



A University of Sussex PhD thesis

Available online via Sussex Research Online:

<http://sro.sussex.ac.uk/>

This thesis is protected by copyright which belongs to the author.

This thesis cannot be reproduced or quoted extensively from without first obtaining permission in writing from the Author

The content must not be changed in any way or sold commercially in any format or medium without the formal permission of the Author

When referring to this work, full bibliographic details including the author, title, awarding institution and date of the thesis must be given

Please visit Sussex Research Online for more information and further details

Mechanisms underlying synaptic phenotypes arising from human disease mutations in NMDA receptors

Marwa Elmasri

Supervised by Dr Andrew Penn

Submitted for the degree of Doctor of Philosophy

University of Sussex

December 2019

Declaration

I hereby declare that this thesis has not been and will not be, submitted in whole or in part to another University for the award of any other degree.

Signature:.....

Acknowledgements

All experimental work included in this thesis was undertaken by Marwa Elmasri, with the exception of:

Electrophysiological recordings from one mouse each for the heterozygous GluN2A and GluN2B KO (Chapter 2). This data was collected by a Postdoc in the lab, Wajeeha Aziz.

Building hGluN2A_S1S2 and hGluN2B_S1S2 model structures and collection of static features (Chapter 3) was done by Andrew Penn.

Preparation, transfection and imaging of dissociated hippocampal cultures for GluN2 trafficking experiments was by project students Daniel Hunter and Does Moolenaar Van der Does. Image analysis was by Daniel Hunter (Chapter 4).

Several mutagenesis reactions were performed by project student Eirini Karachaliou.

The mice for the experiments in this thesis were a gift from Kenji Sakimura (Niigata University, Japan).

I would like to thank my supervisor, Andrew Penn, for his continuous support and guidance throughout my PhD. I would also like to thank him for all the code that he wrote to help with analysis and statistics, teaching me electrophysiology, and for allowing me to be a part of his lab.

I would like to thank my co-supervisor John Atack, thesis committee members Eisuke Koya and Paul Beswick, and Ruth Murrell-Lagnado for their feedback and ideas on my work.

Thanks to all those who made my time at Sussex more enjoyable, especially Petra and Sofie for the endless laughs (and chocolate), and members of the Penn lab: Oli (Jenny), Ella (Ugly Meg), and Daniel.

Finally, I would like to thank my family for helping me through the past few years and always supporting me.

Summary

The *N*-methyl-D-aspartate receptor (NMDAR) is a glutamate-gated ion channel that mediates the late component of excitatory neurotransmission and contributes to synaptic plasticity, processes of learning and memory and excitatory-inhibitory balance. Many diverse combinations of NMDAR subunits can assemble to form the heteromeric structure and each subunit provides unique functional characteristics, creating a heterogeneous receptor pool. Mutations in the GluN2A and GluN2B subunits, which are highly populated in the hippocampus and forebrain, have been found in various seizure and mental disorders. An increasing volume of research to uncover the mechanisms that lead from a genetic alteration to the disease phenotype has so far focused largely on the use of heterologous expression systems, from which, human disease mutants have been characterised into two sub-types: gain-of-function (GOF) and loss-of-function (LOF). GluN2A GOF and LOF mutants have been both implicated in seizure phenotypes whereas GluN2B GOF and LOF mutants have been tentatively linked to distinct phenotypes: seizure and mental disorders, respectively. Despite this, there is still a limited insight into the effects on neuronal and synaptic mechanisms. In this thesis, using the CA3-CA1 synapse in organotypic hippocampal mouse slices and dissociated neuronal cultures, it was found that GluN2A GOF and LOF mutations produced a common synaptic phenotype of prolonged NMDAR-mediated synaptic currents through either an increase in receptor functional properties (GOF) or diminished expression (LOF). GluN2B mutants also exhibited a common synaptic phenotype of rapidly decaying NMDAR-mediated synaptic currents due to a defective expression even for so-called GOF mutants. These findings caution the translation of results from non-neuronal systems into neurons and for predictions of synaptic properties that could influence the disease management in human patients. Instead of counting on the gain/loss distinction of individual subunits, the results suggest that focus should be placed more broadly on the changes in synaptic transmission that result from GluN2 subunit mutations.

Abbreviations

ACSF – Artificial cerebrospinal fluid

AED – Anti-epileptic drug

AMPA – alpha-amino-3-hydroxy-5-methyl-4-isoxazole propionic acid receptor

ASD – Autism spectrum disorder

CDS – Coding Sequence

CTD – C-terminal domain

DG – Dentate gyrus

DIV – Days in vitro

EEG – Electroencephalography

E-I – Excitatory-Inhibitory

ER – Endoplasmic reticulum

EPSC – Excitatory post-synaptic current

EPSP – Excitatory post-synaptic potential

GABAR – Gamma-amino-butyric acid receptor

GFP – Green fluorescent protein

GOF – Gain of function

HEK-293 – Human Embryonic Kidney 293

Het – heterozygous

Hom – homozygous

ID – Intellectual disability

KI – Knock-in

KO – Knock-out

LBD – Ligand-binding domain

LOF – Loss of function

LTP – Long-term potentiation

MC – multiple comparisons

MEG – Magnetoencephalography

mEPSC – Miniature excitatory post-synaptic current

NAM – Negative allosteric modulator

NMDAR – N-methyl-D-aspartate receptor

n.s. – non significant

NTD – Amino-terminal domain

PAM – Positive allosteric modulator

PCA – Principle component analysis

PDF – Probability density function

PSD – Post-synaptic density

RI – Rectification Index

ROBPCA – Robust principle component analysis

ROI – Region of interest

SCE – Single cell electroporation

SEM – Standard error of the mean

SEP – Superecliptic pHluorin

sstype – Sum-of-squares type

TMD – Transmembrane domain

TP – Time point

UnT – Untransfected

WT – Wild-type

Table of Contents

Chapter 1 Introduction	1
NMDAR structure and composition	3
GluN2A and GluN2B function	5
GluN2A and GluN2B trafficking	10
GluN2 impact on AMPAR-mediated synaptic transmission	13
Human disease mutations in GluN2A and GluN2B NMDARs	15
Hypotheses and Aims	21
Chapter 2 Dual or single allele deletion of GluN2A or GluN2B subunits perturbs the NMDAR component of synaptic transmission	24
Abstract	25
Introduction	26
Methods	28
Animals	28
Hippocampal slice culture preparation	28
Single-cell electroporation	29
Slice preparation and recording solutions	31
Electrophysiological recordings	32
Statistical Analysis	32
Results	37
GluN2A homozygous KO produces smaller, slower NMDAR-EPSCs	39
GluN2B homozygous KO produces smaller, faster NMDAR-EPSCs	44
No Left/Right differences in NMDAR-EPSC properties in GluN2A or GluN2B KO	44
GluN2 Heterozygous KO displays haploinsufficiency	45
Discussion	49
Using KO as a model for LOF mutations	49
Conflicting GluN2A KO observations	50
No hemispheric differences in GluN2 subunits	50
The heterozygous condition	51
Conclusions	53
Chapter 3 Synaptic phenotypes arising from diverse mutations in the NMDAR subunits GluN2A and GluN2B	54
Abstract	55
Introduction	56
Methods	59
Mutation selection	59

Molecular Biology	64
Slice preparation, SCE, and electrophysiological recordings	67
Statistical analysis	67
Results.....	71
GluN2A Rescue.....	71
GluN2B Rescue.....	73
Mutant RNA expression	73
Synaptic Phenotypes of GluN2A and GluN2B mutations.....	75
Subunit-specific consequences of GluN2 mutations	87
Discussion.....	88
NMDAR-mediated currents are very sensitive to the amount of GluN2A, but not GluN2B, transfected into CA1 neurons	88
GluN2A mutants and NMDAR currents	88
GluN2B mutants and NMDAR currents.....	91
Mutant GluN2A and GluN2B effects on AMPAR currents	94
Conclusions	96
Chapter 4 Mechanisms underlying synaptic phenotypes of GluN2A and GluN2B NMDAR mutants.....	97
Abstract.....	98
Introduction	99
Methods.....	101
Animals.....	101
Pharmacology experiments	101
Double KO recordings	101
Primary neuronal culture, transfection and imaging.....	102
Statistical analysis	104
Results.....	105
Pharmacological block as an indication of relative expression profiles of mutant GluN2	105
Single mutant subunit expression in CA1 neurons	108
Trafficking to the synapse	112
Discussion.....	114
Limitations of trafficking and expression assays.....	114
LOF mutants.....	116
K669N expression	116
I694T did not exhibit a similar synaptic phenotype to other GluN2A mutants.....	117
Is GluN2B impairment more susceptible to expression defects?	117

Further examination of mutants.....	118
Conclusions	119
Chapter 5 General Discussion	120
Summary of results	121
Methodology: translating heterologous cell research into neurons	121
Effect of decay and amplitude on neuron signalling/function for GluN2A mutants	125
LOF phenotypes of GluN2B mutants	126
Impacts of NMDAR mutants on inhibitory synapses	130
Treatment of patients carrying GluN2 mutations.....	131
Regulation of synaptic efficacy	134
Final Conclusions.....	136
References	137
Appendix	161

List of Figures

Figure 1.1: Structure of the NMDA receptor	6
Figure 1.2: Properties of GluN2A and GluN2B subunits	9
Figure 1.3: Effect of NMDAR activation on AMPAR expression during development and in adult neurons	14
Figure 1.4: Phenotypes of GluN2A and GluN2B mutants	20
Figure 2.1: Experimental procedure.	30
Figure 2.2: Schematic of the recording and stimulation sites in the hippocampal slice cultures.	31
Figure 2.3: ROBPCA method for detection of outliers.....	33
Figure 2.4: Kernel density plots	35
Figure 2.5: Validation of experimental approach.	38
Figure 2.6: GluN2A KO produces smaller and slower currents in CA1 pyramidal neurons in organotypic hippocampal slice culture.	40
Figure 2.7: GluN2A KO in CA1 pyramidal neurons behaves similarly at different time points. ..	41
Figure 2.8: GluN2B KO produces smaller and faster currents in CA1 pyramidal neurons in organotypic slice culture.	42
Figure 2.9: GluN2A and GluN2B KO in CA1 pyramidal neurons do not show hemispheric differences.	43
Figure 2.10: Heterozygous GluN2A and GluN2B KO show a similar trend to the respective homozygous KOs, but with a reduced, intermediate impact.	46
Figure 2.11: The decay kinetics of heterozygous KOs are intermediary but not completely halfway.....	47
Figure 3.1: Mutation selection procedure.	62
Figure 3.2: Location of GluN2 mutants and their associated phenotypes.	63
Figure 3.3: Location of primers annealing to pCI-Neo GRIN2 constructs.	68
Figure 3.4: NMDAR-mediated currents are very sensitive to the amount of GluN2A transfected into CA1 neurons.	72
Figure 3.5: Neurons show saturation with the amount of GluN2B that can be incorporated into the synapse at concentrations tested.....	74
Figure 3.6: Mutant constructs are all expressed at the mRNA level.	75
Figure 3.7: NMDAR conductances are isolated from mixed AMPAR/NMDAR conductances by subtraction of AMPAR conductance.	76
Figure 3.8: GluN2A GOF mutations produce prolonged NMDAR decay at depolarised potentials.	79
Figure 3.9: GluN2A LOF mutations produce prolonged NMDAR decay at depolarised potentials.	81
Figure 3.10: GluN2B LOF mutations produce brief NMDAR decay at depolarised potentials. ..	83
Figure 3.11: GluN2B GOF mutations produce brief NMDAR decay at depolarised potentials...	85
Figure 3.12: A subunit specific effect observed by GluN2A and GluN2B mutants.	86
Figure 4.1: Image analysis procedure using ImageJ.....	103
Figure 4.2: Hypothesised trafficking and expression of GOF and LOF GluN2 mutants and their response to GluN2 blockers.	106
Figure 4.3: Block of GluN2 by ifenprodil or TCN-201 in the presence of mutant subunits.	107
Figure 4.4: Single mutant subunit expression shows diverse effects for GluN2A but not GluN2B mutants.	109

Figure 4.5: Trafficking of GluN2A mutants to dendritic spines differs for a GOF and LOF mutant.	111
Figure 5.1: Synaptic charge transfer predicted from heterologous cells (Swanger et al., 2016) and observed charge transfer from mutants transfected into CA1 neurons.	124

List of Tables

Table 2.1: PCR protocols for genotyping <i>Grin2A</i> -flox and <i>Grin2B</i> -flox mice.....	29
Table 3.1: Primers used to generate mutant GluN2A and GluN2B constructs from WT pCI-Neo <i>GRIN2A</i> and pCI-Neo <i>GRIN2B</i> , respectively, using GeneArt site-directed mutagenesis system.....	65
Table 3.2: Transfected/untransfected ratio of decay time constants and peak amplitudes for the range of GluN2A and GluN2B concentrations tested for successful rescue of KO to regular untransfected levels.....	71
Table 3.3: Electrophysiological properties of GluN2A and GluN2B mutants.....	77

List of Appendices

Appendix A: Raw and ranked scores of static and dynamic features.....	161
Appendix B: Order of mutations from most to least damaging.....	162
Appendix C: Extraction Method for Principal Component Analysis.....	163
Appendix D: Correlation between rankings of predicted deleterious effects and observed effects in heterologous cells of <i>GRIN2A</i> and <i>GRIN2B</i> mutations.....	164
Appendix E: Unadjusted p values for mutant data.....	165
Appendix F: Adjusted p values for mutant data.....	166
Appendix G: Integral of conductance for mutant NMDAR subunits.....	167
Appendix H: NMDAR Current-Voltage curves for untransfected cells and cells transfected with mutant GluN2 subunits.....	168

Chapter 1 Introduction

The neurotransmitter glutamate mediates most of the excitatory signalling in the brain and can act on several receptor classes, which include the ionotropic glutamate receptor family consisting of the *N*-methyl-D-aspartate receptors (NMDARs), alpha-amino-3-hydroxy-5-methyl-4-isoxazole propionic acid receptors (AMPA) and Kainate receptors (Cull-Candy and Leszkiewicz, 2004). Upon binding glutamate, ionotropic glutamate receptors undergo a conformational change that opens a channel in the protein that is capable of conducting ions (Jones et al., 2002). For activation, NMDARs also require the binding of a co-agonist, either glycine (Mayer et al., 1989) or D-serine (Fadda et al., 1988), and removal of pore-blocking magnesium by post-synaptic membrane depolarisation (Mayer et al., 1984, Nowak et al., 1984). The requirement for both agonist binding and membrane depolarization makes the NMDAR a coincidence detector for pre- and post-synaptic activity (Shipton and Paulsen, 2014, Seeburg et al., 1995). This property has made the NMDAR a fundamental component of excitatory synapses, it being essential for many mechanisms regulating synaptic efficacy including the induction of long term potentiation (LTP), which has long been suggested a cellular process underlying learning and memory (Nicoll, 2017).

An imbalance in synaptic excitation and inhibition is generally considered to result in seizure disorders and NMDARs play a large role in excitability (Raol et al., 2001). Sustained states of depolarisation that are mediated through NMDAR plateau potentials lasting hundreds of milliseconds contribute significantly to the supralinear summation of synaptic inputs (Antic et al., 2010) and can contribute to synaptic plasticity (Augusto and Gambino, 2019). Hyperexcitability is thought to be a cause for seizures and epileptic syndromes, where elevation of intracellular calcium can cause neurotoxicity and neurodegeneration (Frasca et al., 2011). In contrast, disrupted NMDAR-mediated synaptic transmission or over-inhibition has been associated with learning and memory impairments (Fernandez and Garner, 2007, Gecz, 2010, Sakimura et al., 1995). Furthermore, many forms of synaptic plasticity and learning behaviours are attenuated when synaptic NMDAR currents are lost (Brigman et al., 2010, Sakimura et al., 1995, Tsien et al., 1996).

In recent years, the number of mutations identified in the GluN2A and GluN2B subunits of the NMDAR have increased dramatically. More than 200 mutations have all been found in patients with various forms of seizure and mental disorders such as intellectual disability, autism spectrum disorders and developmental delay (Lee et al., 2015b, Sun et al., 2017, Dimassi et al., 2013) (see open-access online GRIN database - www.grin-database.de). Investigations into the functional impact of mutations have been performed mainly in non-neuronal, heterologous cells

due to the ease of expression in these systems and the lack of endogenous ion channels that could complicate interpretation of current measurements (Thomas and Smart, 2005). Various studies have reported data for a range of characteristics altered by GluN2 mutants, including agonist potency, peak amplitude, decay time course, sensitivity to magnesium block, proton sensitivity, surface or total expression (Addis et al., 2017, Serraz et al., 2016, Swanger et al., 2016). However, there is often no common method of characterisation between different studies as they do not always use the same expression systems, protocols, concentrations of agonists or co-agonists, so much information is lacking for a lot of mutants. As well as this, very few labs (Fedele et al., 2018, Liu et al., 2017, Ogden et al., 2017) have attempted to extend this research into neurons and to study the impact of human disease NMDAR mutants on synaptic transmission. The aim of this thesis is to study how and to what extent human disease mutations in GluN2A and GluN2B perturb excitatory synaptic currents. This chapter will provide a background overview of the properties and differences between NMDAR subunits GluN2A and GluN2B and will review the current literature on GluN2 human disease mutants.

NMDAR structure and composition

The NMDAR is formed by the oligomerization of four subunits into a tetrameric complex (fig. 1.1a,b). The NMDAR subunits can be split into three different sub-types: GluN1, GluN2 and GluN3. GluN1 subunits are encoded by the *GRIN1* gene which can be alternatively spliced into eight different isoforms that each differ in their functional properties and regional expression (Laurie and Seeburg, 1994, Laurie et al., 1995, Tolle et al., 1995, Yi et al., 2018). GluN2 subunits are subdivided into GluN2A, GluN2B, GluN2C and GluN2D and are encoded by four different genes: *GRIN2A*, *GRIN2B*, *GRIN2C* and *GRIN2D*, respectively. The remaining type of NMDAR subunits, the GluN3, are GluN3A and GluN3B, which are encoded by the *GRIN3A* and *GRIN3B* genes, respectively.

Two glycine- or D-serine-binding GluN1 subunits are obligatory for the formation of the complete receptor (Incontro et al., 2014, Vyklicky et al., 2014). Each obligatory GluN1 subunit interacts with a regulatory subunit, either GluN2 or a GluN3, which then oligomerise as a dimer-of-dimers (Karakas and Furukawa, 2014, Schöler et al., 2008). NMDARs can assemble as either di- or triheterotetramers (Paoletti et al., 2013): Diheterotetramers are composed of two GluN1 subunits along with two of the same GluN2 or GluN3 subunits whereas triheterotetramers are composed of two GluN1 subunits and a different combination of GluN2 or GluN3 subunits. Due to the high diversity of possible subunit combinations, NMDARs can have very different functional properties and can be used to mediate very diverse signalling processes (Sanz-

Clemente et al., 2013). In the hippocampus, the NMDAR composition: di- or triheterotetramers is still a matter of debate, although it is likely that triheterotetramers of GluN1, GluN2A and GluN2B are the major NMDAR type expressed (Gray et al., 2011, Paoletti et al., 2013, Stroebel et al., 2018).

Each NMDAR subunit has four domains, each specialized for different tasks ultimately giving the receptor its unique function (Lee et al., 2014). These are: the amino-terminal domain (NTD), ligand-binding domain (LBD), transmembrane domain (TMD) and carboxy-terminal domain (CTD) (fig. 1.1). The NTD (fig. 1.1c) is an extracellular domain that is important for modulating receptor activity as it binds many allosteric ligands. This includes protons which inhibit NMDARs by binding to GluN1a subunits (Traynelis et al., 1995) and polyamines which relieve proton inhibition of NMDARs due to their positive charge (Huggins and Grant, 2005, Traynelis et al., 1995). Zinc ions also modulate NMDAR activity by causing a conformational change in the protein through closure of the NTD clamshell that is transmitted to the LBD to narrow the pore size and inhibit the passage of ions (Jalali-Yazdi et al., 2018, Mayer and Vyklícký, 1989, Vergnano et al., 2014). GluN2A is more sensitive to block by zinc as nanomolar concentrations affectively inhibit currents whereas micromolar concentrations are required to inhibit GluN2B (Paoletti et al., 1997). At micromolar concentrations, zinc may also have potentiating effects on GluN2B-containing NMDARs thereby enhancing LTP through activation of the Src family of tyrosine kinases (Sullivan et al., 2018). The NTD is also the site of binding for many pharmacological tools that are used to manipulate NMDAR activity, such as the GluN2A selective blocker TCN-201 (Hansen et al., 2012) and the GluN2B selective blocker, ifenprodil (Perin-Dureau et al., 2002).

The NTD and LBD are large structures present in the extracellular region and protrude a total of 10-12 nm into the synapse which can be roughly 40 nm wide (Zhu and Gouaux, 2017). The LBD forms a clamshell-like structure (fig. 1.1a,b) that contains the binding sites for glutamate (GluN2) or the co-agonist (GluN1, GluN3) required for receptor activation (Lu et al., 2017). The glutamate binding site in the GluN2 subunit contains positively charged residues that guide the glutamate molecule into its binding pocket through several ligand-protein interactions (Yu and Lau, 2018). The glycine binding site is present in GluN1 and glycine binding differs in that the process is less controlled by surrounding residues and the molecule diffuses into place at random (Yu and Lau, 2018). Binding of the agonists induces closure of the cleft structure of the LBD and through this conformational change, pulls the connected M3 helices in the TMD away from the pore axis (Suzuki et al., 2013, Twomey and Sobolevsky, 2017, Zheng et al., 2017). In particular, the GluN2 subunits are closer to the central axis and have a privileged role in gating the channel (Karakas

and Furukawa, 2014, Lee et al., 2014, Twomey and Sobolevsky, 2017). Interactions between the LBDs of different subunits are also crucial for receptor function (Bledsoe et al., 2017).

The TMD contains the channel pore, which allows ions to traverse the neuronal membrane. The channel is formed from the TMDs of the four NMDAR subunits; three transmembrane segments (M1, M3, M4) from each subunit form the TMD and the M2 re-entrant loops form the pore (Cao et al., 2011) (fig. 1.1d). This pore is normally blocked by a magnesium ion at resting membrane potential (Mayer et al., 1984, Nowak et al., 1984) as the positively charged large cation cannot pass through the ~0.5 nm diameter of the constricted region of the pore (Villarroel et al., 1995). Membrane depolarization releases the magnesium block at resting membrane potential by providing a driving force to repel the cation from its binding site in the pore (Zarei and Dani, 1994), thus permitting smaller cations (i.e. sodium, potassium and calcium) to permeate. Magnesium is particularly potent at blocking the channels containing GluN2A or GluN2B, whereas magnesium block is weaker for GluN2C, GluN2D and GluN3A-containing channels. The whole TMD seems necessary for the NMDAR to form a functional receptor since subunits that are truncated before the final TMD (M4) show no currents when expressed in HEK cells (Sceniak et al., 2019, Schorge and Colquhoun, 2003).

The CTD (fig. 1.1d) is an intracellular domain that is responsible for interacting with intracellular proteins such as PSD-95, SAP102 and calmodulin and also has a role in the trafficking of the receptor and incorporation into the post synaptic density (Sans et al., 2003, Shipton and Paulsen, 2014, Wenthold et al., 2003a, Wenthold et al., 2003b), as well as affecting receptor function (Maki et al., 2012). NMDARs with truncated CTDs have irregular localisation at the synapse (Mohrmann et al., 2002, Steigerwald et al., 2000) and also show some functional abnormalities (Maki et al., 2012). Mice that have a truncated GluN2B CTD die perinatally and those with a truncated GluN2A CTD have impaired synaptic plasticity and altered kindling behaviour (Sprengel et al., 1998). The C-terminal tails of GluN2A and GluN2B have been found to have diverse roles in signalling processes, including regulation of receptor biophysics (Aman et al., 2014, Murphy et al., 2014), excitotoxicity (Martel et al., 2012), and learning (Ryan et al., 2013).

GluN2A and GluN2B function

Neurons in the adult forebrain tune NMDAR properties largely by controlling the relative expression of the regulatory subunits, GluN2A and GluN2B (Gray et al., 2011, Monyer et al., 1994, Watanabe et al., 1992). The extracellular and membranous regions of the two subunits

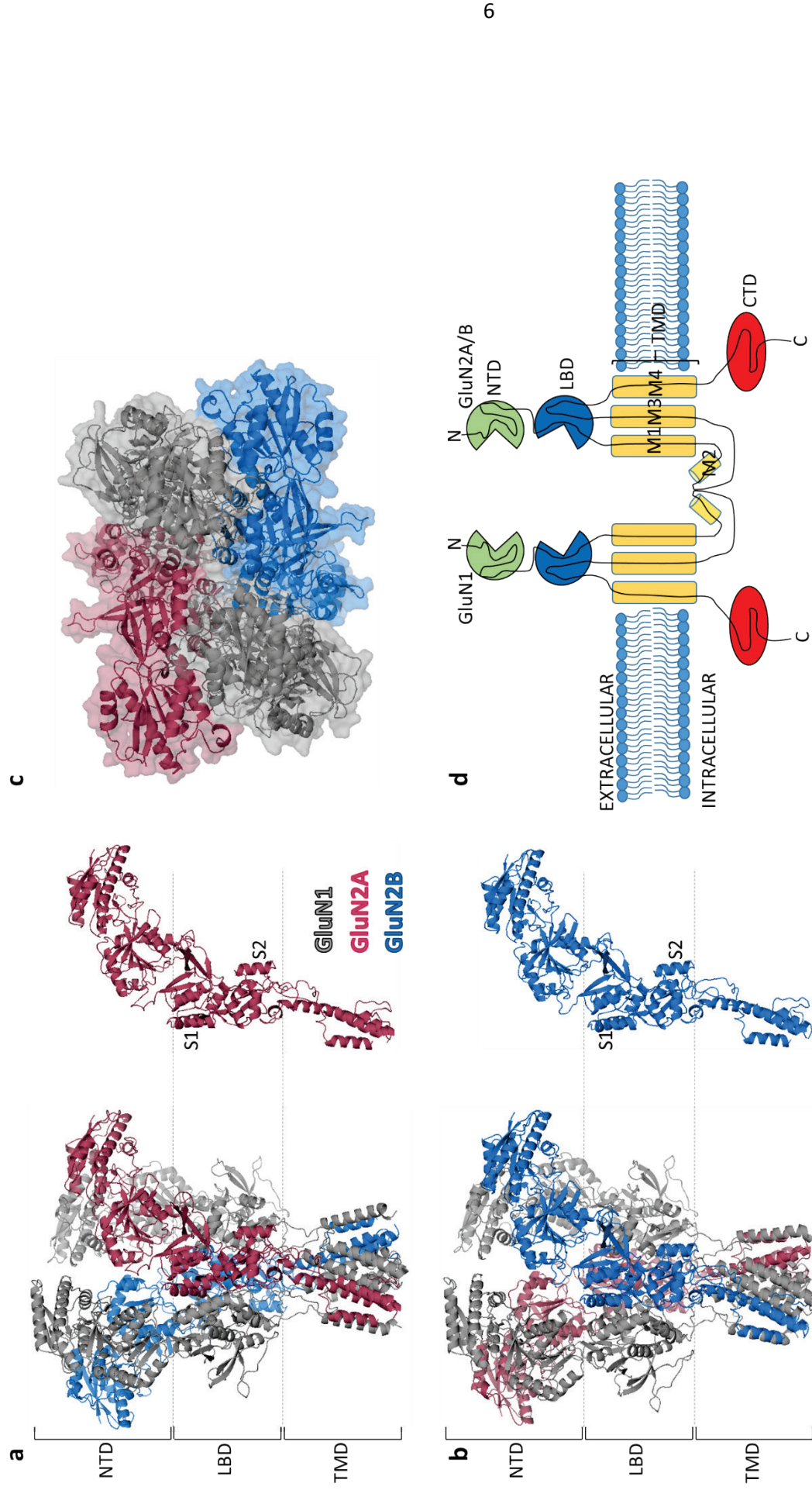


Figure 1.1: Structure of the NMDA receptor

a) Left. Model of NMDAR tetramer composed of a dimer-of-dimers (GluN1-GluN2A and GluN1-GluN2B) with the GluN2A subunit in front view. b) same as a) with GluN2B in front view. a and b) Right. Models of GluN2A and GluN2B alone show the high similarity in structure between the two subunits. c) view from above showing the NTD association of different subunits. d) Schematic of NMDAR with extracellular NTD and LBD which form clamshell structures, TMD composed of three domains which fully span the membrane: M1, M3, M4, the M2 loop (which forms the channel pore), and the intracellular CTD.

have an overall sequence similarity and identity of 85% and 72% respectively in humans, and their structures have a root mean squared deviation of the backbone alpha carbon atoms of 4.2 Å (pdb 5uow). Despite this similarity, the GluN2A and GluN2B subunits differ in their agonist and modulator affinities, channel kinetics, open probabilities and desensitisation (Gray et al., 2011, Kohr et al., 1994, Wright et al., 1999, Yuan et al., 2015, Zhou et al., 1999) (fig. 1a,b). Compared to GluN2B, GluN2A has a higher open probability, lower affinity for glutamate and glycine, faster glutamate unbinding and deactivation (Sheng et al., 1994, Vicini et al., 1998), while both subunits have similar conductance, magnesium sensitivity and calcium permeability (fig. 1.2) (see Paoletti et al. (2013) for review). The properties of different GluN2 subunits can also be modulated by the GluN1 isoform present. GluN1a and GluN1b differ in a 21 amino acid sequence encoded by exon 5 of the *GRIN1* gene (Yi et al., 2018), which is present in GluN1b but spliced out from the GluN1a isoform. This leads to large changes in the deactivation kinetics of GluN1/GluN2B receptors – more than 3 times slower decay with GluN1a. In contrast, the differences in deactivation are less marked for GluN1/GluN2A receptors containing GluN1a or b (fig. 1.2) (Rumbaugh et al., 2000, Yi et al., 2018). Expression of both GluN1a and GluN1b has been detected in embryonic stages in rat at low levels that increase as development progresses into adult; the levels of GluN1a are higher than GluN1b at all stages and in the hippocampus (Laurie and Seeburg, 1994).

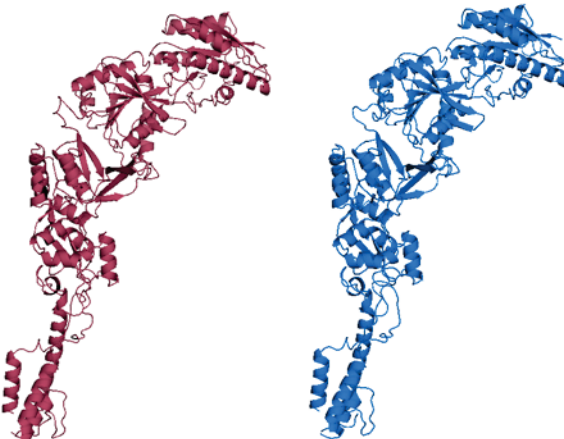
Due to these diverse functional properties within the NMDAR population, different NMDAR compositions can be utilised to achieve various signalling outcomes (Wyllie et al., 2013). In different brain regions and at different time points throughout development, distinct NMDAR compositions are expressed and these correlate with changes in synaptic responses (Gray et al., 2011, Hestrin, 1992, Sanz-Clemente et al., 2013). It has been observed in the forebrain that the subunit composition switches from predominantly GluN2B containing receptors to GluN2A during the early post-natal period (McKay et al., 2012, Punnakal and Dominic, 2018, van Zundert et al., 2004); GluN2B is already expressed during embryonic stages and is maintained into adulthood whereas GluN2A expression begins after birth and increases dramatically in the early post-natal period (fig. 1.2) (Monyer et al., 1994, Sheng et al., 1994). The increase in GluN2A content into synapses containing NMDARs leads to developmental speeding of NMDAR-mediated EPSCs (Hestrin, 1992, McKay et al., 2018). This switch is thought to be activity-dependent (Audinat et al., 1994, Matta et al., 2011) and result more from increasing GluN2A expression rather than GluN2B expression repression or removal from synapses (McKay et al., 2018). The NMDAR subunit composition may have a role in determining the direction of synaptic plasticity, as suppression of GluN2B subunits prevents long term depression (LTD) but

suppression of GluN2A prevents long term potentiation (LTP) at CA1 synapses (Liu et al., 2004). Furthermore, synapse development in the critical period may also depend on the GluN2B to GluN2A switch since cortical neurons from a mouse line that do not undergo the subunit switch have immature dendritic spine morphology, neurodegeneration and increased susceptibility to excitotoxicity (Koster et al., 2019). The switch may also be involved in synapse elimination, pruning of existing synaptic connections and the development of the inhibitory neuronal network; GluN2B levels are reduced in spinal cord synapses at the end of the synapse elimination critical period, while the inhibitory network activity is enhanced (Isoo et al., 2016). This period is extended when GluN2B decline is prevented and can be triggered after the normal cessation with GluN2B overexpression. Inhibition of inhibitory interneurons in the spinal cord also leads to aberrant GluN2B activity and prolonging of the critical period (Isoo et al., 2016). Roles in synaptogenesis and synapse maturation and stabilization have also been implicated for the subunit switch as earlier GluN2A expression onset results in fewer synapses that are of lower volume and less dynamic (Gambrill and Barria, 2011).

Changes in the function or expression of GluN2A or GluN2B during the critical period will likely lead to severe consequences for the development, maturation and pruning of neuronal circuitry (Baez et al., 2018), synapse number and morphology (Gray et al., 2011, Koster et al., 2019), and the excitatory-inhibitory (E-I) balance (Mori et al., 2019). Changes to these processes in development may be implicated in the pathogenesis of disorders whose features include developmental abnormalities or delays and seizure disorders (Zhou et al., 2015). This can be appreciated from knock-out (KO) studies of NMDAR subunits, which have severe effects on behaviour and development. Null deletion of GluN1 in mice causes death within 8-20 hours of birth due to respiratory failure and inability to suckle or feed (Forrest et al., 1994, Li et al., 1994). The GluN1 subunit is essential for the formation of functional NMDARs thus implicating GluN1 in neonatal survival.

GluN2A KO mice are capable of surviving after birth and many have found that they do not exhibit any morphological abnormalities (Kadotani et al., 1996, Kannangara et al., 2015, Sakimura et al., 1995) as GluN2A begins to be expressed after birth and development seems more dependent on GluN2B (Koster et al., 2019). However, a more recent study found various abnormalities in the brain microstructure of the cortex, hippocampus, thalamus and corpus callosum transiently occurring at P30, which were no longer present when mice were a month older (P56) (Salmi et al., 2018). In addition, epileptiform activity was present in electroencephalography (EEG) recordings during slow-wave sleep by the third post-natal week

(Salmi et al., 2019). GluN2A KO mice also have impairments in spatial learning and have been reported to be 'jumpy', although no behavioural hallmarks of seizures were reported by these research groups (Kannangara et al., 2015, Sakimura et al., 1995). In addition, GluN2A subunits with truncated CTDs have irregular kindling behaviour where more stimulations are required to induce seizures but once initiated, seizures last twice as long (Sprengel et al., 1998).



	GluN2A	GluN2B
P _o	0.5	0.1
Glutamate EC ₅₀	4 μM	2 μM
Glycine EC ₅₀	~ 2 μM	0.6 μM
Glutamate unbinding	40 ms	300 ms
Decay	Fast*	Slow*
Decay with different GluN1 isoforms	1a – 49ms [#] 1b – 32 ms	1a – 511 ms [#] 1b – 151 ms
Conductance	50 pS	50 pS
Mg ²⁺ sensitivity (IC ₅₀)	2 μM	2 μM
Ca ²⁺ permeability (P _{Ca} /P _{CS})	~ 8	~ 8
Expression	Post-natal and adult [‡]	Embryonic, post-natal and adult [‡]

Figure 1.2: Properties of GluN2A and GluN2B subunits

P_o, open probability. Data from Paoletti et al., (2013) except *Vicini et al., (1998), [#]Yi et al., (2018), [‡]Monyer et al., (1994).

The GluN2B subunit seems to play a larger role in development than GluN2A, consistent with the higher expression of GluN2B in the forebrain at embryonic stages. The GluN2B KO mice die

shortly after birth due to absence of a suckling response unless supported by hand feeding (Kutsuwada et al., 1996). Due to the obligatory heteromeric assembly of NMDARs, knock-out of GluN2B results in a significant loss of NMDARs, particularly during early developmental stages, with the residual NMDARs largely containing GluN2D or GluN3 (Ciabarra et al., 1995, Kehoe et al., 2013, Monyer et al., 1994, Watanabe et al., 1992). Mice generated to have a replacement of GluN2B with GluN2A through the germline also die perinatally due to an impaired suckling response implicating GluN2B-containing receptors in supporting this behaviour (Wang et al., 2011). These mice also had impaired homeostatic synaptic plasticity, specifically a defective upscaling of synaptic transmission following pharmacological silencing of network activity. In the absence of GluN2B, the AMPAR component at glutamatergic synapses was greater as was observed by larger miniature excitatory post-synaptic current (mEPSC) amplitudes (Gray et al., 2011, Wang et al., 2011). GluN2B loss has also been associated with hippocampal LTP and LTD impairments and reduced spine density, as well as deficits in performance on behavioural tests such as the Morris water maze (Brigman et al., 2010). As LTD but not LTP was found to be impaired with GluN2B loss previously (Liu et al., 2004), it is likely due to the varying protocols used for the induction of either phenomenon by different research groups.

GluN2A and GluN2B trafficking

Tight control of NMDAR subunit composition is regulated by a combination of gene expression and sequence motifs within the subunit proteins. The main NMDAR subunits expressed in the hippocampus are GluN2A and GluN2B, in complex with the obligatory GluN1 (Gray et al., 2011, Monyer et al., 1994, Watanabe et al., 1992). The hippocampus is focused upon as CA1 receives input from a recurrent network implicated in seizure generation; kindling models of epilepsy have shown high susceptibility of seizure induction and spread in the hippocampus (Bertram, 2007). The tri-synaptic pathway, and in particular, the Schaffer collaterals, have been studied extensively in the field of synaptic plasticity (Knierim, 2015, Neves et al., 2008). While the total expression of GluN2B has been found to be higher than that of GluN2A in the hippocampus (Coultrap et al., 2005, Pian et al., 2010), the surface expression of GluN2A was higher than GluN2B in the adult CA1 region as assessed by immunoblotting (Sun et al., 2016), pharmacological blockade of field EPSPs using subunit specific blockers (Le Bail et al., 2015) and conditional subunit deletion (Gray et al., 2011).

Triheteromeric GluN1/GluN2A/GluN2B NMDARs have unique functional and pharmacological properties compared to GluN2A or GluN2B diheteromeric receptors – deactivation rate is intermediate and modulation by subunit-selective antagonists and their binding sites is

distinctive (Hansen et al., 2014). Whether the GluN2A and GluN2B subunits exist in diheteromeric or triheteromeric structures continues to be a subject of debate; Al-Hallaq et al. (2007) have suggested that less than 20% of NMDARs at P7 and only one third at P42 are triheteromeric in the CA1/CA2 region of the rat hippocampus from immunoprecipitation. Thus, the majority of receptors were considered to be diheteromeric GluN1/GluN2A or GluN1/GluN2B receptors. Recently, using super resolution microscopy in cultured hippocampal neurons, it was found that GluN2A and GluN2B cluster in separate, mostly non-overlapping nanodomains that have different properties, including size and shape (Kellermayer et al., 2018). Specifically, only 20-40% of GluN2A and GluN2B nanodomains overlapped, suggesting that most NMDAR in the hippocampus are diheterotetramers, although this was based on overexpression of epitope-tagged GluN2 subunits (Kellermayer et al., 2018). Conversely, using comparisons of voltage dependent decay times of NMDAR EPSCs in mouse neurons, others have found that at least 50% of NMDARs at CA3-CA1 synapses in adult mice are triheteromeric (Rauner and Kohr, 2011) or even two thirds of receptors are triheteromeric GluN1/GluN2A/GluN2B in hippocampal neurons taken from P0-1 mice and cultured for 10–16 days *in vitro* (Tovar et al., 2013). The most widely held view currently is that triheteromeric receptors form a major proportion of NMDARs (Gray et al., 2011, Paoletti et al., 2013, Stroebel et al., 2018). By selectively expressing recombinant triheteromeric GluN1/GluN2A/GluN2B receptors at the membrane, distinct pharmacological properties have been found from the respective diheteromeric receptors for subunit selective antagonists (Hansen et al., 2014, Stroebel et al., 2018), which will aid in interpreting studies evaluating subunit composition using these antagonists.

Expression of the GluN1 or GluN2 subunits alone does not lead to the formation of functional receptors capable of trafficking to the neuron surface and to synapse; instead, the subunit is retained in the endoplasmic reticulum (ER) (McIlhinney et al., 1998). Co-expression of GluN1 with a GluN2 subunit results in surface detection through a mechanism by which the receptor is forward trafficked from the ER (Barria and Malinow, 2002). Both GluN1 and GluN2 subunits contain specific sequences that determine this trafficking behaviour. An ER retention sequence is present in the NTD of GluN2A (Qiu et al., 2009) which is thought to be masked by subunit assembly, allowing the NMDARs to be exported to the Golgi where they are processed and packaged into vesicles to be delivered to the plasma membrane (Cao et al., 2011, Horak et al., 2014). The CTD of GluN2B also contains ER retention signals and a sequence motif that acts as a signal for release from the ER (Hawkins et al., 2004). The latter is a four amino acid sequence (HLFY) in the GluN2B CTD, which when mutated results in accumulation of the assembled, functional receptor in the ER, suggesting that it is necessary for export out of the ER (Hawkins

et al., 2004). However, Yang et al. (2007) found that truncated GluN2A and GluN2B constructs with only three amino acids after M4 were capable of surface expression. In fact, these M4 proximal amino acids were necessary for escaping the ER since GluN2 subunits truncated only two amino acids after M4 could not be detected at the surface. Furthermore, the amino acid residues after M4 did not need to be HLFY as alanine mutants (AAAA) did not alter the surface trafficking compared to HLFY. Others have found ER retention signals to also be present in the M3 TMD of GluN2B since GluN2B truncated before M3 and expressed alone in heterologous cells can be detected at the cell surface whereas GluN2B truncated after M3 is ER-retained (Horak et al., 2008). GluN1 also contains ER retention sequences in the M3 and M4 TMDs and CTD (Horak et al., 2008, Horak and Wenthold, 2009, Standley et al., 2000). Masking of the retention sequences in both GluN1 and GluN2 by their association is the mechanism by which the complex is released from the ER (Horak et al., 2014).

The mechanisms of trafficking of GluN2A- and GluN2B-containing receptors also seem to differ from one another. GluN2B is constitutively expressed owing to the M3-M4 segment of the LBD harbouring an N-glycosylation site (Storey et al., 2011). In contrast, in GluN2A this N-glycosylation site is absent and GluN2A is expressed in an activity-dependent manner (Barria and Malinow, 2002, Storey et al., 2011). The CTDs have been suggested to play a role in determining the localisation and binding to post-synaptic density (PSD) proteins; different subunits interact with different PSD proteins (see Sanz-Clemente et al. (2013) for review). GluN2B is thought to diffuse more freely on the neuronal surface and its incorporation and removal from the synapse is at a higher rate than GluN2A, which are more stable at synapses (Groc et al., 2006b, Lavezzari et al., 2004). Antibody labelling of chimeras of major histocompatibility complex class II alpha or beta chains and GluN2A or GluN2B CTDs showed that recycling and internalisation of GluN1/GluN2A/GluN2B triheteromers is indistinguishable from that of GluN1/GluN2B diheteromers in hippocampal neurons, and is distinct from the processes for GluN1/GluN2A (Tang et al., 2010). This suggested that unlike for functional properties, such as zinc inhibition and the decay time course (Wang and Furukawa, 2019), GluN2B is dominant in the triheteromeric complex for processes involving receptor trafficking and the membrane-distal portion of the CTD of GluN2B was responsible for this (Tang et al., 2010). Sanz-Clemente et al. (2010) showed that phosphorylation of the GluN2B CTD at S1480 (but not but the equivalent position S1460 in GluN2A) caused the GluN2B subunit to dissociate PDZ-domain proteins that otherwise anchor NMDARs at the synapses.

GluN2 impact on AMPAR-mediated synaptic transmission

NMDAR signalling is implicated in the regulation of postsynaptic AMPARs, which together mediate the majority of excitatory synaptic transmission (Groc and Choquet, 2006). AMPARs are from the same family of glutamate-gated ion channels and form as tetramers composed of either GluA1, GluA2, GluA3 or GluA4 subunits, either as homomers or heteromers (Groc et al., 2006a). LTP, a widely-known phenomenon whereby synaptic strength can be enhanced by high-frequency stimulation, is accomplished through modifications to AMPAR function and expression and results from activation of NMDARs (Lu et al., 2001). Strong activation of synaptic NMDARs results in calcium influx and to the activation of multiple intracellular signalling pathways, some of which, can regulate how AMPARs behave and traffic to synapses (Benke et al., 1998, Halt et al., 2012). The enhancement of AMPAR levels and signalling in the adult brain by LTP is opposed to the inhibitory effects of NMDAR signalling on AMPAR recruitment to synapses during development (fig. 1.3) (Hall and Ghosh, 2008).

In the adult, NMDAR activation and calcium influx activates protein kinases such as calcium/calmodulin-dependent kinase II (CaMKII), which phosphorylates AMPARs to increase their conductance and the insertion of AMPARs into the post-synaptic membrane from extrasynaptic reserve pools and intracellular stores (Granger et al., 2013, Luscher and Malenka, 2012, Penn et al., 2017, Wu et al., 2017) (fig 1.3). Long-term depression, a phenomenon caused by prolonged low frequency synaptic stimulation, can also be triggered by NMDARs in the adult brain. The resulting lower NMDAR channel activity and calcium influx activity is associated with de-phosphorylation of AMPARs and their subsequent removal from synapses by internalisation (Luscher and Malenka, 2012).

Early postnatal genetic deletion of either GluN2A or GluN2B in mice results in enhanced evoked AMPAR peak amplitudes in CA1 pyramidal neurons (Gray et al., 2011, Lu et al., 2011) and basal NMDAR activity inhibits AMPAR incorporation into the synapse (Kannangara et al., 2015, Sutton et al., 2006). GluN2A KO also resulted in an increase in mEPSC amplitude and GluN2B KO increased mEPSC frequency (Gray et al., 2011), suggesting that these subunits normally act to suppress the strength and number of AMPAR-containing synapses during development (fig. 1.3).

In agreement, both GluN2B inhibition with ifenprodil and GluN2B knockdown produced an increase in surface AMPAR subunit GluA1 levels and overexpression of GluN2B produced reduced GluA1 levels, probably because GluN2B is upstream of AMPAR internalisation (Kim et al., 2005). In contrast, although GluN2A knockdown reduced surface GluA1 (Kim et al., 2005),

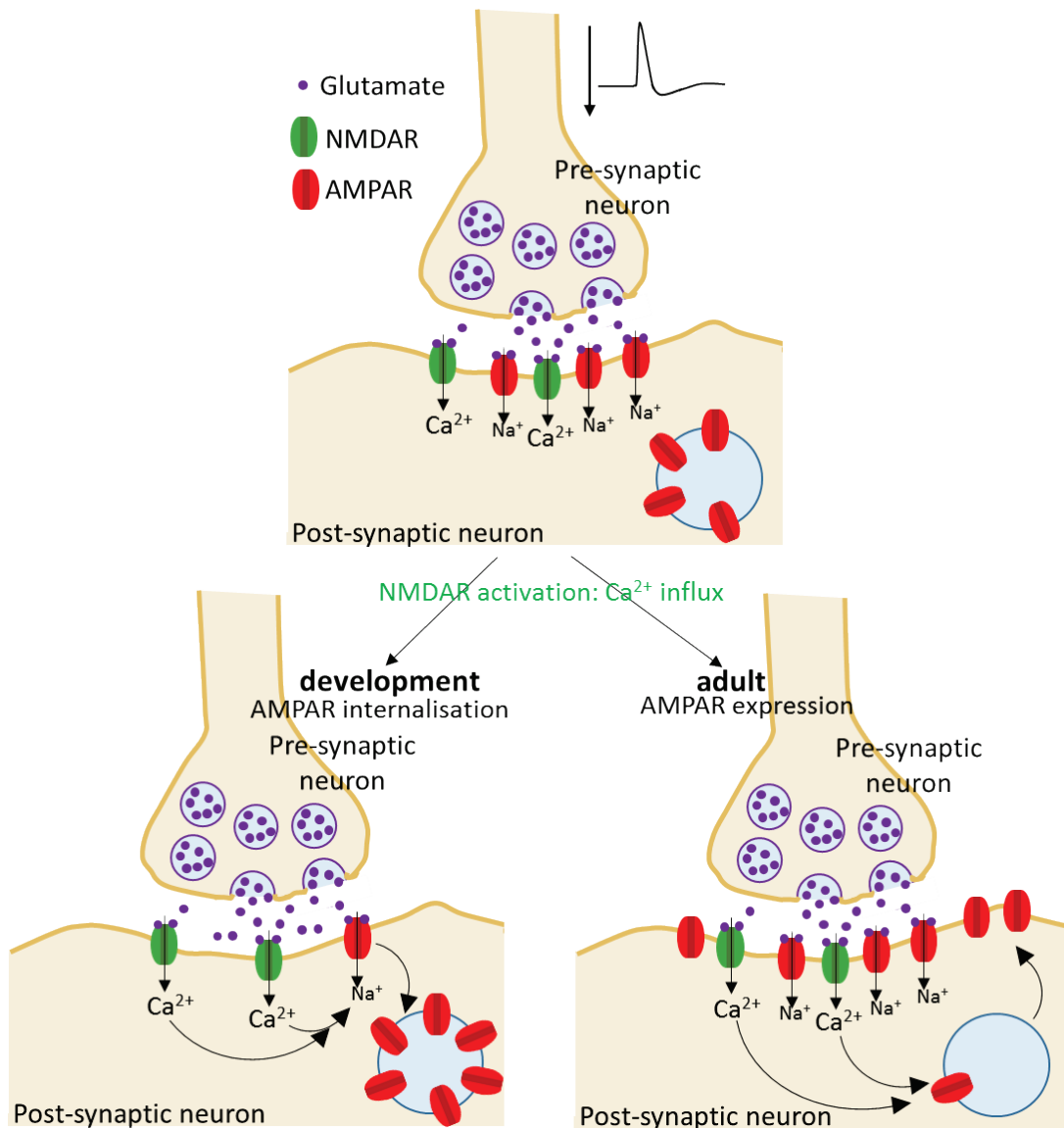


Figure 1.3: Effect of NMDAR activation on AMPAR expression during development and in adult neurons

Activation of NMDARs by glutamate (with concurrent post-synaptic depolarisation) causes the permeation of calcium ions through the channel into the post-synaptic neuron. Calcium is an activator of many intracellular signalling processes, some of which, can lead to regulation of AMPAR expression at the post-synaptic membrane by mobilising AMPARs into and out of intracellular pools. During development, NMDAR signalling acts as a suppressor of synaptic AMPAR expression to regulate excitatory signalling whereas in adult neurons, NMDAR signalling can enhance AMPAR expression or function, leading to phenomena such as LTP.

GluN2A overexpression had no effect on GluA1 expression. Overall consistent with these results, knock-in (KI) mice with GluN2B replaced with GluN2A exhibited an increase in the number of functional AMPARs at the synapse – both GluA1 protein levels and mEPSC amplitude were increased, as well as the number of TARP proteins which regulate AMPAR trafficking (Hamada

et al., 2014). Furthermore, in wild-type (WT) mice the switch from GluN2B to GluN2A during early post-natal development removes the inhibitory influence of GluN2B on synaptic AMPAR content (Hall et al., 2007). Together, this evidence demonstrates diverse roles for GluN2A and GluN2B in the regulation of synaptic AMPARs.

Human disease mutations in GluN2A and GluN2B NMDARs

More than 200 single amino acid substitutions, frameshift mutations, duplications, insertions, truncations and deletions have been observed in the genes encoding human GluN2A and GluN2B NMDAR subunits, *GRIN2A* and *GRIN2B*, respectively (Burnashev and Szepietowski, 2015, Hu et al., 2016, Strehlow et al., 2019). All these genetic abnormalities are heterozygous and have been discovered in the past decade. These mutations have been found to affect all domains and regions of the GluN2 subunits and the effects on receptor activity and expression have been very diverse when investigated in heterologous expression systems (Addis et al., 2017, Endeley et al., 2010, Platzer et al., 2017, Swanger et al., 2016). However, despite the heterogeneity at the molecular level in non-neuronal models, mutations in GluN2A exhibit a common disease phenotype and GluN2B mutations exhibit a different disease phenotype. The majority of mutations in the GluN2A subunit (~90 %) have a link to seizure and epilepsy disorders (fig. 1.4a,c) whereas those in GluN2B (~70 %) are linked to a variety of mental disorders (including intellectual disability (ID), autism spectrum disorders (ASD) and developmental delay) and the majority do not exhibit seizures (fig. 1.4a,b,c) (www.grin-database.de, CFERV database <http://functionalvariants.emory.edu/>). Many patients with GluN2A mutations also exhibit ID (~80 %) (fig. 1.4b) but a much smaller proportion have ID only compared to GluN2B and a much smaller proportion of patients with GluN2B mutants only display seizures without ID (fig. 1.4b). In many cases, ID and epilepsy are co-present in patients (fig. 1.4b) (Brooks-Kayal, 2010, Canitano, 2007, Canitano et al., 2005, Gillberg and Billstedt, 2000, Rubenstein et al., 2018, Tuchman and Cuccaro, 2011) and the prevalence of epilepsy in ID populations is significantly greater than in the general population (McGrother et al., 2006).

Understanding how GluN2 missense mutations disturb the function of NMDARs and lead to synaptic dysfunction may provide clues for understanding the pathogenesis of NMDAR-related disorders. Several studies have attempted to characterise the impact of many different GluN2A and GluN2B mutations on NMDAR function and expression (Adams et al., 2014, Addis et al., 2017, Amin et al., 2017, Amin et al., 2018, Carvill et al., 2013, Endeley et al., 2010, Fedeley et al., 2018, Lemke et al., 2013, Lemke et al., 2014, Lesca et al., 2013, Ogden et al., 2017, Pierson et al., 2014, Serraz et al., 2016, Swanger et al., 2016, Vyklicky et al., 2018, Yuan et al., 2014, Yuan

et al., 2015). However, each study has focused on a certain aspect of NMDAR function so that comparisons between the effects of different mutations have been difficult to make.

Based on the existing available data on mutations in recombinant receptors in heterologous cells at the time, Lemke et al. (2014) suggested a genotype-phenotype correlation for GluN2B mutations where the GOF/LOF distinction correlated to disease outcome – seizure/mental disorders, respectively. This hypothesis arose because the LOF mutation E413G in the LBD from a patient with ID (Adams et al., 2014), led to a fifty times reduction in glutamate potency, reducing receptor activity. Also, truncating, frameshift and deletion mutations which are predicted to have LOF effects from lack of receptor expression had only been found to occur in patients with ID and ASD (Kenny et al., 2014). In contrast, the GOF mutations N615I and V618G discovered in West Syndrome patients and R540H from a patient with both focal epilepsy and ID all resulted in a reduction in the voltage-dependent magnesium block of the channel and thus had increased calcium permeability (Lemke et al., 2014). N615I and V618G were located in the ion channel forming region of the transmembrane domain (TMD) and R540H in the S1 domain of the LBD. R540H was more modest and did not alter glutamate binding efficacy, despite its location in the LBD, and interestingly, the severity of the disease was correlated to the degree of GOF (Lemke et al., 2014). The functional data on mutants was very limited; several mutants had been identified, however, the functional characterisation had been done for few (Awadalla et al., 2010, Conroy et al., 2014, de Ligt et al., 2012, DeVries and Patel, 2013, Epi et al., 2013, Freunscht et al., 2013, Girirajan et al., 2013, Hamdan et al., 2011, Kenny et al., 2014, Klassen et al., 2011, Myers et al., 2011, O'Roak et al., 2012, Talkowski et al., 2012, Tarabeux et al., 2011, Venkateswaran et al., 2014, von Spiczak et al., 2011). Since that time, many mutants have been identified but have also not had their effect on receptor function characterized (Bobbili et al., 2018, Bowling et al., 2017, Butler et al., 2017, D'Gama et al., 2015, Della Mina et al., 2015, Dymment et al., 2015, Farwell et al., 2015, Kyriakopoulos et al., 2018, Lelieveld et al., 2016, Lionel et al., 2018, Nilsson et al., 2017, Pan et al., 2015, Retterer et al., 2015, Takasaki et al., 2016, Trujillano et al., 2017, Sculier et al., 2017, Vissers et al., 2017, von Stulpnagel et al., 2017, Wang et al., 2016, Yu et al., 2018, Zhang et al., 2015).

Early discovery and characterisation of GluN2A mutants identified six mutants that increased receptor activity, albeit through different mechanisms. N615K located in the P-loop that regulates voltage-dependent magnesium channel block resulted in a reduction in this blockade leading to current influx at resting membrane potentials (Allen et al., 2016, Endeley et al., 2010). A243V in the NTD impaired the negative allosteric modulation by zinc, thereby enhancing

receptor activity (Lemke et al., 2013). LBD mutations R518H and T531M and TMD mutation F652V all led to a lengthened mean duration of channel opening (Carvill et al., 2013, Lesca et al., 2013). L812M in the linker region before TMD M4 caused a greater agonist potency, reduced response to negative modulators and increased channel opening (Pierson et al., 2014, Yuan et al., 2014). These mutations were all in patients with various epileptic syndromes, including early onset epileptic encephalopathy, Rolandic epilepsy and epilepsy with continuous spike-waves during slow wave sleep.

Despite evidence for GOF mutations in GluN2A in epilepsy patients, many LOF mutations have also been documented. Deletions in the chromosome region 16p13 which encompassed *GRIN2A* were one of the first seizure-related *GRIN2A* mutations discovered (Reutlinger et al., 2010). Carvill et al. (2013) identified epilepsy-aphasia patients with GluN2A mutations at the methionine translation initiation codon (pM1T) and at a splice site which both likely cause haploinsufficiency. pM1T produces either an absence of the GluN2A protein or a truncated, probable non-functional form, from translation initiation at a downstream methionine and the splice site mutation likely results in nonsense-mediated mRNA decay. Furthermore, Lesca et al. (2013) discovered several truncating mutations, frameshift mutations and *GRIN2A* deletions in patients with epileptic syndromes also predicting haploinsufficiency. Therefore, unlike GluN2B, there appeared to be no genotype-phenotype correlation for GluN2A mutations, as both LOF and GOF are associated with epilepsy.

The contribution of GluN2A LOF mutations to seizure disorders is supported by efforts to systematically examine mutation effects on NMDAR function in heterologous expression systems. Addis et al. (2017) studied ten GluN2A mutations in patients with epilepsy-aphasia spectrum disorders. The mutations P79R, C231Y, C436R, G483R, M705V, and D731N prevented glutamate-mediated toxicity of HEK-293 cells by diminishing receptor trafficking and expression or reducing receptor function. P79R, C231Y, C483R and M705V caused reduced agonist potency whereas C436R and D731N were unresponsive to glutamate and glycine. All these mutants also had reduced surface expression. E714K was also trafficking and expression impaired and C436R had almost no surface expression. Therefore, all the epilepsy-associated mutations exhibited LOF.

While evidence accumulates linking NMDAR mutations to mental and seizure disorders, some groups have reported not finding any effects for some missense mutations from patients with NMDAR-related disorders. Serraz et al. (2016) investigated one LBD mutation (C436R), seven new missense NTD mutations (P79R, F183I, I184S, C231Y, A290V, G295S, R370W) and further

examined A243V in GluN2A. Six of those from the NTD, including A243V, showed no altered effect on current amplitude, glutamate and glycine sensitivity or channel open probability, so had no known effects, although, R370W caused a greater sensitivity to inhibition by zinc. This was in contrast to Addis et al. (2017) for P79R who found reduced agonist potency. Surprisingly, A243V did not appear to have an effect on zinc inhibition, in contrast to the findings by Lemke et al. (2013). LOF mutations P79R, C231Y in the NTD and C436R in the LBD produced a reduced expression of GluN2A-containing receptors, in agreement with Addis et al. (2017). Moreover, P79R receptors also had a decreased sensitivity to allosteric modulation by zinc, a more complicated effect on NMDAR characterisation results. These mutations were also all present in patients with diverse epileptic phenotypes. If and how these mutations contribute to the patients' disorders is still poorly understood.

Comprehensive studies into the effects of missense mutations within the glutamate-binding domains of GluN2 subunits have confirmed the wide-ranging effects seen in case studies. Swanger and colleagues characterised the peak amplitudes, decay time constants and glutamate and glycine potencies for 18 GluN2A and 7 GluN2B LBD missense mutations as well as the expression for a subset of these mutations (Swanger et al., 2016). All GluN2A mutations were epilepsy related, except V452M which was implicated in schizophrenia. These mutations exhibited diverse GOF and LOF effects on the parameters investigated in HEK-293 cells and *Xenopus* oocytes, including complete abolishment of currents (C436R, R518H, T531M), prolonged current decay (K669N), reduced glutamate potency (G483R, V685G, D731N), with the remaining mutants exhibiting milder effects and affecting multiple NMDAR properties, including expression. The GluN2B mutants were all linked with ID, with three also exhibiting epilepsy (C436R, C461F, R540H). C436R, a mutant also present in GluN2A, had diminished current amplitude, as did C456Y and C461F. GluN2B mutants also had very diverse decay profiles with some causing 2-3 times slower decay (R540H, R696H) while others had much faster decay (E413G, C461F), and varying glutamate and glycine potencies and expression profiles too. So, despite common disease phenotypes associated with mutants in each GluN2A and GluN2B subunit (GluN2A – seizures, GluN2B – ID), effects of mutants on NMDAR function and expression were extremely divergent from these studies.

The wide ranging effects of GluN2 mutations on NMDARs have been a common theme in most studies where characterisation has been performed in heterologous expression systems (Adams et al., 2014, Addis et al., 2017, Amin et al., 2017, Amin et al., 2018, Carvill et al., 2013, Chen et al., 2017, Endeley et al., 2010, Fernandez-Marmiesse et al., 2018, Gao et al., 2017, Lemke et al.,

2013, Lemke et al., 2014, Lesca et al., 2013, Mullier et al., 2017, Platzer et al., 2017, Serraz et al., 2016, Sibarov et al., 2017, Swanger et al., 2016, Vyklicky et al., 2018, Wells et al., 2018, XiangWei et al., 2018, Xu and Luo, 2018, Xu et al., 2018, Yuan et al., 2014). A lot of information is now present on the effects of mutant NMDAR subunits when overexpressed in isolation, however, very few studies have extended this research into more biologically relevant model systems: at synapses and in neurons. Only recently has the focus for GluN2 mutants been shifted into neurons, mainly using dissociated neuronal culture, although the characterisation has been mostly limited and uncomprehensive. Ogden et al. (2017) reported the reduced neuronal viability of GluN2A mutant P552R associated with epilepsy and the EPSP rise time of the equivalent mutant engineered in GluN2B (P553R), in order to investigate the role of this proline across the NMDAR subunits and found that the rise time was slower than WT. Marwick et al. (2015) studied cortical primary neurons in culture transfected with the epilepsy-associated N615K mutant in GluN2A where magnesium block and current density were reduced compared to WT GluN2A neurons. Marwick et al. (2017) found that the epilepsy-associated R586K mutant in GluN2A did not affect any property tested in oocytes or cultured neurons (magnesium block, current density and ifenprodil sensitivity) and concluded that it was unlikely to be pathogenic.

One group investigated the effects of West syndrome GluN2B GOF mutants N615I and V618G in hippocampal neuronal dissociated cultures in greater detail and found an intriguing result (Fedele et al., 2018). N615I and V618G were previously found to have abolished sensitivity to magnesium block (Lemke et al., 2014) and the same was found by Fedele et al. (2018) in HEK-293 cells. Magnesium ions were even found to permeate through the NMDAR pore with the V618G mutant. When overexpressed in neurons, magnesium was still capable of inhibiting the currents for both mutants, although to a lesser degree (~90% inhibition for WT GluN2B and ~70% inhibition for the mutants). In HEK-293 cells, magnesium had no effect on the glutamate activated currents of these receptors (Fedele et al., 2018), but in neurons the NMDAR response is mediated by both GluN2A and GluN2B NMDARs so there was still some inhibition by magnesium. Instead of overexpression, one recent study used molecular replacement to study GluN2 mutants in acute brain slices (Liu et al., 2017). The authors examined the effects of three CTD GluN2B ASD- and schizophrenia-associated mutants: S1415L, L1424F and S1452F. Although in *Xenopus* oocytes and HEK-293 cells, no differences to WT were found for any of the mutants for the range of properties investigated (agonist potencies, magnesium inhibition, proton sensitivity, current amplitudes, deactivation, rise time and charge transfer), in neurons, transfection with S1413L (rodent equivalent of human S1415L) only rescued currents to ~60% of WT. This reduction in current amplitude corresponded to the reduced surface expression of

this mutant found in dissociated rat hippocampal cultures in the same study. Despite the unaltered functional properties of the S1413L mutant NMDARs in heterologous expression systems, the incomplete rescue of synaptic currents emphasises the importance for study of both functional and expression/trafficking mechanisms that may be impaired by disease mutants and the value of assessing the effects of ion channel mutants in their native setting.

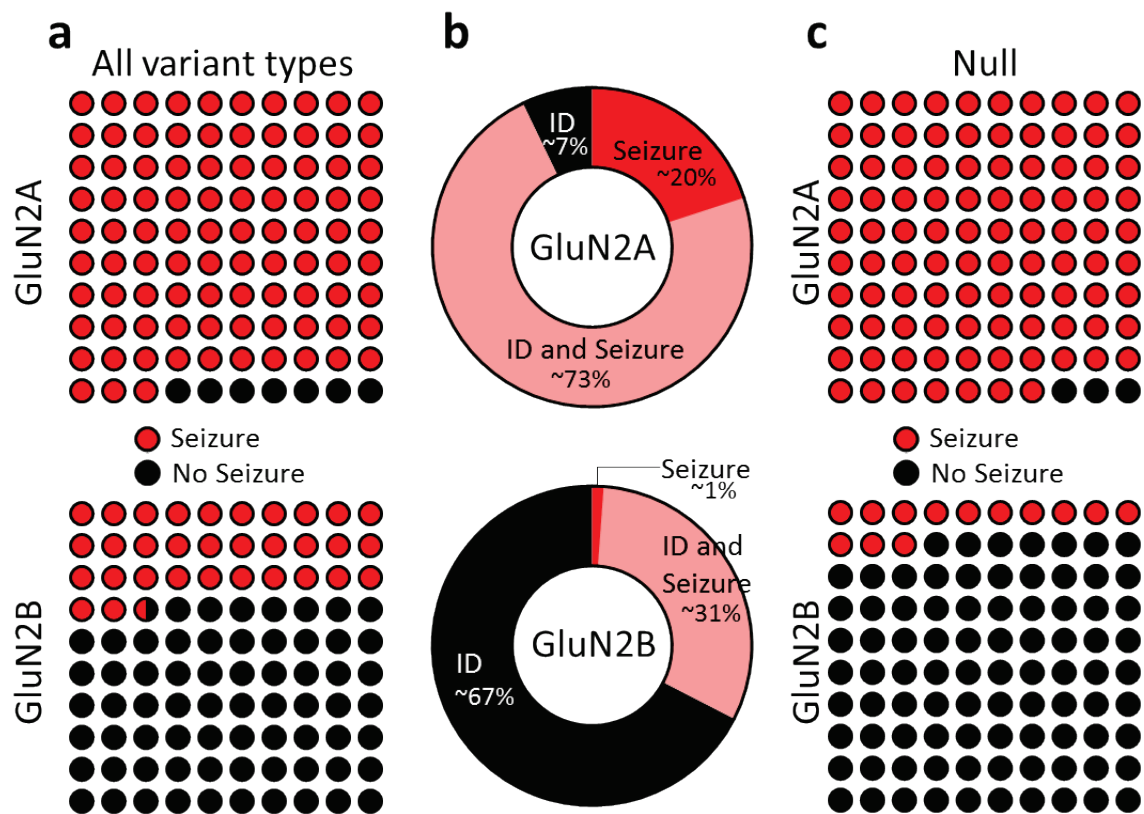


Figure 1.4: Phenotypes of GluN2A and GluN2B mutants

a) and b) All variant types include missense, frameshift, deletions, insertions, duplications, nonsense and splice-site mutations. c) Null mutations include frameshift, deletions, insertions or duplications that alter the open reading frame and nonsense. Data collected from an open-access online database: www.grin-database.de.

In summary, the research field has struggled to associate GluN2 mutation effects with clinical phenotypes. There may be a number of reasons for this: trafficking differences in heterologous cells compared to neurons, not accounting for the other GluN2 subunits that are typically expressed in neurons and the issue of overexpression. NMDAR functional effects of GOF or LOF GluN2 mutations measured in heterologous cells may be concealed by attenuated trafficking of receptors containing the mutant subunit. For example, mutants that show GOF effects or are

not different to WT with overexpression may in fact present as LOF if they do not actually incorporate into the synapse in neurons. Conversely, mutants which exhibit LOF effects on receptor function may appear similar to untransfected cells if their trafficking is enhanced in neurons.

Hypotheses and Aims

It is clear that there is a large gap in the literature and in our understanding of how human disease mutations in GluN2A and GluN2B contribute to disease phenotypes. Although there has been extensive characterisation of mutant NMDAR subunits, investigation into the synaptic consequences and the overall impact on signalling in neurons has so far been minimal. It also remains unclear why such diverse functional alterations to NMDAR activity in GluN2A can converge to produce a common underlying disease phenotype and why for GluN2B, different clinical phenotypes may present depending on the GOF/LOF distinction.

The work of Gray et al. (2011) showed KO of GluN2A led to a higher charge transfer, slower decay kinetics and increased mEPSC amplitude. Based on this, the link between LOF mutants which either prevent GluN2A expression or cause it to be non-functional and elevated neuronal activity that is found in seizure disorders is conceivable. They also observed reduced peak amplitudes and charge transfer and faster NMDAR-EPSCs with GluN2B KO, as would be expected from LOF mutants (Gray et al., 2011). This would produce a diverging consequence for synaptic transmission than GluN2B GOF mutants which expectedly enhance NMDAR activity. Hence, loss of GluN2A, but not GluN2B subunits can lead to greater NMDAR and AMPAR-mediated transmission which is consistent with the genotype-phenotype relationships across patients with *GRIN2* mutations.

Based on these KO experiments which, to some extent model LOF GluN2 mutants, the following hypotheses are made:

Hypothesis 1: Both GluN2A GOF and LOF mutations will prolong the duration of the NMDAR component of synaptic transmission. The mechanisms for GOF and LOF GluN2A mutants in producing this common synaptic phenotype are expected to differ.

Hypothesis 2: GluN2B GOF and LOF mutations will have opposing effects on the duration of NMDAR-mediated synaptic currents in neurons owing to the diverse disease phenotypes they are associated with and each phenotype results from distinct mechanisms.

To address these hypotheses, this thesis aims to:

Aim 1: Replicate the findings by Gray et al. (2011), with respect to the effects of GluN2A and GluN2B KO on NMDAR mediated EPSCs, using organotypic hippocampal slices from *Grin2A*- or *Grin2B*-flox mice (Chapter 2).

The majority of disease-associated GluN2 mutations are deletions, frameshift, premature stop codons or splice site mutations (Burnashev and Szepietowski, 2015, Hu et al., 2016, Strehlow et al., 2019). These will likely have consequences on GluN2 expression that resemble null alleles. As a first approximation, one can model these by genetically knocking-out expression of GluN2 alleles. This will allow investigation of how NMDAR synaptic currents change upon GluN2 allele deletion.

- Does GluN2 KO, which models the effects of LOF GluN2 mutations, produce enhanced NMDAR activity with GluN2A and reduced NMDAR activity with GluN2B?

Patients with NMDAR-related disorders only carry a single mutated allele of the NMDAR subunit genes. To what extent is there haploinsufficiency at the level of synaptic transmission?

- How does a homozygous deletion differ to a heterozygous deletion, considering that human disease mutations in GluN2A and GluN2B are all heterozygous?

Aim 2: Investigate the synaptic phenotypes of selected human disease mutations in CA1 pyramidal neurons of organotypic hippocampal slices (Chapter 3).

A significant fraction of disease-linked mutations in NMDAR subunits exchange an amino acid with another (i.e. missense mutation) with different physicochemical properties. Many of these mutations are de novo and evidence for them being disease causing is limited.

Furthermore, the consequences of missense mutations can vary substantially, leading to no effect or loss or gain of protein function. What impact do missense mutations, with severe and contrasting effects on NMDARs, have on synaptic NMDAR currents? What is the impact of the altered NMDAR signalling on the regulation of synaptic efficacy?

- Can a mouse KO of GluN2A or GluN2B be rescued by the human WT subunits in order to investigate the impacts of *human* disease mutants on synaptic transmission?
- Select missense mutations that are predicted to have a significant impact on the functioning or expression of NMDARs using bioinformatics tools and the current literature on GluN2 disease mutants.

- Investigate the impacts on NMDAR- and AMPAR-EPSCs, when mutants are transfected into CA1 neurons, using dual whole-cell patch clamp recordings of a transfected neuron and an adjacent control untransfected neuron to assess the synaptic phenotypes produced by GluN2A and GluN2B mutants.

Aim 3: Investigate the mechanisms by which the observed synaptic phenotypes (in aim 2 – Chapter 3) are produced by GOF/LOF GluN2A and GluN2B mutants (Chapter 4).

There are numerous possibilities by which NMDAR subunits could be affected by missense mutations. LOF mutations could lower NMDAR protein expression, stability or the ability to fold and assemble into functional receptors. Some LOF mutants may assemble well but may fail to be delivered to the neuronal surface or synapse. Alternatively, mutant NMDARs may be delivered to synapses but may fail to respond normally during synaptic transmission, either having GOF or LOF. What are the consequences of NMDAR mutations on the delivery of NMDARs to synapse and what is their effective functional incorporation? How do these relate to the synaptic phenotypes observed in addressing aim 2?

- Study the expression and trafficking of GluN2 GOF and LOF mutants to differentiate between synaptic phenotypes caused by changes to receptor function or changes in receptor expression/trafficking.
 - Use pharmacological tools to assess the relative expression levels of GOF and LOF mutants at the synapse and their relative contribution to synaptic currents in slices.
 - Express mutant GluN2 subunits in GluN2A-GluN2B double floxed mice to observe the extent of functional rescue of current by mutant subunits.
 - Investigate receptor trafficking in dissociated hippocampal cultures using the ability of different GluN2 subunits to take fluorescent GluN1 subunits to the synapse

The overall aim of this thesis is to better understand the effects of human disease mutants in neurons on synaptic signalling.

Chapter 2 Dual or single allele deletion of GluN2A or GluN2B subunits perturbs the NMDAR component of synaptic transmission.

Abstract

The NMDAR subunits GluN2A and GluN2B are widely expressed in the adult hippocampus and forebrain and their dysfunction is linked to various neurological diseases. Mouse KOs have been used as models for human disease mutations in the respective genes: *GRIN2A* and *GRIN2B*. The majority of the mutations characterized thus far are associated with a loss of NMDAR subunit expression, for example through impaired gene expression or aberrant protein folding, stability or trafficking. With the growing discovery and characterization of GluN2 disease mutations, it is becoming apparent that LOF mutants of *GRIN2A* and *GRIN2B* are associated with different brain disorders. With the main role of NMDARs played at excitatory synapses, the effect of reduced GluN2A and GluN2B subunit expression on synaptic transmission could provide important insight into the pathogenesis of these disorders. This chapter investigates properties of NMDAR-EPSCs after homozygous or heterozygous deletion of GluN2 subunits from neurons within CA1 of the hippocampus. Findings initially described by others in the homozygous GluN2 KO using acute slices were largely reproduced here after postnatal GluN2 deletion in the more experimentally tractable organotypic hippocampal slice. Consistent with earlier reports, smaller and faster decaying NMDAR currents were observed in GluN2B KO neurons. In the GluN2A KO, NMDAR current decays were more prolonged, but the NMDAR charge transfer was not enhanced since the amplitudes of the currents were smaller. The heterozygous KOs showed an intermediate effect to the homozygous KOs, indicating that GluN2 mutants would still produce an observable dysfunctional synaptic phenotype. In summary, the results of this chapter reveal: 1) The power of using single-cell transfection in organotypic slices for the control of gene expression; 2) The major contributions of both GluN2A and GluN2B subunits to the NMDAR-component of synaptic transmission at Schaffer collateral synapses in organotypic hippocampal slices; and that 3) Haploinsufficiency is evident from the properties of NMDAR-mediated synaptic currents following deletion of a single allele of both GluN2A and GluN2B. Therefore, synaptic disruption resulting from GluN2 mutations, which are all heterozygous, cannot be compensated for by the remaining WT allele and is likely to contribute to disease pathology.

Introduction

The majority of disease-linked mutations found in the NMDAR subunits have demonstrated or predicted LOF (Burnashev and Szepietowski, 2015, Hu et al., 2016, Strehlow et al., 2019). LOF mutations by definition reduce the capability of a protein to perform its normal function. More than half of the mutations identified in *GRIN2A* and *GRIN2B* are putative protein-truncating mutations, either due to microdeletions, nonsense mutations that lead to incorporation of a premature stop codon, mutants that disrupt splicing, or insertion/deletion (indels) that cause a shift in the open reading frame (Kenny et al., 2014, MacArthur et al., 2012). The remaining (missense) mutations reflect substitutions of amino acids in the coding sequence. The majority of the *GRIN2A* and *GRIN2B* missense mutants characterized thus far exhibit some LOF either through attenuating NMDAR function directly or impairing expression or trafficking (Addis et al., 2017, Endeley et al., 2010, Lemke et al., 2013, Lemke et al., 2014, Lesca et al., 2013, Serraz et al., 2016, Swanger et al., 2016, Yuan et al., 2014). In summary, a large majority of NMDAR mutations appear to result in LOF.

Patients with putative LOF mutations in human *GRIN2B* most often present with intellectual disability (<80 %) and their clinical features resemble some of the phenotypes observed in germline *Grin2b* KO mouse models, including a range of learning impairments (Sakimura et al., 1995, Wang et al., 2011) and memory deficits (Brigman et al., 2010). Spatial working memory and recognition memory impairments were also observed in mice with conditional KO of GluN2B from excitatory neurons in the forebrain (von Engelhardt et al., 2008). Examination of the synaptic currents in CA1 of these mice revealed that synapses had 50% smaller NMDAR/AMPA ratios and NMDAR currents that decayed more than 2-fold faster. Qualitatively similar results were obtained by Gray et al. (2011) using sparse transfection of Cre recombinase in floxed *Grin2b* mice (*Grin2b^{fl/fl}*) to KO expression of GluN2B in individual CA1 pyramidal neurons. The critical role of NMDARs in the induction of synaptic plasticity has prompted researchers to examine synaptic plasticity following conditional *Grin2b* KO (Akashi et al., 2009, Brigman et al., 2010, von Engelhardt et al., 2008), *Grin2b* knockdown by RNA interference (Clayton et al., 2002) or overexpression of GluN2B (Cao et al., 2007, Cui et al., 2011, Tang et al., 1999, Wang et al., 2009). Together with clinical phenotype data of patients with putative LOF mutations in *GRIN2B*, these findings indicate a positive correlation between GluN2B expression level, LTP and learning and imply that attenuated GluN2B expression is sufficient to cause intellectual disability.

While intellectual disability is also found in about two-thirds of patients with mutations in *GRIN2A*, the most common clinical features in about 90% of patients are epilepsy and language

disorders (www.grin-database.de). In fact, GRIN2A mutations currently represent the best-known genetic cause of Epilepsy-Aphasia Spectrum (EAS). Various phenotypes in *Grin2a* KO mice support the causative role of GluN2A in EAS. Similar to the patients, GluN2A KO mice exhibit epileptiform activity in EEG recordings, including spontaneous spike-wave discharges during slow-wave sleep (Salmi et al., 2019). Further comparisons can be made between the frequently observed language impairments in patients and the abnormal vocalizations in *Grin2a* KO mice (Salmi et al., 2018, Salmi et al., 2019), or the patient's intellectual disability and poor performance of the mice in hippocampal-dependent learning tasks (Kiyama et al., 1998, Sakimura et al., 1995). The GluN2A KO mice also have abnormalities at the level of excitatory synaptic transmission. GluN2A KO is associated with more than a 50% reduction in NMDAR/AMPA ratios (Sakimura et al., 1995) but single-cell deletion of *Grin2A* resulted in similar size NMDAR currents but enhanced NMDAR-EPSC charge transfer due to currents persisting for much longer (Gray et al., 2011). This characteristic slow decay time was proposed to result from activation of the remaining NMDARs which are composed of mainly GluN2B and provides a mechanism by which a loss of GluN2A could lead to enhanced NMDAR-mediated synaptic conductance (Gray et al., 2011). The smaller NMDAR/AMPA ratios may actually reflect a larger AMPAR-mediated synaptic conductance since GluN2A subunit deletion was associated with increased strength of unitary synaptic connections (Gray et al., 2011).

An important distinction to make is that patients with mutations in *GRIN2* subunits are exclusively heterozygotes and the disorder is transmitted with autosomal dominant inheritance. Yet almost all data using KO mouse models has come from those with a homozygote genotype. This chapter sets out to confirm key observations made for NMDAR-EPSCs in homozygotes and test the hypothesis that heterozygotes exhibit haploinsufficiency. The experimental approach used single-cell conditional KO of *Grin2A* and *Grin2B* in CA1 pyramidal neurons of organotypic mouse hippocampal slices.

Overall, the findings are as follows: 1) The effects of a GluN2B KO in CA1 pyramidal neurons in organotypic slices are consistent with those seen in acute slices where NMDAR-EPSCs are smaller and faster decaying than WT; 2) GluN2A KO exhibited prolonged decay of NMDAR-EPSCs but peak amplitudes of GluN2A KO were reduced and this observation was reproducible even after extended periods of expression and across slices obtained from either brain hemispheres; 3) The effects observed were intermediate in the heterozygous KOs, thus demonstrating haploinsufficiency.

Methods

Animals

WT mice used were C57Bl/6J and were purchased from Charles River Laboratories (UK). Heterozygous *Grin2A*-flox (*Grin2A*^{WT/fj}) and *Grin2B*-flox (*Grin2B*^{WT/fj}) mice were a gift from Kenji Sakimura (Niigata University, Japan). Generation of these mice is described by Akashi et al. (2009) and Gray et al. (2011). Homozygous *Grin2A*-flox (*Grin2A*^{fj/fj}) and *Grin2B*-flox (*Grin2B*^{fj/fj}) mice were generated by mating the respective heterozygous mice. The colonies were maintained as homozygous lines taking care to avoid brother-sister matings. Ear clip biopsies obtained for identification and genotyping were incubated in lysis buffer (100 mM NaCl, 10 mM Tris-HCl (pH 8), 0.3 mg/ml Proteinase K) and shaken (1100 rpm) at 55°C until the tissue was digested (typically 1 hour). Following this, proteinase K in the sample was heat-inactivated by a 10 minute incubation at 95°C and insoluble tissue was pelleted by centrifuging the samples at 13,000 rpm for 5 minutes. Genotyping with 3 µL supernatant was achieved by polymerase chain reaction (PCR) in a 25 µL volume using KOD XL DNA polymerase (0.05 U/µL final concentration) with buffer for KOD XL DNA polymerase (Merck KGaA, Germany), 0.2 mM dNTPs and 0.2 µM of each primer. Primers used for *Grin2A*-flox genotyping were: 5'-GAAATGTGGTAAAATCCAGTTAG-3' (forward), and 5'-TAGGCAGTAAACTTTCCTCATC-3' (reverse). Primers used for *Grin2B*-flox genotyping were: 5'-CCCCACTGTCTATAAAAATAGAGG-3' (forward) and 5'-GCCACATAAGTTGGTCTCTT-3' (reverse). Genotyping PCRs were run on a ProFlex PCR system (Thermofisher Scientific, UK) with ramp rate adjusted to 3°C/s. The PCR cycle conditions are shown in table 2.1. Reaction products were run on 1% agarose gels stained with ethidium bromide. Product sizes for *Grin2a*-flox genotyping were 800 bp for the WT allele and 1100 bp for the *Grin2a*-flox allele. Product sizes for *Grin2b*-flox genotyping were 900 bp for the WT allele and 600 bp for the *Grin2b*-flox allele.

Hippocampal slice culture preparation

The hippocampi were dissected from *Grin2A*- and *Grin2B*-floxed mice at postnatal age 6-8 days in cold sterile filtered dissection medium composed of (in mM): CaCl₂ (0.5), KCl (2.5), KH₂PO₄ (0.66), MgCl₂ (2), MgSO₄ (0.28), NaCl (50), Na₂HPO₄ (0.85), glucose (25), NaHCO₃ (2.7), sucrose (175) and HEPES (2) (pH 7.3, 330 mOsm). Hippocampi were sliced into 350 µm transverse sections using a McIlwain tissue chopper (Abbotsbury Engineering Ltd., UK), placed on quartered membranes (FHLCO1300, Millipore, UK) in Millicell cell culture inserts (PICM03050, Millipore, UK) and cultured in 6-well plates (fig. 2.1) (0030720113, Eppendorf). Slices were taken from all along the rostral-caudal axis. The culture medium (1 ml per well) was composed of Minimum

Essential Medium (MEM) supplemented with 15% heat-inactivated horse serum (26050-088, Gibco), B27 supplement (17504044, Gibco), 25 mM HEPES, 3 mM L-glutamine, 1 mM CaCl₂, 1 mM MgSO₄, 0.25 mM ascorbic acid and 5 g/L glucose. Slice culture plates were kept in an incubator at 34°C with 5% CO₂ and 95% humidity. The culture medium was changed twice a week, with pre-warmed slice culture medium supplemented with 10 µg/ml gentamicin.

Table 2.1: PCR protocols for genotyping *Grin2A-flox* and *Grin2B-flox* mice.

			<i>Grin2A</i>	<i>Grin2B</i>
Initial Denaturation			98 °C – 10 s	94 °C – 10 m
3 CYCLES	Denaturation		98 °C – 15 s	
	Annealing		64 °C – 2 s	
	Extension		74 °C – 2 m	
5 CYCLES	Denaturation		98 °C – 15 s	
	Annealing		60 °C – 2 s	
	Extension		74 °C – 2 m	
27 CYCLES	Denaturation		98 °C – 15 s	
	Annealing		56 °C – 2 s	
	Extension		74 °C – 2 m	
35 CYCLES	Denaturation			94 °C – 30 s
	Annealing			47 °C – 5 s
	Extension			74 °C – 4 m
Final extension				74 °C – 10 m
Hold			4 °C – ∞	4 °C – ∞

Single-cell electroporation

At 6-8 days *in vitro* (DIV) CA1 pyramidal neurons in organotypic slices were transfected with 3 ng/µL pLenti CMV Cre-eGFP plasmid (gift from Christophe Mulle, IINs, Bordeaux, France) by single-cell electroporation (SCE; fig. 2.1). pLenti CMV Cre-eGFP plasmid DNA was transformed into chemically competent *E. Coli* (NEB Stable competent *E. Coli*, NEB Inc, UK) and prepared from

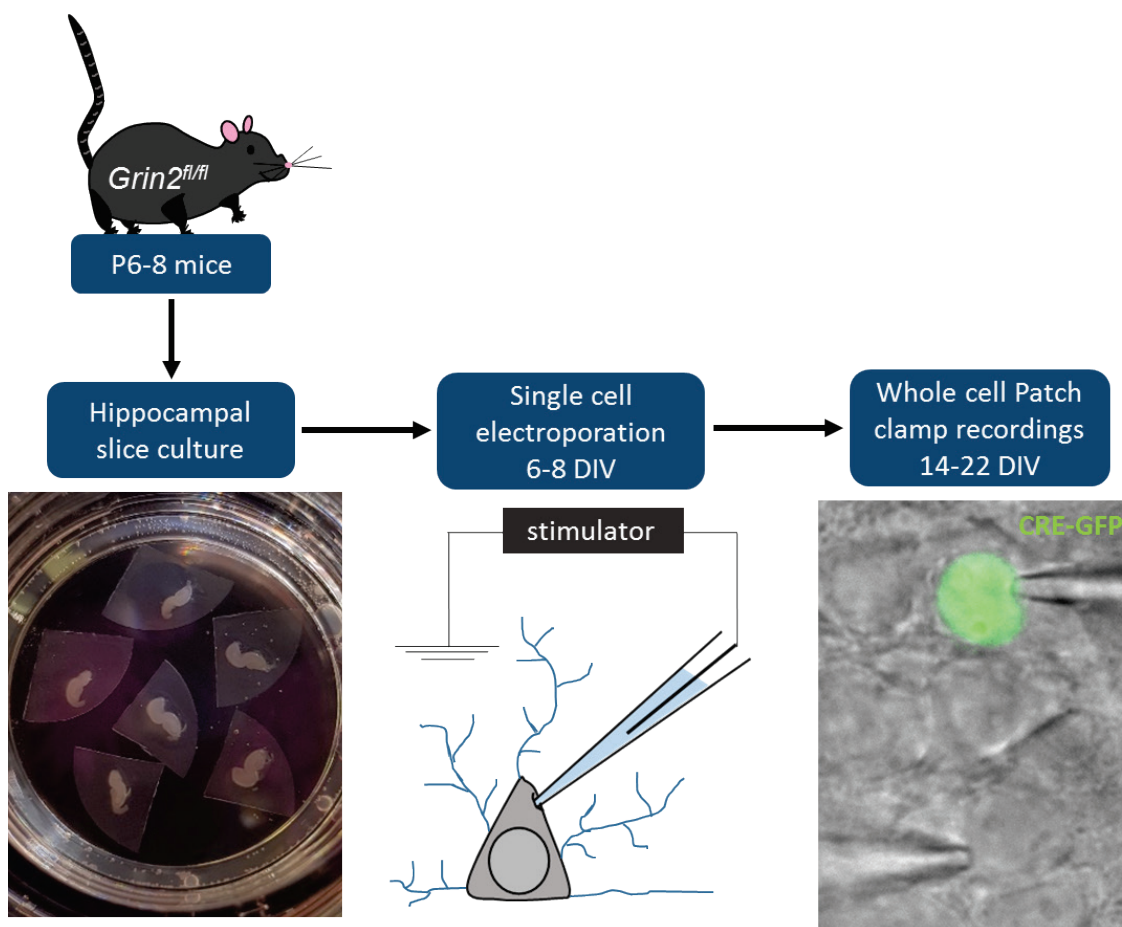


Figure 2.1: Experimental procedure.

*The hippocampus is dissected out from P6-8 floxed mice and sliced into 350 μm sections. Slices are cultured at 34°C with 5% CO_2 for 6-8 days, after which, CA1 pyramidal neurons are electroporated with pLenti CMV Cre-eGFP to KO the floxed *GluN2* gene. The slices are then maintained in culture till the day of recording. NMDAR-EPSCs are recorded by dual whole cell patch clamp of a transfected neuron and a neighbouring untransfected neuron.*

bacterial cultures using EZNA Endo-free Plasmid Maxi kit (VWR International, UK). Plasmid DNA was precipitated upon addition of 0.5 volume of PEG solution (30% PEG 8000 (w/v) in 30 mM MgCl_2 to isolate it from residual lipopolysaccharide endotoxin. The DNA precipitate was pelleted by centrifugation at 10,000 rcf for 15 minutes, washed with 70% ethanol and the air-dried pellet was redissolved in TE buffer (10 mM Tris-HCl, 1 mM EDTA). This protocol for plasmid preparation was followed for all plasmid DNA constructs used for experiments in this thesis. Within a week of transfection, plasmid DNA was diluted to 0.53 nM (3 ng/ μL) in intracellular solution containing (in mM): $\text{CH}_3\text{SO}_3\text{H}$ acid (135), KOH (135), NaCl (4), MgCl_2 (2), HEPES (10), Na-ATP (2), Na-GTP (0.3), spermine dihydrate (0.15), EGTA (0.06) and CaCl_2 (0.01) (pH 7.25, 285 mOsm). DNA-containing intracellular solution was centrifuged at >10,000 rcf for 15 minutes at 4°C to pellet

debris before using it to fill patch pipettes (8-10 M Ω), which were pulled with a Flaming/Brown Micropipette puller from thick-walled borosilicate glass capillaries (GB150F-8P, Science Products).

Slices were then transferred to the recording chamber on an upright microscope (BX51, Olympus) containing room temperature HEPES-buffered aCSF solution composed of (in mM): NaCl (140), KCl (3), MgCl₂ (1), CaCl₂ (2), glucose (10), Na-pyruvate (1), NaHCO₃ (2), HEPES (6), Na-HEPES (4) (pH 7.35, 300 mOsm). The patch pipette was positioned in the slice under visual guidance using a mechanical manipulator (PatchStar, Scientifica). CA1 pyramidal cells were approached with positive pressure (20 mbar). Upon dimple formation, the pressure was released to form a loose-patch seal. Immediately, a 12 V stimulus train was applied (100–200 Hz for 0.25–0.5 s; pulse-width 0.25–0.5 ms) from a stimulus isolator (IsoFlex, A.M.P.I.) triggered by ACQ4 (Campagnola et al., 2014) through a USB-X Series Multifunctional DAQ interface (National Instruments). Ten CA1 pyramidal neuron transfections were attempted in each slice. Average success rate of transfections was 50%.

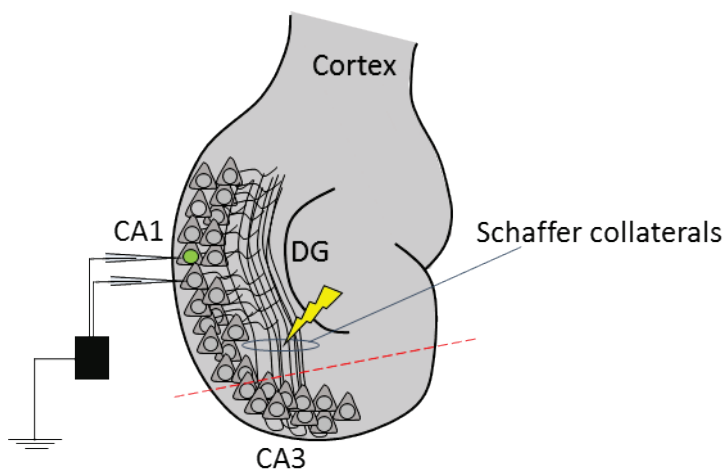


Figure 2.2: Schematic of the recording and stimulation sites in the hippocampal slice cultures.

The pre-synaptic CA3 axons – the Schaffer collaterals – were stimulated with a stimulation electrode to elicit the post-synaptic response in CA1 neurons which were patched in whole-cell mode. The CA3 cell body layer was cut prior to recording to prevent re-current excitation (red dashed line) (Dumas et al., 2018).

Slice preparation and recording solutions

The electrophysiology method utilized was whole-cell voltage clamp using patch clamp. The CA3 cell body layer of the hippocampal slice was cut off using a blade (fig. 2.2) and the slice was

placed into the chamber under a SliceScope Pro 2000 upright microscope (Scientifica). The tissue was held down with a slice anchor and perfused with artificial cerebrospinal fluid (ACSF) solution containing (in mM): NaCl (125), KCl (2.5), NaHCO₃ (25), glucose (10), Na-pyruvate (1), MgCl₂ (1) and CaCl₂ (2). To isolate NMDAR current, the ACSF included 50 μ M picrotoxin (ab120315, Abcam) and 10 μ M gabazine (SR95531, Abcam) to block gamma-amino-butyric acid receptors (GABARs) and 10 μ M NBQX (1044, Tocris Biosciences) to block AMPARs. 5 μ M 2-chloroadenosine (ab120037, Abcam) was also added to prevent seizure activity. The ACSF was bubbled with carbogen (95% oxygen, 5% carbon dioxide) and maintained at 30°C with an in-line heater and heated chamber. A stimulation electrode was placed to stimulate the Schaffer collateral pathway (fig. 2.2). 2-4 M Ω patch pipettes for whole-cell patch clamp recordings were filled with intracellular solution composed of (in mM): CH₃SO₃H (120), CsOH (120), CsCl (20), MgCl₂ (2.5), HEPES (10), Na-ATP (4), Na-GTP (0.4), phosphocreatine disodium salt (5) and EGTA (0.2) (pH 7.25) and coated with Sigmacote (Sigma-Aldrich, SL2). Osmolarity of intracellular and extracellular solutions was checked and adjusted on the day of each experiment (NaCl or water was added to the ACSF and CsCl or water was added to the ICS).

Electrophysiological recordings

Two CA1 neurons were patched simultaneously – one transfected (fluorescence of Cre-GFP seen under blue light (475 nm) and one neighbouring untransfected neuron (fig. 2.1). The procedure for patching was as follows: upon formation of a gigaseal, the fast and slow pipette capacitances were compensated using MultiClamp Commander software controlling a Multiclamp 700B (Molecular Devices, LCC). The cell was broken into using light suction and the ‘zap’ feature (a +1V pulse which aids breaking into whole-cell mode).

Once two cells were successfully patched in whole-cell mode and the access resistance and holding current were stable, the membrane potential was raised from -75 mV to +20 mV at a rate of 0.5 mV per second. Once held at +20 mV, a stimulation of a 20-40 V pulse was applied at the Schaffer collaterals for 50 μ s, where the intensity and polarity were adjusted to obtain reliable NMDAR EPSCs <200 pA in untransfected neurons. Recorded signals were low-pass filtered (4 kHz, 4-pole Bessel) and digitized (25 kHz) directly to hard disk. The stimulation was repeated 30 times with a 10 s cycle time.

Statistical Analysis

Recordings were discarded if the access resistance between two cells differed considerably (5-8 M Ω). Stimfit 0.13 (Guzman et al., 2014) was used to obtain an average of the 30 traces recorded at +20 mV and weighted decay time constant tau (τ_w), peak amplitude and charge transfer values

were obtained from the averaged trace using a custom python module available at <https://github.com/acp29/penn/blob/master/analysis.py>. For τ_w , the non-linear exponential (with offset) fitting problems were solved initially by the Chebyshev algorithm and the fit values were used as starting values for iterative least-squares minimization by the Levenberg-Marquardt algorithm. The fit began from the peak of the current and ended 900 ms after the stimulus artefact for NMDAR-EPSCs. For AMPAR-EPSCs, the fit ended 100 ms after the stimulus artefact. If the fit failed, (this usually occurred when the decay could be fit well with a single exponential with offset) the time constant for a single exponential was used. Amplitudes from the pre-stimulus baseline were measured to the average of the peak \pm 5 sample points. Charge transfer was measured by trapezoidal numerical integration.

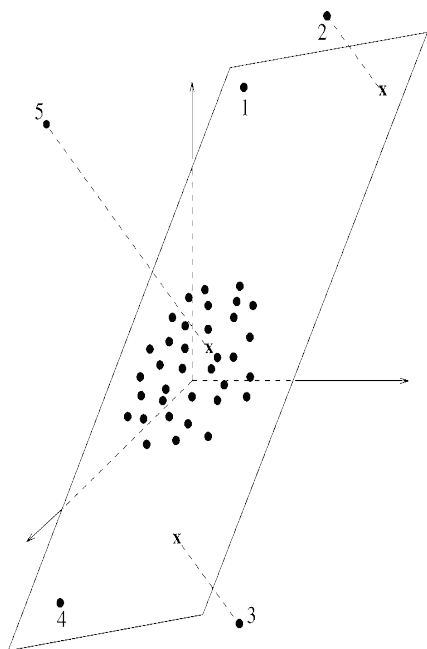


Figure 2.3: ROBPCA method for detection of outliers.

Figure taken from Hubert et al. (2005). Hubert et al. describe four types of data observations:

a) Regular observations that cluster together and form a homogenous group that are close to the PCA space (rectangle). b) Good leverage points that do not lie within the regular observations, but are on the same plane (eg. 1 and 4). c) Orthogonal outliers which have a large orthogonal distance from the PCA space but project outwards from the regular observations (eg. 5). d) Bad leverage points which both do not lie within the regular observations and have a large orthogonal distance (eg. 2 and 3). c and d are considered outliers. b are not considered outliers as they follow the pattern of the majority of the data (Alguraibawi et al., 2015).

Outliers

Outliers were identified using the robust principle component analysis (ROBPCA) developed by Hubert et al. (2005). This outlier detection method was utilised because it is a multivariate approach which is advantageous over univariate outlier detection because instead of discarding outlying values from a cell for each parameter measured, e.g., peak amplitude, decay, charge, etc., it instead highlights individual cells that have outlying responses over the range of parameters measured. Outliers highly influence the values of the principle components (PCs) in a regular PCA. ROBPCA excludes outliers to produce PCs that are representative of the trend of the majority of the data with lower influence from extreme values. The output of ROBPCA

includes an outlier map which is a plot of score distance and orthogonal distance to identify irregular observations. Values with a high orthogonal distance (orthogonal outliers) and values with both high orthogonal and score distances (bad leverage points) are considered outliers (fig. 2.3).

To perform the ROBPCA analyses for KO experiments the variables included were: whole-cell properties (WCP), NMDAR peak amplitude, decay, charge and 20-80% rise times. WCPs were obtained for each cell at +20 mV in Stimfit 0.13. The WCPs included series resistance (Mohm), cell capacitance (pF), input resistance (Mohm), and specific membrane resistance (kohm.cm^2) - see <https://github.com/acp29/penn/blob/master/analysis.py>. Relative values (the log ratio of transfected/untransfected) were calculated for all features and absolute values (log average (transfected + untransfected)) were also calculated for all features except for peak amplitudes and charge as absolute values of these depend on the stimulation intensity, which is manipulated by the experimenter. There were 14 relative and absolute values for KO data. Multivariate outlier detection was applied because pairs of neurons were used for comparing multiple AMPAR and NMDAR features; instead of univariate outlier detection for each feature, outlying responses across the range of features examined were identified. The ROBPCA was applied in MATLAB 9.2. The number of PCs used was the number that explained 90% of the variance. The output produced a plot which shows the outlier values. These values were excluded from the dataset for further statistical analyses.

Statistical testing and data presentation

Following multivariate outlier removal, each NMDAR-EPSC variable (peak, tau, charge) was compared between matched transfected and untransfected cells by univariate multilevel modelling (MLM) in MATLAB 9.2 using the general linear modelling function 'anovan'. Analyses were performed on log-transformed data. The model built resembled a paired t-test with nesting included to account for the hierarchical data structure: Groups of matched cell recordings (i.e. cell pairs) were nested in slices, slices were nested in hemisphere or animal. Fixed-effect factors were condition (transfected or untransfected) and hemisphere (left or right). Random-effect factors were pair, slice and animal. Paired responses were tested for an interaction for hemisphere, but this was not significant (interactions were considered significant at a level of 0.1 because the power is lower for evaluating interactions as the central focus is assessing the impact of main effects (Marshall, 2007)). The sum-of-squares type (sstype) used was type III as nesting was used, taking into account interactions between main effects. p values were adjusted for multiple comparisons with MATLAB 9.2 using 'multicomp' Holm-Bonferroni

method (<https://uk.mathworks.com/matlabcentral/fileexchange/61659-multicomp>). p values of all three variables (peak, decay, and charge) were adjusted for each condition separately. Information was not available for the allocation of slices to animals in one recording set (Cre-GFP in WT slices), in which case only nesting in slices was considered. All error bars shown are standard error of the mean (SEM) unless stated otherwise. For paired or matched data, within-subjects standard error bars were calculated (Cousineau, 2005).

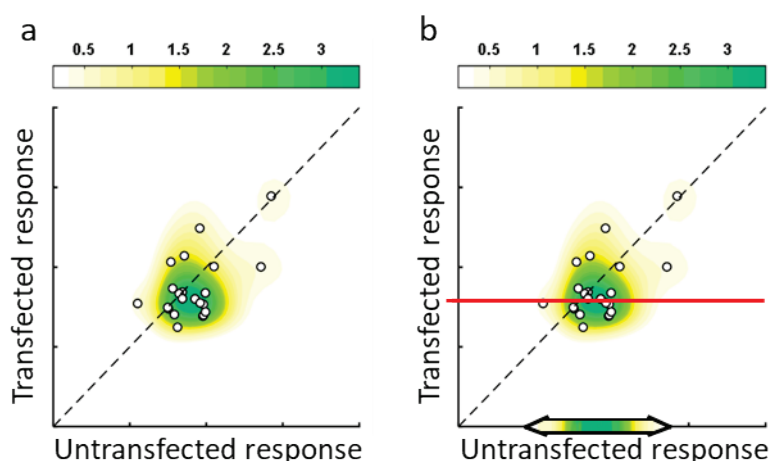


Figure 2.4: Kernel density plots

a) example kernel density plot with sample data from untransfected neurons and neurons transfected with Cre-GFP from WT mice (fig 2.5). b) The distribution of untransfected values (two headed arrow) for a given transfected value (red line) using a kernel density estimate. Darker colours indicate higher probability.

A paired t-test in GraphPad Prism 7 was used for the before and after AP5 experiment. One-way ANOVA was performed to compare different time points of GluN2A KO also using GraphPad Prism 7. One-way MANOVA was performed in SPSS for the multiple NMDAR-EPSC properties (charge, amplitude, decay time constant) between hippocampi from left and right brain hemispheres. The reported Wilk's Λ is an indication of the variance in the NMDAR properties that are not explained by the independent variable (hemisphere). Values closer to zero would indicate that the variance is due to the independent variable. The partial η^2 is a measure of effect size for differences between the hemispheres. $p < 0.05$ was considered to be significant. All statistical tests were two tailed and $p < 0.05$ was considered to be significant.

In this thesis, some of the data is presented as a scatter plot with a kernel density plot overlay (eg. fig. 2.4). These figures show the individual data points (white circles) of the responses from the transfected neurons plotted against the responses of untransfected neurons. The dashed line represents the line of unity, which reflects no difference between the responses of

transfected and untransfected neurons. As the response differs more between transfected and untransfected cells, the data points become further from the line of unity. The data points are overlaid with a 2-D kernel density estimate (fig. 2.4), which estimates the probability density function (PDF) for the bivariate data sample. The probability is colour coded low-to-high as light-to-dark colours. These plots were generated in MATLAB 9.2 using the `kde2d` function (Botev et al., 2010).

Results

Single-cell conditional KOs were utilised to investigate the cell autonomous effects of manipulating GluN2 subunit expression while avoiding the problems with viability of germline GluN2B knockout mice. The conditional KO system used was the Cre-Lox system, which relies on the Cre recombinase enzyme to detect and bind to specific DNA sequences known as LoxP sites. LoxP sites are 34 bp sequences which flank the gene(s) of interest, *Grin2A* and/or *Grin2B*, and are joined together through a recombination reaction by Cre recombinases to KO the gene (Nagy, 2000). The *Grin2B*-flox mice used for the experiments in this thesis contained LoxP sites that flanked exon 14 of *Grin2B* which encodes the M4 TMD. GluN2B subunits that lack the M4 segment are non-functional (Akashi et al., 2009) and in the presence of Cre, Akashi et al. (2009) showed no detectable GluN2B expression by immunohistochemistry and immunoblots. For *Grin2A*-flox, LoxP sites flanked exon 10 of the *Grin2A* gene that encodes TMD segments M2 and M3 (Gray et al., 2011). The result of recombination at the two LoxP sites was a frameshift mutation in *Grin2A* that resulted in a non-functional protein that was degraded, leading to loss of the GluN2A subunit. Crossing of these two floxed mice resulted in completely abolished NMDAR-mediated currents, suggesting that all GluN2A and GluN2B subunits are lost by the implementation of the Cre-Lox system (Gray et al., 2011).

For the application of the Cre-Lox system in this thesis, organotypic hippocampal slices were prepared from homozygous *Grin2A*- or *Grin2B*-floxed mice and individual CA1 pyramidal neurons were transfected with Cre-GFP by single-cell electroporation after 6-8 DIV (fig. 2.1). After 14-22 days of culture (8-14 days after transfection), Cre-containing CA1 neurons (identified with the green fluorescence emission of GFP upon excitation with blue light) were patched in whole-cell configuration, along with a neighbouring control untransfected neuron (fig. 2.1).

The Cre-Lox system has been known to result in off-target effects and even toxicity in some tissues (Heffner et al., 2012). To confirm that Cre recombinase does not modify NMDAR-mediated EPSCs by means not attributable to the specific KO of the targeted floxed gene, Cre-recombinase was first transfected into CA1 neurons of slices prepared from WT mice on the same background (C57Bl/6J) as the *Grin2* floxed lines. Between one and two weeks after transfection, electrophysiological recordings were performed. Figure 2.2 shows a schematic of the hippocampal slice with the location of recording electrodes and stimulation site.

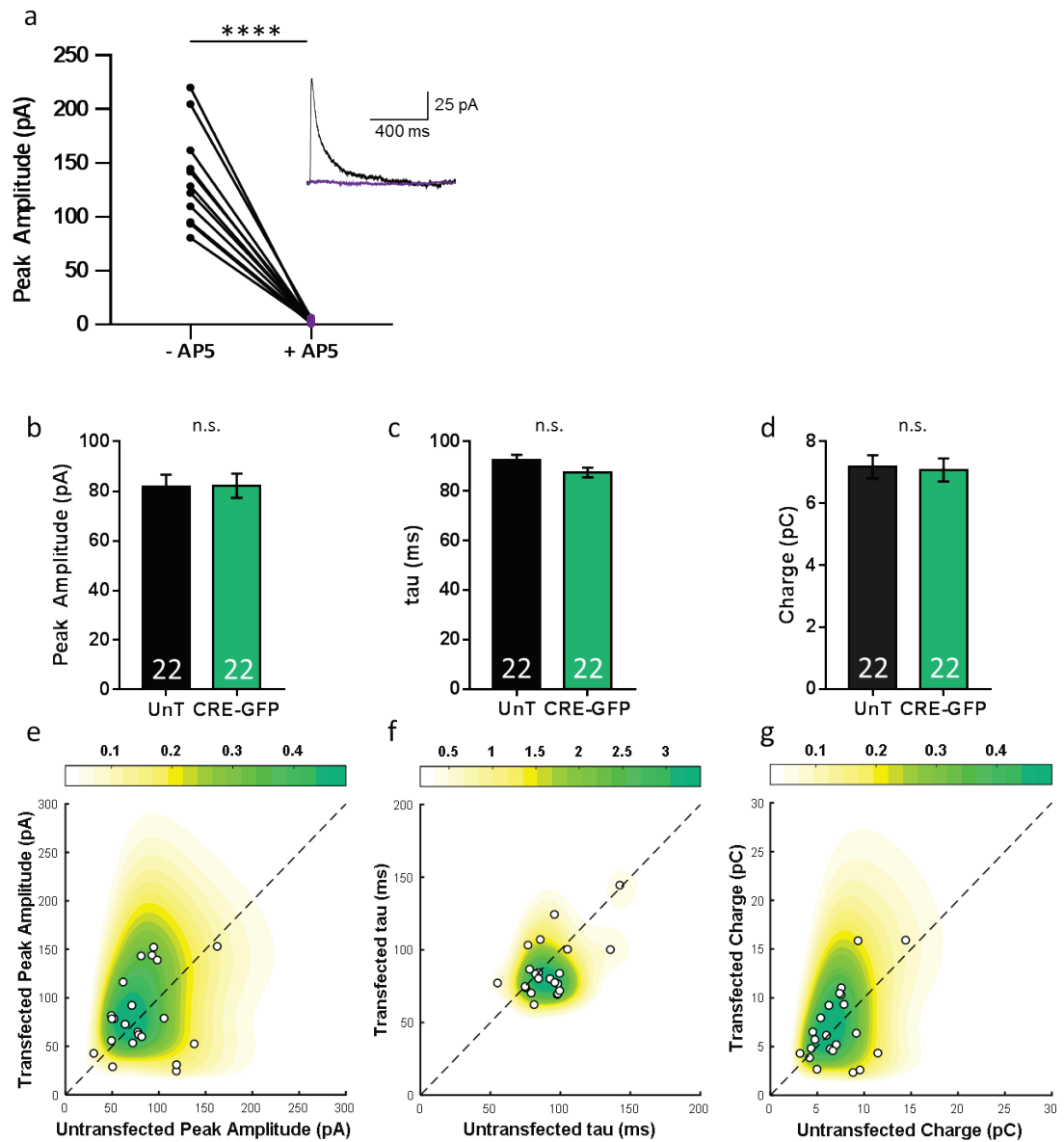


Figure 2.5: Validation of experimental approach.

a) Peak amplitudes of NMDAR-EPSCs before and after the addition of NMDAR antagonist AP5 (100 μ M), with representative traces (before – black, after – purple). Data from 1 mouse. b-d) bar charts of peak amplitudes, tau and charge transfer for untransfected neurons (UnT) and neurons transfected with Cre-GFP from WT mice that do not have any floxed genes. Data from 3 mice. e-g) Kernel density plots corresponding to b-d, showing individual data points.

Post-synaptic responses were recorded from CA1 neurons in voltage clamp after stimulation of the Schaffer collateral pathway, which are axons originating from CA3 neurons. NMDAR-EPSCs were isolated by including AMPAR blocker NBQX and GABA_AR blockers picrotoxin and gabazine in the ACSF and compared between simultaneously recorded Cre-GFP-expressing CA1 neurons and neighbouring untransfected neurons. Fig. 2.5e-g shows the individual data points with the response from the transfected neuron plotted against the response from the untransfected

neuron with a kernel density estimate overlaid representing the 2D-distribution of the sample points. These graphs show that the data points are clustered around the line of unity, suggesting similar responses from transfected and untransfected neurons for all properties measured. These observations were also borne out with statistical hypothesis testing (MLM): there was no significant effect on the NMDAR-EPSC peak amplitude (mean \pm within-subjects SEM: untransfected 81.73 ± 4.89 pA, transfected 82.21 ± 4.89 pA, $p = 0.7101$), decay time constant (τ_w) (mean \pm within-subjects SEM: untransfected 92.64 ± 1.98 ms, transfected 87.42 ± 1.98 ms, $p = 0.1922$), or charge transfer (mean \pm within-subjects SEM: untransfected 7.179 ± 0.38 pC, transfected 7.078 ± 0.38 pC, $p = 0.4475$) (fig. 2.5b-d). This data indicated that the Cre-recombinase construct used in these and further experiments does not alter NMDAR-EPSC properties through non-specific off target effects in CA1 pyramidal neurons.

To ensure that recordings were pure NMDAR-EPSCs, EPSCs were recorded from WT untransfected neurons before and after the addition of an NMDAR antagonist, D-AP5. Fig. 2.5a shows the peak amplitude of responses before (- AP5) and after addition of 100 μ M D-AP5 (+ AP5). A complete inhibition of current to baseline was observed with the addition of AP5 (mean \pm SEM: - AP5 136.70 ± 13.51 pA, + AP5 2.87 ± 0.47 pA, $p < 0.0001$, paired t-test), showing that the current recorded was solely NMDAR-mediated.

GluN2A homozygous KO produces smaller, slower NMDAR-EPSCs

Once it was confirmed that the Cre-GFP construct had no undesirable effects and that the evoked EPSCs recorded were in fact NMDAR mediated, a homozygous KO of GluN2A was performed in CA1 pyramidal neurons by single-cell electroporation of Cre-GFP in hippocampal slices from homozygous *Grin2A*-flox mice. As previously described (fig. 2.1, 2.2), both a transfected and untransfected neuron were recorded simultaneously after stimulation of the Schaffer collaterals. Fig. 2.6a shows the timeline from dissection to recording. NMDAR-EPSCs from GluN2A KO had a significantly lower peak amplitude than control (mean \pm within-subjects SEM: untransfected 99.85 ± 3.06 pA, transfected 61.68 ± 3.06 pA, $p < 0.0001$, MLM) (fig. 2.6b,d,g). Whilst the smaller NMDAR-EPSC amplitude is at odds with similar amplitudes reported in a similar experiment in acute slices (Gray et al., 2011), it is consistent with the smaller NMDAR/AMPA ratios and indistinguishable input-output curves of (presumably AMPAR-mediated) fEPSPs in germline GluN2A KO mice (Sakimura et al., 1995). Similar to Gray et al. (2011), a prolonged current decay time constant was observed in GluN2KO cells (mean \pm within-subjects SEM: untransfected 80.52 ± 2.66 ms, transfected 155.7 ± 2.66 ms, $p < 0.0001$, MLM) (fig. 2.6c,e,h). The resulting charge transfer, which is dependent on both peak amplitude and

decay time, was consequently not significantly different to control (mean \pm within-subjects SEM: untransfected 8.18 ± 0.37 pC, transfected 9.03 ± 0.37 pC, $p = 0.8103$, MLM) (fig. 2.6f,i).

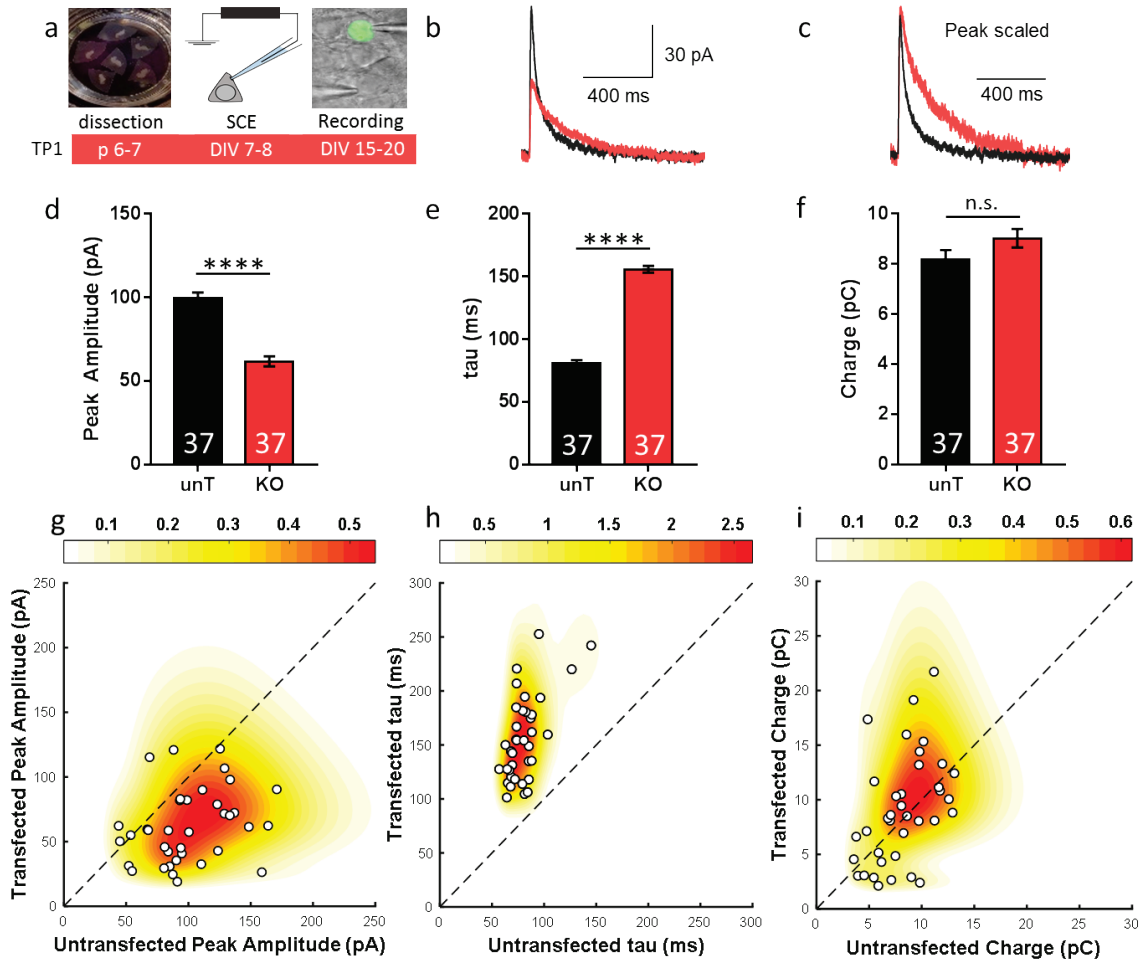


Figure 2.6: *GluN2A* KO produces smaller and slower currents in CA1 pyramidal neurons in organotypic hippocampal slice culture.

a) Timeline of procedure for recording NMDAR-EPSCs from hippocampal neurons from *Grin2A*-floxed mice. TP1 = time point 1. *b*) representative traces from untransfected (black) and *GluN2A* KO (red). *c*) Peak scaled traces highlighting difference in decays from two conditions. *d-e*) bar charts of peak amplitudes, tau and charge transfer for untransfected neurons (unT) and *GluN2A* KO. *g-i*) Kernel density plots corresponding to *d-e*, showing individual data points. Data from four mice (10 cell pairs each from mice 1, 2, 3, and 7 pairs from mouse 4), **** $p < 0.0001$, n.s., non-significant.

As there was some discrepancy with the results seen for single-cell *GluN2A* KO in acute slices (Gray et al., 2011), it was next investigated whether these differences were due to the time points in development when the KO was performed. There is known to be a developmental switch that occurs during early post-natal life where the NMDAR subunit composition shifts from

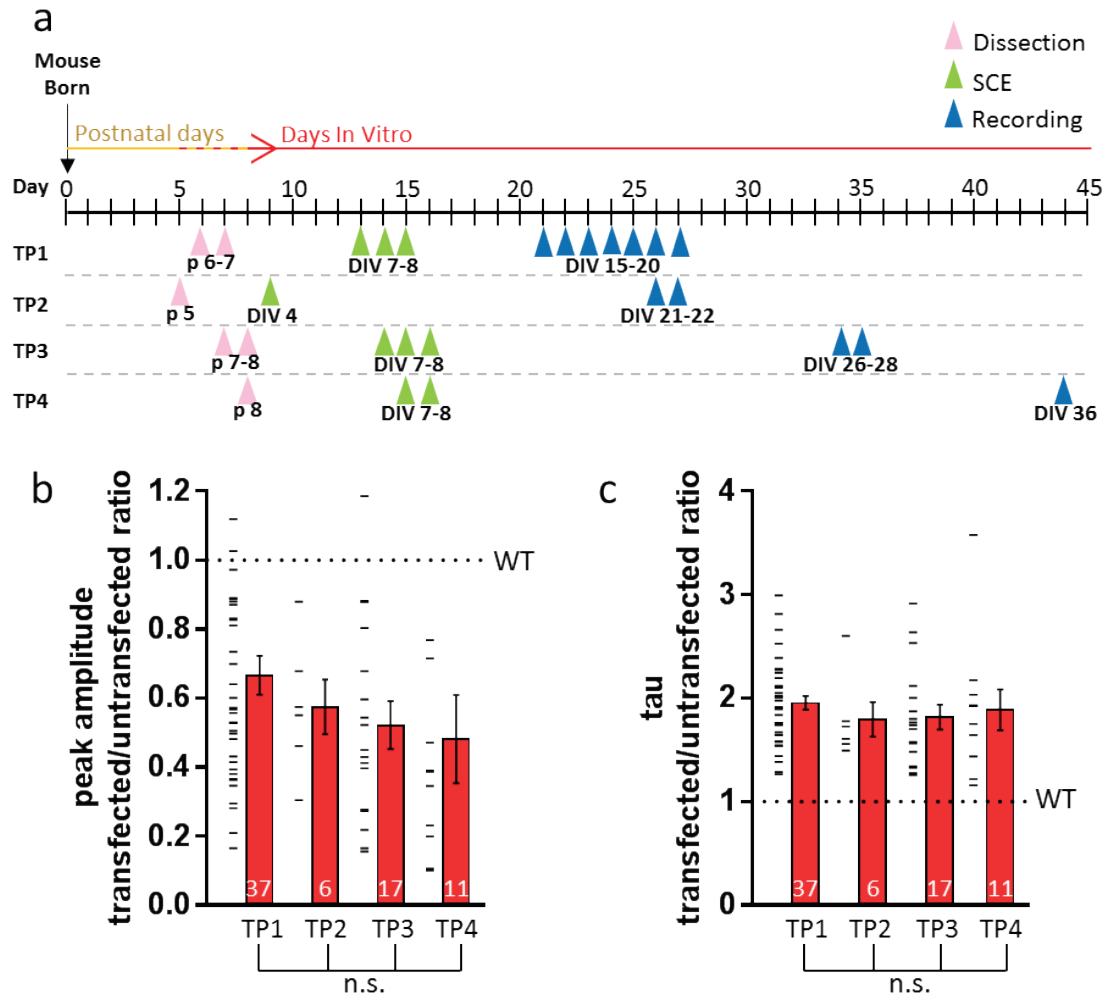


Figure 2.7: GluN2A KO in CA1 pyramidal neurons behaves similarly at different time points.

a) Timeline of four different GluN2A KO procedures that vary in mouse age, slice age and transfection time. TP = time point. b) Peak amplitudes of varying GluN2A KOs. c) Decay times of varying GluN2A KOs. Data from 4 mice (TP1), 2 mice (TP2), 3 mice (TP3), 1 mouse (TP4). n.s., non-significant. Error bars are SEM.

containing predominantly GluN2B to GluN2A subunits (Monyer et al., 1994). Therefore, the length of time the culture is maintained before recording could determine the properties of NMDAR-EPSCs if the switch was still in progress and had not already been complete. Whether the subunit switch occurs or the time at which it is complete in mouse organotypic slices is not yet known, but is reported to quantitatively differ in cultured dissociated neurons compared to *in vivo* (Corbel et al., 2015). Therefore, the length of time the culture is maintained before recording could determine the properties of NMDAR-EPSCs if the switch was still in progress and had not already been complete. The expression levels of GluN2B remaining after GluN2A KO could differ through the 'switch' period, so it was next examined whether any differences were

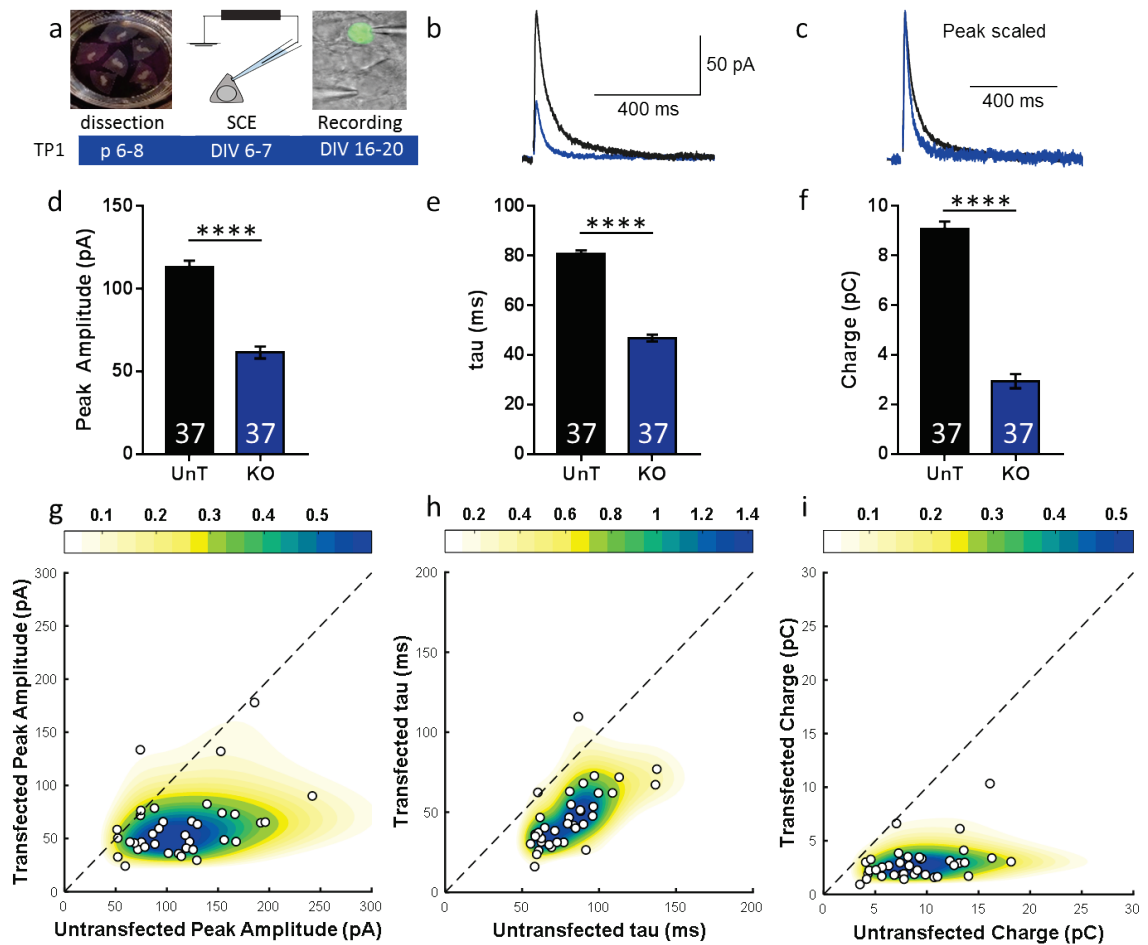


Figure 2.8: *GluN2B* KO produces smaller and faster currents in CA1 pyramidal neurons in organotypic slice culture.

a) Timeline of procedure for recording NMDAR-EPSCs from hippocampal neurons from *Grin2B*-floxed mice. TP1 = time point 1. *b*) representative traces from untransfected (black) and *GluN2B* KO (blue). *c*) Peak scaled traces highlighting difference in decays from two conditions. *d-e*) bar charts of peak amplitudes, tau and charge transfer for untransfected neurons (UnT) and *GluN2B* KO. *g-i*) Kernel density plots corresponding to *d-e*, showing individual data points. Data from four mice (8 cell pairs from mouse 1, 13 pairs from mouse 2, 6 pairs from mouse 3, and 10 pairs from mouse 4), **** $p < 0.0001$.

present in evoked NMDAR-EPSCs in *GluN2A* KO when measured at different time points. Gray et al. (2011) transfected at p0 and recorded from acute slices taken from p16-25 mice; at this time *in vitro*, *GluN2A* expression levels in cultured hippocampal neurons are known to exceed those of *GluN2B* (Corbel et al., 2015). The time of the *GluN2A* KO recordings in fig. 2.6 (Time Point 1 –TP1) are similar to this time period (21-27 days after birth – fig. 2.7a) however, a lot of this time is *in vitro* and the time between transfection and recording is shorter. To address this, *GluN2A* KO was tested using slices that were cultured for a longer time after transfection (26-28

DIV: TP3; and 36 DIV: TP4) and using slices prepared from younger mice that were transfected earlier and cultured for longer (TP2) (fig. 2.7a).

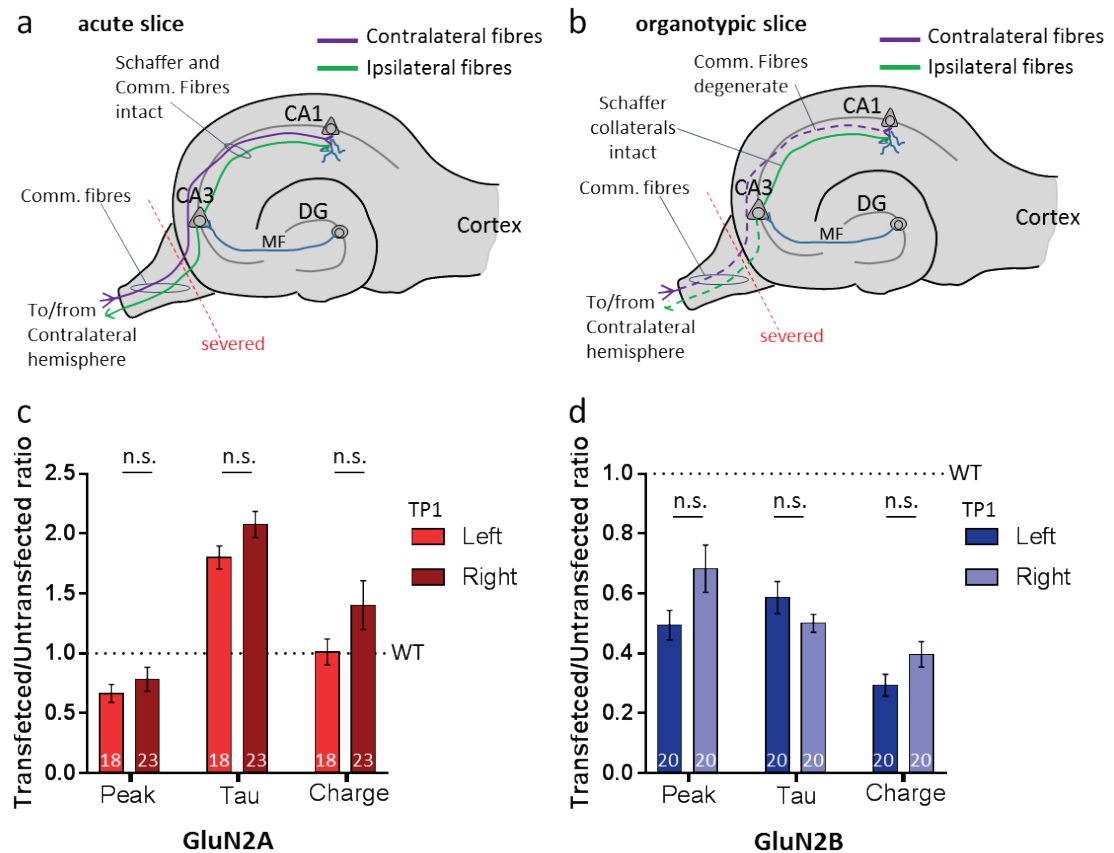


Figure 2.9: GluN2A and GluN2B KO in CA1 pyramidal neurons do not show hemispheric differences.

a) and b) Schaffer and commissural fibre pathways in acute and organotypic hippocampal slices, respectively. DG, dentate gyrus; MF, mossy fibres. c) Peak amplitudes, decay times and charge transfer of GluN2A KO in the left and right hippocampal hemispheres. d) Same as c) for GluN2B. Data from 4 mice for GluN2A and 4 mice for GluN2B. n.s., non-significant; TP, time point.

At all of the time points examined, the same results as TP1 were observed; NMDAR-EPSC peak amplitude was reduced compared to control and there was no significant difference between each time point (one-way ANOVA on transfected/untransfected peak amplitude ratio, $F(3, 67) = 1.258$, $p = 0.2960$) (fig. 2.7b). EPSC decay was also significantly slower in GluN2A KO neurons than in untransfected neurons with no difference between each time point (one-way ANOVA on transfected/untransfected tau ratio, $F(3, 67) = 0.4334$, $p = 0.7298$) (fig. 2.7c). This suggested that the GluN2 subunit expression was not fluctuating during this time period and that GluN2A and GluN2B levels were stable around the DIV 15-20 time point (TP1).

GluN2B homozygous KO produces smaller, faster NMDAR-EPSCs

After the unexpected findings for the GluN2A KO, the next aim was to discover whether a GluN2B KO would show behaviour in organotypic slice culture consistent with published findings. A homozygous KO of GluN2B was performed in the same procedure as that of GluN2A, except with slices dissected from homozygous *Grin2B*-flox mice (fig. 2.8a). This GluN2B KO resulted in NMDAR-EPSCs with significantly smaller peak amplitudes compared to control (mean \pm within-subjects SEM: untransfected 113.3 ± 3.71 pA, transfected 61.44 ± 3.71 pA, $p < 0.0001$, MLM) (fig. 2.8b,d,g).

Synaptic currents from GluN2B KO were also much quicker to decay to baseline compared to WT untransfected cells (mean \pm within-subjects SEM: untransfected 80.79 ± 1.38 ms, transfected 46.78 ± 1.38 ms, $p < 0.0001$, MLM) (fig. 2.8c,e,h). This resulted in a subsequent reduction in charge transfer (mean \pm within-subjects SEM: untransfected 9.09 ± 0.29 pC, transfected 2.94 ± 0.29 pC, $p < 0.0001$, MLM) (fig. 2.8f,i). These results observed for GluN2B KO in organotypic hippocampal slices are identical to those found previously in acute slices (Gray et al., 2011) and consistent to findings in the conditional GluN2B KO in forebrain excitatory neurons (von Engelhardt et al., 2008).

No Left/Right differences in NMDAR-EPSC properties in GluN2A or GluN2B KO

Asymmetrical CA1 synaptic glutamate receptor expression has been found depending on the origin of synaptic inputs; synapses formed from CA3 neurons projecting to CA1 from the left and right hemispheres differ in their GluN2A and GluN2B densities (Kawakami et al., 2003, Shinohara et al., 2008). CA3 projections form two major pathways in the hippocampus, one pathway innervates the CA1 of the ipsilateral hippocampus and is termed the Schaffer collateral pathway and the other projects to the CA1 neurons in the hippocampus of the contralateral hemisphere – the commissural fibre pathway. Inputs that originate from the left CA3 form synapses with a high GluN2B density (Kawakami et al., 2003, Shinohara et al., 2008) – these pathways are the Schaffer collaterals in the left hippocampus and the commissural fibres in the right hippocampus. These two synaptic inputs are present in CA1 of acute hippocampal slices (fig. 2.9a) and both GluN2B dominant and GluN2B non-dominant synapses could be stimulated in slices from both hemispheres (Kohl et al., 2011). However, organotypic slices undergo processes of reorganisation and pruning of axonal projection pathways while being maintained for several days in culture, unlike acute slices. In organotypic slices, the commissural fibre pathway that innervates CA1 from the contralateral CA3 degenerates as the fibres are severed and are thought to be no longer present after several days of culture (Frotscher et al., 1997, Humpel,

2015) but the Schaffer collateral pathway from the ipsilateral CA3 to CA1 remains intact (fig. 2.9b). This means that activation of the left Schaffer collateral pathway, which is GluN2B dense, may have a different current profile compared to activation of the Schaffer collateral fibre pathway in the right hemisphere of GluN2A or GluN2B KO in organotypic slices.

In the results presented in fig. 2.6g and fig. 2.6i, there was an overall reduction in peak amplitude and no overall difference in charge transfer between GluN2A KO and control. However, responses from cell pairs were quite varied, particularly for the amplitude measurement. Therefore, it was explored whether the different extremes of responses could be due to a difference in the hemispheres the recordings were taken from. The responses were separated from the GluN2A KO TP1 (fig. 2.6) from the left and right hippocampi and the EPSC properties were compared for each hemisphere. No significant differences were found in the responses for NMDAR-EPSC peak amplitude, decay or charge transfer from the left and right hemispheres (one-way MANOVA, $F(3, 37) = 1.82$, $p = 0.161$; Wilk's $\Lambda = 0.871$, partial $\eta^2 = 0.129$) (fig. 2.9c).

It was also examined whether the GluN2B KO effect would be more prominent in one hemisphere over another due to the lateralised GluN2B densities. Responses were separated from the GluN2B KO (fig. 2.8) from the left and right hippocampi, but once again, no left/right differences were found for NMDAR-EPSC peak amplitude, decay time or charge transfer (one-way MANOVA, $F(3, 36) = 1.92$, $p = 0.144$; Wilk's $\Lambda = 0.862$, partial $\eta^2 = 0.138$) (fig. 2.9d).

Although there may be small differences in the densities of receptor expression at synapses from the left and right hemispheres in organotypic slices, the effect size may not be big enough to detect as significant with the sample size used ($n=18-23$). It also cannot significantly account for the variability in responses seen for GluN2A KO or why differences to KO in acute slices were observed.

GluN2 Heterozygous KO displays haploinsufficiency

Homozygous KOs are a very valuable technique for inferring the functions or characteristics of individual proteins. Although they provide a sense of the possible consequences of LOF GluN2 mutations, human disease mutations in GluN2A and GluN2B subunits are all *heterozygous* mutations. Thus, it still remained elusive as to whether a single WT allele was sufficient to maintain normal synaptic NMDAR currents. Therefore, the effects of a heterozygous GluN2A and GluN2B KO in CA1 pyramidal neurons on evoked NMDAR currents were investigated next. For GluN2A, the heterozygous KO produced similar effects as the homozygous KO, but with a more mild effect: the peak amplitude appeared reduced but was no longer significant (mean \pm within-subjects SEM: untransfected 83.25 ± 2.51 pA, transfected 71.5 ± 2.51 pA, $p = 0.1262$,

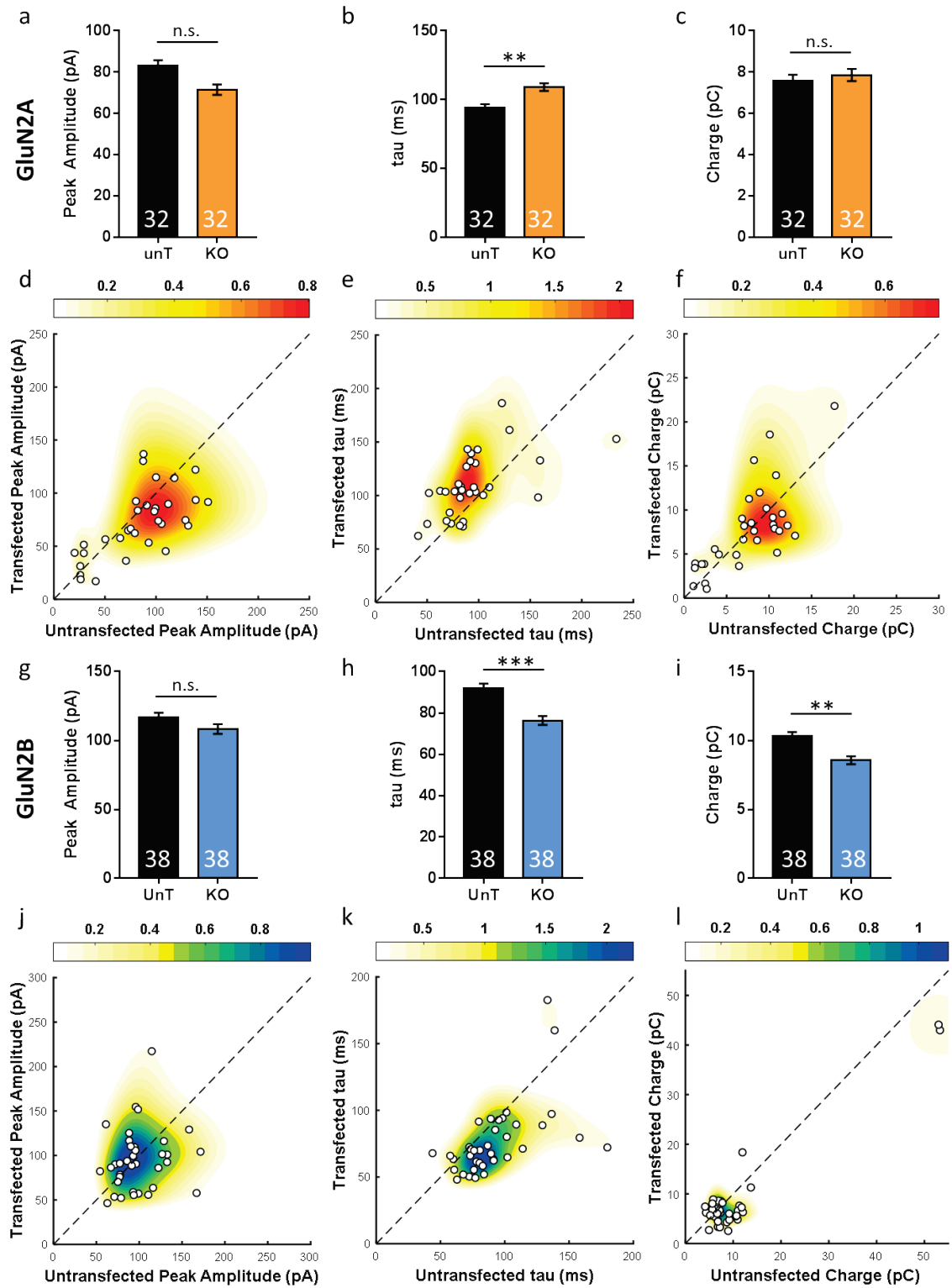


Figure 2.10: Heterozygous GluN2A and GluN2B KO show a similar trend to the respective homozygous KOs, but with a reduced, intermediate impact.

a-c) bar charts of peak amplitudes, tau and charge transfer for untransfected neurons (UnT) and neurons with a heterozygous GluN2A KO. d-f) Kernel density plots corresponding to a-c, showing individual data points. g-i) bar charts for GluN2B heterozygous KO. j-l) Kernel density plots corresponding to g-i. Data from six mice for GluN2A and six mice for GluN2B, ** $p < 0.01$, *** $p < 0.001$, n.s., non-significant.

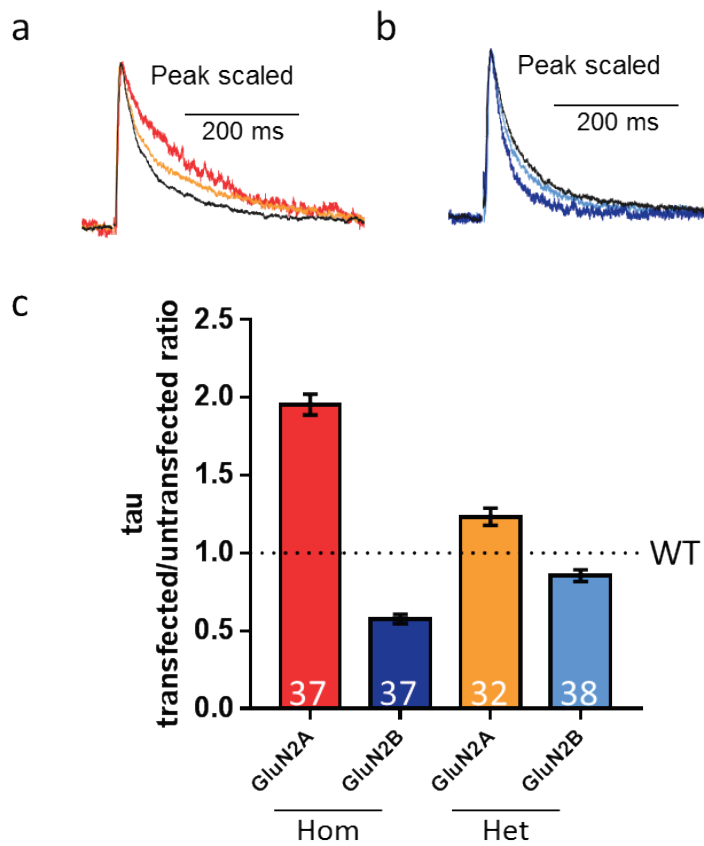


Figure 2.11: The decay kinetics of heterozygous KOs are intermediary but not completely halfway.

a) peak scaled representative traces from homozygous (red), heterozygous (orange) GluN2A KO and untransfected neurons (black). b) same as a) for GluN2B, homozygous (dark blue), heterozygous (light blue) and untransfected (black). c) transfected/untransfected ratio of NMDAR-EPSC decay time showing range of NMDAR decay kinetics.

MLM) (fig. 2.10a,d), the current decay time constant was still significantly longer (mean \pm within-subjects SEM: untransfected 93.81 ± 2.76 ms, transfected 109.1 ± 2.76 ms, $p = 0.0027$, MLM) (fig. 2.10b,e) and the charge transfer was similar to WT (mean \pm within-subjects SEM: untransfected 7.58 ± 0.29 pC, transfected 7.85 ± 0.29 pC, $p = 0.5805$, MLM) (fig. 2.10c,f). Similarly, heterozygous GluN2B KO also showed a smaller, milder effect compared to homozygous KO; there was no longer a significant effect on peak amplitude (mean \pm within-subjects SEM: untransfected 116.6 ± 3.56 pA, transfected 108.3 ± 3.56 pA, $p = 0.2563$, MLM) (fig. 2.10g,j), but decay and charge transfer were still reduced (MLM, decay mean \pm within-subjects SEM: untransfected 91.97 ± 2.16 ms, transfected 76.31 ± 2.16 ms, $p = 0.0003$, (fig. 2.10h,k), charge transfer mean \pm within-subjects SEM: untransfected 10.32 ± 0.29 pC, transfected 8.564 ± 0.29 pC, $p = 0.009$) (fig. 2.10i,l). In summary, while the effects produced by the heterozygous

KOs were not all significant, the effects appeared to be intermediate between WT and homozygous. This is illustrated for the decay kinetics in fig. 2.11.

GluN2 heterozygous gene deletion appears to result in haploinsufficiency. Although, the currents produced by the remaining WT allele in each case was very close to the WT (untransfected) level and was not half-way between (fig. 2.11c), this suggests that there may have been a certain – yet incomplete – degree of compensation by the remaining WT allele. From these results, it would be expected that the effects for heterozygous missense mutations in GluN2A and GluN2B to also have a more subtle outcome than a homozygous mutation would show. The mild deficiencies in NMDAR-EPSCs observed for the heterozygous GluN2 KO and the neurological phenotypes of patients with GluN2 mutations suggest that forebrain circuits are particularly sensitive to perturbations of NMDAR-mediated synaptic transmission.

Discussion

The main aims of this chapter were to replicate the findings of homozygous GluN2A and GluN2B KO in organotypic hippocampal slices and to determine whether single allele expression would result in haploinsufficiency, as an indication of the effects of heterozygous LOF human disease mutations. It was found that homozygous GluN2A KO produced prolonged, yet smaller NMDAR currents, consistent along different time points in *in vitro* development and different brain hemispheres. In contrast, homozygous GluN2B KO produced currents that were brief and small, identical to the characteristics observed previously in acute cultures. Heterozygous GluN2 deletion resulted in intermediate effects that indicated that both functional alleles are required for normal NMDAR currents. The results imply that heterozygous LOF mutations are capable of producing alterations in NMDAR-mediated synaptic currents and that even small perturbations to synaptic NMDARs likely have pathological consequences.

Using KO as a model for LOF mutations

The extent to which the KO model suitably reflects the effects of LOF mutations is limited. For truncations, frameshifts, indels, splice site, nonsense, missense and deletion mutations, the protein expression can be lost through rapid decay of the mRNA, complete lack of protein trafficking from the ER, or rapid targeting and degradation of the protein. In these situations, the KO could appropriately model the effects of the mutation. However, some LOF mutations could potentially have much milder phenotypes that result in only partial LOF on NMDAR properties. Such mutations include those affecting only the terminal tail of the protein, which may still produce a receptor that is trafficked and expressed at the synapse, but may have functional aberrations. Another example is CTD mutations that may reduce subunit expression but not completely abolish it (such as GluN2B-S1415L, (Liu et al., 2017)). Other examples include mutants that may affect both receptor function and expression to reduce the activity of the mutant subunit, but not completely, resulting in a moderate LOF phenotype. Mutants may cause a more severe defect in NMDAR-EPSCs by acting in a dominant negative fashion, where the presence of the mutant may affect the activity or delivery of normal native proteins. This could occur if the mutant subunit accumulates in the ER and sequesters GluN1 from assembling with other GluN2 alleles. In cases such as these, the presence of a dominant negative mutant protein could cause more severe consequences than complete lack of the protein. Therefore, the KO model used in this chapter applies to only specific cases and it was used to test the hypothesis that enhancement of some properties of NMDAR-EPSCs could result from LOF of GluN2A. It is

interesting to speculate whether the observed prolongation of NMDAR-EPSCs could contribute to the seizure phenotypes associated with GluN2A LOF mutations (Liu et al., 2019).

Conflicting GluN2A KO observations

In contrast to GluN2A KO in acute slices with viral injection where the peak amplitude was unchanged, leading to an enhanced charge transfer from prolonged receptor opening (Gray et al., 2011), in organotypic slices using SCE, this effect was not seen. GluN2B is expressed highly during embryonic stages and is gradually replaced with GluN2A through the course of development, a phenomena termed the 'switch' (McKay et al., 2018). GluN2A expression emerges during the first few post-natal days and is maintained into adulthood, mostly in the hippocampus, cerebellum and cortex. GluN2B expression is high throughout the brain and spinal cord in the embryo and declines but still persists in the hippocampus and cortex in the adult (Monyer et al., 1994, Watanabe et al., 1992). The switch begins in the early post-natal days and takes between 3-5 weeks in rodents (Corbel et al., 2015, Monyer et al., 1994, Watanabe et al., 1992). Experiments in acute slices were performed at P16-25 with injection of viral Cre-GFP at P0 whereas the experiments in this thesis were performed on P6-7 mice cultured for 15-20 DIV. The switch is known to occur *in vitro*, as well as *in vivo* (Corbel et al., 2015, Li et al., 1998, Stocca and Vicini, 1998). In case the differences were due to different relative expression levels of GluN2A and GluN2B, the culture duration and transfection duration were increased. However, no significant change in the peak amplitudes or decay kinetics of the GluN2A KOs was seen, suggesting stable levels of GluN2A and GluN2B at these times, and that the switch was already completed. This is consistent with the timings of stable GluN2 protein expression levels in dissociated hippocampal culture which were found to be around 15-20 DIV (Corbel et al., 2015). More recent GluN2A homozygous KO in rat cortical culture also found no compensation by GluN2B with regards to protein expression with western blotting (Strehlow et al., 2019).

No hemispheric differences in GluN2 subunits

Due to the putative degeneration of the commissural fibre pathway in organotypic hippocampal slices (Frotscher et al., 1997, Humpel, 2015), which remains intact in acute slices, differences were expected in the NMDAR mediated currents that originated in either brain hemisphere. Research into left/right NMDAR asymmetries is limited. Publications show that the GluN2B density in the left CA3-to-CA1 Schaffer collateral synapse on apical dendrites is higher than in the right CA3-to-CA1 synapse (Kawakami et al., 2003, Shinohara et al., 2008). The overall GluN2B expression is similar in neurons of both hemispheres, however the density is greater in the left due to the number of other glutamate receptors. GluN2A, on the other hand, is expressed at a

higher level in the right CA3-to-CA1 Schaffer collateral synapse in apical dendrites, but the overall densities are equivalent in the two hemispheres (Kawakami et al., 2003, Shinohara et al., 2008). Furthermore, the GluN2B antagonist Ro 25-6981 blocked NMDAR current to a greater degree in the left than in the right hippocampal hemisphere in acute slices (Kohl et al., 2011). Despite these observations, no detectable differences in the NMDAR currents were found in this thesis in either GluN2A or GluN2B KO (fig. 2.9). KO of GluN2B in the left would have been expected to eliminate a higher proportion of the current than in the right; for GluN2A, the opposite would have been expected. These asymmetrical differences have been reported in the apical dendrites of CA1 neurons in the stratum radiatum; it is possible that the current results do not show the same trends due to the activation of both apical and basal dendritic synapses in the current experimental procedure of this thesis. The glutamate receptor densities and morphological features of basal dendritic spines have not been as extensively studied, in fact, Kawakami et al. (2003) show that the inhibition by Ro 25-6981 is greater in the right hemisphere when examining basal dendrites in the stratum oriens. This may result in a similar level of inhibition if both apical and basal dendrites are activated, as would be the case in the current experiments as there is no selectivity towards certain dendritic compartments. An alternative explanation could be that competing inputs from contralateral and ipsilateral CA3 may be required to maintain input specific GluN2 content in the left and right hippocampi.

The heterozygous condition

GRIN2A mutations in human patients are associated with clinical phenotypes despite the patients still having one copy of the mutant allele. In this thesis, neurons heterozygote for a *Grin2a* null allele exhibited NMDAR-EPSC properties intermediate between WT and homozygous knockout. Intermediate effects have been reported for the epilepsy-associated GluN2A mutant L812M when expressed in both HEK293 cells and *Xenopus* oocytes. In these systems, the glutamate and glycine potencies are enhanced to a greater degree with two mutant alleles compared to one. This is also true for the current decay which is more prolonged in the homozygous condition than in the heterozygous (Yuan et al., 2014). The P552R mutant in GluN2A in epilepsy patients also exhibited an intermediate effect when heterozygous for glutamate and glycine potencies, decay time course and charge transfer, although, the rise time was only affected when the mutant was homozygous (Ogden et al., 2017). In dissociated hippocampal neurons, overexpression of four heterozygous GluN2B mutants with WT subunits still produced aberrant NMDAR currents (Fedele et al., 2018). Together with the findings in this thesis, this supports the idea that heterozygosity for mutant GluN2 alleles may cause a

significant defect in NMDAR currents. Heterozygous mutants may even have dominant negative effects, as seen for the GluN2A mutant R518H which produces severely reduced peak amplitudes in both heterozygous and homozygous conditions in HEK293 cells. Interestingly, the decay kinetics of R518H were found to be more perturbed with a single mutant allele than with two, producing an even longer channel opening with heterozygous than homozygous (Sibarov et al., 2017). It is important to note that the NMDAR population in neurons will consist of various combinations of WT and mutant GluN2 subunits in diheteromeric or triheteromeric receptors. Therefore, the overall effect observed in neurons is difficult to predict but will be dictated by the dominating NMDAR subunit composition (Vyklícký et al., 2018), which may differ depending on the neuron type.

Conclusions

Using single-cell conditional KO of GluN2A or GluN2B genes in the CA1 area of the hippocampus in organotypic slice culture, it was found that GluN2A KO produced prolonged currents but with a smaller amplitude and GluN2B KO produced faster and smaller currents than WT neurons. Using KO as a model for LOF mutants, the observation was reproduced that loss of GluN2A and GluN2B could result in opposite synaptic phenotypes. It was also shown, for the first time, that heterozygous GluN2 KOs produce an intermediate effect, suggesting that one WT allele is not sufficient to fully compensate for the loss of the second allele and expect heterozygous GluN2 mutants to still produce an observable dysfunctional synaptic phenotype. Since patients with *GRIN2*-related disorders have a single mutant allele, the findings here suggest that relatively small perturbations to NMDAR-EPSCs have profound pathological consequences.

Chapter 3 Synaptic phenotypes arising from diverse mutations in the NMDAR subunits GluN2A and GluN2B.

Abstract

Recent published work describes experiments performed in heterologous expression systems being used to characterize disease-linked mutants of recombinant human GluN2A and GluN2B subunits. The mutations lie on a spectrum with the extremes of GOF and LOF, depending on how they affect NMDAR biophysics or expression. Both types of mutations in GluN2A are implicated in various seizure-related disorders, however, for GluN2B, a genotype-phenotype correlation has been suggested where: GOF and LOF mutations are associated with seizure and mental disorders, respectively. These mutations have not been extensively studied in neurons and the synaptic phenotypes of LOF vs GOF have not been identified. In order to understand the underlying mechanisms of GluN2 mutants in relation to the respective disease phenotypes, the endogenous mouse GluN2 was knocked out and replaced with the WT or mutant human GluN2 subunit and the cell-autonomous effects on NMDAR- and AMPAR-mediated currents were examined at the Schaffer collateral synapses in the hippocampus. In this chapter, it is shown that most GluN2A mutations produced a similar synaptic phenotype, irrespective of the GOF-LOF distinction, of prolonged NMDAR-mediated current decays. However, GluN2B GOF and LOF mutations also exhibited a common synaptic phenotype of brief NMDAR currents, despite the differences in their associated disorders. Instead of a distinction in synaptic phenotype between GOF and LOF, there is a strong effect on NMDAR-mediated synaptic currents depending on the subunit affected – mutations in GluN2A vs GluN2B produce opposing synaptic phenotypes. The results question the validity of classifying GluN2 mutations based on their expression and function in heterologous systems.

Introduction

In an attempt to determine how GluN2A and GluN2B missense mutations affect NMDAR signalling and how they may be related to certain disease phenotypes, many research groups have adopted the use of heterologous expression systems, namely *Xenopus* oocytes and HEK-293 cells (Addis et al., 2017, Serraz et al., 2016, Swanger et al., 2016). Mutations that have been observed to increase NMDAR activity, either through longer channel opening, reduced magnesium block, enhanced glutamate and glycine potencies, etc., have been termed GOF mutations while those that reduce receptor activity or reduce receptor trafficking have been termed LOF mutations (Lemke et al., 2014). Interestingly, the majority of mutations in GluN2A, irrespective of their effect on the NMDAR, are implicated in seizure disorders, so that both GluN2A hypofunction and hyperfunction are potentially pro-epileptic. On the other hand, the majority of LOF GluN2B mutations have been found in patients with ID without the incidence of seizures, while those with mutations classed as GOF exhibit seizure disorders (Lemke et al., 2014). These classifications have been useful in order to understand why some of these mutations may converge to produce a similar phenotypic consequence. As these mutations are all very diverse, identifying groups of mutations with similar overall effects on individual subunit characteristics may aid in determining disease mechanisms. However, this has not been yet possible as classifications based on single subunit outcome may not reflect the wider impact to NMDAR function or synapse function. Swanger et al. (2016) have attempted to incorporate data from heterologous expression systems into models to address the consequences on synaptic properties of mutant NMDAR transmission. However, their predictions have not yet been validated because of the current focus of research which has barely entered into neuronal territory. A characterisation based on synapse function may be beneficial in dissecting the mechanisms leading to dysfunction for NMDAR mutations.

Mutations in the NMDAR subunits have been identified throughout the protein sequences, spanning all domains, and cause a variety in aberrant NMDAR biophysics and expression. Although many functional characterisations have now been done on numerous GluN2 mutants (see chapter 1 for review of current characterised mutants), it still remains elusive as to why disruption to GluN2A, in seemingly opposite and divergent ways, is pro-epileptic and how the GOF-LOF alterations to GluN2B function result in a distinction in clinical phenotypes. Heterologous expression systems have not provided answers to these questions, but have shown the diversity in consequences than can result from mutations in NMDARs. Whether the effects observed in these models persist in neuronal cells has also not been extensively studied.

The impact of mutations in receptors and ion channels has been studied in non-neuronal cells which has been useful in identifying the biophysical properties of subunit mutants and how they differ to WT subunits (Addis et al., 2017, Serraz et al., 2016, Swanger et al., 2016). However, these studies have been limited by the fact that regulatory and auxiliary proteins which are normally involved in receptor function are absent in these systems. Another approach that does not have this drawback is the use of WT neurons as expression systems for mutant receptors (Fedele et al., 2018, Marwick et al., 2015, Marwick et al., 2017, Ogden et al., 2017). In these experiments, mutant subunits are overexpressed on the background of endogenous WT subunits, making it hard to determine whether native receptors may be contributing or compensating for the effects of observed. As seen in the previous chapter, KO of endogenous subunits can be used to model LOF mutations. As germline KOs are problematic due to their potential lethality – such as GluN2B KO (Kutsuwada et al., 1996) – and the possibility of developmental compensation (Granger et al., 2011), a cell-autonomous KO was utilised to model LOF mutants. However, KO models become limited if LOF mutations do not cause a complete and total loss of the subunit or GOF mutants are also to be studied. For this purpose, molecular replacement of endogenous subunits with mutants is essential. Conditional KI mice have been used to study certain GluN2A and GluN2B mutants (Sprengel et al., 2017) but these have the same disadvantages as germ-line KO, as well as having large time and cost concerns. Therefore, this limits the feasibility of this approach for large-scale mutant studies. Cell-autonomous molecular replacement in single neurons overcomes these limitations. Animals will still develop normally and survive post-natally, no opportunity for developmental compensation is permitted, native receptors will not intervene once the replacement has been achieved, and the issue of overexpression can be overcome by using the appropriate concentrations of the selected mutant subunits.

In this chapter, the aim was to study the impact of selected human mutant GluN2 subunits in neurons and the consequences to synaptic transmission. Whether the WT mouse GluN2 could be replaced with WT human GluN2 was first tested in order to assess the effects of the *human* disease variants. After a successful replacement of the mouse to human proteins, single-cell conditional replacement with the mutant variants in CA1 pyramidal neurons of organotypic mouse hippocampal slices was performed. Mutants were assessed for their effects on AMPAR- and NMDAR-mediated synaptic currents.

The findings were as follows: the properties of the individual mutant GluN2A or GluN2B subunits identified in isolation in heterologous expression systems were not apparent when studied in

neurons. In neurons, the overall synaptic responses were not completely dominated by the mutant. As a result, many differences to the reported characteristics of mutant NMDAR currents were present. Both GluN2A and GluN2B mutants showed a common synaptic phenotype; GluN2A mutants led to slower NMDAR decay kinetics whereas GluN2B mutants displayed faster decay kinetics. Despite the wide varieties of effects on NMDARs reported for GluN2A mutants, a common synaptic phenotype is fitting with the common disease phenotype reported. However, for GluN2B, this result was surprising and shows the value of expression and function studies of ion channel mutants in neuronal systems that cannot always be modelled well by heterologous systems.

Methods

Mutation selection

Homology modelling

Multiple template homology modelling using full length GluN2B crystal structures 4PE5 (rat) and 4TLL (Xenopus) chains B and D were used to build a model of the soluble, human GluN2B LBD using Modeller 9.13. Since 4PE5 and 4TLL are low resolution (3.96 Å and 3.59 Å, respectively), the soluble ligand-binding domain structure of GluN2A 4NF8 (rat, 1.86 Å) chain B was also included in the alignment. This is justified by GluN2A and GluN2B having highly conserved sequences (~80 % LBD protein sequence identity in humans). The human GluN2A model was built using 4NF8 chain B and 5H8F (human, 1.81 Å) chain A as templates. Alignment of GluN2A and GluN2B structure sequences was performed using MAFFT (Katoh et al., 2002) and their quality was inspected manually. Initial structures were created using *automodel* function with a *slow* automatic schedule of the variable target function method with conjugate gradients. This was followed by refinement using molecular dynamics (CHARMM 22 forcefield) with simulated annealing at the *very slow* refinement level in Modeller. For each subunit, 20 models were made and the best model (lowest DOPE score; DOPE assesses the quality of structural models) was selected. Models were built by Dr Andrew Penn. Note that 4PE5, 4NF8 and 5H8F are crystal structures of the receptor bound to its endogenous agonists and the agonists were not included in the templates used for homology modelling. The models created will be referred to as hGluN2A_S1S2 and hGluN2B_S1S2.

Bioinformatics

The homology models or their primary sequences were used to obtain features that predicted how damaging GluN2 mutations were on the structure and function of NMDARs. Mutations that would have a greater impact on NMDAR properties were more likely to be disease-causing. Disease-associated mutations were more desirable to study and this method reduced the possibility of investigating false positive mutations that do not actually link to the presence of disease. Below, methods are presented relating to data gathering and prediction of the static and dynamic features used in the mutation selection. Static refers to the property that the feature remains fixed regardless of what the amino acid is mutated to. Three categories of static features were considered:

Sequence features. Highly conserved amino acid positions are typically intolerant to mutation (Choi et al., 2012). Consurf normalised conservation score (Ashkenazy et al., 2010) and HSSP sequence entropy (Schneider and Sander, 1996) are sequence-based bioinformatics metrics

related to sequence conservation at amino acid positions within proteins. These metrics are calculated through alignment of sequences of related proteins or of the same protein across different species. Consurf gives a conservation score for an amino acid in a protein calculated from phylogenetic trees of sequence homologues, while inversely HSSP sequence entropy is a measure of sequence variability at each position in the amino acid chain. Consurf scores were derived from the full length human GluN2A and GluN2B FASTA sequences using default settings (freely available at <http://consurf.tau.ac.il/>) and HSSP sequence entropy scores were derived from GluN2A chain B of crystal structure 4NF8 and GluN2B chain D of crystal structure 4TLL (freely available on the MRS search engine for biological and medical databanks at <http://mrs.cmbi.ru.nl/>). Z-scores of these metrics were calculated by subtracting the mean and dividing by the standard deviation for residues within the LBDs.

Structural features. c-beta accessibility and c-beta density are structure-based estimates that provide information about the relative accessibility/exposure of each residue when mutated to an alanine and the number of carbon-betas within a diameter of 10 Angstroms, respectively, in the 3D protein structure. These were calculated with the WHATIF server (Vriend, 1990) (freely available: <http://swift.cmbi.ru.nl/servers/html/index.html>) and the custom script *cbdensity* written in python using the hGluN2A_S1S2 and hGluN2B_S1S2 model structures as input. These measure how much amino acid positions are exposed or buried within the protein, where more buried amino acid positions are more likely to be destabilizing upon mutation (Saunders and Baker, 2002). The WT residue's solvent accessibility was also calculated using PoPMuSiC v2.0 for hGluN2A_S1S2 and hGluN2B_S1S2 (Dehouck et al., 2011), freely available at <http://www.dezyme.com/>.

The B-factor conveys the uncertainty of an atom position due to the spread of electron density and it is deposited in the coordinate files for crystal structures. Since B-factors increase with local disorder and flexibility they can be used as a metric for how integral the residue is for the protein's structure. Normalised B-factors were obtained for the c-alpha positions of residues in GluN2A chain B of 4NF8 and GluN2B chain D of 4TLL from the B-factor column of the PDB files using the custom python script *cabfactor*. Z-scores of the B-factors were calculated by subtracting the mean and dividing by the standard deviation for residues within the LBDs. c-beta values and b-factors were obtained by Dr Andrew Penn.

Energy features. The tolerance of an amino acid to mutation can be estimated in a protein by mutating residues one at a time to all 20 amino acids (a.k.a. saturation mutagenesis) and then predicting the change in the free energy of unfolding, denoted $\Delta\Delta G$. Amino acid positions

predicted to result in greater variation of $\Delta\Delta G$ upon saturation mutagenesis have greater mutational sensitivity and are thus likely to result in deleterious effects upon mutation. FOLDX Saturation mutagenesis (Schymkowitz et al., 2005) (freely available tool at: <http://foldx.embl.de/>) and MAESTRO Saturation mutagenesis (Laimer et al., 2016) (freely available tool at: <https://biwww.che.sbg.ac.at/maestro/web>) were used to calculate changes in protein stability. For each position in the LBD, the median absolute deviation (MAD) of $\Delta\Delta G$ predictions for all 20 mutations was calculated. Both FOLDX and MAESTRO use protein structure to obtain $\Delta\Delta G$ values, but use different algorithms to do so; MAESTRO uses statistical potentials whereas FOLDX uses a forcefield for calculation. hGluN2A_S1S2 and hGluN2B_S1S2 model structures were used. Saturation mutagenesis and energy predictions were obtained by Dr Andrew Penn.

Dynamic features. Dynamic features are features that change in value depending on what the amino acid is mutated to. Generally, the tools available predict whether or not mutations are deleterious. SIFT (Sorts Intolerant From Tolerant amino acid substitutions) uses alignments of homologous sequences to construct position specific probabilities for amino acid changes (Ng and Henikoff, 2001). Similarly, PROVEAN (Choi and Chan, 2015) (freely available at: <http://provean.jcvi.org>) uses alignments and a weighted set of scores, including gap penalties and the BLOSUM62 substitution matrix to predict whether sequence changes in proteins will have deleterious consequences. Polyphen-2 uses probabilistic classifier that was trained to identify structural and sequence features associated with disease-causing mutations annotated in the UniProt database (Adzhubei et al., 2013). SIFT and Polyphen-2 predictions were obtained from the VEP server (freely available at: <http://www.ensembl.org/Tools/VEP>). These methods do not include a prediction of protein stability, so the PoPMuSiC v2.0 tool (<http://www.dezyme.com/>) was employed for a prediction of the change in free energy resulting from substitution of WT to mutant residues ($\Delta\Delta G$) in the hGluN2A_S1S2 and hGluN2B_S1S2 model structures (Dehouck et al., 2011).

Mutation selection

A literature search identified 20 *GRIN2A* and 6 *GRIN2B* LBD mutations. The LBD was chosen because sufficient structural data was available in the public domain for model building of the domain structure for the use of *in silico* programmes that could predict mutation effects. In comparison, no NTD structure was available for GluN2A, all TMD structures were incomplete and of low resolution and no CTD structural data was available. The LBD also has a big effect on

how the receptor can assemble, its function and its expression/trafficking to the cell surface (Adams et al., 2014, Carvill et al., 2013, Lemke et al., 2014, Lesca et al., 2013, She et al., 2012).

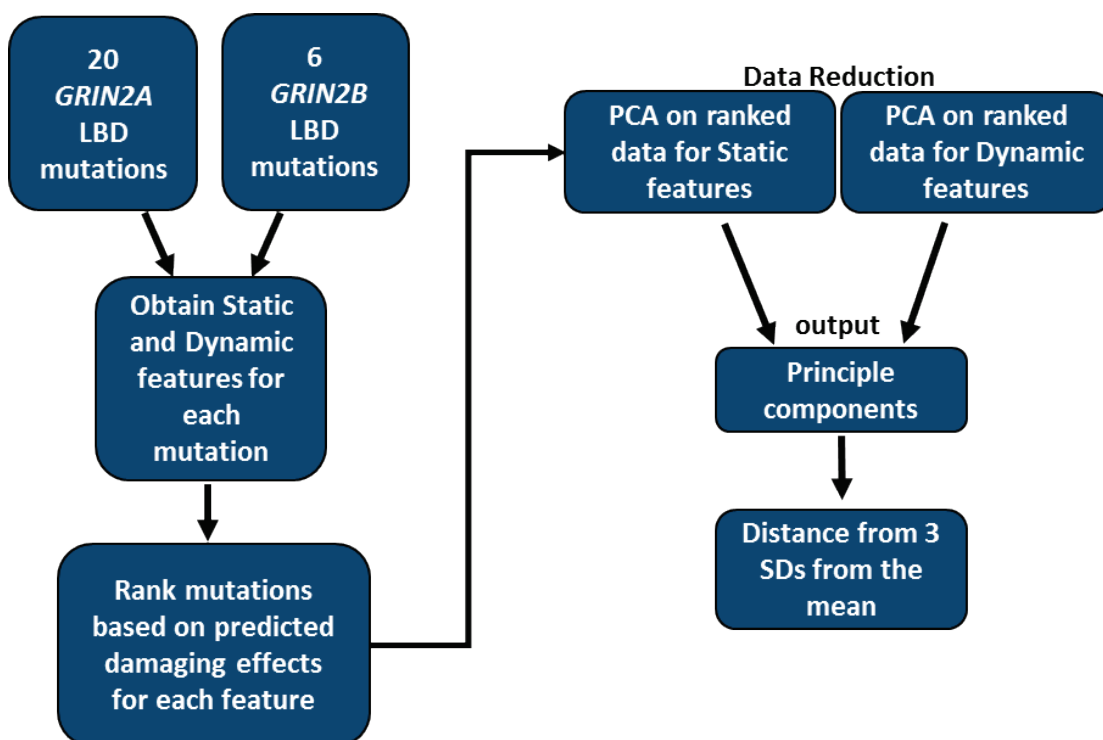


Figure 3.1: Mutation selection procedure.

A literature search identified 20 GluN2A and six GluN2B mutations. Six mutations were selected based on their predicted propensity to disturb NMDAR function from in silico programmes. LBD, ligand-binding domain; PCA, principle component analysis; SD, standard deviation.

Static features were obtained for all LBD residues and dynamic features were obtained for the 26 mutations (Appendix A). After tied rank transformation of the data for each feature (Appendix A), a principle component analysis (PCA) was implemented to perform data reduction using IBM SPSS Statistics 23. This analysis reduces a large dataset of many variables, each with many observations, into a fewer number of principle components (PCs) that explain most of the variance in the original dataset. Data reduction is used as it is easier to identify or analyse trends when working with fewer variables compared to the original high dimensional data.

PCAs were performed separately for static and dynamic features. Assumptions of sampling adequacy and correlated variables were met for the statistical analysis, measured using the Kaiser-Meyer-Olkin Measure of Sampling Adequacy and Bartlett's test of sphericity,

respectively. Two PCs were produced from the static features data and two from the dynamic features data (Appendix B), so for each mutation there were a total of four PCs. PCs with negative values corresponded to more deleterious effects upon mutation - high sequence conservation, low solvent accessibility, high beta density, low B-factors, positive $\Delta\Delta G$, low SIFT and PROVEAN and high PolyPhen2 (Appendix C). Using the PCs for each mutation as coordinates in 4D space, the distance from 3 standard deviations (SD) of the mean (-3,-3,-3,-3) was calculated. PCs are z-scores so have a mean of zero and a SD of one. The distance from 3 SDs was used because within a normal distribution, 99.7% of data points lie within 3 SDs of the mean. Those at the extreme negative end of the scale (more deleterious) would be closer to this value. The mutations were reordered according to their distances (Appendix B, fig. 3.1). The top six mutations were selected: *GRIN2A*-C436R, *GRIN2B*-C461F, *GRIN2B*-C456Y, *GRIN2A*-R518H, *GRIN2A*-T531M, *GRIN2A*-I694T. Fig. 3.2 shows the location of these mutants in the GluN2A or GluN2B structures.

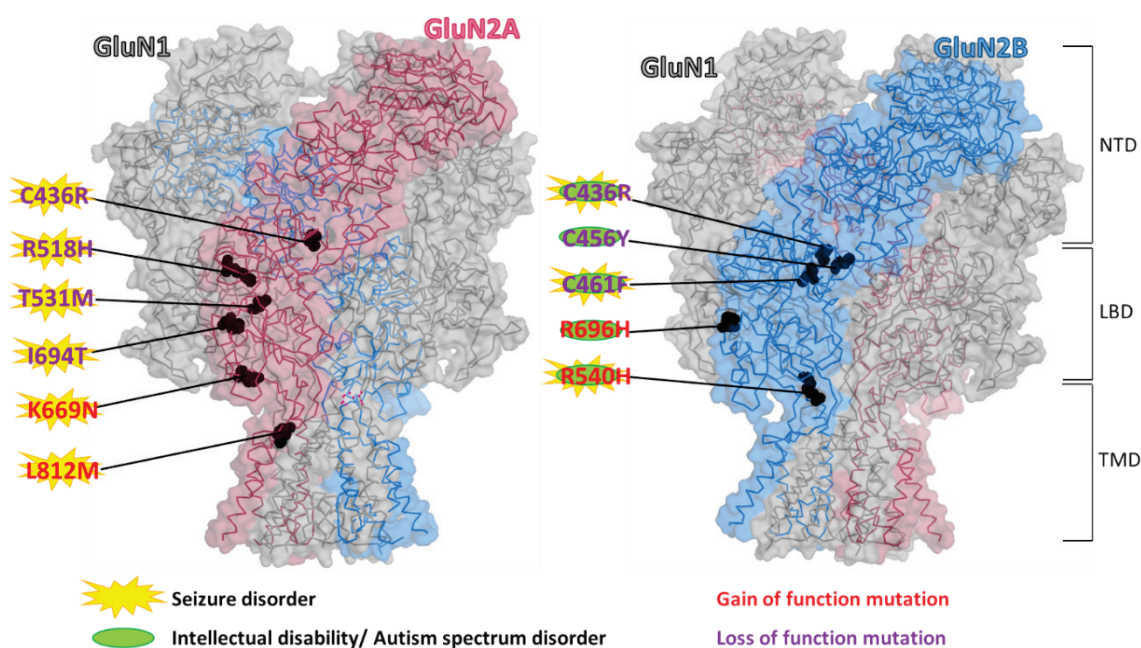


Figure 3.2: Location of GluN2 mutants and their associated phenotypes.

The mutation selection procedure above preceeded the recent boom in experimental studies systematically evaluating the functional effect of multiple mutations (Serraz et al., 2016, Swanger et al., 2016), CFERV database <http://functionalvariants.emory.edu/>. To assess the ability of the mutation selection approach to reliably predict the ranks of mutants based on

damaging effects, the ranks of the mutants were correlated to the ranks of a PCA performed on mutant data from Swanger et al. (2016) (Appendix D). This showed a significant positive correlation between predicted and actual effects of mutations in heterologous cells ($n = 22$, $r = 0.748$, $p < 0.001$), suggesting that this *in silico* method based on unsupervised statistical techniques could efficiently determine possible deleterious effects of mutations in GluN2A and GluN2B.

The PCA identified mutations which were predicted to have deleterious (damaging) effects on NMDAR properties to cause an altered protein expression or function. These mutations selected using PCA were all LOF mutations, based on the research in heterologous cells (Swanger et al., 2016). To effectively test the hypotheses that:

- Both GOF and LOF GluN2A mutations would have similar effects on NMDAR properties
- GOF and LOF GluN2B mutations would have opposing effects on NMDAR properties,

a mixture of GOF and LOF mutations were needed. A literature search identified putative GOF mutations:

GRIN2A-K669N (LBD), which had markedly slower NMDAR decay (Swanger et al., 2016).

GRIN2A-L812M (in linker between LBD and TMD), produced multiple effects to enhance NMDAR functional activity, including increased agonist potency, slower deactivation, abolished magnesium block and reduced susceptibility to negative modulators (Yuan et al., 2014).

GRIN2B-R540H (LBD), reduced magnesium sensitivity, however, had a relatively mild effect (Lemke et al., 2014). This mutation was included in the PCA analysis but had a low ranking.

GRIN2B-R696H (LBD), produced significantly slower current decay (Swanger et al., 2016).

In addition, ***GRIN2B-C436R*** (LBD), a LOF mutation with almost no response to agonist and almost absent current (Swanger et al., 2016) was also chosen as it is also present in GluN2A.

These mutants are shown in fig. 3.2 in the GluN2A and GluN2B structures.

Molecular Biology

Mutagenesis

Mutagenesis was performed on the pCI-Neo *GRIN2A* and pCI-Neo *GRIN2B* plasmids to create single nucleotide changes in the gene's coding sequence and substitutions of single amino acid residues in the peptide sequence, i.e. missense mutations. Primers were designed that contain a single base substitution using the GeneArt® Primer and Construct Design Tool, available at

<http://www.thermofisher.com/order/oligoDesigner/mutagenesis>. Primers were synthesised by Integrated DNA Technologies (IDT, Belgium) and the cloning of the selected mutations was performed using the GeneArt® Site-Directed Mutagenesis Kit (Invitrogen, A13282). The primers used are listed in Table 3.1. The presence of each desired mutation was confirmed by DNA sequencing and the whole coding sequence was also examined to ensure that no other alteration (e.g. PCR error) was present. Plasmids were transformed and prepared as described in chapter 2.

Table 3.1: Primers used to generate mutant *GluN2A* and *GluN2B* constructs from WT *pCI-Neo GRIN2A* and *pCI-Neo GRIN2B*, respectively.

MUTATION	FORWARD PRIMER (5' TO 3')	REVERSE PRIMER (5' TO 3')
<i>GRIN2A</i>		
C436R	AGGAACACCGTGCCACGTCGGAAGTTCGTCA	TGACGAACTCCGACGTGGCACGGTGTTTCCT
R518H	CCATCAATGAGGAACATTCTGAAGTGGTGGGA	TCCACCACTTCAGAATGTTCTCATTGATGG
T531M	TGCCCTTTGTGGAAATGGGAATCAGTGTCAT	ATGACACTGATTCCCATTTCACAAAGGGCA
K669N	CCTCAGTGACAAAAATTTTCAGAGACCTCAT	ATGAGGTCTCTGAAAATTTTGTCACTGAGG
I694T	GCACGGAGAGAAACACTCGGAATAACTATCC	GGATAGTTATTCCGAGTGTTTCTCTCCGTGC
L812M	GTGATGAGCAGCCAGATGGACATTGACAACA	TGTTGTCAATGTCCATCTGGCTGCTCATCAC
<i>GRIN2B</i>		
C436R	AGGAACACAGTCCCCCGCCAAAAACGCATAG	CTATGCGTTTTTGGCGGGGGACTGTGTTTCCT
C456Y	GTTACATCAAAAAATACTGCAAGGGGTTCTG	CAGAACCCCTTGCAATTTTTTGTGATGTAAC
C461F	GCTGCAAGGGGTTCTTTATTGACATCCTTAA	TTAAGGATGTCAATAAAGAACCCCTTGACAGC
R540H	GTGTCATGGTGTACACAGCAATGGGACTGT	ACAGTCCCATTGCTGTGTGACACCATGACAC
R696H	CAGAGAGAAATATTCACAATAACTATGCAGA	TCTGCATAGTTATTGTGAATATTTCTCTCTG

HEK-293 cell culture, transfection, RNA extraction and cDNA synthesis

The transcription of all mutant plasmids was assessed and confirmed as follows. The plasmids with the WT and mutant *GRIN2A* and *GRIN2B* cDNAs contain a vector-derived chimeric intron after the CMV promoter sequence. In cells that express these cDNAs, the mature mRNA will have the intron spliced out. This provided a means to determine whether the plasmids could be transcribed. A primer pair was thus designed to yield two different sized PCR products (fig. 3.3): – a first sequence that included the intron, amplified from plasmid DNA (*GRIN2A* 439 bp, *GRIN2B* 477 bp)

- a second, shorter sequence that did not contain the intron, amplified from cDNA of the mature mRNA (*GRIN2A* 306 bp, *GRIN2B* 344 bp)

The forward primer annealed to the sequence after the CMV promotor but before the chimeric intron and the reverse primer annealed to the 5' end of the *GRIN2* coding sequence.

Forward primer 5'-AGCCTTGCAGAAGTTGGTCG-3'

GRIN2A Reverse primer 5'-TGTCACGTCGTGGCTGTGA-3'

GRIN2B Reverse primer 5'-TCGGAAGTGCCCACGAGGAT-3'

Presence of the shorter PCR product would indicate that the gene was being expressed at the transcription level.

For this purpose, HEK-293T cells were plated in 6-well plates and cultured for 48 hours at 37°C and 5% CO₂ in DMEM+ (supplemented with 10% foetal bovine serum (FBS) and 100 U/ml penicillin/streptomycin). The medium was changed two hours before cells were transfected using Polyethylenimine (PEI) (linear 250kDa, Polysciences, Cat. No. 24314-2, Machida et al., 2012). For one well of a 6-well plate, 2.3 µg/µl total plasmid DNA was added to 100µl DMEM- (no FBS or Pen/Strep). 4.8 µg/µl PEI was added to 100µl DMEM- in a separate tube. Both tubes were vortexed thoroughly and the PEI-DMEM- solution was added to the DNA-DMEM- solution dropwise and incubated for 15 minutes at room temperature. After the incubation, the DNA-PEI solution was added to the cells dropwise and cells were incubated at 37°C and 5% CO₂ for 6-8 hours.

The medium was then replaced with fresh DMEM+ with 100 µM 7-chlorokynurenic acid and 50 µM D-AP5. 48 hours after PEI transfection, RNA was extracted from HEK-293T cells using the Invitrogen PureLink® RNA Mini Kit (Cat. 12183018A). The extracted and purified RNA was then converted to cDNA with the Invitrogen SuperScript™ IV First-Strand Synthesis System (Cat. 18091050) using Oligo-d(T)₂₀ primers included in the kit. DNase I, Amplification Grade (1 unit/µL) (Cat. 18068-015) was used only in control experiments to remove plasmid DNA from the RNA sample and confirm the identity of bands on the gel at later steps.

After cDNA synthesis (with or without DNase treatment), a PCR was performed on the samples with WT or mutant cDNA. cDNA was quantified using Qubit ssDNA Assay Kit (Life Technologies, Q10212) with a Qubit 3.0 fluorometer (Life Technologies) and 14 ng was added as template for PCR. The PCR thermocycling conditions were as follows: Denaturation 94°C for two minutes, 30 cycles of denaturation, annealing and extension (94°C – 15s, 58.5°C – 30s, 74°C – 1 min, respectively) and a final extension at 74°C for 5 mins. PCR products were analysed on 2% agarose gel and imaged using DNR Bio-Imaging systems F-ChemiBIS 3.2M.

Slice preparation, SCE, and electrophysiological recordings

Hippocampal slice culture preparation and SCE were identical to the methods described in chapter 2 for *Grin2A*- and *Grin2B*-floxed mice, with the following exceptions:

- Rescue experiments had the addition of the WT GluN2A or GluN2B plasmid during the electroporation procedure, as well as the pLenti CMV Cre-eGFP.
- Mixed AMPAR and NMDAR recordings had the addition of the mutant GluN2A or GluN2B construct during the electroporation procedure, as well as the pLenti CMV Cre-eGFP.

For rescue experiments, electrophysiological recordings were also identical to those previously described (Ch2).

For mixed AMPAR- and NMDAR-mediated EPSCs (mutant experiments), the following alterations were made:

- 3mM QX314 was added to the intracellular solution to block sodium channels.
- 2 μ M CGP52432 was added to the ACSF solution that perfused the slice to block GABA_B receptors.
- NBQX was not included in the ACSF.
- EPSCs were recorded at the following holding potentials: -100, -40, 0 and 20 mV. At each holding potential, 10 EPSCs were recorded from patched neurons after a 20-40 V stimulation pulse of the Schaffer collaterals for 50 μ s, 10 s cycle time.

Recordings for mutant NMDAR responses were randomized and performed blind.

Statistical analysis

Recordings were discarded if the access resistance between two cells differed considerably (5-8 M Ω). Analysis including Stimfit 0.13 procedures, outlier tests, anovan (MLM) and multicomp in MATLAB 9.2 were also identical to those described in chapter 2 for rescue experiments.

For mixed AMPAR- and NMDAR-mediated EPSCs (mutant experiments), averaged current traces were converted to conductance traces in Stimfit 0.13 using a custom python module available at <https://github.com/acp29/penn/blob/master/analysis.py>. To obtain the NMDAR component from the mixed traces, the conductance of the -100 mV trace (assumed to be solely AMPAR conductance) was subtracted from the conductance traces at all other holding potentials (since GluA2-containing AMPARs have a linear current-voltage relationship and so should have the same conductance at each holding potential). Note that even GluA2-lacking AMPARs should have a near linear I-V relationship since no spermine was included in the patch pipettes and

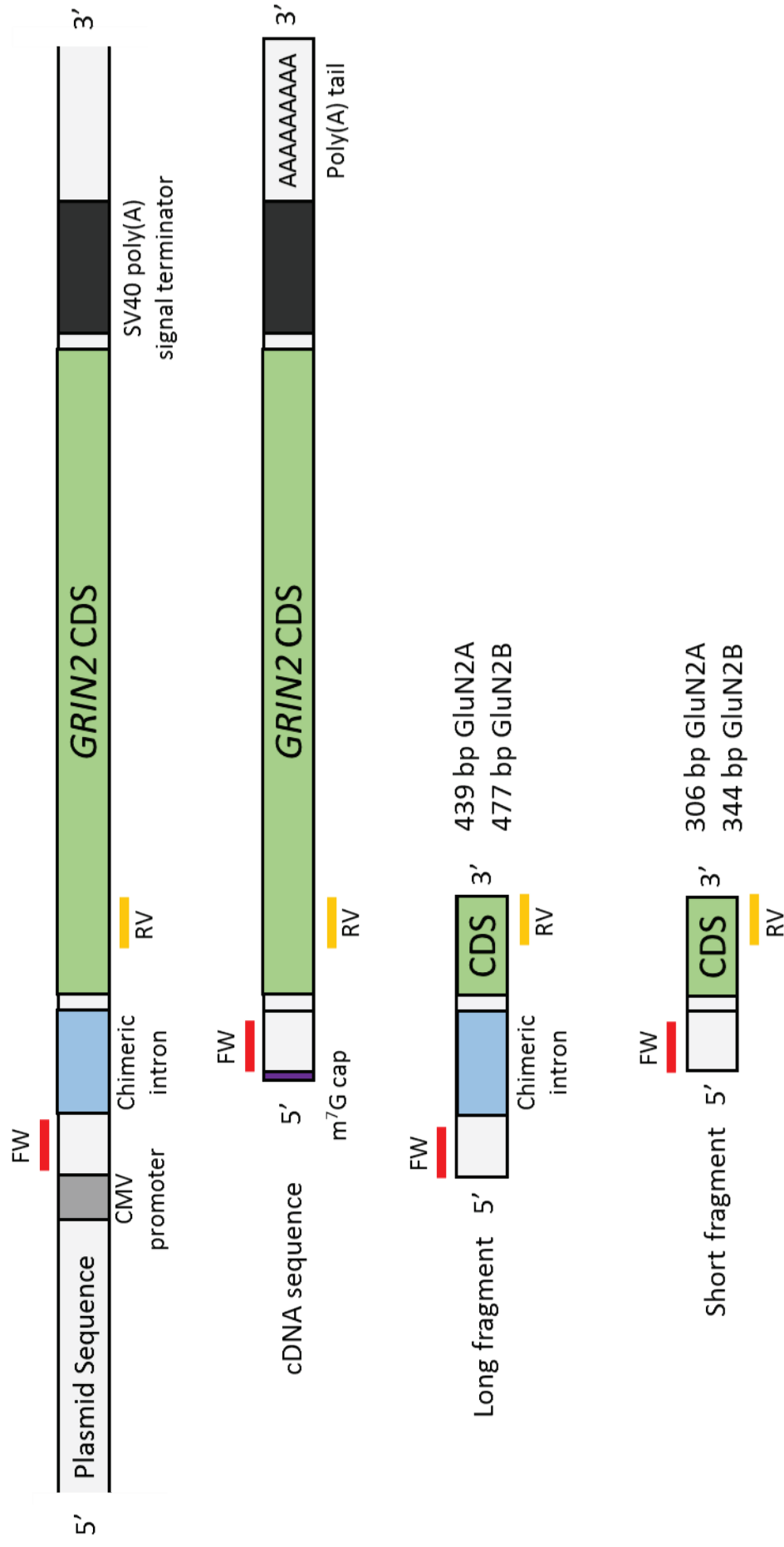


Figure 3.3: Location of primers annealing to pCI-Neo GRIN2 constructs.

Primers anneal before and after chimeric intron sequence in plasmid DNA, amplifying the 'long fragment'. In the cDNA, the sequence does not contain the chimeric intron due to splicing; PCR amplification produces the 'short fragment'. FW, forward; RV, reverse; CMV, cytomegalovirus; CDS, coding sequence.

endogenous spermine is washed out during whole-cell recording (Rozov et al., 2012). This method was chosen, as opposed to the alternative method of measuring the amplitude at +40 ms where AMPAR responses would have seized, as the mutants could potentially affect the NMDAR decay, and so the amplitude at +40 ms would be inaccurate. τ_w , peak amplitude and charge transfer values were taken for the AMPAR current traces at -100 mV and for the NMDAR conductance at +20 mV. Peak amplitudes were also taken for the NMDAR conductance at -40 mV for calculation of the rectification indices which measure the relative contribution of responses at negative and positive holding potentials and can be used as an indirect measure of mutants on the magnesium block of NMDARs. This was calculated by: the peak amplitude at -40 mV divided by the peak amplitude at +20 mV.

Outlier detection

ROBPCA analysis was performed as described in chapter 2. For rescue experiments, the procedure was identical to the outlier tests in chapter 2. For mutant experiments, the variables used were: WCPs, NMDAR peak amplitude, decay, charge, AMPAR peak amplitude, decay, charge, AMPAR 20-80% rise time, AMPAR/NMDAR ratio, latency of AMPAR peak, latency of beginning of AMPAR event and baseline at -100 mV. These extra variables were included because of the addition of the AMPAR component to these recordings, which was not present for the KO or rescue experiments.

Latency of the AMPAR peak measures the time between the stimulation (the stimulus artefact) and the peak of the AMPAR current. Latency of beginning of AMPAR event measures the time between stimulation and the onset of AMPAR current. These were obtained in Stimfit 0.13.

Relative values (the log ratio of transfected/untransfected) were calculated for all features and absolute values (log average (transfected + untransfected)) were also calculated for all features except for peak amplitudes and charge, AMPAR/NMDAR ratio and baseline at -100 mV. Peak amplitudes and charge were not included in absolute values because they depend on the stimulation. AMPAR/NMDAR ratio was not included because this is already a relative value.

There were 14 relative and absolute values for rescue data and 24 for mutant data. The ROBPCA was run in MATLAB 9.2. As previously mentioned, the number of PCs used was the number that explained 90% of the variance. The output produced is a plot which showed the outlier values. These values were excluded from the dataset for further statistical analyses.

Hypothesis testing

Analyses were performed on log-transformed data. A nested ANOVA was performed in MATLAB 9.2 as in chapter 2 for both rescue and mutant experiments. p values were adjusted for multiple

comparisons with MATLAB 9.2 using multicmp Holm-Bonferroni method (<https://uk.mathworks.com/matlabcentral/fileexchange/61659-multicmp>). p values of all six variables (+20 mV peak and decay, -40 mV peak, AMPAR peak and decay, and RI) were adjusted for each mutant separately (a MC test was performed for each mutant: each row of table 3.3). $p < 0.05$ was considered to be significant.

Results

To be able to examine the effects of *human* missense mutations on synaptic transmission, it was necessary to establish whether WT human GluN2 subunits are capable of rescuing NMDAR-EPSCs in the respective mouse GluN2 KO. A rescue was first attempted of the GluN2A and GluN2B homozygous KOs in mice with human WT GluN2A or GluN2B. It was also necessary to establish the concentration of GluN2A and GluN2B required for this effective molecular replacement. The homozygous genetic manipulation was chosen instead of heterozygous due to the much larger effect sizes observed with the homozygous KOs in chapter 2. This allowed the use of smaller sample sizes and therefore, more ethically, fewer animals for the experiments.

Table 3.2: transfected/untransfected ratio of peak amplitudes and decay time constants for the range of WT GluN2A and GluN2B concentrations tested for rescue of KO.

[ng/μl]	[nM]	Transfected/Untransfected Ratio (Mean ± SEM)				
[GluN2A]		Peak amplitude	Decay	n	slices	animals
1.1	0.2	0.74 ± 0.08	1.69 ± 0.18	9	5	1
3.3	0.5	0.95 ± 0.07	1.29 ± 0.13	14	6	2
3.8	0.6	1.12 ± 0.14	1.08 ± 0.10	15	8	3
4.4	0.7	1.00 ± 0.09	0.80 ± 0.05	15	7	2
5.6	0.9	0.68 ± 0.10	0.79 ± 0.05	16	9	2
10.9	1.7	0.93 ± 0.10	0.81 ± 0.06	16	6	2
[GluN2B]						
3	0.4	0.82 ± 0.08	0.88 ± 0.07	14	7	2
10	1.5	0.82 ± 0.11	1.11 ± 0.08	16	8	3

GluN2A Rescue

CA1 hippocampal neurons in organotypic slice culture from *Grin2A*-flox mice were co-transfected with Cre-GFP and human WT GluN2A. Multiple rescue experiments were performed with varying WT GluN2A concentrations and the simultaneous postsynaptic responses (NMDAR-

EPSCs) from stimulation of the Schaffer collateral pathway were compared between transfected and untransfected neurons.

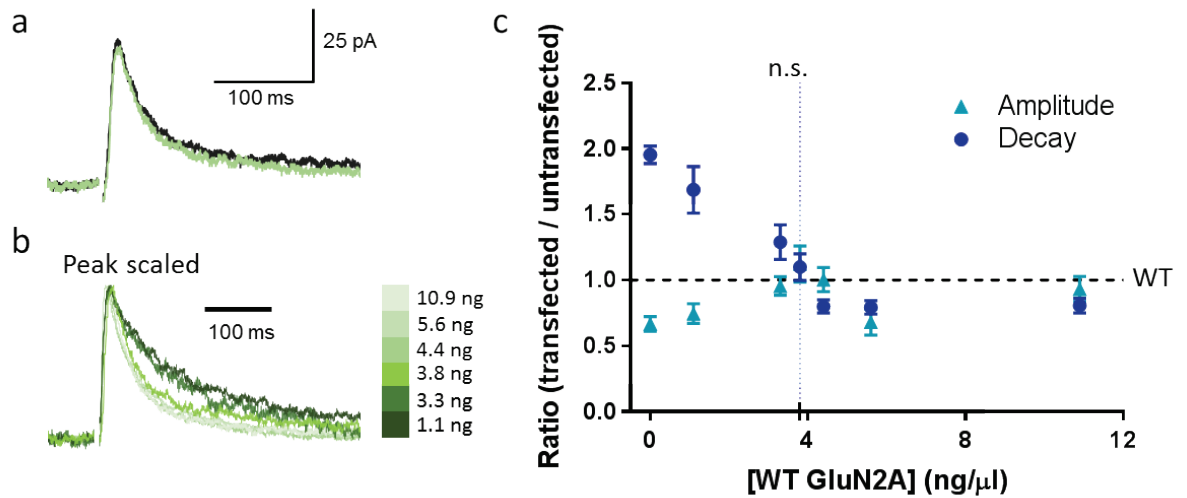


Figure 3.4: NMDAR-mediated currents are very sensitive to the amount of GluN2A transfected into CA1 neurons.

a) NMDAR currents from untransfected (black) and transfected (green) neurons with 3.8 ng/μl GluN2A which successfully rescued responses. b) Peak scaled NMDAR responses from the range of GluN2A concentrations tested which shows the changes in decay at each concentration. c) Plot of amplitudes and decays of GluN2A concentrations tested, mean and SEM shown. n.s., non-significant.

It was found that human WT GluN2A could successfully rescue NMDAR-EPSC decay and peak amplitude in mouse KO when cells were electroporated using intracellular solution containing 3.8 ng/μl (0.62 nM) pCI-Neo WT *GRIN2A* (peak mean \pm within-subjects SEM: untransfected 97.38 ± 7.78 pA, transfected 85.55 ± 7.78 pA, $p = 0.2998$, paired t-test, decay mean within-subjects SEM: untransfected 85.01 ± 6.85 ms, transfected 93.55 ± 6.85 ms, $p = 0.3919$, charge mean \pm within-subjects SEM: untransfected 8.52 ± 0.82 pC, transfected 8.47 ± 0.82 pC, $p = 0.9653$) (fig. 3.4a,c). Interestingly, the NMDAR-EPSC decay was especially sensitive to the amount of WT GluN2A transfected, where small differences in the concentration resulted in large effects on the kinetics of current decay (fig. 3.4b, table 3.2). The decay time decreased in transfected cells with increasing GluN2A concentrations (from ~ 1 to ~ 4.5 ng/μl), consistent with the idea that GluN2B dominates at the synapse with absent or low GluN2A levels (to produce NMDARs with slow EPSCs) and as the concentration of GluN2A increases (which increases GluN2A incorporation at the synapse), the decay becomes less slow as GluN2A-containing NMDARs have faster currents. At concentrations above ~ 4.5 ng/μl, there was no further change in the decay

and it remained constant (table 3.2, fig. 3.4c), suggesting that there is a limit to the amount of GluN2A that can be inserted at the synapse.

GluN2B Rescue

Neurons from *Grin2B*-flox mice transfected with Cre-GFP and 10 ng/ μ l (1.57 nM) WT GluN2B resulted in a successful rescue; NMDAR-EPSCs were not significantly different from control untransfected cells (peak mean \pm within-subjects SEM: untransfected 100.78 ± 9.40 pA, transfected 72.57 ± 9.40 pA, $p = 0.0509$, paired t-test, decay mean within-subjects SEM: untransfected 95.15 ± 4.64 ms, transfected 106.00 ± 4.64 ms, $p = 0.1191$, charge mean \pm within-subjects SEM: untransfected 8.95 ± 0.84 pC, transfected 6.99 ± 0.84 pC, $p = 0.1210$) (fig. 3.5). To assess whether currents were also sensitive to the amount of GluN2B transfected, 3 ng/ μ l WT GluN2B was also examined. In contrast to GluN2A, NMDAR-EPSC decay was not observed to be as affected by the amount of GluN2B transfected. Both 3 ng/ μ l and 10 ng/ μ l produced a successful rescue of GluN2B decay time (3 ng/ μ l paired t-test, peak $p = 0.0744$, decay $p = 0.1489$, charge $p = 0.0744$) (fig 3.5a, b), and responses were not significantly different to each other (unpaired t-test, peak $p = 0.4036$, decay $p = 0.077$). This may be a result of GluN2B having occupied all available positions at the synapse and increasing the amount of GluN2B could not cause any further incorporation. It is possible that in transfected cells decays may be faster and resemble the GluN2B KO at lower concentrations of GluN2B cDNA. However, currents slower than untransfected cells do not seem likely as both 3 and 10 ng/ μ l concentrations of GluN2B produced decay similar to untransfected cells. This is unlike GluN2A where the decay time constant in untransfected neurons was approximately midrange of the decay time constants measured across the GluN2A concentrations tested, and was at the steepest part of the relationship between GluN2A concentration and transfected cell decay time constants. This suggests a capability of adding GluN2A into the synapse at levels higher than there normally would be, but this may not be possible for GluN2B.

Mutant RNA expression

After successfully rescuing NMDAR currents with human GluN2A or GluN2B in the corresponding GluN2 subunit KO, selected human mutations (see methods) were cloned into the pCI-Neo *GRIN2A* or *GRIN2B* plasmids using site directed mutagenesis and the mutation and integrity of the remaining coding sequence was confirmed by DNA sequencing. The *GRIN2A* mutations generated were GOF L812M, K669N and LOF C436R, T531M, R518H and I694T. *GRIN2B* mutations were GOF R540H, R696H and LOF C461F, C456Y and C436R (see fig. 3.2).

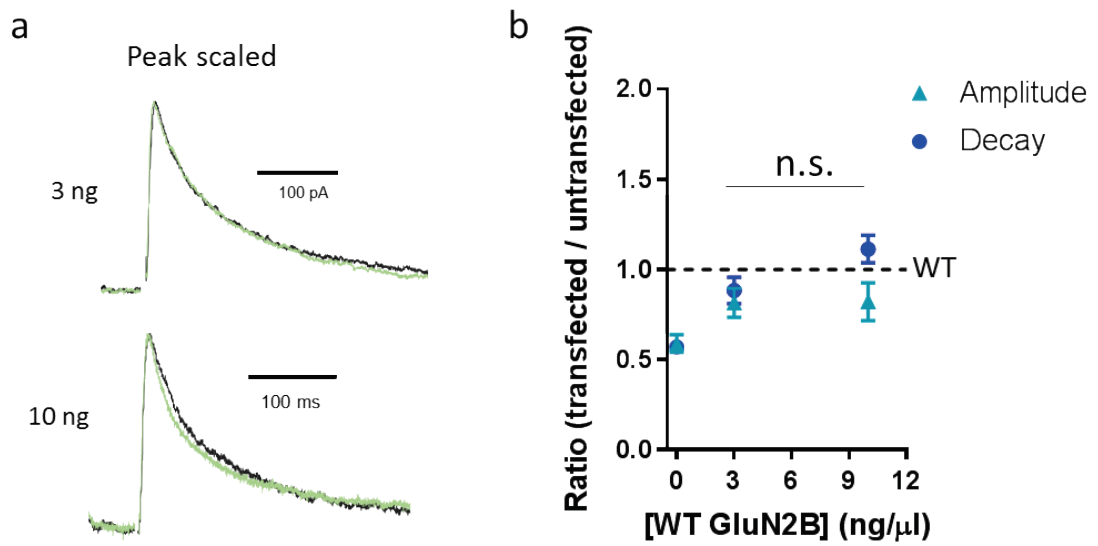


Figure 3.5: Neurons show saturation with the amount of GluN2B that can be incorporated into the synapse at concentrations tested.

a) Representative peak scaled current traces from untransfected neurons (black) and transfected neurons (green) with 3 and 10 ng/μl GluN2B. b) Plot of amplitudes and decays of GluN2B concentrations used, mean and SEM shown. n.s., non-significant.

Although the coding sequence and untranslated regions of the *GRIN2* cDNAs appeared as expected by DNA sequencing, it is possible that PCR errors elsewhere in the plasmid may perturb transcription of the cDNA. To ensure that these mutant constructs were capable of being transcribed, the polyadenylated mRNA levels were examined using RT-PCR when mutant plasmids were transfected into HEK-293T cells as a verification of successful transcription. The pCI-Neo *GRIN2A* WT, pCI-Neo *GRIN2B* WT and mutant plasmids all contain a chimeric intron after the CMV promoter which enabled an assay for detection of the mature mRNA as the chimeric intron would be spliced out during mRNA processing (fig. 3.3). RNA extracted from HEK-293 cells transfected with WT or mutant GluN2 was converted to cDNA (without DNase I treatment) and RT-PCR products were run on an agarose gel. This showed two bands, a band that corresponded to the size of plasmid DNA (containing the chimeric intron) and a second band, which corresponded to the size of an amplicon of the mature mRNA (without the intron). For *GRIN2A* constructs, the plasmid and cDNA bands were 439 and 306 bp, respectively. For *GRIN2B* constructs, the plasmid band was 477 bp and the cDNA was 344 bp (fig. 3.6a). Different sized bands were produced for *GRIN2A* and *GRIN2B* due to a different reverse primer that was used for each construct. A third (much weaker) band was also present in all *GRIN2A* and *GRIN2B* constructs that got weaker but persisted with DNase I (amplification grade) digestion (fig. 3.6b),

so it was uncertain whether this was plasmid DNA or transcript or a combination. The cDNA band was detected for all the mutants, indicating that all constructs were being transcribed and the pre-mRNA processed into its mature form (fig 3.6c,d). Overall, this indicated that the integrity of mutant construct transcription is unaffected and that any defects we may observe will be at the level of the protein.

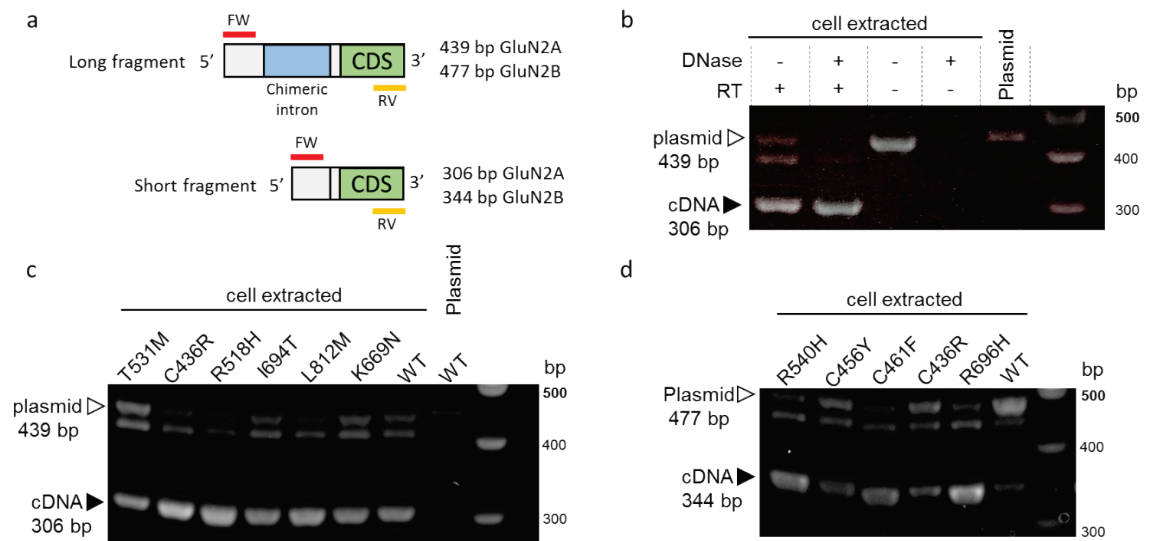


Figure 3.6: Mutant constructs are all expressed at the mRNA level.

a) Fragments generated from amplification of the plasmid DNA (long fragment) and cDNA (short fragment), CDS, coding sequence. b) Plasmid and cDNA bands with and without DNase and reverse transcriptase (RT) treatment. c,d) Short and long fragments for GluN2A and GluN2B mutants, respectively. Data from 3 experiments.

Synaptic Phenotypes of GluN2A and GluN2B mutations

All electrophysiological experiments shown so far in this and in the previous chapter were performed with the voltage clamped at +20 mV and currents recorded were isolated NMDAR-EPSCs. In the next series of experiments shown in this chapter, a mixed current mediated by both AMPAR and NMDARs was recorded at four different holding potentials (-100, -40, 0, +20 mV) to examine the wider possible impacts of GluN2A and GluN2B mutations on basal synaptic transmission. Excitatory postsynaptic currents were recorded from CA1 pyramidal neurons after stimulation of the Schaffer collateral pathway, as previously described. To isolate the NMDAR component from each current trace, the AMPAR conductance was subtracted from the mixed AMPAR+NMDAR conductance, as the AMPAR conductance can be assumed to be approximately the same at all holding potentials (linear I-V curve and no spermine used in patch pipette) (fig

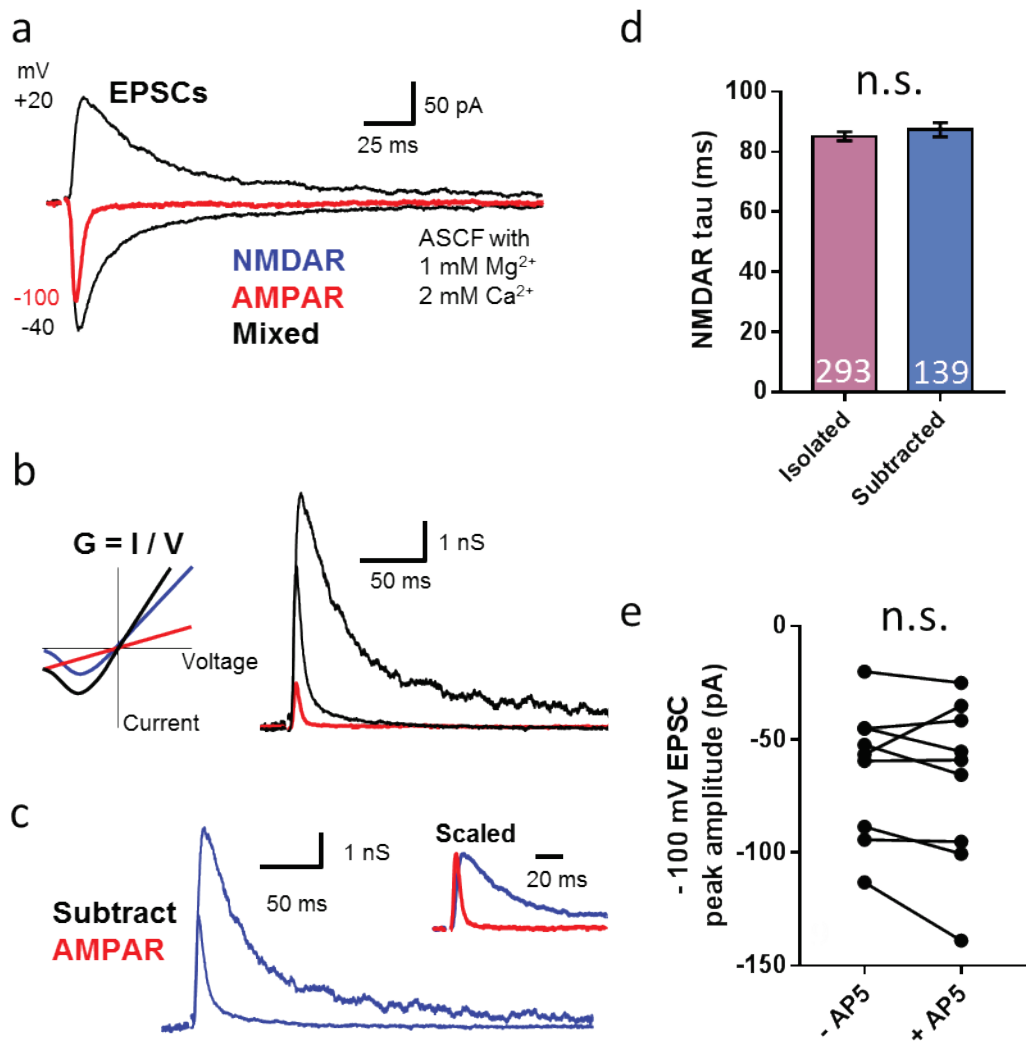


Figure 3.7: NMDAR conductances are isolated from mixed AMPAR/NMDAR conductances by subtraction of AMPAR conductance.

a) representative traces of mixed EPSCs recorded at -100, -40 and +20 mV. b) currents are converted to conductances using $G = I/V$. c) assuming a linear I/V relationship for AMPAR, the AMPAR conductance is subtracted from the mixed AMPAR/NMDAR conductance to produce NMDAR conductance. d) NMDAR decay from isolated NMDAR-EPSCs recorded in the presence of AMPAR blocker NBQX compared to NMDAR decay using subtraction method of a-c. e) peak amplitude of EPSCs at -100 mV before and after addition of NMDAR blocker AP5 (100 μM). n.s., non-significant.

3.7a,b,c) (Boulter et al., 1990). AMPAR currents and NMDAR conductances were compared between mutant-transfected and WT untransfected cells. To confirm that the NMDAR decay was not disrupted with this subtraction procedure, the NMDAR decays in untransfected neurons were compared between the conditions of pharmacologically isolating NMDAR currents (using 10 μM NBQX, 50 μM picrotoxin and 10 μM gabazine) to those obtained through subtraction of the AMPAR conductance (ACSF did not include AMPAR blocker NBQX). There was no significant

Table 3.3: Electrophysiological properties of GluN2A and GluN2B mutants

GluN2	+ 20 mV NMDAR		- 40 mV NMDAR		AMPA		RI (-40 mV / +20 mV)
	Peak Amplitude (pA)	Decay (ms)	Peak Amplitude (pA)	Decay (ms)	Peak Amplitude (pA)	Decay (ms)	
GluN2A WT	0.96 ± 0.12	1.10 ± 0.10					
GluN2A KO	0.64 ± 0.08****	1.88 ± 0.09****					
K669N	0.91 ± 0.11	1.62 ± 0.24	1.18 ± 0.16		1.13 ± 0.21	1.09 ± 0.07	1.30 ± 0.15
L812M	0.67 ± 0.06***	1.55 ± 0.17**	1.03 ± 0.12		0.84 ± 0.11	1.68 ± 0.27	1.68 ± 0.22#
T531M	0.72 ± 0.06**	1.93 ± 0.14****	0.58 ± 0.06#		1.10 ± 0.10	1.26 ± 0.19	0.78 ± 0.09
C436R	0.77 ± 0.12*	1.88 ± 0.15****	0.71 ± 0.15		1.26 ± 0.21	1.25 ± 0.29	0.92 ± 0.10
R518H	0.71 ± 0.08**	1.81 ± 0.11****	0.74 ± 0.12		1.27 ± 0.21	0.96 ± 0.08	1.06 ± 0.13
I694T	0.76 ± 0.06*	1.18 ± 0.15	0.74 ± 0.09		1.17 ± 0.20	0.98 ± 0.08	1.02 ± 0.09
GluN2B WT	0.85 ± 0.12	1.11 ± 0.08					
GluN2B KO	0.60 ± 0.05****	0.58 ± 0.03****					
C461F	0.95 ± 0.18	0.58 ± 0.14****	0.63 ± 0.07		0.88 ± 0.14	1.13 ± 0.10	0.93 ± 0.17
C456Y	0.87 ± 0.10	0.49 ± 0.05****	0.74 ± 0.08		1.39 ± 0.27	0.92 ± 0.08	0.95 ± 0.12
C436R	0.83 ± 0.09	0.37 ± 0.06****	0.82 ± 0.15		0.85 ± 0.12	1.0 ± 0.05	0.98 ± 0.14
R540H	0.86 ± 0.15	0.70 ± 0.08**	1.07 ± 0.22		1.19 ± 0.22	0.94 ± 0.08	1.60 ± 0.33
R696H	0.78 ± 0.07*	0.70 ± 0.10*	0.87 ± 0.14		1.35 ± 0.29	0.98 ± 0.05	1.20 ± 0.21

Ratio of Transfected/Untransfected. Values are Mean ± SEM. MLM* $p < 0.05$, ** $p < 0.01$, *** $p < 0.001$, **** $p < 0.0001$. Paired t-test # $p < 0.05$.

p values adjusted for multiple comparisons with MATLAB 9.2 multcomp, Holm-Bonferroni. p values of all six variables (+20 mV peak and decay, -40 mV peak, AMPAR peak and decay, and Rectification Index (RI)) were adjusted for each mutant separately (a MC test was performed for each mutant: each row of the table).

difference in the NMDAR decays between the two conditions (unpaired t-test, $p = 0.4289$, pharmacologically isolated NMDAR-EPSC $n = 293$, conductance subtracted $n = 139$) (fig. 3.7d). To further justify the procedure, synaptic currents were also recorded at -100 mV before and after the addition of NMDAR blocker D-AP5 (100 μ M), and there was no difference in current amplitude (paired t-test $p = 0.3250$) (fig. 3.7e), confirming that no NMDAR current was subtracted off in the procedure.

GluN2A GOF mutations

Expression of GluN2A GOF mutations K669N and L812M altered the properties of typical evoked EPSCs and showed some dissimilarities to each other. There was no difference in the NMDAR-EPSC peak amplitude at $+20$ mV for K669N compared to WT, and L812M expressing neurons had NMDA-EPSCs with lower NMDAR peak amplitude (fig. 3.8a,c, table 3.3), resembling more the current amplitude of GluN2A KO. The decay of the NMDAR response was prolonged for both GOF mutants (~ 1.5 times slower than WT NMDARs) (fig 3.8b,d, table 3.3), suggesting that receptor activity that was aberrantly sustained, albeit to a lesser extent than the decay of GluN2B-only NMDARs in the GluN2A KO. However, the prolonged decay for K669N was no longer significant after correcting for multiple comparisons (MCs) (see methods and table 3.3; Appendices E and F for unadjusted and adjusted p values, respectively).

The rectification index (RI) of NMDAR peak amplitudes ($G_{-40\text{ mV}} / G_{+20\text{ mV}}$) was measured to identify any possible alterations to current ratios between mutant and untransfected neurons at different holding potentials where the magnesium blockade of the NMDAR would normally differ. Changes in the ratios of peak amplitudes at -40 mV to $+20$ mV would indicate altered current flow through the receptor compared to WT, which could suggest that mutants may change the degree of magnesium block at the channel pore. There was no significant deviation in the rectification index for K669N (fig. 3.8e, table 3.3), suggesting it did not alter the magnesium block of the channel pore, and the currents at -40 mV were similar to untransfected neurons. However, L812M was found to have an increased rectification index compared to NMDAR-EPSCs in untransfected neurons (fig. 3.8e, table 3.3), indicating that there are larger currents at negative holding potentials compared to positive potentials. Previous work on L812M has also found this effect with expression in *Xenopus* oocytes (Yuan et al., 2014). To see whether this enhanced rectification index reflected enhanced current at negative holding potentials and therefore reduced magnesium block, the peak amplitudes were compared at -40 mV between L812M-transfected and neighbouring untransfected neurons. There was no significant difference in the peak amplitudes at -40 mV (fig. 3.8g, table 3.3), indicating that although the currents were greater when normalised to the $+20$ mV conductance, the increased

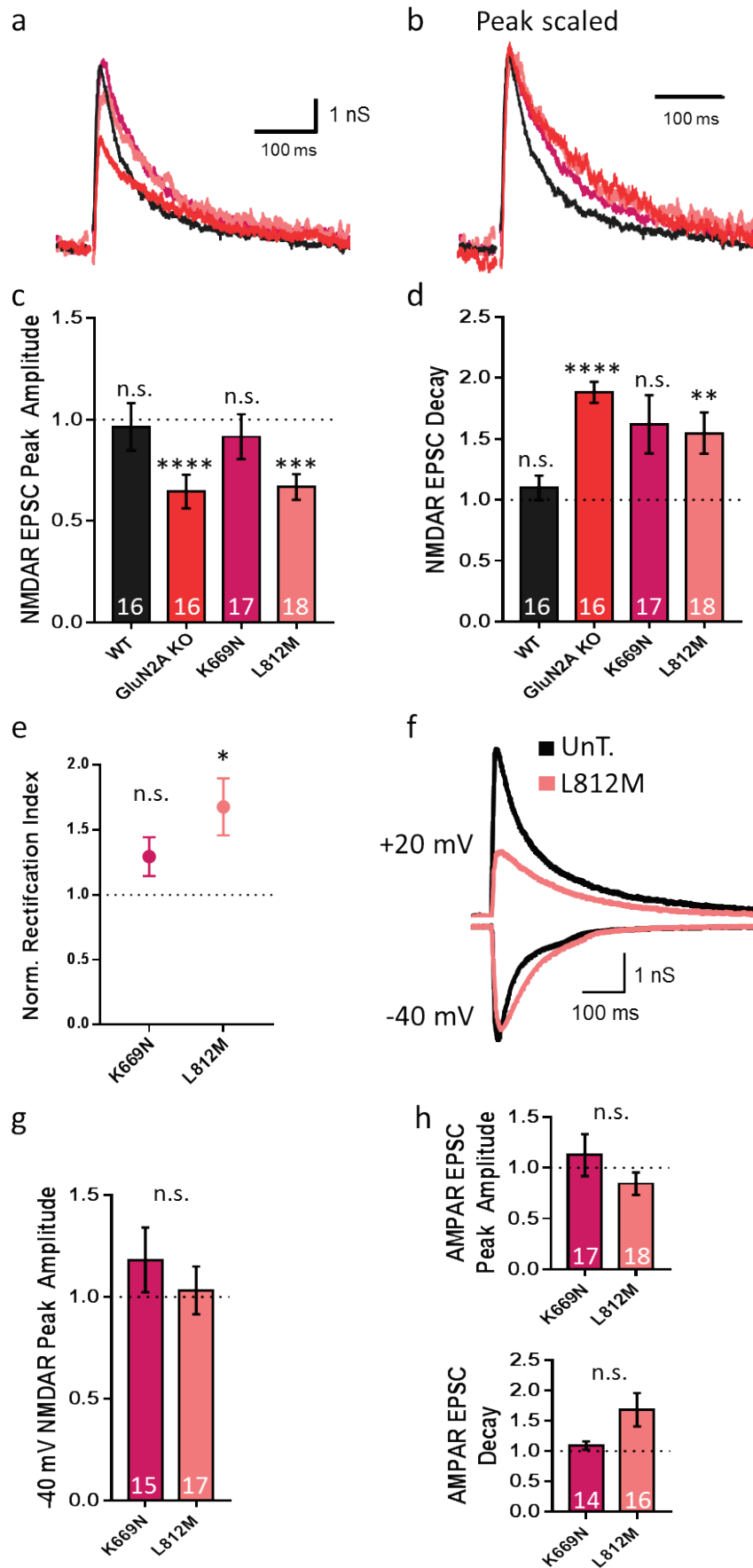


Figure 3.8: GluN2A GOF mutations produce prolonged NMDAR decay at depolarised potentials.

a) Representative NMDAR traces from GluN2A GOF mutations and untransfected (black). b) Peak scaled traces demonstrating prolonged decay time. c) NMDAR peak amplitude ratio of transfected/untransfected of mutants compared to WT and GluN2A KO. d) NMDAR decay ratio of transfected/untransfected of mutants compared to WT and GluN2A KO. e) Normalised rectification index of GOF mutants (-40 mV / +20 mV, normalised to untransfected). f) Representative traces of GOF mutants at -40 mV and +20 mV. g) Peak amplitudes of GOF mutants at -40 mV. h) Peak amplitudes and decays of GOF mutants at -100 mV (AMPA mediated). Data from 3 mice for K669N and 4 mice for L812M.

RI was actually due to the reduced amplitude at +20 mV only (fig. 3.8f). Studies that describe relative currents at negative potentials versus positive potentials (i.e. rectification indices) have not reported the actual currents observed at depolarised potentials for mutants vs WT (Pierson et al., 2014, Yuan et al., 2014). Although the peak amplitudes of L812M NMDAR-EPSCs are similar to untransfected cells at -40 mV, because the decay kinetics are slower, the overall conductance (using the integral) is actually enhanced (mean \pm SEM: untransfected 644.49 ± 146.53 pS.ms, transfected 832.31 ± 184.06 pS.ms, $p = 0.0196$). As predicted by the rectification index, K669N-transfected neurons had peak amplitudes (at either holding potential) that were not significantly different to untransfected (fig. 3.8g, table 3.3).

Since NMDARs are key regulators of synaptic AMPAR content and function, AMPAR-EPSC properties were also assessed. No changes were found in AMPAR peak currents for K669N or L812M, and the decay of AMPAR-EPSCs with the K669N mutant was also not altered (fig. 3.8h, table 3.3). However, L812M-transfected neurons had a slower decay of AMPAR-EPSCs (~1.7 fold slower decay), although this did not survive correction for MCs (fig. 3.8h, table 3.3). This raises the question of whether there may be some small NMDAR component contaminating the AMPAR current at -100 mV. However, since the current at -100 mV is still very brief compared to the currents at +20 mV, this would likely have very little effect on the subtraction method to obtain pure NMDAR conductance traces.

In summary, L812M resulted in slower NMDAR-EPSC decays but produced smaller NMDAR currents at positive holding potentials. At these depolarised potentials, the net effect is ambiguous as slower responses are a GOF whereas the reduced amplitude is a LOF. However, neurons will not likely spend much time at extremely depolarised potentials and will more likely be at a more physiologically relevant potential such as -40 mV. At this potential, a GOF effect is seen as although the peak amplitudes are similar to untransfected cells, the charge is enhanced due to the slower decay kinetics of L812M mutant GluN2A NMDARs. K669N also

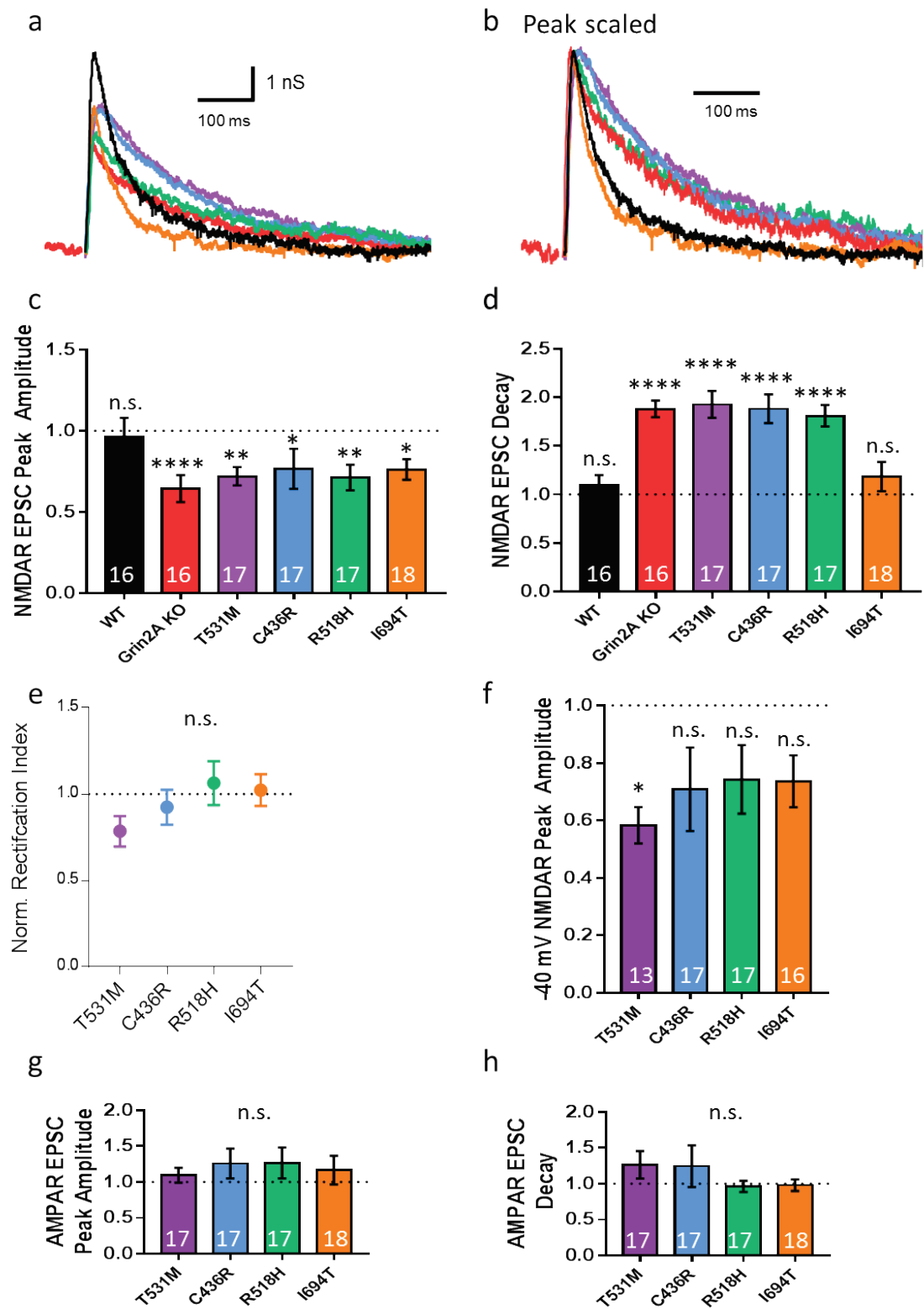


Figure 3.9: GluN2A LOF mutations produce prolonged NMDAR decay at depolarised potentials.

a) Representative NMDAR traces from GluN2A LOF mutations and untransfected (black). b) Peak scaled traces demonstrating prolonged decay time. c) NMDAR peak amplitude ratio of transfected/untransfected of mutants compared to WT and GluN2A KO. d) NMDAR decay ratio of

transfected/untransfected of mutants compared to WT and GluN2A KO. e) Normalised rectification index of LOF mutants (-40 mV / +20 mV, normalised to untransfected). f) Peak amplitudes of LOF mutants at -40 mV. g) AMPAR-EPSC peak amplitudes of LOF mutants h) AMPAR-EPSC decays of LOF mutants. Data from 3 mice for T531M, 6 for C436R, and 4 mice for R518H and I694T.

showed slower NMDAR decay at +20 mV (although no longer significant) and maintained its amplitude. However, overall, the charge transfer was unchanged (Appendix G).

GluN2A LOF mutations

All GluN2A LOF mutations studied – T531M, C436R, R518H and I694T – had a reduced NMDAR peak amplitude that was similar to the response in the GluN2A KO (fig. 3.9a,c, table 3.3). T531M, C436R and R518H also phenocopied the GluN2A KO with respect to the decay of the NMDAR response, which was approximately doubled in both KO and mutant conditions compared to untransfected (fig. 3.9b,d, table 3.3). Thus, an enhanced NMDAR function was observed, despite these mutations having only ‘LOF’ effects in heterologous expression systems. However, NMDAR decay was not altered with the I694T mutation as it was not significantly different to NMDAR decay in untransfected neurons (fig. 3.9b,d, table 3.3).

The rectification index of NMDAR peak amplitudes ($G_{-40\text{ mV}} / G_{+20\text{ mV}}$) was reduced for T531M, suggesting that the conductance at -40mV is even lower than the diminished peak amplitude at +20 mV; however, this did not survive correction for MCs. There was no significant change in the rectification index for the remaining LOF GluN2A mutations (fig. 3.9e, table 3.3, Appendix H). This index suggested that an equivalent reduction in peak amplitude was present at negative holding potentials to that seen at +20 mV. To confirm this, the -40 mV NMDAR peak amplitudes of mutant-transfected vs untransfected were compared (fig. 3.9f, table 3.3) and showed an agreement with this index; amplitudes were reduced at -40 mV, although not significantly for C436R, R518H and I694T after correction for MCs. This indicated that NMDAR dysfunction was present and equivalent at both positive and negative holding potentials, in contrast to the GluN2A GOF mutation L812M which appeared to show reduced amplitudes only at positive holding potentials.

Finally, the AMPAR currents were assessed from mutant vs untransfected neurons and no significant differences were present in the AMPAR current amplitude or decay for LOF GluN2A mutants (fig. 3.9g,h, table 3.3), indicating preserved AMPAR function, even with conditions that are thought to mimic GluN2A KO.

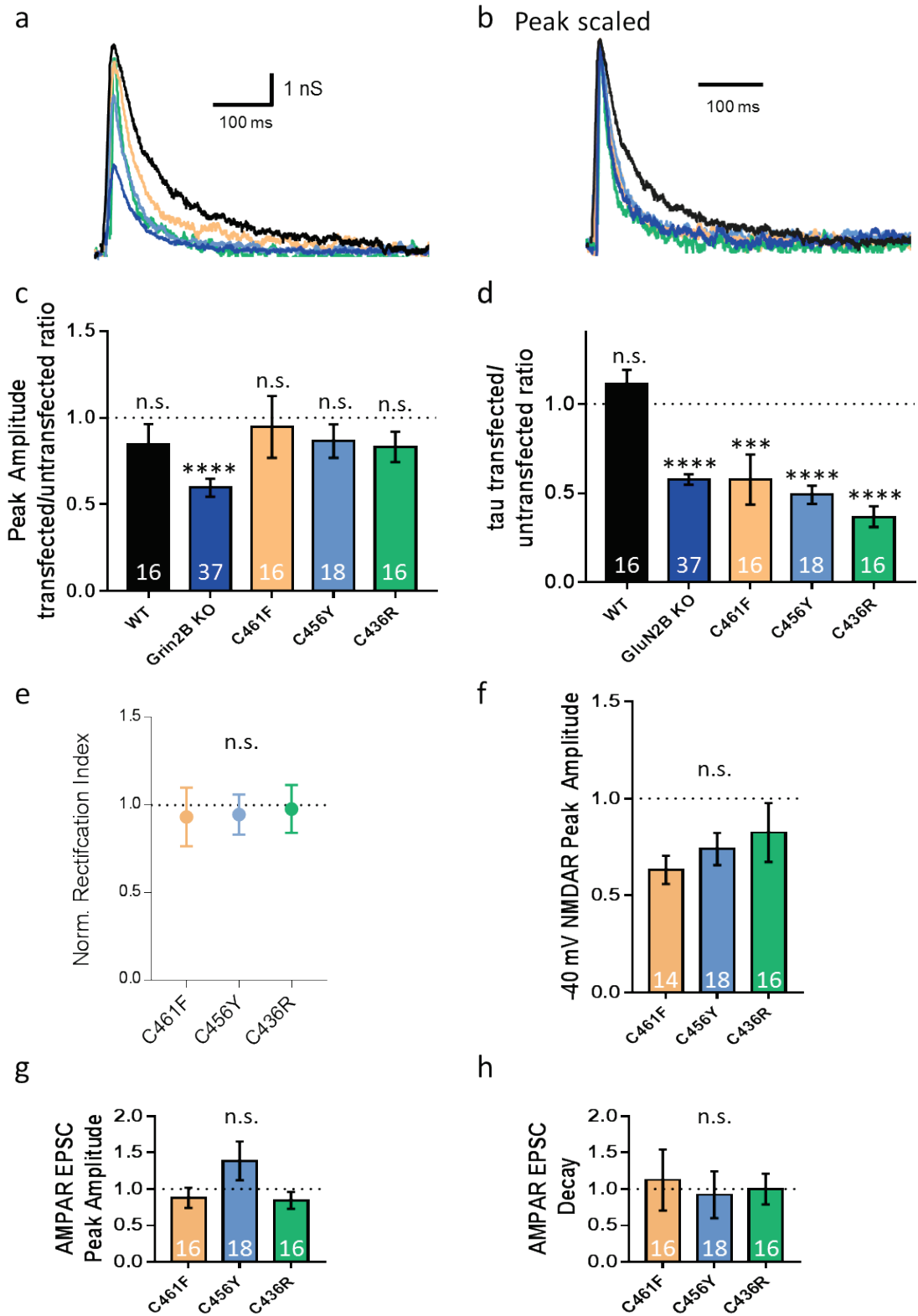


Figure 3.10: GluN2B LOF mutations produce brief NMDAR decay at depolarised potentials.

a) Representative NMDAR traces from GluN2B LOF mutations and untransfected (black). b) Peak scaled traces demonstrating faster decay time. c) NMDAR peak amplitude ratio of transfected/untransfected of mutants compared to WT and GluN2B KO. d) NMDAR decay ratio of transfected/untransfected of mutants compared to WT and GluN2B KO. e) Normalised rectification index of LOF mutants (-40 mV / +20 mV, normalised to untransfected). f) Peak amplitudes of LOF mutants at -40 mV. g) AMPAR-EPSC peak amplitudes of LOF mutants h) AMPAR-EPSC decays of LOF mutants. Data from 3 mice for C461F, 6 for C456Y, and 3 mice for C436R.

GluN2B LOF mutations

GluN2B LOF mutants were expected to phenocopy the responses of GluN2B KO as all three mutants were predicted to abolish GluN2B expression, however, C461F produced similar NMDAR peak amplitudes as WT and the peaks for C456Y and C436R were not significantly different to WT after correction for MCs (fig. 3.10a,c, table 3.3). However, the decay time constant was significantly reduced for all these mutants (fig. 3.10b,d, table 3.3), resulting in currents that resembled the brief-decaying characteristic of a GluN2A-only population. Remarkably, for C436R, the decay was even slower than in the GluN2B KO.

The rectification index suggested no differences in the NMDAR peak amplitudes at positive and negative holding potentials for all LOF GluN2B mutations (fig. 3.10e, table 3.3, Appendix H). In agreement, currents at -40 mV were also not significantly different to untransfected neurons (fig. 3.10f, table 3.3). Thus, unlike the LOF GluN2A mutants which had altered peak amplitudes at both positive and negative holding potentials and reflected the synaptic phenotype of a loss of GluN2A, GluN2B LOF mutants appear to produce a more complex result than a simple loss of the GluN2B subunit.

Gray et al. (2011) showed that homozygous null alleles of GluN2B increased evoked AMPAR-mediated EPSCs. Here, AMPAR-mediated currents were unaffected by LOF GluN2B mutations (fig. 3.10g,h, table 3.3), again producing an unexpected result as mutants which mimic a loss of GluN2B were anticipated to impact AMPAR function or expression.

GluN2B GOF mutations

No GOF effects were seen on the peak amplitudes of GluN2B GOF mutations R540H and R696H; the peak was unaffected with R540H (not significant after MC correction) and was actually reduced with R696H (fig. 3.11a,c, table 3.3). Most unexpectedly, the NMDAR decay properties from mutants transfected into hippocampal neurons show stark contrasts to the NMDAR properties observed when GluN2B GOF mutants were overexpressed on their own in heterologous systems. In these heterologous systems, R540H and R696H showed NMDAR

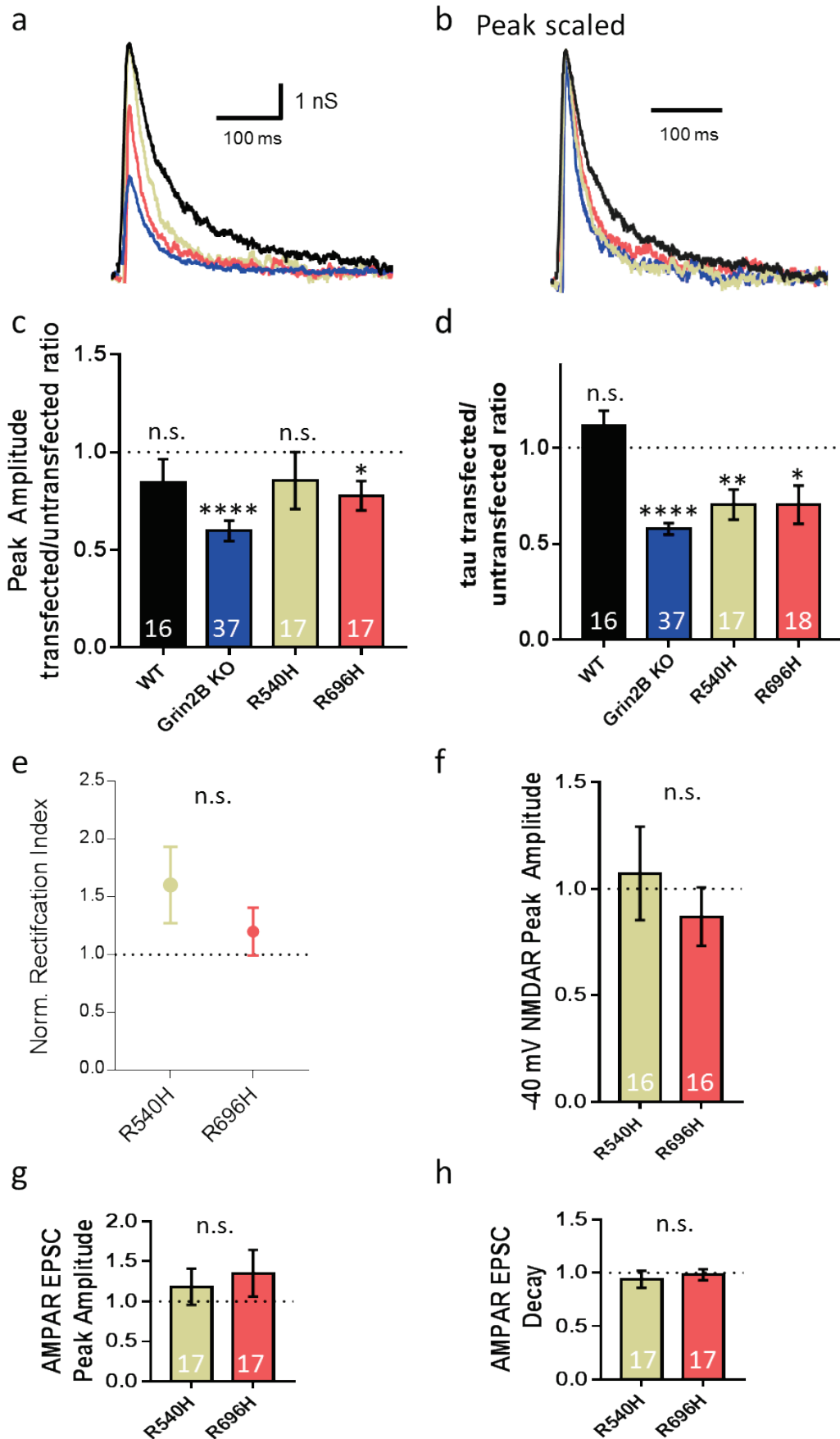


Figure 3.11: GluN2B GOF mutations produce brief NMDAR decay at depolarised potentials.

a) Representative NMDAR traces from GluN2B GOF mutations and untransfected (black). b) Peak scaled traces demonstrating prolonged decay time. c) NMDAR peak amplitude ratio of transfected/untransfected of mutants compared to WT and GluN2B KO. d) NMDAR decay ratio of transfected/untransfected of mutants compared to WT and GluN2B KO. e) Normalised rectification index of GOF mutants (-40 mV / $+20$ mV, normalised to untransfected). f) Peak amplitudes of GOF mutants at -40 mV. g) AMPAR-EPSC peak amplitudes of GOF mutants h) AMPAR-EPSC decays of GOF mutants. Data from 4 mice for R540H and R696H.

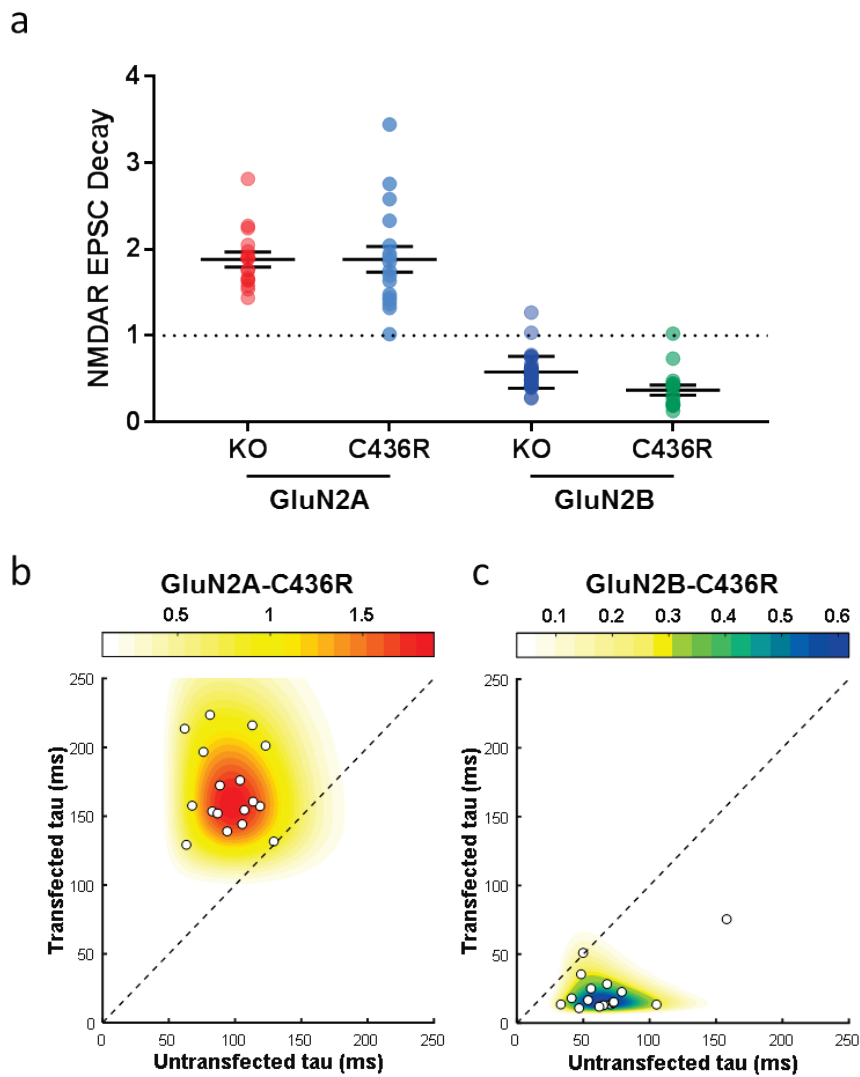


Figure 3.12: A subunit specific effect observed by GluN2A and GluN2B mutants.

a) NMDAR decay comparison between GluN2A and GluN2B that contain the same C436R mutation, with KO for comparison. This mutant behaves in an opposite manner depending on the subunit it is present in. b,c) Individual responses of transfected vs untransfected decay for C436R in GluN2A and GluN2B, respectively.

currents that were extremely prolonged. Here, *faster* NMDAR currents were observed in neurons with GluN2B 'GOF' mutations, similar to GluN2B KO (fig. 3.11b,d, table 3.3).

From the RI, no differences in the peak amplitudes at -40 mV compared to +20 mV were evident, suggesting no change to the magnesium blockade properties of the receptor as a result of these two mutants (fig. 3.11e, table 3.3, Appendix H). R696H peak amplitude at -40 mV was reduced, but was not statistically significant and the peak for R540H at -40 mV was unaffected, in accordance with the RI (fig. 3.11f, table 3.3).

Lastly, GluN2B GOF mutations had no significant effects on AMPAR peak amplitude or decay time constant (fig. 3.11g,h, table 3.3), as exhibited by almost all other mutants.

Subunit-specific consequences of GluN2 mutations

These data have shown that most GluN2A and GluN2B mutations phenocopy the respective subunit's KO. For GluN2A, this resulted in slowed NMDAR decay kinetics while in GluN2B, the decay kinetics were faster. No genotype-phenotype correlation was observed for GluN2B mutations, but instead, it appeared that the consequences on synaptic transmission were a result of the specific subunit affected. This is demonstrated well by the mutation C436R which is present in both GluN2A and GluN2B, and caused completely opposite outcomes for NMDAR activity in each subunit (fig. 3.12). The NMDAR-EPSC decay was slow when C436R occurred in GluN2A (fig. 3.12b), but fast when GluN2B was affected (fig. 3.12c), and these decay speeds were similar to the decays of the KO for each subunit (fig. 3.12a).

Discussion

A successful molecular replacement of endogenous mouse GluN2A and GluN2B subunits was performed with the respective human variants and similar characteristic NMDAR-EPSC properties were obtained compared to untransfected neurons. This allowed examination of the cell autonomous effects of human disease mutations using the mouse hippocampal circuitry as a model to compare evoked NMDAR- and AMPAR-mediated transmission between mutant and WT neurons.

NMDAR-mediated currents are very sensitive to the amount of GluN2A, but not GluN2B, transfected into CA1 neurons

The amount of GluN2A transfected into pyramidal neurons for the rescue was highly impactful on the NMDAR-EPSC decay especially, whereas for GluN2B, relatively large differences in the amount transfected did not significantly alter NMDAR properties. This resulted from the GluN2A successful rescue concentration lying within the steepest part of the curve (fig. 3.4), with the numbers of GluN2A at the synapse readily adjusted and changed. However, for GluN2B, the decay kinetics were similar at both 3 and 10 ng/ μ l concentrations tested, which may be due to a limit in the amount of GluN2B that could be incorporated into the synapse. It has been observed that the total expression levels of GluN2B are higher than GluN2A (Coultrap et al., 2005, Pian et al., 2010), but the surface expression of GluN2A is higher than GluN2B in the CA1 region (Le Bail et al., 2015, Sun et al., 2016). This also implies that the post-synaptic density is capable of incorporating more GluN2A than GluN2B, even though higher non-synaptic levels of GluN2B exist, possibly due to the higher turnover and mobility of GluN2B subunits than GluN2A (Groc et al., 2006b, Lavezzari et al., 2004, Sanz-Clemente et al., 2010). Recently, the developmental switch from GluN2B to GluN2A has been suggested to occur through the increase in expression of GluN2A (McKay et al., 2018), which also shows the capacity for the post-synaptic density to alter its GluN2A content.

GluN2A mutants and NMDAR currents

It was hypothesised that GluN2A mutants would show a common synaptic phenotype of enhanced synaptic activity since the majority of GluN2A mutations are associated with seizure disease phenotypes. In agreement with this, it was found that five out of the six mutations investigated had a sustained NMDAR channel opening by 1.5-2 times more than WT.

The K669N mutant results in alterations to the charges of the residue at position 669, from a positively charged lysine to a smaller and neutral asparagine. Furthermore, the 669 residue is

located in a region that forms an α -helix, whereas asparagine does not favour the formation of this secondary protein structure (Venselaar et al., 2010). Therefore, it is likely that both the structural formation of the GluN2A subunit and its functional properties will be affected. K669N was the only GluN2A mutant investigated in this chapter that did not show any LOF effects on NMDAR-EPSC properties. The decay was ~ 1.5 times slower than WT NMDARs, less than would have been expected from previous reports in HEK-293 cells where the decay of K669N mutants was four times slower than WT GluN2A subunits (Swanger et al., 2016). Although there is a difference in the two experimental conditions – the presence of the GluN2B subunit which contributes to the overall decay profile – the degree to which this mutant alters NMDAR properties is less than anticipated from studies in heterologous cells. The prolonged decay may affect the degree of summation of post-synaptic potentials. Slower postsynaptic currents can more readily summate at lower rates of transmission across synapses during on-going synaptic activity, and therefore lead to a greater probability of postsynaptic firing (Augustinaite and Heggelund, 2007, Hunt and Castillo, 2012). At the network level, GluN2A-NMDARs are highly expressed in hippocampal neurons and in the cortex (Monyer et al., 1994), so mutant GluN2A subunits are present in a high proportion of neurons in the brain. Global increases in neuronal activity in large populations of neurons may be a likely result. However, for the remaining mutations (L812M, C436R, T531M, R518H) exhibiting reduced peak amplitude, as well as a prolonged decay, the overall effect that may be produced by these mutations is more difficult to interpret. While prolonged events increase the probability of the membrane depolarisation of successive events to accumulate, those membrane depolarisations are smaller than normal; reaching a threshold for neuronal firing may require more of these small inputs to summate.

The putative GluN2A LOF mutants, C436R, T531M and R518H phenocopied the GluN2A KO, whereas the decay for L812M was also prolonged but not as slow. In HEK-293 cells, the peak amplitudes of currents in response to 1 mM glutamate were similar to WT for both L812M mutant receptors with one and two mutant GluN2A subunits in the NMDAR complex. In addition, the decay of the homozygous L812M mutant NMDAR was ~ 10 times slower than WT GluN2A-comprising NMDARs, with the heterozygous WT/L812M exhibiting almost three times slower decay than the WT (Yuan et al., 2014). Considering that the GluN2B subunits, which are also present in CA1 pyramidal neurons (Gray et al., 2011), have slower decay kinetics than GluN2A, it suggests that the L812M mutant is either not well modelled in heterologous systems, or that the contribution of current by this mutant is very low and that the majority of current is mediated by native healthy receptors. In this case, the expression of this mutant would give a good indication of the relative contributions to NMDAR currents it provides.

L812M is a mutation which occurs in the LBD-TMD linker in a highly conserved region and although both amino acids have the same properties of being non-polar and hydrophobic, methionine has a larger side chain (Venselaar et al., 2010). This may impact the folding and structural properties of the subunit, leading to alterations in the protein's functions. Interestingly, as others have reported, L812M produced larger currents at negative compared to positive holding potentials. This has been interpreted as a reduction in the magnesium sensitivity of L812M, leading to enhanced activity at resting membrane potentials. However, it was found that at negative holding potentials, the recorded current amplitude was not significantly different to WT untransfected neurons. The difference between positive and negative holding potentials that many have observed actually reflects a marked reduction in the currents at positive potentials, rather than an enhancement at negative potentials. All studies (Pierson et al., 2014, Yuan et al., 2014) that have reported L812M as having reduced magnesium block have all concluded this from plots of current normalised to the current at more depolarised states (around +20 mV) or to the maximal current in response to agonists, failing to account this to the much smaller response of L812M at ~+20 mV than WT.

C436R, T531M and R518H have been predicted to abolish subunit expression, owing to the complete lack of currents when expressed in HEK-293 cells (Swanger et al., 2016). As a result, measures of decay with these mutant subunits have not been possible. All three residues are conserved amino acids; the C436R mutations disrupts the formation of a cysteine-cysteine disulphide bridge with C456 and likely results in severe misfolding and degradation. It also introduces a larger positively charged and less hydrophobic residue in place of the neutral WT residue that is buried within the core of the protein. T531M occurs in a β -strand region, a secondary structure that is not favoured by methionine residues (Venselaar et al., 2010). Additionally, the methionine is a larger more hydrophobic residue. The likely result is a destabilised and misfolded conformational structure that is likely to also be degraded. R518H results in an incorporation of an amino acid with a smaller side chain that could impact protein folding and conformation as well (Venselaar et al., 2010). Therefore, lack of GluN2A expression is highly likely with these LOF mutations, in a manner similar to a complete GluN2A KO. Validation through expression studies would help to confirm these ideas. Although, the aberrant NMDAR properties at both negative and positive holding potentials for LOF mutants would support this, in contrast to the GOF mutants which showed more aberrant effects at positive holding potentials, suggesting a functional alteration as a consequence of these mutants.

I694T did not follow the pattern shown by all other GluN2A mutants studied; I694T results in a smaller more hydrophobic threonine residue in place of the highly conserved isoleucine (Venselaar et al., 2010). It showed a phenotype of a reduced synaptic activity – reduced peak amplitudes, without any observable GOF. This mutation is also associated with seizure disorders including Landau-Kleffner syndrome, Benign epilepsy with centrotemporal spikes, epileptic encephalopathy with continuous spike and wave during slow-wave sleep and autosomal dominant Rolandic epilepsy (UniProtKB/Swiss-prot Q12879). Previously, this mutant was found to have a reduced peak amplitude in HEK-293 cells, with no effect on current decay (Swanger et al., 2016), consistent with the results found in this chapter. With regard to epilepsy disorders, one simple explanation is that this mutation is not the direct cause of this disease phenotype and other factors may contribute to the development of seizures. I694T is also implicated in mental retardation and speech dyspraxia and the observed synaptic phenotype may relate to these instead. Another possibility, which is the drawback of the current experimental design, is that these mutations may alter the splicing instead of the mature cDNA sequence. In this case, the current design would not detect the possibility of these effects.

GluN2B mutants and NMDAR currents

It was surprising that for GluN2B mutants, a common synaptic phenotype was also present: all mutants had brief decaying currents compared to WT. This was surprising, firstly, due to the diverse disease phenotypes that are associated with these mutations - all share the association with ID, but C461F, R540H and C436R also present with seizure disorders whereas C456Y and R696H do not. Secondly, these mutants did not fit into the classification of 'GOF' and 'LOF' subtypes as the individual properties of each mutant subunit identified in isolation were not reflected in the overall synaptic activity that was observed. These receptor subunits do not exist in solitude and contribute only a portion to the overall synaptic transmission that is mediated by a collection of different receptor types, each with several isoforms or subunit combinations. Therefore, the results from studies in heterologous expression systems were not reflective of the results in neurons.

The first note is that GluN2B LOF mutations did not fully phenocopy the KO, with respect to the peak amplitudes, as they would have with a complete lack of trafficking and expression. This was surprising, especially for C436R and C456Y which are known to disrupt the formation of disulphide bridges (C436-C457 and C456-C429) that will all be expected to lead to a complete misfolding of the protein with severe consequences for stability and trafficking (Venselaar et al.,

2010). C436R also alters the charge of the buried residue at the core of the protein from neutral to positive (Venselaar et al., 2010). These residues, as well as C461F, are all conserved residues.

If expression of these subunits is diminished in neurons, as is predicted from the above mentioned changes to properties of residues, their disruption to structural bonds, and as was found in HEK cells (Swanger et al., 2016), then it could suggest that the remaining receptors at the synapse have compensated, either through the number of remaining receptors or the size of responses, to produce an amplitude of receptor signalling that is closer to the regular state. Compensatory mechanisms involving NMDARs have been reported in many circumstances, including potent block of NMDARs, KO of individual subunits or KO of the obligatory GluN1 subunit and is exhibited through upregulation of the NMDAR itself or through non-NMDAR pathways (Gray et al., 2011, Nagy et al., 2005, Reiprich et al., 2005). However, it is surprising as to why possible compensatory mechanisms could be present for the LOF mutants but not for the GluN2B KO. It has been found that some ion channel mutants show a more damaging effect on signalling than having a total loss of the protein in KOs of ion channel genes (Single et al., 2000). This is possible due to the mutant subunit having adverse effects on the folding, assembly and trafficking processes so that the WT protein is unable to be processed as the cellular machinery is saturated with the dysfunctional variant. This may be the case for the LOF mutations studied, especially C456Y and C436R, which show a more severe effect on the decay of NMDARs than the GluN2B KO, and could result in a greater likelihood that compensatory pathways would be activated as the intensity of dysfunction is much larger. Although how, if at all, this putative compensation may occur or which channels may be involved is for future research to uncover.

Alternatively, if the mutant subunits have defective trafficking and are stuck in the ER, but the CTD is still contributing to NMDAR signalling, this could explain the fast decay of NMDARs with the maintained peak amplitude. While in the ER, NMDARs are membrane bound with the NTD in the ER lumen and the CTD in the cytoplasm (Fukaya et al., 2003). The CTD is involved in many downstream signalling processes, including activation of CAMKII-alpha (McKay et al., 2018) and MAGUK (membrane associated guanylate kinase) binding proteins (Ryan et al., 2008). CTD signalling from the ER for NMDARs has not been reported or investigated.

The other possibility is that mutant GluN2B subunits are still trafficked to the synapse and form heterotetramers so that the amplitudes of currents are maintained but the kinetic properties of GluN2B have been functionally altered. However, this possibility is less likely considering the severe consequences to structure, folding, and stability caused by these mutants. The decays of

C436R and C456Y have not been reported due to the complete lack of current when these mutants are transfected into HEK-293 cells, however, C461F still produced a very small current that had 20 times faster decay than WT GluN2B receptors and twice as fast as GluN2A receptors (Swanger et al., 2016). Considering the decay of C461F-transfected neurons in this chapter had a similar decay to GluN2A subunits (GluN2B KO), it again suggests that this mutant subunit is not contributing to NMDAR-mediated currents.

Next, 'GOF' mutants did not show any GOF effects, but in fact, had LOF NMDAR-EPSC properties such as reduced peak amplitude of R696H and faster decays of both R540H and R696H. Both these mutants affect conserved residues and R696 also forms a salt bridge with E692 and is in contact with other domains in the subunit (Venselaar et al., 2010); substitution to the histidine will likely result in an impairment to the integrity of the structure and stability of the subunit. R540H showed an unaltered peak amplitude, but is known to have a more mild dysfunctional effect on both receptor properties and disease phenotype (Lemke et al., 2014). In HEK cells, R540H and R696H were found to have roughly a 50% and 20% reduction, respectively, in total and surface/total expression (Swanger et al., 2016). Furthermore, in HEK cells, both these mutants had slower NMDAR decays of 2 times longer (R540H) and 3.6 times longer (R696H) than WT GluN2B NMDARs. If the expression and trafficking of these mutant subunits in heterologous cell lines is assumed to be translatable to the processes in neurons, decay that is close to that of GluN2A-containing NMDARs at the synapse would not be expected. With a 50% reduction in surface expression compared to WT but double the decay time of those subunits, the expected overall outcome would be decay that resembles untransfected neurons. In the case of R696H, an overall slower decay would be expected. The current results suggest that the trafficking and expression of these 'GOF' mutants in neurons may be diminished – to a greater degree than seen in HEK cells, leading to an overall GluN2B KO-resembling phenotype. The fact that the mutants' decay is very slightly slower than the KO would suggest that there is still some expression present at the synapse, but despite the mutant subunits having a GOF effect individually, these effects are not dominant as other receptor subunits (GluN2A) are mediating the majority of NMDAR responses.

An important point to realise is that expression of GluN2A and GluN2B in heterologous cells is most commonly done with co-expression of the GluN1a isoform. There are eight different GluN1 isoforms that exist that are generated through alternative splicing and all display varied kinetic properties. In particular, exon 5 of the GluN1 gene is a vital decider of the kinetic and gating properties that the subunit will have; exon 5 is present in the 1b isoforms but is spliced out of

the 1a isoforms and leads to 1a having much slower rates of decay (Rumbaugh et al., 2000, Vance et al., 2012). Research by Yi et al. (2018) investigated the differences in decay kinetics between the 1a and 1b GluN1 isoforms in both GluN2A and GluN2B NMDARs and found that the decay of diheteromeric GluN2B-NMDARs differed immensely depending on the GluN1 isoform present: GluN1a/GluN2B receptors were much slower (~500 ms) than GluN1b/GluN2B receptors (~150 ms). Conversely, the diheteromeric GluN2A-NMDAR decay was less significantly impacted by the GluN1 isoform (~50 ms with 1a, 30 ms with 1b). From P7 to adult stages in rat, both 1a and 1b isoforms are expressed in the CA1 of the hippocampus, although GluN1a levels are higher (Laurie and Seeburg, 1994). For mouse and human, it is still undetermined; if it is similar to the rat, and both 1a and 1b isoforms are present, then the degree of the decay kinetics measured in HEK cells with only the GluN1a isoform may be an overestimation of the effect sizes that the mutants produce on NMDAR decay. This has major impacts on interpreting the results of these mutations in systems that do not model well the endogenous native environment in which these genetic abnormalities develop.

Mutant GluN2A and GluN2B effects on AMPAR currents

The effects of human disease mutants on AMPAR transmission have not been studied; the focus so far, has been on NMDAR properties. As NMDAR signalling is known to affect the numbers of AMPARs at the synapse and their function, and many groups have found changes to AMPAR properties with NMDAR KO, inhibition or overexpression (Gray et al., 2011, Hall et al., 2007, Hall and Ghosh, 2008, Hamada et al., 2014, Kim et al., 2005), it was surprising to find that all mutants had no discernible effects on AMPAR properties. The only exception was the GOF mutation in GluN2A, L812M, which exhibited slower current decay, although this was no longer a significant change after multiple comparison correction. As similar effects that were exhibited by L812M were also exhibited by other mutants – decay and peak amplitude, it is puzzling why only L812M showed a trend in altered AMPAR properties. However, no other mutants exhibited this combination of properties, as the LOF GluN2A mutants had a slower decay than L812M. It may be that this combination of effects was capable of activating the pathways leading to alterations in AMPAR behaviour. Alternatively, it may be due to a property which was not examined; the downstream effectors activated by NMDAR signalling are diverse and involve many different pathways, including CaMK, CREB, ERK1/2, nNOS, Akt, which may alter the activity of certain proteins or induce changes in gene expression leading to many more diverse outcomes (Papadia and Hardingham, 2007).

One possibility is that the AMPAR current was contaminated by NMDAR activity if the L812M mutant results in NMDAR activation at negative holding potentials and from interference with magnesium block. If this is the case, this may impact the AMPAR conductance subtraction procedure to obtain pure NMDAR traces (fig. 3.7). However, since the -100 mV current is small compared to the +20 mV current (Appendix E) and the -100 mV current is much more brief, this does not pose a huge problem and not a lot of current is subtracted off erroneously.

Conclusions

Both GluN2A LOF and GOF mutants, with the exception of I694T, exhibited a common prolonged decay of NMDAR currents, which are expected to enhance neuronal excitability and contribute to the seizure phenotypes associated with these mutations. Unexpectedly, both LOF and GOF GluN2B mutations also showed a common synaptic phenotype where decays were briefer. This was surprising as diverse disease phenotypes are associated with GluN2B mutations so diverse consequences at the synapse were expected.

How these synaptic phenotypes are caused: through functional changes to the mutant subunit or changes in expression, and whether this differs for GOF and LOF mutants are the next unanswered questions. GluN2A mutants that do not express may be capable of producing prolonged postsynaptic responses due to the remaining population of GluN2B receptors which are known to have slow kinetics. On the other hand, those that do express may alter the kinetic properties of the subunit itself. For GluN2B, there is the possibility that although certain mutations overexpressed in isolation produce a GOF phenotype, in neurons, it may be that the LOF effect seen is due to diminished expression. The distinction between these mechanisms or whether other processes are occurring to result in the observed synaptic phenotypes for GluN2A and GluN2B mutants are the next focus and will be addressed in the next chapter.

Chapter 4 Mechanisms underlying synaptic phenotypes of GluN2A and GluN2B NMDAR mutants

Abstract

In the previous chapter, it was shown that the NMDAR-mediated component of synaptic transmission in neurons expressing GluN2A and GluN2B human disease mutants within the ligand-binding domain and linker phenocopied the respective subunit KOs. In particular, there was no genotype-phenotype correlation for GluN2B mutants, as originally suspected from work in non-neuronal systems. Instead, it was observed that mutation effects on synaptic currents segregated by subunit: prolonged currents when GluN2A was mutated and more rapidly decaying currents when GluN2B was mutated. In this chapter, the mechanisms by which GluN2 mutants produce their respective synaptic phenotypes are investigated to distinguish between alterations in NMDAR function or aberrant expression at the synapse. To assess functional incorporation of mutant receptors, the CA3-to-CA1 synapse was used in cultured mouse hippocampal slices and the cell autonomous effect of GluN2 mutants were examined on the decay of NMDAR-mediated synaptic currents in CA1 neurons, where the mutant GluN2 subunit was expressed following deletion of both the native GluN2A and GluN2B. To examine the expression and trafficking competence of the mutant GluN2 subunits, the synaptic localization of NMDARs was imaged in cultured hippocampal neurons overexpressing GluN2 mutants together with a Super Ecliptic pHluorin (SEP)-tagged GluN1. It was found that the GluN2A GOF mutation K669N enabled robust expression of NMDARs at synapses and directly enhanced the GluN2A kinetics. In contrast, the LOF GluN2A mutation C436R had poor synaptic expression implying that the more prolonged NMDAR component in the GluN2A-C436R rescue experiment of Chapter 3 was mediated by GluN2B-containing NMDARs. For GluN2B, both GOF and LOF, R696H and C456Y respectively, resulted in defective functional incorporation of the NMDAR subunit GluN2B. This suggests that the NMDAR-EPSC phenotype measured in the GluN2B mutant rescue experiments in Chapter 3 were mediated by remaining GluN2A-containing NMDARs. Interestingly, the 'GOF' R696H mutant, produced severely prolonged currents in isolation, however, its contribution to the overall current at regular synapses was negligible, producing an overall 'LOF' phenotype in neurons. These results highlight the importance of using more biologically relevant model systems to understand disease-associated ion channel mutations, and the importance of studying both function and expression phenotypes of disease mutants.

Introduction

The last chapter showed subunit specific synaptic phenotypes for GluN2A and GluN2B human disease mutations expressed in CA1 pyramidal neurons. The GOF/LOF distinction that has been adopted from research in heterologous expression systems was not reflective of the effects that these mutant subunits have on the NMDAR-EPSCs in neurons and on synaptic function. Mutants that exhibit strong alterations in the individual subunit's characteristics, such as 'GOF' GluN2B mutants R540H and R696H which have 2x and 3.6x slower NMDAR currents when expressed in isolation, respectively (Swanger et al., 2016), produced an unexpected synaptic phenotype with *faster* NMDAR-EPSC decay when expressed in neurons.

In order to fully understand the mechanisms behind the association between GluN2 mutations and disease phenotypes, it is also necessary to examine the trafficking and expression profiles, as well as the electrophysiological properties of mutant subunits in their native environment. The amount of mutant subunits that are incorporated into the synapse can indicate the degree to which synaptic currents are functionally altered by the mutant and to what extent the current is mediated by alternate healthy native NMDAR compositions. Furthermore, measuring NMDARs at synapses implicitly captures mutation effects on allosteric modulation by small molecule endogenous ligands, including Zn^{2+} co-released with glutamate (Paoletti et al., 2009), pH changes in the synaptic cleft (Low et al., 2003, Regan et al., 2019), and cholesterol content in the plasma membrane at synapses (Korinek et al., 2015).

In this chapter, the synaptic expression and functional incorporation of select GOF and LOF GluN2A and GluN2B mutants are examined. The hypothesis was that GOF GluN2A mutations would produce an enhancement in the GluN2A functional properties leading to prolonged current decay whereas LOF GluN2A mutations would have defective functional incorporation, trafficking or expression. For GluN2B, the hypothesis was that both GOF and LOF mutants would have defects in functional incorporation or trafficking to synapses, leading to faster NMDAR currents mediated by the remaining GluN2A subunits at the synapse. Even though GOF GluN2B mutations have an enhanced NMDAR function when expressed in heterologous expression systems, it is possible that they do not contribute significantly to the overall currents in neurons, due to their low or absent numbers at the synapse, and so, actually produce a LOF phenotype.

To test these hypotheses, three different experiments were performed, using one GOF and one LOF mutant from each GluN2 subunit – K669N (GOF) and C436R (LOF) from GluN2A, and R696H (GOF) and C456Y (LOF) from GluN2B. The first experiment involved pharmacological block of

GluN2 subunits to get an indication of the relative expression levels of GluN2A and GluN2B at the synapse with GOF or LOF mutants. The second experiment involved expression of a single mutant subunit after KO of both endogenous GluN2A and GluN2B subunits and using the amount of current that was rescued as an indication of the mutant's expression levels at the CA3-to-CA1 synapse. The final experiment focused on the trafficking of mutant subunits using the GluN1 subunit with a Super Ecliptic pHluorin (SEP) tag as a readout of receptor expression in dendritic spines.

It was observed that the GluN2A GOF mutation K669N was expressed at the synapse and contributed a significant proportion of the total NMDAR current, whereas LOF GluN2A mutation C436R and both GOF and LOF GluN2B mutations R696H and C456Y were not functionally incorporated into synapses. Where mutants made little or no functional contribution to NMDAR-EPSCs, the properties of the remaining NMDAR subunit(s) will have sole influence on the synaptic currents.

Methods

Animals

For the pharmacological experiments with GluN2 blockers, homozygous *Grin2a*-flox (*Grin2a^{fl/fl}*) and *Grin2b*-flox (*Grin2b^{fl/fl}*) mice were used (see chapter 2).

For the expression of single GluN2 mutant subunits alone in neurons, *Grin2a-Grin2b* double floxed mice (both *Grin2a* and *Grin2b* genes are floxed - *Grin2a^{fl/fl}Grin2b^{fl/fl}*) were generated by mating homozygous *Grin2a*-flox mice with homozygous *Grin2b*-flox mice (see chapter 2). This generated mice which were heterozygous for the *Grin2a*-flox gene and heterozygous for the *Grin2b*-flox gene (*Grin2a^{+fl}Grin2b^{+fl}*). Subsequently, *Grin2a^{+fl}Grin2b^{+fl}* mice were mated together and the offspring were genotyped (see chapter 2 methods for genotyping) to identify the homozygous *Grin2a-Grin2b* double floxed mice (*Grin2a^{fl/fl}Grin2b^{fl/fl}*).

WT Sprague-Dawley rats aged P1-P2 were used for dissociated hippocampal cultures for trafficking experiments.

Pharmacology experiments

Hippocampal slice culture preparation and SCE were identical to the methods described in chapter 2 for *Grin2a^{fl/fl}* and *Grin2b^{fl/fl}* mice, with the following exceptions: the cotransfection of the mutant or WT GluN2A or GluN2B and pLenti CMV Cre-eGFP construct during the electroporation procedure.

Electrophysiological recordings were also identical to those previously described in chapter 2, with the following differences in the procedure. A stimulation of 20-40 V for 50 μ s (20 repetitions; 10 s cycle time) was applied to the Schaffer collaterals and NMDAR-EPSCs were recorded postsynaptically from only transfected CA1 neurons. For GluN2A mutants, after this first recording, 3 μ M Ifenprodil hemitartrate (Abcam ab120111) was added to the ASCF and allowed to perfuse through the tissue for 12 minutes. One recording was taken every 30 seconds during this period (20-40 V for 50 μ s) and another recording of 20 traces was taken after the 12 minutes. For GluN2B, the slices were perfused with 10 μ M TCN-201 (Tocris 4154) instead of Ifenprodil.

Double KO recordings

Hippocampal slice culture preparation, SCE and electrophysiological recordings were identical to the methods described in chapter 2 for *Grin2a-Grin2b* double floxed mice. The transfected neurons from these slices expressed either GluN2A or GluN2B WT or mutant subunits only.

Primary neuronal culture, transfection and imaging

Sprague-Dawley rats aged P0-P2 were used for dissociated hippocampal cultures. The hippocampus was dissected on ice and the meninges were removed in dissection medium composed of HBSS (Invitrogen 14155048) with 10 mM HEPES (Sigma H0887) and 1% Pen/Strep (Invitrogen 15140122). The hippocampi were then triturated in 2 ml of pre-warmed plating medium which was composed of MEM (GIBCO 51200087) supplemented with 20 mM glucose, 1% Pen/Strep, 1 mM sodium pyruvate (Sigma S8636), 25 mM HEPES, 1x N2 (Invitrogen 17502048) and 10% HI-horse serum (Gibco 26050088). The homogenised tissue was then diluted into 6.5 ml total volume of plating medium. 500 μ l of this was plated per well into 12-well plates that contained 16 mm diameter coverslips (ThermoFisher 10755354) that had been previously coated (for 3 hours) with 50 μ g/ml poly-D-lysine (Sigma P0899) and (overnight with) 2 μ g/ml laminin (Sigma L2020). Neurons were allowed to settle and adhere for 3 hours at 37 °C, 5% CO₂, after which, they were supplemented with culture medium containing: Neurobasal-A (Fisher 12349), 1 ml B-27 (Gibco 17504044), 1% Pen/Strep, and Glutamax (Gibco 35050). Cultures were returned to 37 °C, 5% CO₂ and fed twice a week with culture medium supplemented with antimetabolic agents: 0.1 μ M uridine, 0.1 μ M fluorodeoxyuridine and 0.1 μ M cytosine arabinoside. Neurons were transfected at 8 DIV with the calcium phosphate method. For this, coverslips were transferred to a fresh plate containing 500 μ l culture medium that contained 1 mM kynurenic acid to acidify the medium for smaller precipitates. 50 μ l 2.5M CaCl₂ with DNA solution was added dropwise to 50 μ l 2xHEPES buffered saline (Sigma-Aldrich). DNA constructs used were pCaMKII α -Homer1c tdTomato at 1 μ g per coverslip with pCI-SEP-NRI (Addgene plasmid #23999) at 1.5 μ g per coverslip. This was used alone or in addition to one WT or mutant GluN2 at 1.5 μ g per coverslip. The DNA/CaCl₂-HEPES solution was incubated for 20 minutes at room temperature and then added to one well of the 12-well plate containing the neurons. After a 90-minute incubation at 37 °C, 5% CO₂, the coverslips were transferred to a new 12-well plate that had been pre-incubated at 37 °C, 10% CO₂ and placed for 20 minutes at 37 °C, 5% CO₂. Coverslips were transferred back to the original 12-well plate and incubated until the day of imaging, DIV 11.

Neurons were imaged using a Zeiss AxioVert.A1/Jenoptik ProgRes GRYPHAX Arktur microscope with a 40x objective; 0.65 numerical aperture. Coverslips were placed in HEPES ASCF with 4 mM CaCl₂ and 4 mM MgCl₂. Neurons were imaged for the GFP signal at 395 nm (fig. 4.1c) and the tdTomato signal at 554 nm (fig. 4.1a). Five images were taken from each coverslip. These 8-bit images were converted to grayscale in ImageJ (fig. 4.1d) and the fluorescence was normalised

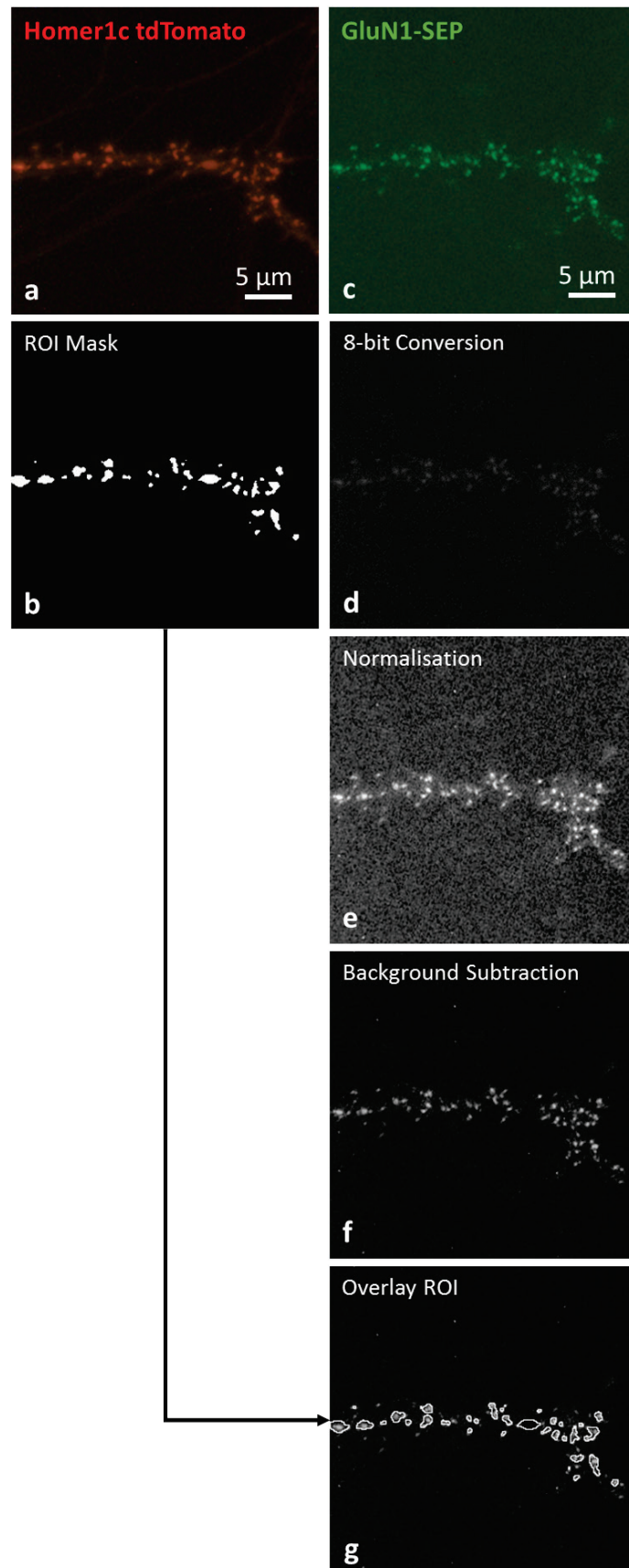


Figure 4.1: Image analysis procedure using ImageJ.

a) Homer1c-tdTomato signal. b) ROIs selected in five dendritic compartments. c) SEP-GluN1 signal. d) GluN1 converted to grayscale. e) fluorescence normalisation within image. f) background subtraction. g) ROIs selected from Homer1c-tdTomato signal overlaid onto SEP-GluN1 signal. The fluorescence of the SEP-GluN1 signal is measured at these ROIs. Figure used with permission from Daniel Hunter, University of Sussex.

within each image using a custom built macro (fig. 4.1e) as the transfection efficiency between neurons was variable. The background fluorescence was subtracted (fig. 4.1f) and the Homer1C-tdTomato signal was used to select five regions of interest (ROIs) that corresponded to five different dendritic compartments that contained dendritic spines (fig. 4.1b). The ROIs were overlaid onto the SEP-GluN1 signal (fig. 4.1g) and the fluorescence at these ROIs was measured.

Statistical analysis

For pharmacology experiments with ifenprodil and TCN-201, recordings were discarded if the access resistance between two recordings (before and after drug) differed considerably (5-8 MΩ). In Stimfit 0.13, an average of the 20 traces was taken and the peak amplitudes were compared before and after drug addition to obtain the percent block of the EPSC peak amplitudes by Ifenprodil or TCN-201. A one-way ANOVA was used to compare the percent inhibition by ifenprodil or TNC-201 for the GOF, LOF and WT subunits in GraphPad Prism 7. For double KO experiments, a paired t-test was used to compare the double KO and untransfected peak amplitudes and a one-way ANOVA was used to compare the various constructs transfected into the double KO background. GraphPad Prism 7 was used for these analyses.

For imaging experiments, one-way ANOVA in GraphPad Prism 7 was used to compare the fluorescence with and without the WT subunits, a two-way ANOVA was used for the fluorescence before and after the addition of trypan purple and a one-way ANOVA in GraphPad Prism 7 was used for comparisons of fluorescence for the various mutants tested.

Results

Pharmacological block as an indication of relative expression profiles of mutant GluN2

Mutant NMDAR subunits that still express and traffic to the synapse may be expected to have similar relative synaptic expression of GluN2A and GluN2B to WT neurons (fig. 4.2a). With GluN2A LOF mutants, which are predicted to reduce expression or trafficking of the subunit to the synapse, the remaining GluN2B subunit is expected to contribute relatively more to NMDAR-EPSCs (fig 4.2c). In these situations, GluN2B-selective antagonist ifenprodil should block a larger proportion of the NMDAR current. Likewise, for GluN2B LOF mutants, the relative contribution of GluN2A-containing receptors should be higher, so GluN2A-selective antagonist TCN-201 should block a larger proportion of the NMDAR current. Thus, experiments were designed to use these negative allosteric modulators to assess the subunit composition of NMDARs contributing to NMDAR-EPSCs. Negative allosteric modulators were selected to target the non-mutated GluN2 subunit (as described above), since interpretation of the block by antagonists targeting the mutated subunit is arguably more likely confounded by direct effects of the mutation on drug potency or efficacy.

NMDAR-EPSCs were recorded from CA1 neurons transfected with one GOF and one LOF mutant for both GluN2A and GluN2B, with and without ifenprodil or TCN-201 addition, respectively. GOF and LOF mutants K669N and C436R respectively were characterized further in this chapter. For GluN2B, GOF mutant R696H and LOF mutant C456Y were chosen.

GluN2A GOF and LOF mutant NMDAR subunits are differentially blocked by ifenprodil

The NMDAR-EPSC peak amplitude after the addition of ifenprodil to the ASCF was reduced to 61.92 ± 7.11 % for K669N-transfected neurons and 30.94 ± 2.20 % for C436R-transfected CA1 neurons in hippocampal slices. The GluN2A human WT subunit was intermediate with an EPSC peak amplitude of 41.49 ± 6.27 % in the presence of ifenprodil (fig. 4.3a,b). Fig. 4.3a shows the EPSC size with increasing time exposure to ifenprodil. The two mutant responses were significantly different to each other (one-way ANOVA with Tukey's MC test $F(50,2) = 8.38$, $p = 0.0007$; C436R vs K669N $p = 0.0006$), however the WT response did not significantly differ to either mutant (WT vs C436R $p = 0.4801$, WT vs K669N $p = 0.0628$). This result suggests a difference in the GluN2A and GluN2B ratios at the synapse with the GOF and LOF GluN2A mutants where a higher proportion of the EPSC is mediated by GluN2B in cells expressing the LOF mutant C436R. Although the WT GluN2A was not significantly different to either mutant, possibly due to the sample size.

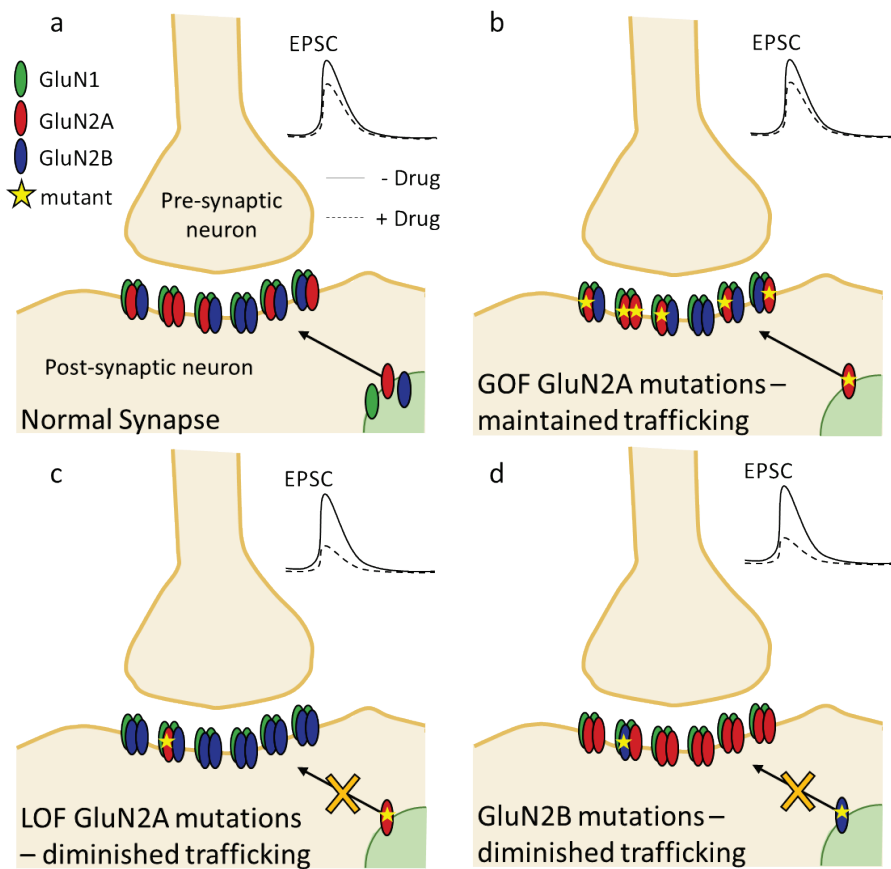


Figure 4.2: Hypothesised trafficking and expression of GOF and LOF GluN2 mutants and their response to GluN2 blockers.

a) A regular synapse with GluN1, GluN2A and GluN2B normally trafficked to the synapse. b) A GOF GluN2A mutation would be predicted to not disrupt the trafficking or expression of the GluN2A subunit, leading to mutant subunits present at the synapse. The block by ifenprodil would produce a similar level of block as the normal synapse due to similar levels of GluN2A and GluN2B in both. c) GluN2A LOF mutations are predicted to disrupt the trafficking of the GluN2A subunit to the synapse, leading to a higher GluN2B density at the synapse. EPSCs from this population of neurons are predicted to be blocked by ifenprodil to a greater degree. d) GluN2B GOF and LOF mutations which are both predicted to disrupt GluN2B trafficking to the synapse would both result in a GluN2A rich synapse, from which, EPSCs would be blocked to a greater degree by TCN-201 than the normal synapse.

GluN2B GOF and LOF mutant NMDAR subunits are equally blocked by TCN-201

The percent block by TCN-201 for neurons transfected with GluN2B mutants R696H and C456Y were not significantly different to each other (NMDAR-EPSC size after TCN-201 addition: R696H: 43.52 ± 3.51 %, C456Y: 39.69 ± 3.41 %, one-way ANOVA with Tukey's MC test $F(37,2) = 7.05$, $p = 0.0025$; C456Y vs R696H $p = 0.7764$ Fig. 4.3c,d). The block recorded in cells transfected with the human GluN2B WT subunit was significantly lower than these (61.34 ± 5.884 % EPSC size, WT vs

C456Y $p = 0.0026$; WT vs R696H $p = 0.0159$), suggesting that for both of these mutants, there was a greater proportion of GluN2A-containing NMDARs contributing to the NMDAR-EPSC than in neurons expressing WT human GluN2B. Fig. 4.3c shows the EPSC size with increasing time exposure to TCN-201. Despite R696H having a GOF characterisation, this experiment suggests that its expression is similar to the LOF C456Y, and that both mutants likely have disrupted expression and trafficking.

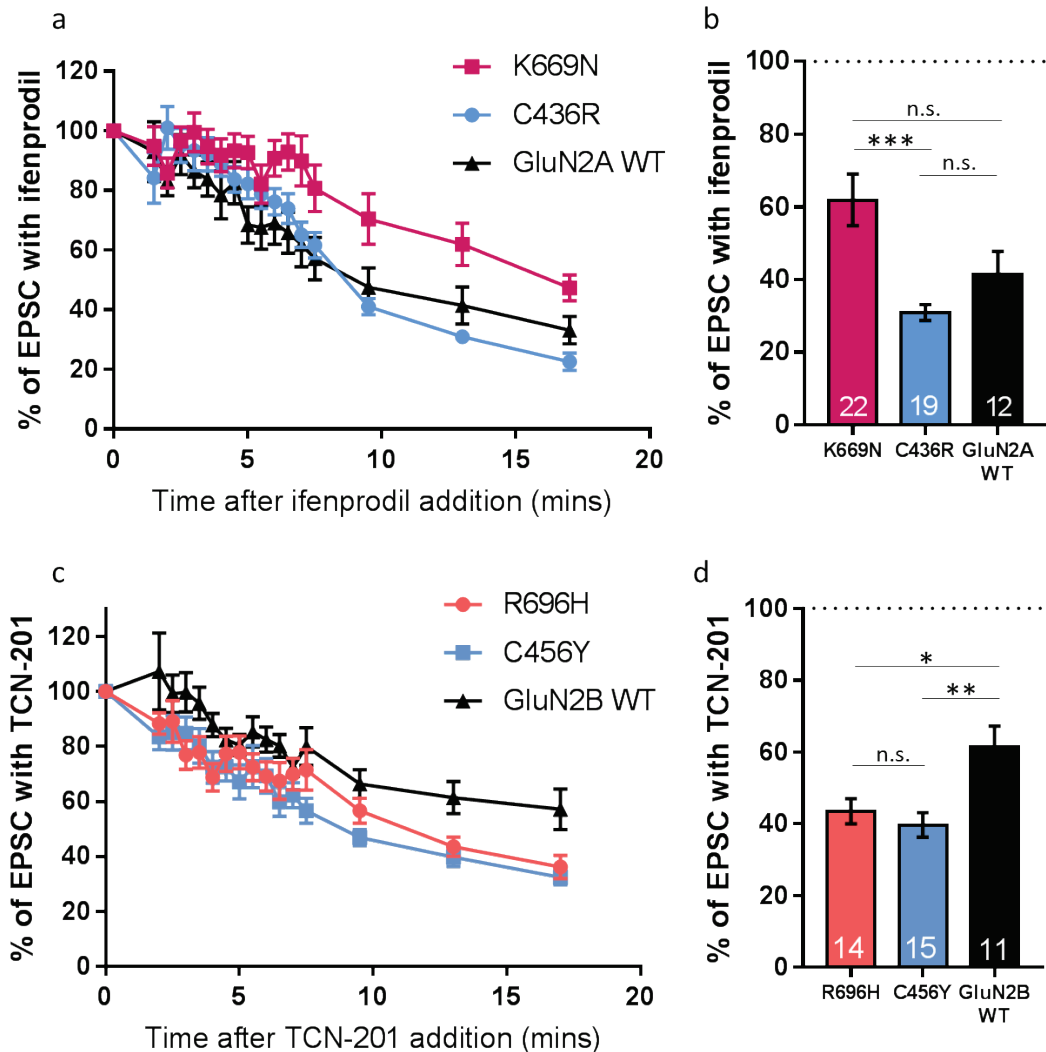


Figure 4.3: Block of GluN2 by ifenprodil or TCN-201 in the presence of mutant subunits.

a) Size of EPSC (%) after the addition of ifenprodil for mutant or WT GluN2A transfected into CA1 pyramidal neurons in hippocampal slices. b) Mean size of EPSC after the addition of ifenprodil at 12 minutes. Data from 3 animals for mutants and 2 for WT. c) Size of EPSC (%) after the addition of TCN-201 for mutant or WT GluN2B. d) Mean size of EPSC after the addition of TCN-201 at 12 minutes. Data from 2 animals each.

This experiment supported the predictions of the expression profiles of different mutants in heterologous expression systems – C456Y shows no current when transfected into HEK-293 cells

and R696H shows 75% less current than GluN2B WT (Swanger et al., 2016). However, the drawback of pharmacological readouts of mutant expression is that mutations may alter the drug potency or efficacy through long-range allostery from the mutation site. This is possible since GluN2A and GluN2B are capable of forming triheteromeric receptors, in complex with GluN1, where they associate in close proximity. Single amino acid residue changes that lead to a side chain with different hydrophobicity, polarity or charge, in the place of the original side chain may alter the folding and structure of the receptor complex that may in turn alter the conformations relevant to the pathway of inhibition. This may directly alter the potency or efficacy of the drug, leading to errors in the interpretation of subunit expression. As a result, experiments described next were conducted to investigate subunit trafficking/expression using approaches that are not subject to these caveats.

Single mutant subunit expression in CA1 neurons

Grin2a-Grin2b double floxed mice were transfected with Cre-GFP and mutant GluN2 subunits to examine their functional incorporation and properties at synapses without interference from the remaining GluN2 subunits. First, double KO (without co-expression of any GluN2A or GluN2B subunits) was done to confirm that the majority of the synaptic NMDARs are composed of GluN2A and B subunits. Most of the current was abolished with the transfection of Cre-GFP only (fig. 4.4a,b) and less than 20% of the current remained (fig. 4.4c). To determine whether this residual current was due to an incomplete KO by Cre recombinase or whether it may be mediated by non-GluN2A and GluN2B currents, the double KO was repeated for a longer time period (21 DIV instead of 8/13 DIV), but once again, a similar level of residual current was found (fig. 4.4c). It may be possible that a small proportion of current is mediated by other receptor subtypes in CA1 neurons or the efficiency of the KO is not complete. Since this current was minimal, it was not expected to produce a large impact on the currents mediated by mutant GluN2 subunits.

GluN2A GOF mutant, K669N, is expressed at the synapse whereas LOF mutant, C436R, is not WT human GluN2A expressed in slices from *Grin2a-Grin2b* double floxed mice rescued the current to roughly 70 % of untransfected neurons (fig. 4.4d). This was not significantly different to the peak amplitude of the NMDAR-EPSCs in GluN2B KO neurons, which are thought to be mediated by mostly GluN2A-containing NMDARs (unpaired t-test, $p = 0.1475$) (fig. 4.4d) (Gray et al., 2011). The decay of the human WT GluN2A subunits also matched the fast decay of the GluN2B KO (unpaired t-test, $p = 0.9873$) (fig. 4.4e), supporting the notion that the receptors remaining in the GluN2B KO are GluN2A-containing NMDARs.

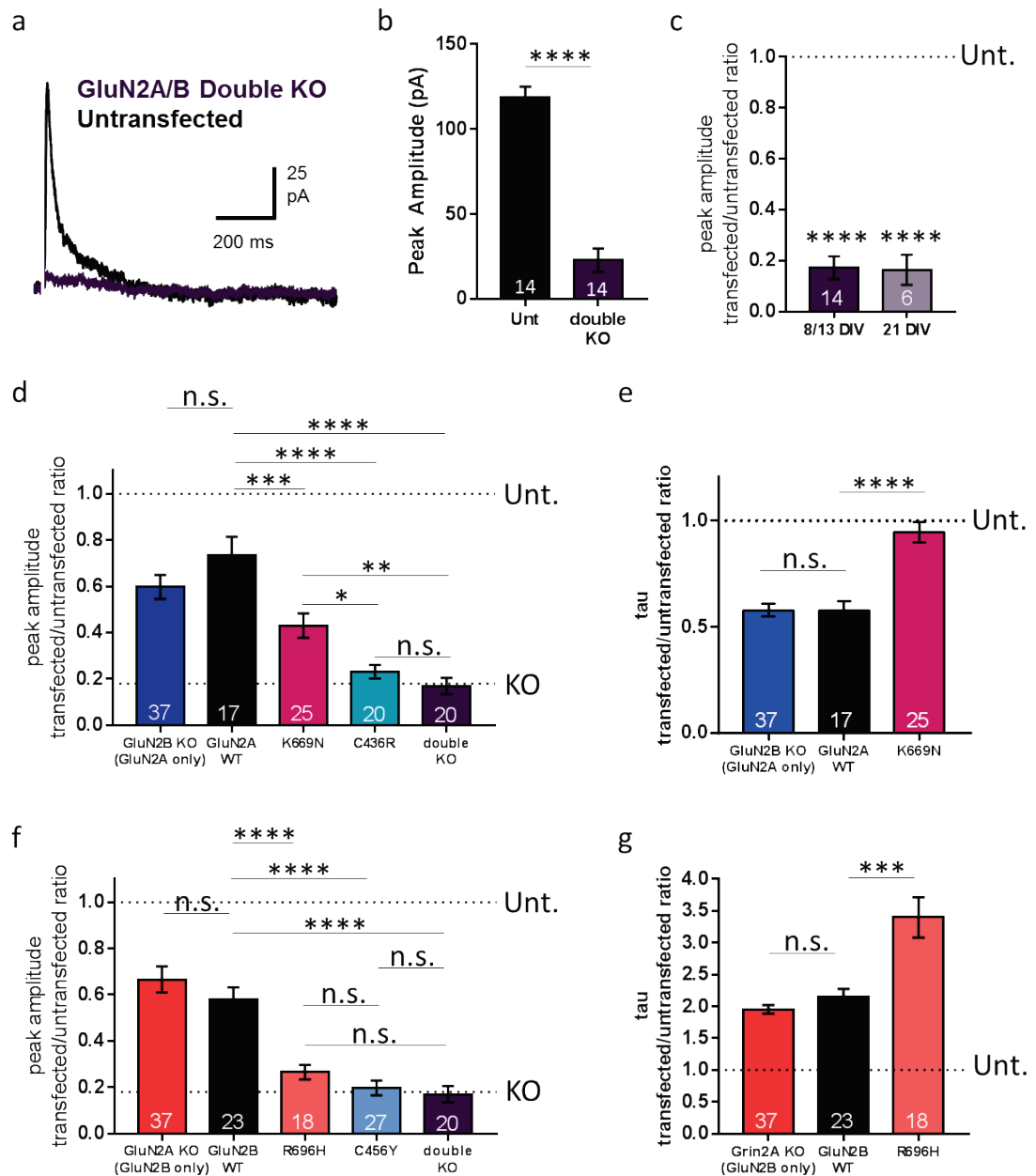


Figure 4.4: Single mutant subunit expression shows diverse effects for GluN2A but not GluN2B mutants.

a) Representative traces from untransfected neurons (black) and double KO neurons (purple) in hippocampal slices at 8/13 DIV. b) Peak amplitudes of untransfected (black) and double KO (purple) at 8/13 DIV. Data from 2 animals. Paired t-test, $p < 0.0001$. c) Ratios of transfected/untransfected of peak amplitudes for double KO at two different time points. 21 DIV data from 1 animal. Paired t-tests of transfected vs untransfected $p < 0.0001$. d) Ratios of transfected/untransfected of peak amplitudes for GluN2A mutants and WT. GluN2B KO: 4 animals; GluN2A WT, K669N, C436R: 3 animals; double KO: 2 animals. e) Ratios of transfected/untransfected for tau of K669N and WT. f) Ratios of transfected/untransfected of peak amplitudes for GluN2B mutants and WT. GluN2A KO: 4 animals; GluN2B WT: 2 animals; R696H, C456Y: 3 animals; double KO: 2 animals. g) Ratios of transfected/untransfected for tau of R696H and WT. * $p < 0.05$, ** $p < 0.01$, *** $p < 0.001$, **** $p < 0.0001$.

GluN2A K669N or C436R were then subsequently transfected into slices from the *Grin2a-Grin2b* double floxed mice to compare their current profiles to the human GluN2A WT (fig. 4.4d). GluN2A K669N rescued the current to roughly 40%; which was about 40% less than the WT subunit rescue (one-way ANOVA with Tukey's MC test $F(78,3) = 21.82$, $p < 0.0001$; K669N vs WT $p = 0.0005$) and lower than predicted from the previous experiment in this chapter, but still indicating that K669N is functionally incorporated into synapses, as this was significantly more current than the KO (one-way ANOVA with Tukey's MC test K669N vs KO $p = 0.0019$). In contrast, C436R produced currents that were not significantly different to the double KO but reduced compared to K669N (C436R vs KO $p = 0.8336$; C436R vs K669N $p = 0.0273$), indicating impaired functional incorporation into synapses, as the previous experiment in this chapter suggested. The decay of the GluN2A K669N-containing NMDARs was slower than for the WT GluN2A expressed in the double KO background (unpaired t-test $p < 0.0001$) (fig. 4.4e), which supported findings published by others showing enhanced functional properties for this GOF mutation leading to prolonged current decay (Swanger et al., 2016). The decay of C436R was not included as the currents were too small for reliable fits of exponential decay times, but the current amplitude being comparable with the double KO (fig. 4.4d) is evidence for poor functional synaptic incorporation. Since the decay of the K669N mutant was shown to be significantly longer than WT in the double-flox in the current chapter (fig. 4.4), it further supports the trend of prolonged current for the same mutant in the single-flox experiments (fig. 3.8).

GluN2B GOF and LOF mutants have impaired expression at synapses

Expression of human WT GluN2B in hippocampal neurons from the *Grin2a-Grin2b* double floxed mice produced currents that were roughly 60% the size of currents from untransfected neurons, comparable to the peak currents of GluN2A KO (unpaired t-test $p = 0.3018$) (fig. 4.4f). The decay of GluN2B NMDARs expressed alone showed the characteristic slow kinetics of these subunits and was not significantly different to the NMDAR-EPSCs recorded in the GluN2A KO cells (unpaired t-test $p < 0.1631$) (fig. 4.4g).

Consistent with the previous observations and predictions of the expression profiles for both GOF and LOF GluN2B mutants (Chapter 3), R696H and C456Y produced very small currents, close to the double KO level (one-way ANOVA with Tukey's MC test $F(84,3) = 23.8$, $p < 0.0001$; R696H vs KO $p = 0.3876$; C456Y vs KO $p = 0.9574$; R696H vs C456Y $p = 0.6215$; R696H vs WT $p < 0.0001$; C456Y vs WT $p < 0.0001$) (fig. 4.4f), consistent with the hypothesis of disrupted trafficking and expression. Interestingly, the decay of the small population of R696H NMDARs in the double KO was roughly 3.5x slower than untransfected neurons (~1.5x slower than WT

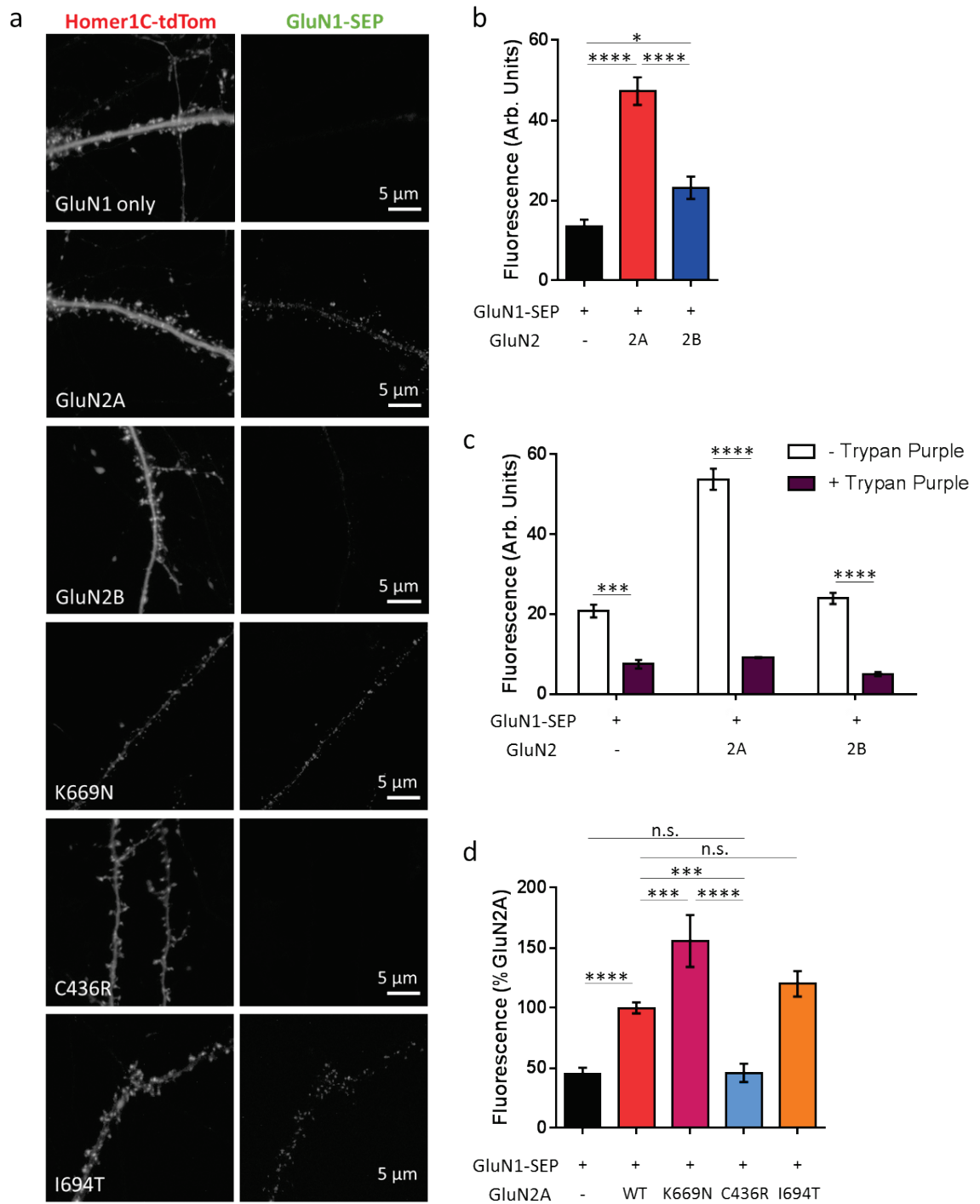


Figure 4.5: Trafficking of GluN2A mutants to dendritic spines differs for a GOF and LOF mutant.

a) representative images of the Homer1C-tdTomato fluorescence which labels post-synaptic densities and SEP-GluN1 signal for the various GluN2 constructs. b) fluorescence, in arbitrary units, for the SEP-GluN1 signal for WT GluN2 subunits. c) fluorescence, in arbitrary units, before and after addition of Trypan purple to estimate surface expression of SEP-GluN1/GluN2 tetramers. d) Percent of GluN2A fluorescence for GluN2A mutants. Data from three cultures of rat hippocampal neurons. * $p < 0.05$, ** $p < 0.01$, *** $p < 0.001$, **** $p < 0.0001$.

GluN2B) (unpaired t-test WT vs R696H $p = 0.0003$) (fig. 4.4g), which was different to the decay found from overexpression in HEK-293 cells (~ 3.6 x slower than WT GluN2B) (Swanger et al., 2016). Therefore, it seems that the functional enhancement to NMDAR time course did not influence much the NMDAR-EPSC decay in the experiments in chapter 2 because GluN2B R696H subunits make little functional contribution to the currents. This suggests that a synaptic expression defect may dominate in the effect of this mutation on NMDAR-EPSCs, thus leading to a 'LOF' synaptic phenotype in neurons.

Trafficking to the synapse

In the above experiments, a functional signature of NMDAR trafficking to synapses was used. However, such experiments cannot distinguish between those mutations that disrupt trafficking to synapses, with those that disrupt the ability of NMDARs to function at synapses. To address this, an imaging assay was carried out using SEP-GluN1 as a reporter for synaptic delivery of GluN2 mutants (Ogden et al., 2017). WT dissociated rat hippocampal neurons were transfected with SEP-GluN1, a GluN1 subunit tagged with a pH sensitive GFP that fluoresces at above pH 7, the pH of the extracellular space, so that subunits in acidic intracellular compartments would not fluoresce. The fluorescence of SEP-GluN1 alone was compared to that of SEP-GluN1 and WT or mutant GluN2 to determine the trafficking profiles for each mutant compared to WT. GluN1 subunits are obligatory for the formation of a functional NMDAR, but they cannot assemble or be expressed at the synapse as homomers in neurons; they have to be in a complex with GluN2 or GluN3 for this to happen. Therefore, co-expression of SEP-GluN1 with a WT GluN2 subunit is anticipated to increase the fluorescence in dendritic spines as GluN1 would now be able to be trafficked to the synapse. This assay was based on the work of Barria and Malinow (2002) and has been used by others to establish the trafficking competence of GluN2A mutants (Ogden et al., 2017).

Homer1C-tdTomato was used as a synaptic marker as it is a protein that is highly present at the post-synaptic density, and so is enriched in the heads of dendritic spines. The SEP-GluN1 fluorescence was measured in the dendritic spine compartments that co-localised with the Homer1C-tdTomato signal. With SEP-GluN1 expression alone, there was very little fluorescence in the dendritic spines, which were clearly visible with the Homer1C signal, and mostly the dendritic shaft was labelled (fig. 4.5a). This background fluorescence may be present due to the endogenous GluN2 subunits existing in hippocampal rat neurons that could assemble with SEP-GluN1 and release it from the ER to the plasma membrane. Expression of WT human GluN2A with SEP-GluN1 increased the trafficking of SEP-GluN1 to spines, observed through the increased

spine fluorescence (fig.4.5a,b), compared to SEP-GluN1 expressed alone (one-way ANOVA with Tukey's MC test $F(51,2) = 40.1$, $p < 0.0001$, SEP-GluN1 alone vs SEP-GluN1+GluN2A WT $p < 0.0001$). Expression of GluN2B resulted in a much smaller increase in fluorescence than WT GluN2A (SEP-GluN1 alone vs SEP-GluN1+GluN2B WT $p = 0.0403$, GluN2A vs GluN2B $p < 0.0001$) (fig. 4.5a,b), suggesting that either the trafficking of GluN1 by GluN2B is less efficient than GluN2A, or that the synapse has a greater capacity for GluN2A expression than GluN2B. This effect has been observed by others (Barria and Malinow, 2002) and is similar to the synaptic incorporation of GluN2A and GluN2B in the rescue experiment in chapter 3.

To determine the amount of surface expression of the SEP-GluN1/GluN2 receptors in dendritic spines, the fluorescence was measured before and after the addition of Trypan purple to the hippocampal cultures. Trypan purple is membrane impermeable and quenches GFP fluorescence (Jullie et al., 2014); the remaining fluorescence after the addition of Trypan purple would reflect fluorescence from any intracellular SEP-GluN1 receptors. The majority of the fluorescent signals from the GluN2A and GluN2B WT subunits were abolished after the addition of Trypan purple (fig. 4.5c), indicating that the receptors were expressed mostly at the plasma membrane (two-way ANOVA, $F(6, 2) = 109.60$, $p < 0.0001$) (fig. 2.9c), and very little fluorescence was from intracellular compartments.

The SEP-GluN1 fluorescence with K669N was greater than with the human GluN2A WT subunit – roughly 150% of WT (one-way ANOVA with Tukey's MC test $F(112,4) = 24.78$, $p < 0.0001$; K669N vs GluN2A WT $p = 0.0005$) (fig. 4.5a,d), suggesting an even greater enrichment at synapses for this mutant compared to WT. This was similar to the expression levels predicted from the ifenprodil inhibition in fig. 4.3, but unlike the peak amplitudes of currents for CA1 neurons that expressed the K669N mutant alone in fig. 4.4. C436R produced an equivalent fluorescent signal to the SEP-GluN1 transfected alone (C436R vs SEP-GluN1 alone $p > 0.9999$; C436R vs GluN2A WT $p = 0.0008$; C436R vs K669N $p < 0.0001$) (fig. 4.5a,d), suggesting that this mutant had a complete trafficking impairment. The trafficking of I694T was measured, as it did not fit the trend exhibited by all other GluN2A mutants as it showed a decay time that was comparable to WT untransfected neurons (chapter 3). It was found that I694T had unperturbed trafficking that was not significantly different to the trafficking of SEP-GluN1 by WT GluN2A subunits (I694T vs GluN2A WT $p = 0.4608$ (fig. 4.5a,d), as the decay would have suggested from the previous experiment.

Discussion

The key finding in this chapter in relation to GluN2A mutants is that similarities in the synaptic phenotype of a GOF GluN2A mutant, K669N, and LOF mutant, C436R, can be explained by different mechanisms. The GOF mutant produced prolonged NMDAR currents by a functional enhancement to the subunit's properties whereas the LOF mutant produced this similar synaptic phenotype through disruption of the trafficking of GluN2A to the synapse, resulting in the NMDAR-EPSC being mediated mostly by GluN2B. This finding contrasted with what was observed in GluN2B. The putative 'GOF' GluN2B mutant, R696H, and a LOF mutant, C456Y, both exhibited poor functional incorporation into synapses leading them both to be associated with faster decaying NMDAR currents. Despite the NMDAR-EPSC decay of the R696H being slower when its properties were isolated in the GluN2A/GluN2B double KO, the small functional incorporation of this mutant meant that it did not significantly influence EPSC decay in the molecular replacement experiments of chapter 3. The faster decay observed for the GluN2B mutants in those experiments could be explained by GluN2A-mediated currents over representing the NMDAR-EPSC.

Limitations of trafficking and expression assays

The pharmacological blockade of GluN2 subunits with ifenprodil or TCN-201 was used as a measure of the relative expression levels of GluN2A and GluN2B at the synapse. The currents that remained after blockade of one subunit were used as a measure of the expression of the remaining subunit. In this experiment, the blockade with the GluN2A WT was not significantly different to the GluN2A mutants, although the two mutants were significantly different to each other. This could reflect the smaller sample size for the WT and therefore requires further recordings to uncover whether statistically significant differences may be detected.

There was a significant latency to the blockade by both drugs so that the percent inhibition had still not plateaued after several minutes of incubation of the hippocampal slice with either drug (fig. 4.3a,c). Whether the total blockade could have differed for the WT or mutant subunits once this plateau had been reached may be a possibility, especially as the differences in block between the different constructs was not huge.

Another issue regarding the pharmacology is that no antagonists are available that offer complete and specific block of either the GluN2A- or GluN2B-containing receptors, and their action on triheteromers confounds interpretation. Ifenprodil (3 μ M) was reported to block currents mediated by GluN1/2B diheteromers up to 88% but triheteromer-mediated currents were blocked by only 32% (Hansen et al., 2014). In contrast, TCN-201 (10 μ M) provided up to

91% block of GluN1/2A diheteromer mediated current while also blocking 72% of triheteromer-mediated currents (Hansen et al., 2014). These issues could affect interpretation if the mutation affected the ability of the mutated GluN2 subunit to form triheteromers. There also remains the potential long-range allosteric effect of the mutation to affect the potency or efficacy of the antagonist to inhibit mutant triheteromeric receptors. For this reason, this experiment was used in conjunction with others to confirm the results.

What the residual current is mediated by is currently unclear, especially as it remained consistent even after longer durations of Cre expression. There is a possibility that the residual current could be GluN2D-, or even GluN3-mediated. GluN2C is almost exclusively expressed in the cerebellum (Watanabe et al., 1992). GluN2D is expressed in hippocampal pyramidal neurons in new-born mice (von Engelhardt et al., 2015) and is downregulated through development (Monyer et al., 1994). GluN3A and GluN3B are expressed in early post-natal weeks in hippocampus but later decline (Kehoe et al., 2013, Matsuda et al., 2002). In organotypic slices, there is a possibility that they may persist *in vitro* but this is unknown. As the residual current is small, it does not likely impact the results.

Finally, the overexpression of GluN2 for the measure of assembly and trafficking competency of GluN1 may have put pressure on the cellular machinery that is involved in transport of proteins from the ER to the plasma membrane, especially as the endogenous subunits were still present in these hippocampal neurons. However, as the fluorescence with WT GluN2A increased dramatically compared to the SEP-GluN1 alone, it suggests that there was still a large capability for incorporation of GluN2A subunits into the synapse. This was also seen with the rescue experiments in chapter 3 where increasing GluN2A concentrations produced progressively faster NMDAR-mediated currents. In contrast, the fluorescence increase with expression of WT GluN2B was much more minor, comparable to the saturated expression levels of WT GluN2B in the rescue experiment of chapter 3. Similar levels of expression for GluN2A and GluN2B have been observed before, where GluN2A levels are greater at synapses than GluN2B, even though the total level of the GluN2B protein is higher (Coultrap et al., 2005, Le Bail et al., 2015, Pian et al., 2010, Sun et al., 2016). This low propensity to traffic the GluN2B subunit would make it difficult to distinguish any effects of GluN2B mutants as the fluorescence with and without GluN2B is very similar.

Overall, the experimental results agree that GluN2A K669N is still expressed and contributes to synaptic currents whereas GluN2A C436R, GluN2B R696H and GluN2B C456Y have impaired trafficking and expression in hippocampal neurons.

LOF mutants

C436R in GluN2A and C456Y in GluN2B have been predicted to cause an impairment in expression due to their effects on protein structure and folding; both mutants disrupt a disulphide bridge which is integral for the stability of the subunit. In heterologous cells, currents from C436R- or C456Y-transfected cells have been at or below the limit of detection and surface/total protein levels have been very low – less than 10% for C456Y and C436R was close to zero % (Swanger et al., 2016). C436R also showed no response to maximal concentrations (30 μ M) of glutamate and glycine and western blots showed ~20 % protein levels of WT for C436R, as well as almost absent surface expression (Addis et al., 2017). Serraz et al. (2016) reported no protein expression with immunoblots for C436R. No currents were detected for C456Y with up to 3 mM glutamate in HEK-293 cells (Fedele et al. (2018). This data is consistent with the findings in this chapter, and suggest that currents from neurons transfected with these two mutants is mediated by the remaining GluN2A subunits that are expressed at the synapse.

K669N expression

For C436R, R696H and C456Y, all three experiments produced a similar results of poor functional incorporation at synapses. However, K669N expression was not as consistent between the pharmacology, electrophysiology and imaging experiments. One possibility for why K669N expression and trafficking was higher than WT GluN2A subunits in two experiments but lower in the double KO could be the difference in the ability of this mutant to assemble and express as diheteromeric vs triheteromeric receptors. In the pharmacology experiment, endogenous GluN2B is present and in the dissociated neuronal cultures, both endogenous GluN2A and GluN2B are present, however, in the double KO, receptors are forced into forming diheterotetramers. In heterologous expression systems, it is also diheterotetramers which are formed as mutants are typically expressed without other GluN2 subunits. The current view of NMDAR subunit composition at neuronal synapses is that triheteromeric receptors dominate (Paoletti et al., 2013, Stroebel et al., 2018). However, the possibilities of reduced ifenprodil potency or efficacy are still present for the pharmacology experiment and the overexpression of GluN2 subunits in the imaging experiment with SEP-GluN1 may contribute a degree of error, as previously discussed. Despite this, it is clear that K669N is still capable of trafficking, assembly and expression, whereas the LOF GluN2A mutant is not. The population of diheteromeric K669N NMDARs which made up 40% of the size of untransfected currents had a prolonged decay compared to WT GluN2A subunits, about two times longer. This is less than what was observed in HEK-293 cells where the K669N subunit current was four times slower than WT GluN2A

subunits, but not different in amplitude to WT GluN2A (Swanger et al., 2016). This difference is odd, considering that in both systems, K669N is a diheteromer with GluN1, and the GluN1 isoform does not greatly impact the GluN2A receptor properties like it does for GluN2B (Yi et al., 2018). The reason for this difference is unclear, as the number of receptors expressed would not impact the biophysical properties such as decay time.

I694T did not exhibit a similar synaptic phenotype to other GluN2A mutants

One mutation was very unusual in that it did not present a common phenotype like the other mutations. This mutation, I694T, did not exhibit the trend in NMDAR-EPSC decay kinetics exhibited by all other GluN2A mutants studied in this thesis. This mutant was included in the imaging experiments to determine whether synaptic expression levels could provide insights into its mechanisms. I694T was trafficked similarly to WT GluN2A subunits, as the decay suggested in the previous chapter. This suggests that the reduction in peak amplitude was a functional alteration caused by I694T, producing a much milder phenotype than all other tested GluN2A mutants. The patient with the I694T mutation has Landau-Kleffner syndrome (Lesca et al., 2013), which is a severe variant on the Epilepsy-Aphasia Spectrum, so a mild synaptic phenotype would not be a convincing mechanism for this patient's disorder. It may be that the effects of this mutant are not detected in the experimental paradigm used in this thesis, such as disruptions to splicing, or it may be that other factors contribute to the disease phenotypes in these individuals.

Is GluN2B impairment more susceptible to expression defects?

Since the putative GluN2B 'GOF' mutation do not exhibit their GOF effects in neurons and the overall postsynaptic response appears to be mediated by GluN2A receptors, it is possible that the GluN2B NMDAR subunit has an increased propensity to have disrupted trafficking and expression when mutated in the LBD (She et al., 2012). Most studies on GluN2B mutant expression are conducted in heterologous cells. However, Swanger et al. (2016) showed that GluN2B LBD mutant C461F had reduced total expression in cultured dissociated cortical neurons and a reduced surface/total expression, indicating impaired trafficking. They also showed that most GluN2B mutants they investigated (five out of seven) had impaired expression and trafficking in HEK-293 cells. Other studies have reported similar effects and found impaired GluN2B trafficking and expression also in heterologous expression systems (Liu et al., 2017, Ogden et al., 2017). In COS-7 cells though, only two out of 11 de novo missense GluN2B mutations resulted in impaired trafficking, with no clues given on expression relative to WT (Vyklícký et al., 2018). These discrepancies possibly reflect cell-type specific trafficking

phenotypes. The data in neurons is very limited and whether the same trafficking and expression profiles from heterologous cells will be observed is not certain. The reportedly GOF mutant, R696H (Swanger et al., 2016), was investigated in this chapter and was found to have a poor synaptic expression similar to the LOF mutant. Swanger et al. (2016) showed a reduction in peak amplitude to roughly ~25% of WT GluN2B receptors, which may have been a functional change or an indication of poor expression. The decay of these currents was 3.6 times longer than WT GluN2B receptors, in contrast to the 1.5-2 times longer currents than WT GluN2B observed in this chapter (~3.5x slower than untransfected neurons). Once again, like the difference in decay for the K669N mutant, there was a large difference in the decays for this GluN2B mutant, however, in this case, the difference may be a result of the slow GluN1a isoform used in heterologous cells being different to the native GluN1 isoforms in CA1 mouse neurons. In rat hippocampal CA1 neurons, both 1a and 1b isoforms were detected (P7 to adult stages) (Laurie and Seeburg, 1994), and this may also be likely for mouse. Alternatively, the effect of filtering caused by limited space clamp may have selectively 'slowed' the kinetics of the faster NMDAR-EPSCs, thereby making the effect size smaller.

One approach to determine whether the GluN2B subunit may be more susceptible to trafficking and expression impairments would be to replicate a 'GOF' GluN2B mutation, such as R696H which displays poor trafficking and expression, in the GluN2A subunit. Whether the mutant would also disrupt the GluN2A subunit's trafficking and expression or would result in an observable 'GOF' phenotype would elucidate this.

Further examination of mutants

To confirm that all GluN2B mutations that were studied resulted in fast decay due to lack of expression, further examination of the trafficking and expression profiles of the remaining mutants will be necessary. This will also be necessary to confirm the diverse mechanisms for the remaining GluN2A GOF and LOF mutants that lead to a common synaptic phenotype. It is highly likely that the GluN2B mutants C436R and C461F have impaired expression due to the severely diminished currents observed in HEK-293 cells (Swanger et al., 2016). This also applies to GluN2A mutants T531M and R518H. This leaves GluN2A L812M and GluN2B R540H which are suspected to have increased functional properties and diminished expression, respectively, but this needs verification in order to fully establish their mechanisms. The expression of these mutants in the double KO to uncover the single subunit decay properties would also be needed to determine whether single subunit effects are present or overshadowed by other NMDAR subunit compositions.

Conclusions

To determine whether the synaptic phenotypes of GluN2A and GluN2B mutants resulted from altered NMDAR function or expression, the trafficking and expression levels were investigated, relative to WT, for a GOF and a LOF mutant from each subunit. GluN2A GOF and LOF mutations appeared to produce a slower decaying NMDAR-EPSCs through very different mechanisms; the GOF mutant K669N increased the functional biophysical properties of the GluN2A subunit, whereas the LOF mutant C436R disrupted GluN2A trafficking and expression leading to a synaptic response that was dominated by slow decaying GluN2B NMDARs. Conversely, for GluN2B subunits, both GOF and LOF, led to impaired trafficking and expression in neurons, allowing the synaptic response to be dominated by fast decaying GluN2A NMDARs. It was found that the GOF/LOF distinction, which was based upon research using heterologous expression systems, was unsuitable when applied in neurons. Whether other LOF and GOF mutants also exhibit these mechanisms will be crucial future research to determine whether these results are applicable to the wider population of LBD mutations in GluN2 subunits.

Chapter 5 General Discussion

Summary of results

The aim of the research presented in this thesis was to investigate the synaptic phenotypes arising from human disease mutations occurring in the GluN2A and GluN2B NMDAR subunits. Despite there being wide ranging effects of GluN2A mutations on receptor expression or function, these mutations ultimately converge on patients having an epilepsy phenotype. In contrast, for GluN2B, a genotype-phenotype correlation was postulated relating LOF and GOF mutations to intellectual disability without or with a seizure disorder, respectively (Lemke et al., 2014). Most published research into the effects of GluN2 mutations focussed on the mutant subunit properties when overexpressed in heterologous cells. This thesis describes and discusses unexpected synaptic dysfunction arising from a range of different mutations in the LBD and LBD-TMD linker regions of the GluN2A and GluN2B subunits.

In support of the first hypothesis, all GluN2A mutants tested, with the exception of I694T, prolonged the duration of the NMDAR component of synaptic transmission. For mutants with undisrupted trafficking and expression, such as the GOF mutant K669N, this occurred by a functional increase in the receptor channel properties. For mutants with disrupted trafficking and expression, such as LOF C436R, the prolonged decay was mediated through the remaining GluN2B-containing NMDARs at the synapse, which have characteristically slower decay than GluN2A-containing NMDARs.

Surprisingly, the GluN2B mutation data was in contradiction to the second hypothesis. Specifically, it was found that both putative GOF and LOF GluN2B mutations within the LBD produced synaptic responses that decayed more rapidly than WT, essentially showing a LOF synaptic phenotype. For the putative GOF mutation R696H, NMDAR expression and trafficking was found to be impaired, as was found for the LOF mutation C456Y. Despite the GOF mutation R696H showing prolonged NMDAR activity when studied in isolation in the *Grin2A-Grin2B* double floxed background, these functional properties contributed a minimal amount in the single gene-flox condition and so, the synaptic responses were dominated by the remaining GluN2A subunits at the synapse, which was also true for the LOF mutant.

Methodology: translating heterologous cell research into neurons

Predictions of neuronal and synaptic properties resulting from manipulations made in heterologous expression systems seem to be inconsistent with the empirical measurements described in this thesis. Swanger et al. (2016) predicted the synaptic charge transfer that would result from a variety of GluN2 mutations. The authors estimated the synaptic charge transfer

(Q) from the product of the following parameters: deactivation time constant, channel open probability, surface GluN2 expression and relative agonist responses to peak cleft glutamate and glycine concentrations. The comparison of these predictions by Swanger and colleagues with the empirical measurements of charge transfer from this thesis are plotted in Fig 5.1 for six mutants: K669N, I694T, C456Y, C461F, R540H and R696H.

Discrepancies are clearly evident for the severe LOF GluN2B mutants, C456Y and C461F. Both of these mutants were shown to exhibit low surface/total GluN2 expression ratios, approximately 10-20% respectively relative to WT GluN2B expressed in heterologous cells (Swanger et al., 2016). Combined with effects on agonist potencies, these mutants have miniscule predicted synaptic charge transfer (>1% of WT). This contrasts with the modest drop (to 52-60%) in the measured synaptic charge transfer (fig. 5.1). These discrepancies are not completely explained by trafficking differences of these mutants in heterologous cells compared to neurons as the same authors compared the expression of GFP-tagged GluN2B mutants in neurons and found approximately 45% surface/total for C461F relative to WT GluN2B (Swanger et al., 2016). An alternative explanation for the discrepancy is that the predictions do not account for the other GluN2 subunits that are typically expressed in neurons and contribute to overall synaptic charge transfer. A proportion of the synaptic charge transfer, in hippocampal CA1 neurons, would be mediated by GluN2A. Even with mutants that cause a complete loss of GluN2B so that the predicted charge transfer would be less than 1% of WT GluN2B, diheteromeric GluN2A NMDARs would comprise the remaining charge transfer. The size of this response would depend on the ratios of GluN2B-containing and GluN2B-lacking NMDARs at the synapse.

The explanations for large discrepancies between predicted and observed charge transfer are less clear for other mutants. The putative GOF GluN2B mutant R696H exhibits only 26% lower surface/total expression ratios relative to WT GluN2B expressed in HEK cells (Swanger et al., 2016). The 5-fold high glutamate potency and almost 5-fold slower deactivation of this mutant compensate for the lower expression and are predicted to give a 1.9-fold increase in synaptic charge transfer (Fig 5.1). Poor rescue of GluN2B R696H in GluN2A/GluN2B double KO neurons (Chapter 4) indicates that there is very little functional incorporation of this mutant at synapses. The impact of this is emphasized by the rapid decay time constant of the NMDAR-mediated EPSC in the GluN2B R696H molecular replacement experiment, which resembles more the GluN2B KO (Chapter 3) than the slow deactivation or EPSC decay of GluN1/GluN2B (R696H) (Chapter 4; Swanger et al. 2016). Another explanation could be the parameterization of the model used for

the predictions. Each of the parameters used in the model are equally weighted, which may not be adequate to model changes in synaptic charge transfer. The model also does not account for other factors known to modulate NMDARs, such as cleft pH, co-released zinc, calcium-dependent inactivation, which could also be affected by the mutations. The relevant contribution of these factors is implicit in measurements of NMDAR-mediated synaptic currents following molecular replacement (Chapter 3).

Potential issues with the parametrization of the prediction model of Swanger and colleagues may explain discrepancies for the I694T mutant. Molecular replacement with GluN2A I694T rescued all measured properties of NMDAR-mediated EPSCs similarly to GluN2A WT, except peak amplitude (Chapter 3). In HEK cells, I694T expression was only modestly affected (surface/total ratio ~75% of WT) (Swanger et al., 2016), and I694T had little impact on the synaptic delivery of GluN2B I694T in neurons (Chapter 4). The modest decrease in glutamate potency together with a small drop in open probability combined to predict a 65% drop in synaptic charge transfer for this mutant (Swanger et al., 2016). However, no change was found in measured synaptic charge transfer (fig. 5.1), despite the drop in peak amplitude (Chapter 3). This indicates that the agonist potency and open probability parameters may have a lesser influence on the prediction than anticipated or that other parameters may be more impactful. Alternatively, this mutant may behave differently at the synapse than in the conditions of the experiments underlying the model used to predict synaptic charge transfer.

Together, these comparisons illustrate that to fully understand the impact of GluN2 variants one should not only rely on heterologous expression systems. By examining mutation effects on NMDAR-mediated EPSCs, the receptor trafficking, stoichiometry and allosteric modulation by endogenous ligands are taken into consideration, all within the native environment of the receptor – in neurons at synapses. It is important to note that the effects of GluN2 mutants will be different in diverse neuronal populations that express varied combinations of GluN2 or GluN3 subunits. The influence of this will be most evident for LOF mutations, where the resulting drop in the mutant subunit at the synapse will reveal more the properties of the receptors composed of the remaining regulatory subunits, which can vary for deactivation, magnesium block and open probability (Paoletti et al., 2013, Vicini et al., 1998). In contrast, if no other regulatory subunits are expressed, then the LOF mutant would simply knockdown NMDAR content at synapses. Parvalbumin- and somatostatin-positive interneurons in the hippocampus contain GluN2A, GluN2B and GluN2D NMDARs; block of GluN2B resulted in slowing of NMDAR-EPSCs

from P3-12 but not at P20-25 due to the higher GluN2A expression at the later age (von Engelhardt et al., 2015).

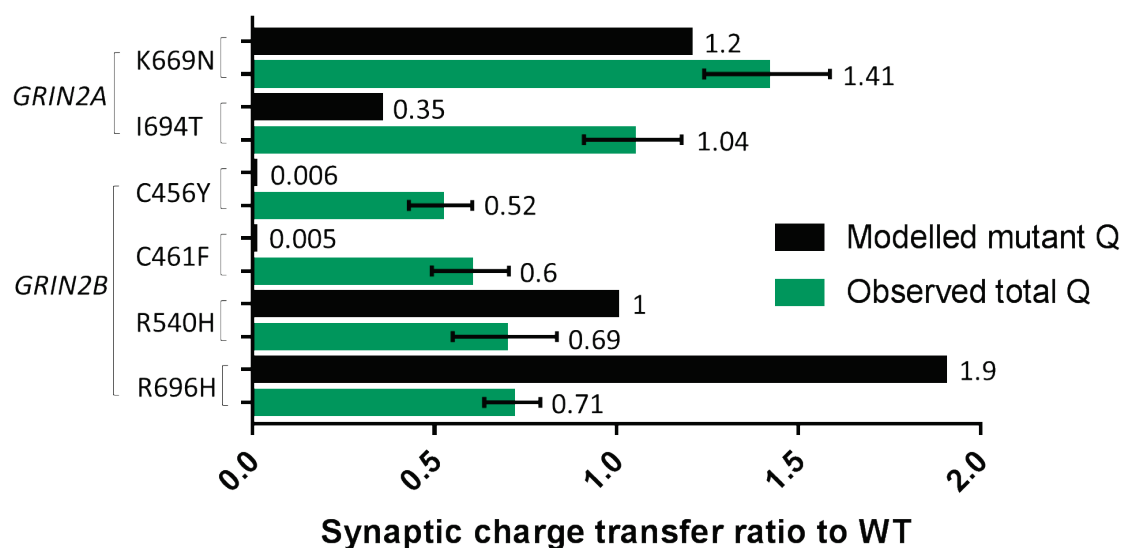


Figure 5.1: Synaptic charge transfer predicted from heterologous cells (Swanger et al., 2016) and observed charge transfer from mutants transfected into CA1 neurons.

Modelled synaptic charge (Q) was done using tau (τ), open probability (P_o), surface protein levels ($Surf$) and relative response to agonist (R), all measured in *Xenopus* oocytes and HEK-293 cells, where $Charge\ transfer_{Synaptic} = \tau_{mut/wt} \times P_{o\ mut/wt} \times Surf_{mut/wt} \times R_{Gly} \times R_{Glu,Synaptic}$ where $R_{agonist} = 1/(1+(agonist\ EC_{50}/[agonist])^{nH})$ and nH is the Hill slope, From Swanger et al. (2016). Observed data: mean \pm SEM from mutants transfected into CA1 neurons in hippocampal slices.

GluN2B GOF mutants in the TMD have been found to still traffic and be expressed at the synapse (Fedele et al., 2018), however the GluN2B LBD mutants studied in this thesis impair NMDARs in this sense. LBD mutations which cause a large change to the glutamate potency have a lower surface/total expression compared to WT (Swanger et al., 2016). The glycine binding site in GluN1 and glutamate binding in GluN2B have been shown to regulate receptor surface trafficking so that mutations which reduce glutamate potency result in reduced receptor trafficking and retention in the ER (Kenny et al., 2009, She et al., 2012). The same has been found for AMPARs (Coleman et al., 2009, Coleman et al., 2010, Penn et al., 2008) and kainate receptors (Gill et al., 2009, Mah et al., 2005). In the LBD, GluN2B mutants may affect the binding of glutamate which facilitates trafficking of the NMDAR out of the ER (She et al., 2012). The present findings may not be relevant to mutations in other subunit domains since they may not have an impact on glutamate potency. Investigation beyond the LBD would help to determine this.

Furthermore, whether binding of glutamate facilitates GluN2A trafficking is unknown and the GOF GluN2A mutants do not suggest any trafficking impairments (chapter 4) so this may be a specific case for GluN2B LBD mutations.

Effect of decay and amplitude on neuron signalling/function for GluN2A mutants

Changes in decay kinetics of NMDAR-mediated EPSCs were a common feature of almost all the mutations tested. The slow time course of NMDAR currents facilitates temporal summation of EPSPs, which increases the probability of the postsynaptic neuron spiking to physiologically relevant patterns of synaptic activity (Augustinaite and Heggelund, 2007, Hunt and Castillo, 2012). In the same way, due to their slower decay, neurons expressing GluN2B subunits have a greater ability to integrate synaptic inputs than those with GluN2A subunits (Hildebrand et al., 2014). In contrast, mice that have had the GluN2B subunits switched for GluN2A exhibit lower levels of integrated synaptic currents, due to the faster deactivation time of GluN2A containing receptors (Wang et al., 2011). A similar result was observed from replacement of the GluN2B for GluN2A in cortical cells induced by light exposure of dark-reared rats; temporal summation of NMDAR-EPSCs was reduced after 40 Hz stimulation from faster decaying GluN2A NMDARs (Philpot et al., 2001). Consistent with these findings, increased amounts of GluN2B expression levels in the CA1 of rat hippocampus after contextual fear learning resulted in greater EPSP-spike coupling, which was inhibited by the GluN2B-selective blocker ifenprodil (Sun et al., 2016). Therefore, it is tempting to speculate that LOF and GOF GluN2A mutations with prolonged decay times will lead to an enhanced neuronal activity and spike generation. It will be important in future experiments to evaluate how sensitive synaptic integration is to graded changes in the time course of NMDAR-mediated EPSCs as it may be that over the population of excitatory neurons, these effects may be sufficient to cause some circuits to undergo synchronous, repetitive discharges, similar to those observed during seizures (Amakhin et al., 2016).

Alterations to the time course of NMDAR-mediated synaptic currents were often accompanied by a reduction in the peak amplitude of currents in GluN2A KO and missense mutations studied (L812M, C436R, T531M and R518H). On first sight this would seem consistent with the idea that there is no compensation by synaptic recruitment of additional GluN2B-containing receptors. However, this is difficult to establish firmly with the evidence presented here alone since GluN2A and GluN2B differ in their open probability (Paoletti et al., 2013). GluN2B-containing receptors have a 5-fold lower open probability so even if GluN2B-containing receptors were to substitute for the reduction in GluN2A, the peak amplitudes will likely be smaller anyway. This is further

complicated by the different negative allosteric modulation of open probability of the GluN2 subunits by zinc, which is co-released with glutamate at the Schaffer collateral synapses (Vergnano et al., 2014).

For mutants with opposing effects on peak amplitude and decay of NMDAR currents, it would be important to ascertain which altered property would have a greater impact on synaptic signalling. One way to investigate this would be to measure the post-synaptic calcium entry using a calcium indicator, such as GCaMP, and imaging of the fluorescent signal upon activation of NMDARs in cultured hippocampal neurons. The size of the calcium signal for the mutants, relative to WT subunits, with recurrent activation of receptors would give an indication of the level of activity of the mutant receptors and whether the reduction in peak amplitude seen for some mutants would be sufficient to balance out the prolonged decay that is simultaneously observed. Another approach could be employed using electrophysiology in organotypic hippocampal slices where the Schaffer collateral pathway can be repeatedly stimulated with high frequency and the summation of post-synaptic CA1 neuron currents or potentials can be recorded. This would enable the detection of the efficiency of summation for each mutant and whether the peak amplitude has any significant impacts that could attenuate the effects of the decay time on synaptic integration.

LOF phenotypes of GluN2B mutants

The NMDAR component of EPSCs exhibited LOF for the full range of GluN2B mutations tested. The functional incorporation of GluN2B mutants at synapses was tested for the putative GOF mutant R696H and the LOF mutant C456Y and the results suggest that loss of synaptic function may be a common phenotype for LBD mutants of GluN2B. These mutations are associated with a range of mental disorders that include intellectual disability, ASDs and neurodevelopmental abnormalities. These disorders have a feature in common: that the E-I balance is disrupted leading to aberrant neuronal network activity. Both enhanced and reduced activity levels through dysregulation of both excitatory and inhibitory systems have been reported (Dani et al., 2005, Frega et al., 2018, Kroon et al., 2013, Rubenstein and Merzenich, 2003, Tabuchi et al., 2007, Takarae and Sweeney, 2017). The reduced NMDAR signalling likely has impact on both intrinsic cell excitability and network level activity due to the possible impairment of synaptic integration of inputs from much quicker and smaller NMDAR responses. A reduction in summation, reduced intrinsic cell excitability and reduced network excitability will likely cause a disruption to the E-I balance which is essential for the processes of neuronal maturation, synapse maturation and dendritic spine formation during the critical periods in early

development (Jedlicka et al., 2018, Lee et al., 2017, Subramanian and Nedivi, 2016). These processes have been shown to be perturbed when the E-I balance is tipped during critical periods as the specific time windows for structural development becomes disrupted, with either delayed onset or complete disruption of these processes (Kroon et al., 2013). GluN2B is known to be involved in the critical periods of development and it is highly expressed at this time (Gambrill and Barria, 2011, Monyer et al., 1994). With the disruption of these structural developments, neuronal populations with aberrant spine morphology or density result, a widely reported observation in many types of mental and neurodevelopmental syndromes that include ID and ASD (He and Portera-Cailliau, 2013, Kaufmann and Moser, 2000, Koyama and Ikegaya, 2015, Purpura, 1974). Ectopic early expression of GluN2A in CA1 of rat hippocampal slices exhibited fewer dendritic spines, indicating fewer synapses, and a reduced spine density and volume (Gambrill and Barria, 2011). Expression of GluN2A also reduced spine motility – additions and retractions of spines – whereas expression of GluN2B enhanced this, without affecting spine density or volume (Gambrill and Barria, 2011). Knockdown of GluN2B reduced the number of functional spines, motility and spine density, whereas knockdown of GluN2A during this period had no significant effects due to the low expression of GluN2A during early post-natal development (Gambrill and Barria, 2011). In contrast, delayed GluN2B to GluN2A switch (resulting from GluD1 KO) increased spine density and the number of spines (Gupta et al., 2015). Eps8 KO mice, which lack an NMDAR-associated actin-regulating protein, show an impaired GluN2B to GluN2A subunit switch and have neurons with immature filopodia-like spines (Morini et al., 2018). A loss of GluN2B, resulting from the missense mutations studied here would likely alter many developmental processes, which include features of spine development and maturation. Interestingly, a common observation in cases of ID and ASD is of thin immature filopodia-like spines (Purpura, 1974), which is likely linked to the cognitive impairments and intellectual deficits as spine morphology is thought to be the structural basis of learning and memory. In the Fragile X mouse model, *Fmr1*^{-/-}, synaptic plasticity impairments are reversed by inhibition of GluN2A, but not GluN2B (Lundbye et al., 2018), suggesting that enhanced GluN2A activity, as would occur with all studied GluN2B mutations that showed a LOF effect in neurons, could be linked to the ID and ASD exhibited in Fragile X syndrome.

Future research could focus on the longer term effects of GluN2 mutants on synaptic structure and properties. Using the same methods as the trafficking experiments with SEP-GluN1 in chapter 4, the cotransfected Homer1C-tdTomato can be used to measure the spine densities and spine lengths. As these mutants may have effects on developmental processes, long term synaptic properties which includes structural features of synapses may be altered. The numbers

of spines, which may reflect synapse number could provide an indication of the changes to activity levels; a higher spine density, assuming mature functional synapses, could suggest the propensity for greater levels of activity. In contrast, reduced spine density or the presence of long, thin immature spines may be a sign of deficient neuronal signalling.

Reduced excitatory NMDAR-mediated transmission in pyramidal neurons is consistent with the idea that deficits in synaptic signalling, learning and developmental abnormalities may underlie the clinical phenotypes of ID and ASD (Guang et al., 2018, Verma et al., 2019). The findings for the GluN2B mutations paint a more complicated picture since some of the mutants tested (C436R, C461F and R540H) are found in patients with seizure disorders. Many studies have reported paradoxically intensified and increased duration of seizures and enhanced synaptic connectivity in conditions of insufficient NMDAR activity, NMDAR antagonists, such as AP5, and low extrasynaptic GluN2B-NMDAR activity (Bausch et al., 2010, McKinney et al., 1999, Sveinbjornsdottir et al., 1993). The different genetic background of human patients may also influence how the changes in NMDAR mutations ultimately affect excitability and plasticity within cortical networks (Myers and Mefford, 2015, Noebels, 2015). Single-gene epilepsies illustrate that many genes are involved in regulating E-I balance and seizure generation (Noebels, 2015). Indeed, the potential of genetic modifiers to influence seizure phenotypes is well illustrated by the effect of genetic background (mouse strain) on the seizure phenotype of mice carrying a LOF allele for the sodium channel subunit (Nav1.1) (Miller et al., 2014, Yu et al., 2006). This could contribute to the spectrum of phenotypes observed in epilepsy-aphasia syndromes for GluN2 mutations.

Epilepsy is often comorbid with other brain disorders with there being a particularly high incidence of seizures in individuals who exhibit ID and ASD (Lee et al., 2015a, Rubenstein, 2010). Published figures show that 80% of patients with ID and ASD have abnormal Magnetoencephalography (MEG) activity and almost 70% exhibit epileptiform activity with electroencephalography (EEG) (Lewine et al., 1999). The ID and ASD in syndromic disorders such as Kleefstra syndrome, Rett syndrome, and Fragile X, are also associated with hyperexcitability and loss of inhibitory signalling and synaptic strength (Doll and Broadie, 2014, Frega et al., 2018, Lee et al., 2017, Takarae and Sweeney, 2017). In a Down's syndrome mouse model, Ts65Dn mouse model, general inhibition of NMDARs with memantine rescued learning and memory impairments (Costa et al., 2008). In human patients, memantine was less affective but did have some performance enhancement in memory recall assessment (Boada et al., 2012). In mouse neurons with knockdown or KO of calcium/calmodulin-dependent serine protein kinase, a

membrane-associated guanylate kinase, there is an impaired E-I balance associated with a reduction in GluN2B expression (Mori et al., 2019). Knockdown of GluN2B specifically disrupted E-I balance (increased frequency of mEPSCs and reduced frequency of mIPSCs) and overexpression of GluN2B rescued these E-I balance impairments (Mori et al., 2019). Gray et al. (2011) also showed that mEPSC frequency is enhanced with a GluN2B KO in acute slices and this has been replicated in organotypic slices along with reduced mIPSCs frequency (unpublished – Wajeeha Aziz, Penn Lab, University of Sussex). Although evoked NMDAR responses were reduced with the GluN2B mutant subunits, spontaneous activity may thus be enhanced, through regulation of AMPAR and GABAR-mediated synaptic transmission. However, the lack of effect of any mutation on evoked AMPAR-mediated EPSCs in chapter 3 are not consistent with these ideas.

An important limitation in the approach used here concerns the period of time that the mutant GluN2 subunits were expressed in CA1 hippocampal neurons. GluN2 disease mutations occur in patients from the beginning of development, whereas here the replacement of endogenous to mutant genes was two weeks after birth (1 week *in vivo* plus 1 week *ex vivo*). In the experimental design, all developmental processes and neuronal maturation proceeded without disruption, whereas in human disease patients it is highly likely that several processes or critical periods in development are perturbed due to GluN2 mutants altering the regular NMDAR activity and function at these times. Since GluN2B expression dominates in early development this may be more of an issue for the investigation of GluN2B mutants than for GluN2A. Furthermore, in the design, only a few cells – up to a maximum of ten per slice – contained mutant GluN2 whereas in disease patients, all neuronal cells that express GluN2A and GluN2B subunits contain the mutant variant. This means that the effects of GluN2 mutants at the network or circuitry level were not captured, which may play a large role in the disease occurrence and contribute to the malfunctioning processes involved. Using LOF mutants as an example, it is known that GluN2B KO is lethal (Kutsuwada et al., 1996) and associated with hippocampal plasticity impairments and reduced spine density and GluN2A KO is associated with transient abnormalities in the brain microstructure (Salmi et al., 2018) and epileptiform activity (Salmi et al., 2019). These macroscopic, multicellular changes are likely to alter network activity and development in ways that cannot be replicated with sparse manipulation and the impacts of these may not be present after normal development in the conditional KO mice. Seizure disorders and disorders involving ID, ASD and related mental disorders are the result of a global network disruption and understanding the mechanisms at this level will also be crucial, alongside the single-cell level. Although examining the cell-autonomous effect of NMDAR mutants may pose difficulties in

relating findings to the disease state, it provides the opportunity to deconvolve the effects directly on NMDARs at synapses. This would be the foundation to uncovering disease mechanisms.

Impacts of NMDAR mutants on inhibitory synapses

Studying excitatory neurons is an important path to understand how synaptic activity can be perturbed by ion channel mutations. However, there is extensive and intricate modulation and control of these neurons by the inhibitory neuronal network. Studying the effect of NMDAR perturbations in only one of these systems provides only a partial image of their impact at a network level. The E-I balance, when aberrant, is implicated in GluN2 disease phenotypes that range from seizure to mental disorders (Eichler, 2008, Ferguson and Gao, 2018). As a result, both excitatory and inhibitory circuits are crucial to examine in order to fully grasp the underlying changes to neuronal activity that may lead to disease states. As GluN2 subunits are involved in the regulation and development of inhibitory neuronal networks, the effect of mutants on this system is crucial to understand.

While the work presented in this thesis focussed on hippocampal pyramidal neurons, it is possible that NMDARs, either at inhibitory synapses or at excitatory synapses onto interneurons, play a significant role in NMDAR related disorders. Immunocytochemical labelling and electron microscopy revealed that both NMDAR subunits GluN2A and GluN2B are present at somatic GABAergic synapses pre- and post-synaptically in the mouse hippocampus (Paquet and Smith, 2000, Szabadits et al., 2011). Furthermore, it has been found that in neurons that lack NMDARs, inhibitory synaptic transmission mediated through GABARs is largely diminished, although, tonic inhibition mediated through extra-synaptic GABARs is enhanced (Gu et al., 2016). Recently, it was found that ambient synaptic glutamate levels are higher at inhibitory synapses than excitatory synapses, and therefore NMDAR activation at either synapse differs; ambient glutamate activated synaptic NMDARs more at inhibitory synapses (Yao et al., 2018). The effect on inhibitory transmission by GluN2B NMDAR mutants may be key to seizure incidence through a reduced excitatory drive to inhibitory interneurons, resulting in possible greater network excitability (Carlen et al., 2012, Korotkova et al., 2010, Su et al., 2018).

NMDAR activity is important for inhibitory synapse function as application of NMDA (NMDAR agonist) to neurons of the superior colliculus caused a premature enhancement to GABA_AR currents at P12 instead of the regular P18 enhancement in rat, due to activation of NMDARs (Aamodt et al., 2000). Although, it was unclear whether it was from NMDARs present on

GABAergic neurons directly or indirectly by activation of NMDARs on other neuronal types. Furthermore, NMDA application increased the size of GABAergic boutons in cerebellar cultures and frequency of spontaneous GABA release (Fisman et al., 2005). NMDAR signalling in individual neurons in the hippocampus during development is crucial for the maturation of GABAergic synapses (Wang et al., 1998) as both spontaneous and evoked GABAR-mediated events are significantly impaired with NMDAR KO due to a reduction in GABAergic synapse number, and increasing NMDAR activity enhances GABAR transmission (Gu et al., 2016). These effects were also present in cortical and midbrain neurons and were not limited to the hippocampus (Gu and Lu, 2018), suggesting a widespread role for NMDARs in the development of GABAergic transmission. The balance between excitation and inhibition is crucial in the maintenance of a regular level of circuit activity (Horn and Nicoll, 2018) and with the possible stunted development of the inhibitory network or NMDAR hypofunction in inhibitory interneurons, it is likely that this would tip the balance and result in aberrant levels of activity.

Since GluN2B is crucial in development, whereas GluN2A signalling begins after birth, GluN2B may have a more significant role in regulating inhibitory synapses. Pre-synaptic GluN2B-containing NMDARs on GABAergic neurons in P12-15 rat cortex act to enhance GABAR transmission, with NMDAR and GluN2B antagonists resulting in a block of this potentiation (Mathew and Hablitz, 2011). Mice that lack GluN2B expression in hippocampal interneurons develop seizures and die between P15-P20 when both alleles are affected; although heterozygous deletion was not fatal for mice and the seizure incidence was not reported (Kelsch et al., 2014). Since GluN2B LBD mutations are likely LOF mutants from impaired trafficking or expression, similar results may develop. Through a combination of reduction in activity of both the inhibitory and excitatory neuronal networks, it is likely that multiple signalling pathways and processes will be disrupted, affecting the E-I balance, basal synaptic signalling, and leading to the presentation of many disease phenotypes, as occurs for GluN2B missense mutants.

Treatment of patients carrying GluN2 mutations

From the mismatches in effects observed in heterologous expression systems and neurons, it suggests that the characteristics of individual mutant subunits cannot be used to interpret the effect in neurons. 'LOF' GluN2A mutations and 'GOF' GluN2B mutations had the opposite effects in neurons as they did in heterologous cells but GOF GluN2A and LOF GluN2B had the predicted outcomes. Pharmacological treatment strategies to correct the activity levels for LOF GluN2A and GOF GluN2B from data collected in heterologous cells may be unsuitable and may in fact worsen disease symptoms. In the case of GluN2A-L812M which did show GOF effects in neurons,

as it did in heterologous cells, treatment with memantine, an uncompetitive NMDAR antagonist, reduced seizure frequency from roughly 11 seizures a week to 3 seizures a week in a patient who exhibited early-onset epileptic encephalopathy and cognitive impairment (Pierson et al., 2014). This strategy was suitable and proved effective for this particular mutant as L812M enhanced GluN2A decay. Memantine has also been studied for its potency and efficacy when applied to HEK-293 cells expressing either GluN2B-R696H or GluN2A-K669N which exhibited GOF in these cells (Swanger et al., 2016). Both potency and efficacy of memantine were similar to WT for both mutants, and it was suggested that memantine could provide beneficial treatment to patients with mutants that have these GOF effects. For K669N, this may, in fact, be beneficial, however, R696H, which showed LOF in neurons, inhibition of NMDAR currents may worsen the disease severity. For a patient with Rett syndrome and intractable epilepsy who had a GluN2B mutation L643P that had not been previously characterised, memantine was given as an adjunctive treatment. This caused the patient to have more frequent seizures and memantine use was therefore discontinued (Kyriakopoulos et al., 2018).

The use of positive allosteric modulators (PAMs) for the treatment of 'LOF' GluN2A mutants to enhance NMDAR function, as proposed by Addis et al. (2017), is also likely to worsen disease symptoms. Addis et al. (2017) found that GluN2A mutations C436R and D731N produced no response to maximal glutamate and glycine application (30 μ M) and several other mutants showed reduced potencies. Therefore, they used the GluN2A-selective PAM, Compound 275, to increase responses to glutamate for the mutants that showed reduced glutamate potencies. This may aid in correcting the reduced peak current amplitudes that were observed in neurons for putative LOF GluN2A mutations, although, the PAM was not at all effective for C436R and D731N, possibly due to the almost complete absence of the GluN2A-C436R subunit at the membrane. Therefore, this approach would only be efficacious for cases where the expression is not completely lacking. Also, considering the disease phenotypes of epileptic disorders exhibited by these mutants, PAMs may not be the ideal choice and may increase seizure incidence as the prolonged NMDAR-mediated EPSC decay for LOF mutations may also be intensified. In five patients with *GRIN2A* mutations that cause truncations, duplication/deletions, and affected splicing, anti-epileptic drugs (AED) that reduced excitation or enhanced inhibition resulted in an improvement in seizures (von Stulpnagel et al., 2017). All patients that had these mutations exhibited epileptic syndromes and had moderate to severe ID. In 3/4 patients who were given Valproic Acid, a GABAR enhancer and voltage-gated sodium channel inhibitor (Drugbank DB00313), there was an improvement in the seizure conditions. Sulthiame, which also blocks sodium channels (Fejerman et al., 2012), caused an improvement

in 3/5 of patients. Clobazam, which enhances GABAergic transmission, improved symptoms for 3/5 patients. Reducing neuronal transmission would be the appropriate course of action for both GOF GluN2A mutants and 'LOF' mutants that still enhance NMDAR signalling. Despite the improvement in the disease conditions for some patients that were given these AEDs, some patients still do not respond well. This suggests that certain neuronal systems and circuitry need to be targeted instead of general enhancement of inhibitory networks or inhibition of excitation, for specific patients. Characterisation of the mutants in neurons will help to narrow the precise pathways and systems that contribute to the disorder in each unique case.

Similar to the case of PAMs for GluN2A mutants described above, negative allosteric modulators (NAMs) for the treatment of GluN2B 'GOF' mutants, such as radiprodil, proposed by Mullier et al. (2017) may also be unsuitable. Mullier et al. (2017) investigated the properties of GluN2B 'GOF' mutants R540H, N615I and V618G. R540H showed a slight enhanced glutamate potency whereas N615I and V618G had completely abolished magnesium blockade and even had greater currents in the presence of magnesium in *Xenopus* oocytes. Therefore, the reasoned therapeutic agent was a NAM to reduce the 'GOF' effects. Radiprodil retained its blocking effects on these mutant GluN2B subunits and therefore was suggested as a 'valuable therapeutic option'. However, R540H showed a 'LOF' effect in neurons (Chapter 3) and the expression and trafficking profiles for N615I and V618G would ultimately determine whether this may be a suitable approach. It would seem that these channel mutants do traffic to synapses as evidenced by less magnesium block of spontaneous NMDAR-mediated EPSCs in neurons overexpressing GluN2B N615I and V618G compared to WT (Fedele et al., 2018). Patients with GluN2B mutants G611V, N615I, V618G, or M818T that were predicted potential GOF mutants were given memantine as part of an adjunctive anti-epileptic drug treatment, however, there were no changes to the seizures that the patients exhibited (Platzer et al., 2017).

For LOF mutant C461F in GluN2B, Pregnenolone sulphate potentiated currents in heterologous cells similar to WT and prolonged the deactivation time course (Swanger et al., 2016). Drugs which may prolong the deactivation kinetics, such as pregnenolone sulphate, may be suited for GluN2B mutants which have brief currents. However, pregnenolone sulfate is also a potent negative allosteric modulator of GABA_ARs, and not surprisingly, is proconvulsant (Harteneck, 2013, Reddy, 2010). Some more specific, GluN2A-selective PAMs also prolong deactivation (Hackos and Hanson, 2017, Villemure et al., 2017, Volgraf et al., 2016), which may be used for prolonging the decay of GluN2A-containing NMDARs if mutants abolish GluN2B expression (Chapter 3 and 4). A GluN2A-selective PAM, GNE-8324, also prolongs NMDAR currents, although

constant glycine application was required and the PAM selectively targeted inhibitory synapses (Hackos et al., 2016). NTD ligands, such as GluN2A-selective zinc and GluN2B-selective ifenprodil have also been found to prolong NMDAR-mediated EPSCs, although, these results were produced with an accompanying reduction in EPSC peak amplitude (Tovar and Westbrook, 2012). Furthermore, if GluN2B expression is impaired, ifenprodil may be ineffective at producing any of the desired effects. D-serine, a co-agonist of the NMDAR, has been shown to prolong NMDAR currents in the CA1 in both pyramidal cells and interneurons (Martina et al., 2003) and can be administered as a dietary supplement as L-serine. A patient with Rett-like syndrome with severe encephalopathy harbouring a GluN2B mutation, P553T, that exhibited smaller and faster currents when expressed in HEK cells was given L-serine for treatment and showed improvement in disease symptoms including motor and cognitive performance and communication (Soto et al., 2019). For GluN2A mutations that give rise to GluN2A-containing synaptic receptors with slower deactivation, a drug with the opposite action may provide therapeutic results. For example, D-cycloserine which is a partial agonist at the NMDAR co-agonist binding site has been found to reduce the decay time of NMDAR currents in post-synaptic neurons but not affect the amplitude (Lench et al., 2015). As D-cycloserine is not GluN2A- or GluN2B-selective and binds GluN1, it can be used to treat both GOF and LOF GluN2A mutations with slower decay kinetics. It is critical that the expression of mutants is always examined in order to determine whether the GOF or LOF effects observed will, in fact, persist or whether an alternate synaptic phenotype is exhibited from loss of the mutant subunit from the synapse. This will be crucial in selecting the appropriate treatment for GluN2 mutants.

Regulation of synaptic efficacy

GluN2A and GluN2B NMDAR subunits are known to have diverse roles in the induction of LTP and LTD (Shipton and Paulsen, 2014). A common hypothesis for the induction of either mechanisms is that the amount of calcium that enters the post-synaptic terminal determines the direction of plasticity: low calcium results in LTD expression and high calcium results in LTP expression (Cummings et al., 1996). As GluN2A and GluN2B have diverse decay kinetics, the post-synaptic calcium concentration is therefore distinct upon activation of GluN2A-containing NMDARs vs GluN2B-containing NMDARs, with GluN2B permitting greater calcium entry due to its slower decay and greater charge transfer. The NMDAR composition therefore allows precise control of calcium levels in the post-synaptic compartment (Shipton and Paulsen, 2014). This is due to the intracellular signalling cascades that can be activated by varying calcium concentrations (Malenka and Bear, 2004, Sheng and Pak, 2000, Sprengel et al., 1998). Block of

GluN2B-containing NMDARs prevents the induction of LTD but not LTP whereas block of GluN2A-containing NMDARs results in the opposite of this (Liu et al., 2004). Similarly, activation of GluN2A NMDARs enabled LTP whereas GluN2B NMDAR activation facilitated LTD (Sil'kis, 2007). However, many contradicting results have been observed (Bartlett et al., 2007, Berberich, 2005, Fox et al., 2006, Ge et al., 2010) owing to the diverse drugs and concentrations used, as well as the LTP/LTD induction protocols which are numerous. Therefore, the literature on subunit-specific mechanisms for the induction and direction of synaptic plasticity is not unified. The stimulation protocol used for the induction of synaptic plasticity can result in varying total charge transfer from GluN2A and GluN2B NMDARs so that with some types of stimulation, GluN2A contributes to a greater charge transfer, and with other protocols, GluN2B contributes to greater charge transfer (Shipton and Paulsen, 2014). Therefore, the level of synaptic activity can also influence the outcome of plasticity.

As well as the distinct calcium levels that GluN2A and GluN2B can contribute to, their diverse CTD sequences can also influence the induction of plasticity (Foster et al., 2010). The GluN2 CTDs couple to distinctive intracellular signalling pathways that have different effects on the induction of plasticity and regulation of synaptic strength (Shipton and Paulsen, 2014). These signalling pathways may include protein kinases and phosphatases which regulate the phosphorylation of AMPARs to alter their activity or insertion/removal from synapses to cause the changes in synaptic efficacy (Malinow and Malenka, 2002). Alterations to either the kinetics of NMDARs or the GluN2A-GluN2B ratio at the synapse could therefore result in changes to the direction of synaptic plasticity. These alterations can result from human disease mutations as shown in this thesis. Mutants which have trafficking impairments may result in a shift in the plasticity to favour the pathways activated by the remaining GluN2 subunit at the synapse.

Alternatively, trafficking-competent mutants that alter subunit function and have slow deactivation approaching that of GluN2B, such as L812M and K669N, may result in a more intermediate effect. The reason for this is that the kinetics of the receptor are altered, however, the GluN2A CTD remains to continue its interactions with its usual signalling molecules. These mutants would be a good tool to examine synaptic plasticity, in comparison to a mutant which does not traffic, such as C436R, T531M or R518H. This can be used to explore whether the NMDAR-EPSC time course and calcium signal or GluN2 subunit identity is more critical in regulating the induction of synaptic plasticity.

Final Conclusions

This research has demonstrated a synaptic phenotype of a GOF for GluN2A and a LOF for GluN2B human disease mutants when expressed at the CA3-CA1 synapse in organotypic hippocampal mouse slices. These mutants mostly impacted the decay time course of NMDAR currents and resulted from either functionally enhanced NMDARs or diminished trafficking and expression. The GOF/LOF distinction from characterisations of mutants in heterologous cells did not accurately reflect the overall impact on NMDAR currents and the expression, as well as function of mutant subunits, was found to be crucial in determining the synaptic properties that resulted. Future work to investigate further NMDAR mutants in GluN2A and GluN2B will reveal the extent of the common synaptic phenotypes in each subunit.

References

- AAMODT, S. M., SHI, J., COLONNESE, M. T., VERAS, W. & CONSTANTINE-PATON, M. 2000. Chronic NMDA exposure accelerates development of GABAergic inhibition in the superior colliculus. *J Neurophysiol*, 83, 1580-91.
- ADAMS, D. R., YUAN, H., HOLYOAK, T., ARAJS, K. H., HAKIMI, P., MARKELLO, T. C., WOLFE, L. A., VILBOUX, T., BURTON, B. K., FAJARDO, K. F., GRAHAME, G., HOLLOMAN, C., SINCAN, M., SMITH, A. C., WELLS, G. A., HUANG, Y., VEGA, H., SNYDER, J. P., GOLAS, G. A., TIFFT, C. J., BOERKOEL, C. F., HANSON, R. W., TRAYNELIS, S. F., KERR, D. S. & GAHL, W. A. 2014. Three rare diseases in one Sib pair: RAI1, PCK1, GRIN2B mutations associated with Smith-Magenis Syndrome, cytosolic PEPCK deficiency and NMDA receptor glutamate insensitivity. *Mol Genet Metab*, 113, 161-70.
- ADDIS, L., VIRDEE, J. K., VIDLER, L. R., COLLIER, D. A., PAL, D. K. & URSU, D. 2017. Epilepsy-associated GRIN2A mutations reduce NMDA receptor trafficking and agonist potency - molecular profiling and functional rescue. *Sci Rep*, 7, 66.
- ADZHUBEI, I., JORDAN, D. M. & SUNYAEV, S. R. 2013. Predicting functional effect of human missense mutations using PolyPhen-2. *Curr Protoc Hum Genet*, Chapter 7, Unit7 20.
- AKASHI, K., KAKIZAKI, T., KAMIYA, H., FUKAYA, M., YAMASAKI, M., ABE, M., NATSUME, R., WATANABE, M. & SAKIMURA, K. 2009. NMDA receptor GluN2B (GluR epsilon 2/NR2B) subunit is crucial for channel function, postsynaptic macromolecular organization, and actin cytoskeleton at hippocampal CA3 synapses. *J Neurosci*, 29, 10869-82.
- AL-HALLAQ, R. A., CONRAD, T. P., VEENSTRA, T. D. & WENTHOLD, R. J. 2007. NMDA di-heteromeric receptor populations and associated proteins in rat hippocampus. *J Neurosci*, 27, 8334-43.
- ALGURABAWI, M., MIDI, H. & IMON, A. H. M. R. 2015. A New Robust Diagnostic Plot for Classifying Good and Bad High Leverage Points in a Multiple Linear Regression Model. *Mathematical Problems in Engineering*.
- ALLEN, N. M., CONROY, J., SHAHWAN, A., LYNCH, B., CORREA, R. G., PENA, S. D. J., MCCREARY, D., MAGALHÃES, T. R., ENNIS, S., LYNCH, S. A. & KING, M. D. 2016. Unexplained early onset epileptic encephalopathy: Exome screening and phenotype expansion. *Epilepsia*, 57, e12-e17.
- AMAKHIN, D. V., ERGINA, J. L., CHIZHOV, A. V. & ZAITSEV, A. V. 2016. Synaptic Conductances during Interictal Discharges in Pyramidal Neurons of Rat Entorhinal Cortex. *Front Cell Neurosci*, 10, 233.
- AMAN, T. K., MAKI, B. A., RUFFINO, T. J., KASPEREK, E. M. & POPESCU, G. K. 2014. Separate intramolecular targets for protein kinase A control N-methyl-D-aspartate receptor gating and Ca²⁺ permeability. *J Biol Chem*, 289, 18805-17.
- AMIN, J. B., LENG, X., GOCHMAN, A., ZHOU, H.-X. & WOLLMUTH, L. P. 2018. A conserved glycine harboring disease-associated mutations is required for slow deactivation and high Ca²⁺ permeability in NMDA receptors. *bioRxiv*, 313452.
- AMIN, J. B., SALUSSOLIA, C. L., CHAN, K., REGAN, M. C., DAI, J., ZHOU, H.-X., FURUKAWA, H., BOWEN, M. E. & WOLLMUTH, L. P. 2017. Divergent roles of a peripheral transmembrane segment in AMPA and NMDA receptors. *The Journal of General Physiology*, 149, 661-680.
- ANTIC, S. D., ZHOU, W.-L., MOORE, A. R., SHORT, S. M. & IKONOMU, K. D. 2010. The decade of the dendritic NMDA spike. *Journal of Neuroscience Research*, 88, 2991-3001.
- ASHKENAZY, H., EREZ, E., MARTZ, E., PUPKO, T. & BEN-TAL, N. 2010. ConSurf 2010: calculating evolutionary conservation in sequence and structure of proteins and nucleic acids. *Nucleic Acids Res*, 38, W529-33.

- AUDINAT, E., LAMBOLEZ, B., ROSSIER, J. & CREPEL, F. 1994. Activity-dependent regulation of N-methyl-D-aspartate receptor subunit expression in rat cerebellar granule cells. *Eur J Neurosci*, 6, 1792-800.
- AUGUSTINAITE, S. & HEGGELUND, P. 2007. Changes in firing pattern of lateral geniculate neurons caused by membrane potential dependent modulation of retinal input through NMDA receptors. *J Physiol*, 582, 297-315.
- AUGUSTO, E. & GAMBINO, F. 2019. Can NMDA Spikes Dictate Computations of Local Networks and Behavior? *Frontiers in Molecular Neuroscience*, 12.
- AWADALLA, P., GAUTHIER, J., MYERS, R. A., CASALS, F., HAMDAN, F. F., GRIFFING, A. R., COTE, M., HENRION, E., SPIEGELMAN, D., TARABEUX, J., PITON, A., YANG, Y., BOYKO, A., BUSTAMANTE, C., XIONG, L., RAPOPORT, J. L., ADDINGTON, A. M., DELISI, J. L., KREBS, M. O., JOOBER, R., MILLET, B., FOMBONNE, E., MOTTRON, L., ZILVERSMIT, M., KEEBLER, J., DAOUD, H., MARINEAU, C., ROY-GAGNON, M. H., DUBE, M. P., EYRE-WALKER, A., DRAPEAU, P., STONE, E. A., LAFRENIERE, R. G. & ROULEAU, G. A. 2010. Direct measure of the de novo mutation rate in autism and schizophrenia cohorts. *Am J Hum Genet*, 87, 316-24.
- BAEZ, M. V., CERCATO, M. C. & JERUSALINSKY, D. A. 2018. NMDA Receptor Subunits Change after Synaptic Plasticity Induction and Learning and Memory Acquisition. *Neural Plast*, 2018, 5093048.
- BARRIA, A. & MALINOW, R. 2002. Subunit-specific NMDA receptor trafficking to synapses. *Neuron*, 35, 345-53.
- BARTLETT, T. E., BANNISTER, N. J., COLLETT, V. J., DARGAN, S. L., MASSEY, P. V., BORTOLOTTI, Z. A., FITZJOHN, S. M., BASHIR, Z. I., COLLINGRIDGE, G. L. & LODGE, D. 2007. Differential roles of NR2A and NR2B-containing NMDA receptors in LTP and LTD in the CA1 region of two-week old rat hippocampus. *Neuropharmacology*, 52, 60-70.
- BAUSCH, S. B., HE, S. & DONG, Y. 2010. Inverse relationship between seizure expression and extrasynaptic NMDAR function following chronic NMDAR inhibition. *Epilepsia*, 51 Suppl 3, 102-5.
- BENKE, T. A., LUTHI, A., ISAAC, J. T. & COLLINGRIDGE, G. L. 1998. Modulation of AMPA receptor unitary conductance by synaptic activity. *Nature*, 393, 793-7.
- BERBERICH, S. 2005. Lack of NMDA Receptor Subtype Selectivity for Hippocampal Long-Term Potentiation. *Journal of Neuroscience*, 25, 6907-6910.
- BERTRAM, E. 2007. The relevance of kindling for human epilepsy. *Epilepsia*, 48 Suppl 2, 65-74.
- BLEDSON, D., TAMER, C., MESIC, I., MADRY, C., KLEIN, B. G., LAUBE, B. & COSTA, B. M. 2017. Positive Modulatory Interactions of NMDA Receptor GluN1/2B Ligand Binding Domains Attenuate Antagonists Activity. *Front Pharmacol*, 8, 229.
- BOADA, R., HUTAFF-LEE, C., SCHRADER, A., WEITZENKAMP, D., BENKE, T. A., GOLDSON, E. J. & COSTA, A. C. 2012. Antagonism of NMDA receptors as a potential treatment for Down syndrome: a pilot randomized controlled trial. *Transl Psychiatry*, 2, e141.
- BOBBILI, D. R., LAL, D., MAY, P., REINTHALER, E. M., JABBARI, K., THIELE, H., NOTHNAGEL, M., JURKOWSKI, W., FEUCHT, M., NURNBERG, P., LERCHE, H., ZIMPRICH, F., KRAUSE, R., NEUBAUER, B. A., REINTHALER, E. M., ZIMPRICH, F., FEUCHT, M., STEINBOCK, H., NEOPHYTOU, B., GELDNER, J., GRUBER-SEDLIMAYR, U., HABERLANDT, E., RONEN, G. M., ALTMULLER, J., LAL, D., NURNBERG, P., SANDER, T., THIELE, H., KRAUSE, R., MAY, P., BALLING, R., LERCHE, H., NEUBAUER, B. A. & CONSORTIUM, E. C. 2018. Exome-wide analysis of mutational burden in patients with typical and atypical Rolandic epilepsy. *Eur J Hum Genet*, 26, 258-264.
- BOTEV, Z. I., GROTHOWSKI, J. F. & KROESE, D. P. 2010. Kernel Density Estimation Via Diffusion. *Annals of Statistics*, 38, 2916-2957.

- BOULTER, J., HOLLMANN, M., O'SHEA-GREENFIELD, A., HARTLEY, M., DENERIS, E., MARON, C. & HEINEMANN, S. 1990. Molecular cloning and functional expression of glutamate receptor subunit genes. *Science*, 249, 1033-7.
- BOWLING, K. M., THOMPSON, M. L., AMARAL, M. D., FINNILA, C. R., HIATT, S. M., ENGEL, K. L., COCHRAN, J. N., BROTHERS, K. B., EAST, K. M., GRAY, D. E., KELLEY, W. V., LAMB, N. E., LOSE, E. J., RICH, C. A., SIMMONS, S., WHITTLE, J. S., WEAVER, B. T., NESMITH, A. S., MYERS, R. M., BARSH, G. S., BEBIN, E. M. & COOPER, G. M. 2017. Genomic diagnosis for children with intellectual disability and/or developmental delay. *Genome Med*, 9, 43.
- BRIGMAN, J. L., WRIGHT, T., TALANI, G., PRASAD-MULCARE, S., JINDE, S., SEABOLD, G. K., MATHUR, P., DAVIS, M. I., BOCK, R., GUSTIN, R. M., COLBRAN, R. J., ALVAREZ, V. A., NAKAZAWA, K., DELPIRE, E., LOVINGER, D. M. & HOLMES, A. 2010. Loss of GluN2B-containing NMDA receptors in CA1 hippocampus and cortex impairs long-term depression, reduces dendritic spine density, and disrupts learning. *J Neurosci*, 30, 4590-600.
- BROOKS-KAYAL, A. 2010. Epilepsy and autism spectrum disorders: Are there common developmental mechanisms? *Brain and Development*, 32, 731-738.
- BURNASHEV, N. & SZEPETOWSKI, P. 2015. NMDA receptor subunit mutations in neurodevelopmental disorders. *Curr Opin Pharmacol*, 20, 73-82.
- BUTLER, K. M., DA SILVA, C., ALEXANDER, J. J., HEGDE, M. & ESCAYG, A. 2017. Diagnostic Yield From 339 Epilepsy Patients Screened on a Clinical Gene Panel. *Pediatr Neurol*, 77, 61-66.
- CAMPAGNOLA, L., KRATZ, M. B. & MANIS, P. B. 2014. ACQ4: an open-source software platform for data acquisition and analysis in neurophysiology research. *Front Neuroinform*, 8, 3.
- CANITANO, R. 2007. Epilepsy in autism spectrum disorders. *Eur Child Adolesc Psychiatry*, 16, 61-6.
- CANITANO, R., LUCHETTI, A. & ZAPPELLA, M. 2005. Epilepsy, electroencephalographic abnormalities, and regression in children with autism. *J Child Neurol*, 20, 27-31.
- CAO, J. Y., QIU, S., ZHANG, J., WANG, J. J., ZHANG, X. M. & LUO, J. H. 2011. Transmembrane region of N-methyl-D-aspartate receptor (NMDAR) subunit is required for receptor subunit assembly. *J Biol Chem*, 286, 27698-705.
- CAO, X., CUI, Z., FENG, R., TANG, Y. P., QIN, Z., MEI, B. & TSIEN, J. Z. 2007. Maintenance of superior learning and memory function in NR2B transgenic mice during ageing. *Eur J Neurosci*, 25, 1815-22.
- CARLEN, M., MELETIS, K., SIEGLE, J. H., CARDIN, J. A., FUTAI, K., VIERLING-CLAASSEN, D., RUHLMANN, C., JONES, S. R., DEISSEROTH, K., SHENG, M., MOORE, C. I. & TSAI, L. H. 2012. A critical role for NMDA receptors in parvalbumin interneurons for gamma rhythm induction and behavior. *Mol Psychiatry*, 17, 537-48.
- CARVILL, G. L., REGAN, B. M., YENDLE, S. C., O'ROAK, B. J., LOZOVAYA, N., BRUNEAU, N., BURNASHEV, N., KHAN, A., COOK, J., GERAGHTY, E., SADLEIR, L. G., TURNER, S. J., TSAI, M. H., WEBSTER, R., OUVRIER, R., DAMIANO, J. A., BERKOVIC, S. F., SHENDURE, J., HILDEBRAND, M. S., SZEPETOWSKI, P., SCHEFFER, I. E. & MEFFORD, H. C. 2013. GRIN2A mutations cause epilepsy-aphasia spectrum disorders. *Nature Genetics*, 45, 1073-+.
- CHEN, W., TANKOVIC, A., BURGER, P. B., KUSUMOTO, H., TRAYNELIS, S. F. & YUAN, H. 2017. Functional Evaluation of a De Novo GRIN2A Mutation Identified in a Patient with Profound Global Developmental Delay and Refractory Epilepsy. *Mol Pharmacol*, 91, 317-330.
- CHOI, Y. & CHAN, A. P. 2015. PROVEAN web server: a tool to predict the functional effect of amino acid substitutions and indels. *Bioinformatics*, 31, 2745-7.
- CHOI, Y., SIMS, G. E., MURPHY, S., MILLER, J. R. & CHAN, A. P. 2012. Predicting the functional effect of amino acid substitutions and indels. *PLoS One*, 7, e46688.

- CIABARRA, A. M., SULLIVAN, J. M., GAHN, L. G., PECHT, G., HEINEMANN, S. & SEVARINO, K. A. 1995. Cloning and characterization of chi-1: a developmentally regulated member of a novel class of the ionotropic glutamate receptor family. *J Neurosci*, 15, 6498-508.
- CLAYTON, D. A., MESCHES, M. H., ALVAREZ, E., BICKFORD, P. C. & BROWNING, M. D. 2002. A hippocampal NR2B deficit can mimic age-related changes in long-term potentiation and spatial learning in the Fischer 344 rat. *J Neurosci*, 22, 3628-37.
- COLEMAN, S. K., MOYKKYNEN, T., HINKKURI, S., VAAHTERA, L., KORPI, E. R., PENTIKAINEN, O. T. & KEINANEN, K. 2010. Ligand-binding domain determines endoplasmic reticulum exit of AMPA receptors. *J Biol Chem*, 285, 36032-9.
- COLEMAN, S. K., MOYKKYNEN, T., JOUPPILA, A., KOSKELAINEN, S., RIVERA, C., KORPI, E. R. & KEINANEN, K. 2009. Agonist occupancy is essential for forward trafficking of AMPA receptors. *J Neurosci*, 29, 303-12.
- CONROY, J., MCGETTIGAN, P. A., MCCREARY, D., SHAH, N., COLLINS, K., PARRY-FIELDER, B., MORAN, M., HANRAHAN, D., DEONNA, T. W., KORFF, C. M., WEBB, D., ENNIS, S., LYNCH, S. A. & KING, M. D. 2014. Towards the identification of a genetic basis for Landau-Kleffner syndrome. *Epilepsia*, 55, 858-865.
- CORBEL, C., HERNANDEZ, I., WU, B. & KOSIK, K. S. 2015. Developmental attenuation of N-methyl-D-aspartate receptor subunit expression by microRNAs. *Neural Dev*, 10, 20.
- COSTA, A. C., SCOTT-MCKEAN, J. J. & STASKO, M. R. 2008. Acute injections of the NMDA receptor antagonist memantine rescue performance deficits of the Ts65Dn mouse model of Down syndrome on a fear conditioning test. *Neuropsychopharmacology*, 33, 1624-32.
- COULTRAP, S. J., NIXON, K. M., ALVESTAD, R. M., VALENZUELA, C. F. & BROWNING, M. D. 2005. Differential expression of NMDA receptor subunits and splice variants among the CA1, CA3 and dentate gyrus of the adult rat. *Brain Res Mol Brain Res*, 135, 104-11.
- COUSINEAU, D. 2005. Confidence intervals in within-subject designs: A simpler solution to Loftus and Masson's method. *Tutorials in Quantitative Methods for Psychology*, 1, 42-45.
- CUI, Y., JIN, J., ZHANG, X., XU, H., YANG, L., DU, D., ZENG, Q., TSIEN, J. Z., YU, H. & CAO, X. 2011. Forebrain NR2B overexpression facilitating the prefrontal cortex long-term potentiation and enhancing working memory function in mice. *PLoS One*, 6, e20312.
- CULL-CANDY, S. G. & LESZKIEWICZ, D. N. 2004. Role of distinct NMDA receptor subtypes at central synapses. *Sci STKE*, 2004, re16.
- CUMMINGS, J. A., MULKEY, R. M., NICOLL, R. A. & MALENKA, R. C. 1996. Ca²⁺ Signaling Requirements for Long-Term Depression in the Hippocampus. *Neuron*, 16, 825-833.
- D'GAMA, ALISSA M., POCHAREDDY, S., LI, M., JAMUAR, SAUMYA S., REIFF, RACHEL E., LAM, A.-THU N., SESTAN, N. & WALSH, CHRISTOPHER A. 2015. Targeted DNA Sequencing from Autism Spectrum Disorder Brains Implicates Multiple Genetic Mechanisms. *Neuron*, 88, 910-917.
- DANI, V. S., CHANG, Q., MAFFEI, A., TURRIGIANO, G. G., JAENISCH, R. & NELSON, S. B. 2005. Reduced cortical activity due to a shift in the balance between excitation and inhibition in a mouse model of Rett syndrome. *Proc Natl Acad Sci U S A*, 102, 12560-5.
- DE LIGT, J., WILLEMSSEN, M. H., VAN BON, B. W. M., KLEEFSTRA, T., YNTEMA, H. G., KROES, T., VULTO-VAN SILFHOUT, A. T., KOOLEN, D. A., DE VRIES, P., GILISSEN, C., DEL ROSARIO, M., HOISCHEN, A., SCHEFFER, H., DE VRIES, B. B. A., BRUNNER, H. G., VELTMAN, J. A. & VISSERS, L. E. L. M. 2012. Diagnostic Exome Sequencing in Persons with Severe Intellectual Disability. *New England Journal of Medicine*, 367, 1921-1929.
- DEHOUCK, Y., KWASIGROCH, J. M., GILIS, D. & ROOMAN, M. 2011. PoPMuSiC 2.1: a web server for the estimation of protein stability changes upon mutation and sequence optimality. *BMC Bioinformatics*, 12, 151.

- DELLA MINA, E., CICCONE, R., BRUSTIA, F., BAYINDIR, B., LIMONGELLI, I., VETRO, A., IASCONE, M., PEZZOLI, L., BELLAZZI, R., PEROTTI, G., DE GIORGIS, V., LUNGI, S., COPPOLA, G., ORCESI, S., MERLI, P., SAVASTA, S., VEGGIOTTI, P. & ZUFFARDI, O. 2015. Improving molecular diagnosis in epilepsy by a dedicated high-throughput sequencing platform. *Eur J Hum Genet*, 23, 354-62.
- DEVRIES, S. P. & PATEL, A. D. 2013. Two Patients With a GRIN2A Mutation and Childhood-onset Epilepsy. *Pediatric Neurology*, 49, 482-485.
- DIMASSI, S., ANDRIEUX, J., LABALME, A., LESCA, G., CORDIER, M. P., BOUTE, O., NEUT, D., EDERY, P., SANLAVILLE, D. & SCHLUTH-BOLARD, C. 2013. Interstitial 12p13.1 deletion involving GRIN2B in three patients with intellectual disability. *Am J Med Genet A*, 161A, 2564-9.
- DOLL, C. A. & BROADIE, K. 2014. Impaired activity-dependent neural circuit assembly and refinement in autism spectrum disorder genetic models. *Frontiers in Cellular Neuroscience*, 8.
- DUMAS, T. C., UTTARO, M. R., BARRIGA, C., BRINKLEY, T., HALAVI, M., WRIGHT, S. N., FERRANTE, M., EVANS, R. C., HAWES, S. L. & SANDERS, E. M. 2018. Removal of area CA3 from hippocampal slices induces postsynaptic plasticity at Schaffer collateral synapses that normalizes CA1 pyramidal cell discharge. *Neuroscience Letters*, 678, 55-61.
- DYMENT, D. A., TÉTREAU, M., BEAULIEU, C. L., HARTLEY, T., FERREIRA, P., CHARDON, J. W., MARCADIÉ, J., SAWYER, S. L., MOSCA, S. J., INNES, A. M., PARBOOSINGH, J. S., BULMAN, D. E., SCHWARTZENTRUBER, J., MAJEWSKI, J., TARNOPOLSKY, M. & BOYCOTT, K. M. 2015. Whole-exome sequencing broadens the phenotypic spectrum of rare pediatric epilepsy: a retrospective study. *Clinical Genetics*, 88, 34-40.
- EICHLER, S. A. 2008. E-I balance and human diseases – from molecules to networking. *Frontiers in Molecular Neuroscience*, 1.
- ENDELE, S., ROSENBERGER, G., GEIDER, K., POPP, B., TAMER, C., STEFANOVA, I., MILH, M., KORTUM, F., FRITSCH, A., PIENKA, F. K., HELLENBROICH, Y., KALSCHUEER, V. M., KOHLHASE, J., MOOG, U., RAPPOLD, G., RAUCH, A., ROPERS, H. H., VON SPICZAK, S., TONNIES, H., VILLENEUVE, N., VILLARD, L., ZABEL, B., ZENKER, M., LAUBE, B., REIS, A., WIECZOREK, D., VAN MALDERGEM, L. & KUTSCHE, K. 2010. Mutations in GRIN2A and GRIN2B encoding regulatory subunits of NMDA receptors cause variable neurodevelopmental phenotypes. *Nat Genet*, 42, 1021-6.
- EPI, K. C., ALLEN, A. S., BERKOVIC, S. F., COSSETTE, P., DELANTY, N., DLUGOS, D., EICHLER, E. E., EPSTEIN, M. P., GLAUSER, T., GOLDSTEIN, D. B., HAN, Y., HEINZEN, E. L., HITOMI, Y., HOWELL, K. B., JOHNSON, M. R., KUZNIECKY, R., LOWENSTEIN, D. H., LU, Y.-F., MADOU, M. R. Z., MARSON, A. G., MEFFORD, H. C., ESMAEELI NIEH, S., O'BRIEN, T. J., OTTMAN, R., PETROVSKI, S., PODURI, A., RUZZO, E. K., SCHEFFER, I. E., SHERR, E. H., YUSKAITIS, C. J., EPILEPSY PHENOME/GENOME, P., ABOU-KHALIL, B., ALLDREDGE, B. K., BAUTISTA, J. F., BERKOVIC, S. F., BORO, A., CASCINO, G. D., CONSALVO, D., CRUMRINE, P., DEVINSKY, O., DLUGOS, D., EPSTEIN, M. P., FIOL, M., FOUNTAIN, N. B., FRENCH, J., FRIEDMAN, D., GELLER, E. B., GLAUSER, T., GLYNN, S., HAUT, S. R., HAYWARD, J., HELMERS, S. L., JOSHI, S., KANNER, A., KIRSCH, H. E., KNOWLTON, R. C., KOSSOFF, E. H., KUPERMAN, R., KUZNIECKY, R., LOWENSTEIN, D. H., MCGUIRE, S. M., MOTIKA, P. V., NOVOTNY, E. J., OTTMAN, R., PAOLICCHI, J. M., PARENT, J. M., PARK, K., PODURI, A., SCHEFFER, I. E., SHELLHAAS, R. A., SHERR, E. H., SHIH, J. J., SINGH, R., SIRVEN, J., SMITH, M. C., SULLIVAN, J., LIN THIO, L., VENKAT, A., VINING, E. P. G., VON ALLMEN, G. K., WEISENBERG, J. L., WIDDESS-WALSH, P. & WINAWER, M. R. 2013. De novo mutations in epileptic encephalopathies. *Nature*, 501, 217.

- FADDA, E., DANYSZ, W., WROBLEWSKI, J. T. & COSTA, E. 1988. Glycine and D-serine increase the affinity of N-methyl-D-aspartate sensitive glutamate binding sites in rat brain synaptic membranes. *Neuropharmacology*, 27, 1183-5.
- FARWELL, K. D., SHAHMIRZADI, L., EL-KHECHEN, D., POWIS, Z., CHAO, E. C., TIPPIN DAVIS, B., BAXTER, R. M., ZENG, W., MROSKE, C., PARRA, M. C., GANDOMI, S. K., LU, I., LI, X., LU, H., LU, H. M., SALVADOR, D., RUBLE, D., LAO, M., FISCHBACH, S., WEN, J., LEE, S., ELLIOTT, A., DUNLOP, C. L. & TANG, S. 2015. Enhanced utility of family-centered diagnostic exome sequencing with inheritance model-based analysis: results from 500 unselected families with undiagnosed genetic conditions. *Genet Med*, 17, 578-86.
- FEDELE, L., NEWCOMBE, J., TOPF, M., GIBB, A., HARVEY, R. J. & SMART, T. G. 2018. Disease-associated missense mutations in GluN2B subunit alter NMDA receptor ligand binding and ion channel properties. *Nat Commun*, 9, 957.
- FEJERMAN, N., CARABALLO, R., CERSOSIMO, R., FERRARO, S. M., GALICCHIO, S. & AMARTINO, H. 2012. Sulthiame add-on therapy in children with focal epilepsies associated with encephalopathy related to electrical status epilepticus during slow sleep (ESES). *Epilepsia*, 53, 1156-61.
- FERGUSON, B. R. & GAO, W.-J. 2018. PV Interneurons: Critical Regulators of E/I Balance for Prefrontal Cortex-Dependent Behavior and Psychiatric Disorders. *Frontiers in Neural Circuits*, 12.
- FERNANDEZ-MARMIESSE, A., KUSUMOTO, H., REKARTE, S., ROCA, I., ZHANG, J., MYERS, S. J., TRAYNELIS, S. F., COUCE, M. L., GUTIERREZ-SOLANA, L. & YUAN, H. 2018. A novel missense mutation in GRIN2A causes a nonepileptic neurodevelopmental disorder. *Mov Disord*, 33, 992-999.
- FERNANDEZ, F. & GARNER, C. C. 2007. Over-inhibition: a model for developmental intellectual disability. *Trends Neurosci*, 30, 497-503.
- FISZMAN, M. L., BARBERIS, A., LU, C., FU, Z., ERDELYI, F., SZABO, G. & VICINI, S. 2005. NMDA receptors increase the size of GABAergic terminals and enhance GABA release. *J Neurosci*, 25, 2024-31.
- FORREST, D., YUZAKI, M., SOARES, H. D., NG, L., LUK, D. C., SHENG, M., STEWART, C. L., MORGAN, J. I., CONNOR, J. A. & CURRAN, T. 1994. Targeted disruption of NMDA receptor 1 gene abolishes NMDA response and results in neonatal death. *Neuron*, 13, 325-38.
- FOSTER, K. A., MCLAUGHLIN, N., EDBAUER, D., PHILLIPS, M., BOLTON, A., CONSTANTINE-PATON, M. & SHENG, M. 2010. Distinct roles of NR2A and NR2B cytoplasmic tails in long-term potentiation. *J Neurosci*, 30, 2676-85.
- FOX, C. J., RUSSELL, K. I., WANG, Y. T. & CHRISTIE, B. R. 2006. Contribution of NR2A and NR2B NMDA subunits to bidirectional synaptic plasticity in the hippocampus in vivo. *Hippocampus*, 16, 907-915.
- FRASCA, A., AALBERS, M., FRIGERIO, F., FIORDALISO, F., SALIO, M., GOBBI, M., CAGNOTTO, A., GARDONI, F., BATTAGLIA, G. S., HOOGLAND, G., DI LUCA, M. & VEZZANI, A. 2011. Misplaced NMDA receptors in epileptogenesis contribute to excitotoxicity. *Neurobiol Dis*, 43, 507-15.
- FREGA, M., SELTEN, M., MOSSINK, B., KELLER, J. M., LINDA, K., MOERSCHEN, R., QU, J., KOERNER, P., JANSEN, S., BIJVANK, E., OUDAKKER, A., KLEEFSTRA, T., BOKHOVEN, H. V., ZHOU, H., SCHUBERT, D. & KASRI, N. N. 2018. Distinct pathogenic genes causing intellectual disability and autism exhibit overlapping effects on neuronal network development. *bioRxiv*, 408252.
- FREUNSCHT, I., POPP, B., BLANK, R., ENDELE, S., MOOG, U., PETRI, H., PROTT, E.-C., REIS, A., RÜBO, J., ZABEL, B., ZENKER, M., HEBEBRAND, J. & WIECZOREK, D. 2013. Behavioral phenotype in five individuals with de novo mutations within the GRIN2B gene. *Behavioral and Brain Functions*, 9, 20.

- FROTSCHER, M., HEIMRICH, B. & DELLER, T. 1997. Sprouting in the hippocampus is layer-specific. *Trends in Neurosciences*, 20, 218-223.
- FUKAYA, M., KATO, A., LOVETT, C., TONEGAWA, S. & WATANABE, M. 2003. Retention of NMDA receptor NR2 subunits in the lumen of endoplasmic reticulum in targeted NR1 knockout mice. *Proc Natl Acad Sci U S A*, 100, 4855-60.
- GAMBRILL, A. C. & BARRIA, A. 2011. NMDA receptor subunit composition controls synaptogenesis and synapse stabilization. *Proc Natl Acad Sci U S A*, 108, 5855-60.
- GAO, K., TANKOVIC, A., ZHANG, Y., KUSUMOTO, H., ZHANG, J., CHEN, W., XIANGWEI, W., SHAULSKY, G. H., HU, C., TRAYNELIS, S. F., YUAN, H. & JIANG, Y. 2017. A de novo loss-of-function GRIN2A mutation associated with childhood focal epilepsy and acquired epileptic aphasia. *PLoS One*, 12, e0170818.
- GE, Y., DONG, Z., BAGOT, R. C., HOWLAND, J. G., PHILLIPS, A. G., WONG, T. P. & WANG, Y. T. 2010. Hippocampal long-term depression is required for the consolidation of spatial memory. *Proceedings of the National Academy of Sciences*, 107, 16697-16702.
- GECZ, J. 2010. Glutamate receptors and learning and memory. *Nat Genet*, 42, 925-6.
- GILL, M. B., VIVITHANAPORN, P. & SWANSON, G. T. 2009. Glutamate binding and conformational flexibility of ligand-binding domains are critical early determinants of efficient kainate receptor biogenesis. *J Biol Chem*, 284, 14503-12.
- GILLBERG, C. & BILLSTEDT, E. 2000. Autism and Asperger syndrome: coexistence with other clinical disorders. *Acta Psychiatr Scand*, 102, 321-30.
- GIRIRAJAN, S., DENNIS, M. Y., BAKER, C., MALIG, M., COE, B. P., CAMPBELL, C. D., MARK, K., VU, T. H., ALKAN, C., CHENG, Z., BIESECKER, L. G., BERNIER, R. & EICHLER, E. E. 2013. Refinement and discovery of new hotspots of copy-number variation associated with autism spectrum disorder. *Am J Hum Genet*, 92, 221-37.
- GRANGER, A. J., GRAY, J. A., LU, W. & NICOLL, R. A. 2011. Genetic analysis of neuronal ionotropic glutamate receptor subunits. *J Physiol*, 589, 4095-101.
- GRANGER, A. J., SHI, Y., LU, W., CERPAS, M. & NICOLL, R. A. 2013. LTP requires a reserve pool of glutamate receptors independent of subunit type. *Nature*, 493, 495-500.
- GRAY, J. A., SHI, Y., USUI, H., DURING, M. J., SAKIMURA, K. & NICOLL, R. A. 2011. Distinct modes of AMPA receptor suppression at developing synapses by GluN2A and GluN2B: single-cell NMDA receptor subunit deletion in vivo. *Neuron*, 71, 1085-101.
- GROC, L. & CHOQUET, D. 2006. AMPA and NMDA glutamate receptor trafficking: multiple roads for reaching and leaving the synapse. *Cell Tissue Res*, 326, 423-38.
- GROC, L., GUSTAFSSON, B. & HANSE, E. 2006a. AMPA signalling in nascent glutamatergic synapses: there and not there! *Trends Neurosci*, 29, 132-9.
- GROC, L., HEINE, M., COUSINS, S. L., STEPHENSON, F. A., LOUNIS, B., COGNET, L. & CHOQUET, D. 2006b. NMDA receptor surface mobility depends on NR2A-2B subunits. *Proc Natl Acad Sci U S A*, 103, 18769-74.
- GU, X. & LU, W. 2018. Genetic deletion of NMDA receptors suppresses GABAergic synaptic transmission in two distinct types of central neurons. *Neurosci Lett*, 668, 147-153.
- GU, X., ZHOU, L. & LU, W. 2016. An NMDA Receptor-Dependent Mechanism Underlies Inhibitory Synapse Development. *Cell Rep*, 14, 471-478.
- GUANG, S., PANG, N., DENG, X., YANG, L., HE, F., WU, L., CHEN, C., YIN, F. & PENG, J. 2018. Synaptopathology Involved in Autism Spectrum Disorder. *Front Cell Neurosci*, 12, 470.
- GUPTA, S. C., YADAV, R., PAVULURI, R., MORLEY, B. J., STAIRS, D. J. & DRAVID, S. M. 2015. Essential role of GluD1 in dendritic spine development and GluN2B to GluN2A NMDAR subunit switch in the cortex and hippocampus reveals ability of GluN2B inhibition in correcting hyperconnectivity. *Neuropharmacology*, 93, 274-84.
- GUZMAN, S. J., SCHLOGL, A. & SCHMIDT-HIEBER, C. 2014. Stimfit: quantifying electrophysiological data with Python. *Front Neuroinform*, 8, 16.

- HACKOS, D. H. & HANSON, J. E. 2017. Diverse modes of NMDA receptor positive allosteric modulation: Mechanisms and consequences. *Neuropharmacology*, 112, 34-45.
- HACKOS, D. H., LUPARDUS, P. J., GRAND, T., CHEN, Y., WANG, T. M., REYNEN, P., GUSTAFSON, A., WALLWEBER, H. J., VOLGRAF, M., SELLERS, B. D., SCHWARZ, J. B., PAOLETTI, P., SHENG, M., ZHOU, Q. & HANSON, J. E. 2016. Positive Allosteric Modulators of GluN2A-Containing NMDARs with Distinct Modes of Action and Impacts on Circuit Function. *Neuron*, 89, 983-99.
- HALL, B. J. & GHOSH, A. 2008. Regulation of AMPA receptor recruitment at developing synapses. *Trends Neurosci*, 31, 82-9.
- HALL, B. J., RIPLEY, B. & GHOSH, A. 2007. NR2B signaling regulates the development of synaptic AMPA receptor current. *J Neurosci*, 27, 13446-56.
- HALT, A. R., DALLAPIAZZA, R. F., ZHOU, Y., STEIN, I. S., QIAN, H., JUNTTI, S., WOJCIK, S., BROSE, N., SILVA, A. J. & HELL, J. W. 2012. CaMKII binding to GluN2B is critical during memory consolidation. *EMBO J*, 31, 1203-16.
- HAMADA, S., OGAWA, I., YAMASAKI, M., KIYAMA, Y., KASSAI, H., WATABE, A. M., NAKAO, K., AIBA, A., WATANABE, M. & MANABE, T. 2014. The glutamate receptor GluN2 subunit regulates synaptic trafficking of AMPA receptors in the neonatal mouse brain. *Eur J Neurosci*, 40, 3136-46.
- HAMDAN, FADI F., GAUTHIER, J., ARAKI, Y., LIN, D.-T., YOSHIZAWA, Y., HIGASHI, K., PARK, A. R., SPIEGELMAN, D., DOBRZENIECKA, S., PITON, A., TOMITORI, H., DAOUD, H., MASSICOTTE, C., HENRION, E., DIALLO, O., SHEKARABI, M., MARINEAU, C., SHEVELL, M., MARANDA, B., MITCHELL, G., NADEAU, A., D'ANJOU, G., VANASSE, M., SROUR, M., LAFRENIÈRE, RONALD G., DRAPEAU, P., LACAILLE, JEAN C., KIM, E., LEE, J.-R., IGARASHI, K., HUGANIR, RICHARD L., ROULEAU, GUY A. & MICHAUD, JACQUES L. 2011. Excess of De Novo Deleterious Mutations in Genes Associated with Glutamatergic Systems in Nonsyndromic Intellectual Disability. *The American Journal of Human Genetics*, 88, 306-316.
- HANSEN, K. B., OGDEN, K. K. & TRAYNELIS, S. F. 2012. Subunit-selective allosteric inhibition of glycine binding to NMDA receptors. *J Neurosci*, 32, 6197-208.
- HANSEN, K. B., OGDEN, K. K., YUAN, H. & TRAYNELIS, S. F. 2014. Distinct functional and pharmacological properties of Triheteromeric GluN1/GluN2A/GluN2B NMDA receptors. *Neuron*, 81, 1084-96.
- HARTENECK, C. 2013. Pregnenolone sulfate: from steroid metabolite to TRP channel ligand. *Molecules*, 18, 12012-28.
- HAWKINS, L. M., PRYBYLOWSKI, K., CHANG, K., MOUSSAN, C., STEPHENSON, F. A. & WENTHOLD, R. J. 2004. Export from the endoplasmic reticulum of assembled N-methyl-d-aspartic acid receptors is controlled by a motif in the c terminus of the NR2 subunit. *J Biol Chem*, 279, 28903-10.
- HE, C. X. & PORTERA-CAILLIAU, C. 2013. The trouble with spines in fragile X syndrome: density, maturity and plasticity. *Neuroscience*, 251, 120-8.
- HEFFNER, C. S., HERBERT PRATT, C., BABIUK, R. P., SHARMA, Y., ROCKWOOD, S. F., DONAHUE, L. R., EPPIG, J. T. & MURRAY, S. A. 2012. Supporting conditional mouse mutagenesis with a comprehensive cre characterization resource. *Nat Commun*, 3, 1218.
- HESTRIN, S. 1992. Developmental regulation of NMDA receptor-mediated synaptic currents at a central synapse. *Nature*, 357, 686-689.
- HILDEBRAND, M. E., PITCHER, G. M., HARDING, E. K., LI, H., BEGGS, S. & SALTER, M. W. 2014. GluN2B and GluN2D NMDARs dominate synaptic responses in the adult spinal cord. *Sci Rep*, 4, 4094.
- HORAK, M., CHANG, K. & WENTHOLD, R. J. 2008. Masking of the endoplasmic reticulum retention signals during assembly of the NMDA receptor. *J Neurosci*, 28, 3500-9.

- HORAK, M., PETRALIA, R. S., KANIAKOVA, M. & SANS, N. 2014. ER to synapse trafficking of NMDA receptors. *Front Cell Neurosci*, 8, 394.
- HORAK, M. & WENTHOLD, R. J. 2009. Different roles of C-terminal cassettes in the trafficking of full-length NR1 subunits to the cell surface. *J Biol Chem*, 284, 9683-91.
- HORN, M. E. & NICOLL, R. A. 2018. Somatostatin and parvalbumin inhibitory synapses onto hippocampal pyramidal neurons are regulated by distinct mechanisms. *Proc Natl Acad Sci U S A*, 115, 589-594.
- HU, C., CHEN, W., MYERS, S. J., YUAN, H. & TRAYNELIS, S. F. 2016. Human GRIN2B variants in neurodevelopmental disorders. *J Pharmacol Sci*, 132, 115-121.
- HUBERT, M., ROUSSEUW, P. J. & VANDEN BRANDEN, K. 2005. ROBPCA: A New Approach to Robust Principal Component Analysis. *Technometrics*, 47, 64-79.
- HUGGINS, D. J. & GRANT, G. H. 2005. The function of the amino terminal domain in NMDA receptor modulation. *J Mol Graph Model*, 23, 381-8.
- HUMPEL, C. 2015. Organotypic brain slice cultures: A review. *Neuroscience*, 305, 86-98.
- HUNT, D. L. & CASTILLO, P. E. 2012. Synaptic plasticity of NMDA receptors: mechanisms and functional implications. *Curr Opin Neurobiol*, 22, 496-508.
- INCONTRO, S., ASENSIO, C. S., EDWARDS, R. H. & NICOLL, R. A. 2014. Efficient, complete deletion of synaptic proteins using CRISPR. *Neuron*, 83, 1051-7.
- ISOO, N., OHNO, T., ISOWAKI, M., FUKUDA, S., MURABE, N., MIZUKAMI, H., OZAWA, K., MISHINA, M. & SAKURAI, M. 2016. The decline in synaptic GluN2B and rise in inhibitory neurotransmission determine the end of a critical period. *Sci Rep*, 6, 34196.
- JALALI-YAZDI, F., CHOWDHURY, S., YOSHIOKA, C. & GOUAUX, E. 2018. Mechanisms for Zinc and Proton Inhibition of the GluN1/GluN2A NMDA Receptor. *Cell*, 175, 1520-1532 e15.
- JEDLICKA, P., MUELLERLEILE, J. & SCHWARZACHER, S. W. 2018. Synaptic Plasticity and Excitation-Inhibition Balance in the Dentate Gyrus: Insights from In Vivo Recordings in Neuroligin-1, Neuroligin-2, and Collybistin Knockouts. *Neural Plasticity*, 2018, 1-11.
- JONES, K. S., VANDONGEN, H. M. & VANDONGEN, A. M. 2002. The NMDA receptor M3 segment is a conserved transduction element coupling ligand binding to channel opening. *J Neurosci*, 22, 2044-53.
- JULLIE, D., CHOQUET, D. & PERRAIS, D. 2014. Recycling endosomes undergo rapid closure of a fusion pore on exocytosis in neuronal dendrites. *J Neurosci*, 34, 11106-18.
- KADOTANI, H., HIRANO, T., MASUGI, M., NAKAMURA, K., NAKAO, K., KATSUKI, M. & NAKANISHI, S. 1996. Motor discoordination results from combined gene disruption of the NMDA receptor NR2A and NR2C subunits, but not from single disruption of the NR2A or NR2C subunit. *J Neurosci*, 16, 7859-67.
- KANNANGARA, T. S., EADIE, B. D., BOSTROM, C. A., MORCH, K., BROCARDO, P. S. & CHRISTIE, B. R. 2015. GluN2A^{-/-} Mice Lack Bidirectional Synaptic Plasticity in the Dentate Gyrus and Perform Poorly on Spatial Pattern Separation Tasks. *Cereb Cortex*, 25, 2102-13.
- KARAKAS, E. & FURUKAWA, H. 2014. Crystal structure of a heterotetrameric NMDA receptor ion channel. *Science*, 344, 992-7.
- KATOH, K., MISAWA, K., KUMA, K. & MIYATA, T. 2002. MAFFT: a novel method for rapid multiple sequence alignment based on fast Fourier transform. *Nucleic Acids Res*, 30, 3059-66.
- KAUFMANN, W. E. & MOSER, H. W. 2000. Dendritic anomalies in disorders associated with mental retardation. *Cereb Cortex*, 10, 981-91.
- KAWAKAMI, R., SHINOHARA, Y., KATO, Y., SUGIYAMA, H., SHIGEMOTO, R. & ITO, I. 2003. Asymmetrical allocation of NMDA receptor epsilon2 subunits in hippocampal circuitry. *Science*, 300, 990-4.
- KEHOE, L. A., BERNARDINELLI, Y. & MULLER, D. 2013. GluN3A: an NMDA receptor subunit with exquisite properties and functions. *Neural Plast*, 2013, 145387.

- KELLERMAYER, B., FERREIRA, J. S., DUPUIS, J., LEVET, F., GRILLO-BOSCH, D., BARD, L., LINARES-LOYEZ, J., BOUCHET, D., CHOQUET, D., RUSAKOV, D. A., BON, P., SIBARITA, J. B., COGNET, L., SAINLOS, M., CARVALHO, A. L. & GROU, L. 2018. Differential Nanoscale Topography and Functional Role of GluN2-NMDA Receptor Subtypes at Glutamatergic Synapses. *Neuron*, 100, 106-119 e7.
- KELSCH, W., LI, Z., WIELAND, S., SENKOV, O., HERB, A., GONGRICH, C. & MONYER, H. 2014. GluN2B-containing NMDA receptors promote glutamate synapse development in hippocampal interneurons. *J Neurosci*, 34, 16022-30.
- KENNY, A. V., COUSINS, S. L., PINHO, L. & STEPHENSON, F. A. 2009. The integrity of the glycine co-agonist binding site of N-methyl-D-aspartate receptors is a functional quality control checkpoint for cell surface delivery. *J Biol Chem*, 284, 324-33.
- KENNY, E. M., CORMICAN, P., FURLONG, S., HERON, E., KENNY, G., FAHEY, C., KELLEHER, E., ENNIS, S., TROPEA, D., ANNEY, R., CORVIN, A. P., DONOHOE, G., GALLAGHER, L., GILL, M. & MORRIS, D. W. 2014. Excess of rare novel loss-of-function variants in synaptic genes in schizophrenia and autism spectrum disorders. *Mol Psychiatry*, 19, 872-9.
- KIM, M. J., DUNAH, A. W., WANG, Y. T. & SHENG, M. 2005. Differential roles of NR2A- and NR2B-containing NMDA receptors in Ras-ERK signaling and AMPA receptor trafficking. *Neuron*, 46, 745-60.
- KIYAMA, Y., MANABE, T., SAKIMURA, K., KAWAKAMI, F., MORI, H. & MISHINA, M. 1998. Increased thresholds for long-term potentiation and contextual learning in mice lacking the NMDA-type glutamate receptor epsilon1 subunit. *J Neurosci*, 18, 6704-12.
- KLASSEN, T., DAVIS, C., GOLDMAN, A., BURGESS, D., CHEN, T., WHEELER, D., MCPHERSON, J., BOURQUIN, T., LEWIS, L., VILLASANA, D., MORGAN, M., MUZNY, D., GIBBS, R. & NOBELS, J. 2011. Exome sequencing of ion channel genes reveals complex profiles confounding personal risk assessment in epilepsy. *Cell*, 145, 1036-48.
- KNIERIM, J. J. 2015. The hippocampus. *Current Biology*, 25, R1116-R1121.
- KOHL, M. M., SHIPTON, O. A., DEACON, R. M., RAWLINS, J. N., DEISSEROTH, K. & PAULSEN, O. 2011. Hemisphere-specific optogenetic stimulation reveals left-right asymmetry of hippocampal plasticity. *Nat Neurosci*, 14, 1413-5.
- KOHR, G., ECKARDT, S., LUDDENS, H., MONYER, H. & SEEBURG, P. H. 1994. NMDA receptor channels: subunit-specific potentiation by reducing agents. *Neuron*, 12, 1031-40.
- KORINEK, M., VYKLYCKY, V., BOROVSKA, J., LICHNEROVA, K., KANIAKOVA, M., KRAUSOVA, B., KRUSEK, J., BALIK, A., SMEJKALOVA, T., HORAK, M. & VYKLYCKY, L. 2015. Cholesterol modulates open probability and desensitization of NMDA receptors. *J Physiol*, 593, 2279-93.
- KOROTKOVA, T., FUCHS, E. C., PONOMARENKO, A., VON ENGELHARDT, J. & MONYER, H. 2010. NMDA receptor ablation on parvalbumin-positive interneurons impairs hippocampal synchrony, spatial representations, and working memory. *Neuron*, 68, 557-69.
- KOSTER, K. P., FRANCESCONI, W., BERTON, F., ALAHMADI, S., SRINIVAS, R. & YOSHII, A. 2019. Developmental NMDA receptor dysregulation in the infantile neuronal ceroid lipofuscinosis mouse model. *Elife*, 8.
- KOYAMA, R. & IKEGAYA, Y. 2015. Microglia in the pathogenesis of autism spectrum disorders. *Neurosci Res*, 100, 1-5.
- KROON, T., SIERKSMA, M. C. & MEREDITH, R. M. 2013. Investigating mechanisms underlying neurodevelopmental phenotypes of autistic and intellectual disability disorders: a perspective. *Front Syst Neurosci*, 7, 75.
- KUTSUWADA, T., SAKIMURA, K., MANABE, T., TAKAYAMA, C., KATAKURA, N., KUSHIYA, E., NATSUME, R., WATANABE, M., INOUE, Y., YAGI, T., AIZAWA, S., ARAKAWA, M., TAKAHASHI, T., NAKAMURA, Y., MORI, H. & MISHINA, M. 1996. Impairment of suckling response, trigeminal neuronal pattern formation, and hippocampal LTD in NMDA receptor epsilon 2 subunit mutant mice. *Neuron*, 16, 333-44.

- KYRIAKOPOULOS, P., MCNIVEN, V., CARTER, M. T., HUMPHREYS, P., DYMENT, D. & FANTANEANU, T. A. 2018. Atypical Rett Syndrome and Intractable Epilepsy With Novel GRIN2B Mutation. *Child Neurol Open*, 5, 2329048X18787946.
- LAIMER, J., HIEBL-FLACH, J., LENGAUER, D. & LACKNER, P. 2016. MAESTROweb: a web server for structure-based protein stability prediction. *Bioinformatics*, 32, 1414-6.
- LAURIE, D. J., PUTZKE, J., ZIEGLGANSBERGER, W., SEEBURG, P. H. & TOLLE, T. R. 1995. The distribution of splice variants of the NMDAR1 subunit mRNA in adult rat brain. *Brain Res Mol Brain Res*, 32, 94-108.
- LAURIE, D. J. & SEEBURG, P. H. 1994. Regional and developmental heterogeneity in splicing of the rat brain NMDAR1 mRNA. *J Neurosci*, 14, 3180-94.
- LAVEZZARI, G., MCCALLUM, J., DEWEY, C. M. & ROCHE, K. W. 2004. Subunit-specific regulation of NMDA receptor endocytosis. *J Neurosci*, 24, 6383-91.
- LE BAIL, M., MARTINEAU, M., SACCHI, S., YATSENKO, N., RADZISHEVSKY, I., CONROD, S., AIT OUADES, K., WOLOSKE, H., POLLEGIONI, L., BILLARD, J. M. & MOTHET, J. P. 2015. Identity of the NMDA receptor coagonist is synapse specific and developmentally regulated in the hippocampus. *Proc Natl Acad Sci U S A*, 112, E204-13.
- LEE, B. H., SMITH, T. & PACIORKOWSKI, A. R. 2015a. Autism spectrum disorder and epilepsy: Disorders with a shared biology. *Epilepsy Behav*, 47, 191-201.
- LEE, C. H., LU, W., MICHEL, J. C., GOEHRING, A., DU, J., SONG, X. & GOUAUX, E. 2014. NMDA receptor structures reveal subunit arrangement and pore architecture. *Nature*, 511, 191-7.
- LEE, E., LEE, J. & KIM, E. 2017. Excitation/Inhibition Imbalance in Animal Models of Autism Spectrum Disorders. *Biol Psychiatry*, 81, 838-847.
- LEE, E. J., CHOI, S. Y. & KIM, E. 2015b. NMDA receptor dysfunction in autism spectrum disorders. *Curr Opin Pharmacol*, 20, 8-13.
- LELIEVELD, S. H., REIJNDERS, M. R., PFUNDT, R., YNTEMA, H. G., KAMSTEEG, E. J., DE VRIES, P., DE VRIES, B. B., WILLEMSSEN, M. H., KLEEFSTRA, T., LOHNER, K., VREEBURG, M., STEVENS, S. J., VAN DER BURGT, I., BONGERS, E. M., STEGMANN, A. P., RUMP, P., RINNE, T., NELEN, M. R., VELTMAN, J. A., VISSERS, L. E., BRUNNER, H. G. & GILISSEN, C. 2016. Meta-analysis of 2,104 trios provides support for 10 new genes for intellectual disability. *Nat Neurosci*, 19, 1194-6.
- LEMKE, J. R., HENDRICKX, R., GEIDER, K., LAUBE, B., SCHWAKE, M., HARVEY, R. J., JAMES, V. M., PEPLER, A., STEINER, I., HORTNAGEL, K., NEIDHARDT, J., RUF, S., WOLFF, M., BARTHOLDI, D., CARABALLO, R., PLATZER, K., SULS, A., DE JONGHE, P., BISKUP, S. & WECKHUYSSEN, S. 2014. GRIN2B mutations in West syndrome and intellectual disability with focal epilepsy. *Ann Neurol*, 75, 147-54.
- LEMKE, J. R., LAL, D., REINTHALER, E. M., STEINER, I., NOTHNAGEL, M., ALBER, M., GEIDER, K., LAUBE, B., SCHWAKE, M., FINSTERWALDER, K., FRANKE, A., SCHILHABEL, M., JAHN, J. A., MUHLE, H., BOOR, R., VAN PAESSCHEN, W., CARABALLO, R., FEJERMAN, N., WECKHUYSSEN, S., DE JONGHE, P., LARSEN, J., MOLLER, R. S., HJALGRIM, H., ADDIS, L., TANG, S., HUGHES, E., PAL, D. K., VERI, K., VAHER, U., TALVIK, T., DIMOVA, P., GUERRERO LOPEZ, R., SERRATOSA, J. M., LINNANKIVI, T., LEHESJOKI, A. E., RUF, S., WOLFF, M., BUERKI, S., WOHLRAB, G., KROELL, J., DATTA, A. N., FIEDLER, B., KURLEMANN, G., KLUGER, G., HAHN, A., HABERLANDT, D. E., KUTZER, C., SPERNER, J., BECKER, F., WEBER, Y. G., FEUCHT, M., STEINBOCK, H., NEOPHYTHOU, B., RONEN, G. M., GRUBER-SEDLIMAYR, U., GELDNER, J., HARVEY, R. J., HOFFMANN, P., HERMS, S., ALTMULLER, J., TOLIAT, M. R., THIELE, H., NURNBERG, P., WILHELM, C., STEPHANI, U., HELBIG, I., LERCHE, H., ZIMPRICH, F., NEUBAUER, B. A., BISKUP, S. & VON SPICZAK, S. 2013. Mutations in GRIN2A cause idiopathic focal epilepsy with rolandic spikes. *Nat Genet*, 45, 1067-72.

- LENCH, A. M., ROBSON, E. & JONES, R. S. 2015. Differential Effects of D-Cycloserine and ACBC at NMDA Receptors in the Rat Entorhinal Cortex Are Related to Efficacy at the Co-Agonist Binding Site. *PLoS One*, 10, e0133548.
- LESCA, G., RUDOLF, G., BRUNEAU, N., LOZOVAYA, N., LABALME, A., BOUTRY-KRYZA, N., SALMI, M., TSINTSADZE, T., ADDIS, L., MOTTE, J., WRIGHT, S., TSINTSADZE, V., MICHEL, A., DOUMMAR, D., LASCELLES, K., STRUG, L., WATERS, P., DE BELLESCIZE, J., VRIELYNCK, P., DE SAINT MARTIN, A., VILLE, D., RYVLIN, P., ARZIMANOGLU, A., HIRSCH, E., VINCENT, A., PAL, D., BURNASHEV, N., SANLAVILLE, D. & SZEPETOWSKI, P. 2013. GRIN2A mutations in acquired epileptic aphasia and related childhood focal epilepsies and encephalopathies with speech and language dysfunction. *Nat Genet*, 45, 1061-6.
- LEWINE, J. D., ANDREWS, R., CHEZ, M., PATIL, A. A., DEVINSKY, O., SMITH, M., KANNER, A., DAVIS, J. T., FUNKE, M., JONES, G., CHONG, B., PROVENCAL, S., WEISEND, M., LEE, R. R. & ORRISON, W. W., JR. 1999. Magnetoencephalographic patterns of epileptiform activity in children with regressive autism spectrum disorders. *Pediatrics*, 104, 405-18.
- LI, J. H., WANG, Y. H., WOLFE, B. B., KRUEGER, K. E., CORSI, L., STOCCA, G. & VICINI, S. 1998. Developmental changes in localization of NMDA receptor subunits in primary cultures of cortical neurons. *Eur J Neurosci*, 10, 1704-15.
- LI, Y., ERZURUMLU, R. S., CHEN, C., JHAVERI, S. & TONEGAWA, S. 1994. Whisker-related neuronal patterns fail to develop in the trigeminal brainstem nuclei of NMDAR1 knockout mice. *Cell*, 76, 427-37.
- LIONEL, A. C., COSTAIN, G., MONFARED, N., WALKER, S., REUTER, M. S., HOSSEINI, S. M., THIRUVAHINDRAPURAM, B., MERICO, D., JOBLING, R., NALPATHAMKALAM, T., PELLECCIA, G., SUNG, W. W. L., WANG, Z., BIKANGAGA, P., BOELMAN, C., CARTER, M. T., CORDEIRO, D., CYTRYNBAUM, C., DELL, S. D., DHIR, P., DOWLING, J. J., HEON, E., HEWSON, S., HIRAKI, L., INBAR-FEIGENBERG, M., KLATT, R., KRONICK, J., LAXER, R. M., LICHT, C., MACDONALD, H., MERCIMEK-ANDREWS, S., MENDOZA-LONDONO, R., PISCIONE, T., SCHNEIDER, R., SCHULZE, A., SILVERMAN, E., SIRIWARDENA, K., SNEAD, O. C., SONDHEIMER, N., SUTHERLAND, J., VINCENT, A., WASSERMAN, J. D., WEKSBERG, R., SHUMAN, C., CAREW, C., SZEGO, M. J., HAYEEMS, R. Z., BASRAN, R., STAVROPOULOS, D. J., RAY, P. N., BOWDIN, S., MEYN, M. S., COHN, R. D., SCHERER, S. W. & MARSHALL, C. R. 2018. Improved diagnostic yield compared with targeted gene sequencing panels suggests a role for whole-genome sequencing as a first-tier genetic test. *Genet Med*, 20, 435-443.
- LIU, H., WANG, H., PETERSON, M., ZHANG, W., HOU, G. & ZHANG, Z. W. 2019. N-terminal alternative splicing of GluN1 regulates the maturation of excitatory synapses and seizure susceptibility. *Proc Natl Acad Sci U S A*, 116, 21207-21212.
- LIU, L., WONG, T. P., POZZA, M. F., LINGENHOEHL, K., WANG, Y., SHENG, M., AUBERSON, Y. P. & WANG, Y. T. 2004. Role of NMDA receptor subtypes in governing the direction of hippocampal synaptic plasticity. *Science*, 304, 1021-4.
- LIU, S., ZHOU, L., YUAN, H., VIEIRA, M., SANZ-CLEMENTE, A., BADGER, J. D., 2ND, LU, W., TRAYNELIS, S. F. & ROCHE, K. W. 2017. A Rare Variant Identified Within the GluN2B C-Terminus in a Patient with Autism Affects NMDA Receptor Surface Expression and Spine Density. *J Neurosci*, 37, 4093-4102.
- LOW, C. M., LYUBOSLAVSKY, P., FRENCH, A., LE, P., WYATTE, K., THIEL, W. H., MARCHAN, E. M., IGARASHI, K., KASHIWAGI, K., GERNERT, K., WILLIAMS, K., TRAYNELIS, S. F. & ZHENG, F. 2003. Molecular determinants of proton-sensitive N-methyl-D-aspartate receptor gating. *Mol Pharmacol*, 63, 1212-22.
- LU, W., DU, J., GOEHRING, A. & GOUAUX, E. 2017. Cryo-EM structures of the triheteromeric NMDA receptor and its allosteric modulation. *Science*, 355.

- LU, W., GRAY, J. A., GRANGER, A. J., DURING, M. J. & NICOLL, R. A. 2011. Potentiation of synaptic AMPA receptors induced by the deletion of NMDA receptors requires the GluA2 subunit. *J Neurophysiol*, 105, 923-8.
- LU, W., MAN, H., JU, W., TRIMBLE, W. S., MACDONALD, J. F. & WANG, Y. T. 2001. Activation of synaptic NMDA receptors induces membrane insertion of new AMPA receptors and LTP in cultured hippocampal neurons. *Neuron*, 29, 243-54.
- LUNDBYE, C. J., TOFT, A. K. H. & BANKE, T. G. 2018. Inhibition of GluN2A NMDA receptors ameliorates synaptic plasticity deficits in the Fmr1(-/y) mouse model. *J Physiol*, 596, 5017-5031.
- LUSCHER, C. & MALENKA, R. C. 2012. NMDA receptor-dependent long-term potentiation and long-term depression (LTP/LTD). *Cold Spring Harb Perspect Biol*, 4.
- MACARTHUR, D. G., BALASUBRAMANIAN, S., FRANKISH, A., HUANG, N., MORRIS, J., WALTER, K., JOSTINS, L., HABEGGER, L., PICKRELL, J. K., MONTGOMERY, S. B., ALBERS, C. A., ZHANG, Z. D., CONRAD, D. F., LUNTER, G., ZHENG, H., AYUB, Q., DEPRISTO, M. A., BANKS, E., HU, M., HANDSAKER, R. E., ROSENFELD, J. A., FROMER, M., JIN, M., MU, X. J., KHURANA, E., YE, K., KAY, M., SAUNDERS, G. I., SUNER, M. M., HUNT, T., BARNES, I. H., AMID, C., CARVALHO-SILVA, D. R., BIGNELL, A. H., SNOW, C., YNGVADOTTIR, B., BUMPSTEAD, S., COOPER, D. N., XUE, Y., ROMERO, I. G., GENOMES PROJECT, C., WANG, J., LI, Y., GIBBS, R. A., MCCARROLL, S. A., DERMITZAKIS, E. T., PRITCHARD, J. K., BARRETT, J. C., HARROW, J., HURLES, M. E., GERSTEIN, M. B. & TYLER-SMITH, C. 2012. A systematic survey of loss-of-function variants in human protein-coding genes. *Science*, 335, 823-8.
- MAH, S. J., CORNELL, E., MITCHELL, N. A. & FLECK, M. W. 2005. Glutamate receptor trafficking: endoplasmic reticulum quality control involves ligand binding and receptor function. *J Neurosci*, 25, 2215-25.
- MAKI, B. A., AMAN, T. K., AMICO-RUVIO, S. A., KUSSIUS, C. L. & POPESCU, G. K. 2012. C-terminal domains of N-methyl-D-aspartic acid receptor modulate unitary channel conductance and gating. *J Biol Chem*, 287, 36071-80.
- MALENKA, R. C. & BEAR, M. F. 2004. LTP and LTD. *Neuron*, 44, 5-21.
- MALINOW, R. & MALENKA, R. C. 2002. AMPA Receptor Trafficking and Synaptic Plasticity. *Annual Review of Neuroscience*, 25, 103-126.
- MARSHALL, S. W. 2007. Power for tests of interaction: effect of raising the Type I error rate. *Epidemiol Perspect Innov*, 4, 4.
- MARTEL, M. A., RYAN, T. J., BELL, K. F., FOWLER, J. H., MCMAHON, A., AL-MUBARAK, B., KOMIYAMA, N. H., HORSBURGH, K., KIND, P. C., GRANT, S. G., WYLLIE, D. J. & HARDINGHAM, G. E. 2012. The subtype of GluN2 C-terminal domain determines the response to excitotoxic insults. *Neuron*, 74, 543-56.
- MARTINA, M., KRASTENIAKOV, N. V. & BERGERON, R. 2003. D-Serine differently modulates NMDA receptor function in rat CA1 hippocampal pyramidal cells and interneurons. *J Physiol*, 548, 411-23.
- MARWICK, K., SKEHEL, P., HARDINGHAM, G. & WYLLIE, D. 2015. Effect of a GRIN2A de novo mutation associated with epilepsy and intellectual disability on NMDA receptor currents and Mg(2+) block in cultured primary cortical neurons. *Lancet*, 385 Suppl 1, S65.
- MARWICK, K. F. M., PARKER, P., SKEHEL, P., HARDINGHAM, G. & WYLLIE, D. J. A. 2017. Functional assessment of the NMDA receptor variant GluN2A (R586K). *Wellcome Open Res*, 2, 20.
- MATHEW, S. S. & HABLITZ, J. J. 2011. Presynaptic NMDA receptors mediate IPSC potentiation at GABAergic synapses in developing rat neocortex. *PLoS One*, 6, e17311.

- MATSUDA, K., KAMIYA, Y., MATSUDA, S. & YUZAKI, M. 2002. Cloning and characterization of a novel NMDA receptor subunit NR3B: a dominant subunit that reduces calcium permeability. *Brain Res Mol Brain Res*, 100, 43-52.
- MATTA, J. A., ASHBY, M. C., SANZ-CLEMENTE, A., ROCHE, K. W. & ISAAC, J. T. 2011. mGluR5 and NMDA receptors drive the experience- and activity-dependent NMDA receptor NR2B to NR2A subunit switch. *Neuron*, 70, 339-51.
- MAYER, M. L. & VYKICKY, L., JR. 1989. The action of zinc on synaptic transmission and neuronal excitability in cultures of mouse hippocampus. *J Physiol*, 415, 351-65.
- MAYER, M. L., VYKICKY, L., JR. & CLEMENTS, J. 1989. Regulation of NMDA receptor desensitization in mouse hippocampal neurons by glycine. *Nature*, 338, 425-7.
- MAYER, M. L., WESTBROOK, G. L. & GUTHRIE, P. B. 1984. Voltage-dependent block by Mg²⁺ of NMDA responses in spinal cord neurones. *Nature*, 309, 261-3.
- MCGROTHER, C. W., BHAUMIK, S., THORP, C. F., HAUCK, A., BRANFORD, D. & WATSON, J. M. 2006. Epilepsy in adults with intellectual disabilities: prevalence, associations and service implications. *Seizure*, 15, 376-86.
- MCILHINNEY, R. A., LE BOURDELLES, B., MOLNAR, E., TRICAUD, N., STREIT, P. & WHITING, P. J. 1998. Assembly intracellular targeting and cell surface expression of the human N-methyl-D-aspartate receptor subunits NR1a and NR2A in transfected cells. *Neuropharmacology*, 37, 1355-67.
- MCKAY, S., GRIFFITHS, N. H., BUTTERS, P. A., THUBRON, E. B., HARDINGHAM, G. E. & WYLLIE, D. J. 2012. Direct pharmacological monitoring of the developmental switch in NMDA receptor subunit composition using TCN 213, a GluN2A-selective, glycine-dependent antagonist. *Br J Pharmacol*, 166, 924-37.
- MCKAY, S., RYAN, T. J., MCQUEEN, J., INDERSMITTEN, T., MARWICK, K. F. M., HASEL, P., KOPANITSA, M. V., BAXTER, P. S., MARTEL, M. A., KIND, P. C., WYLLIE, D. J. A., O'DELL, T. J., GRANT, S. G. N., HARDINGHAM, G. E. & KOMIYAMA, N. H. 2018. The Developmental Shift of NMDA Receptor Composition Proceeds Independently of GluN2 Subunit-Specific GluN2 C-Terminal Sequences. *Cell Rep*, 25, 841-851 e4.
- MCKINNEY, R. A., LUTHI, A., BANDTLOW, C. E., GAHWILER, B. H. & THOMPSON, S. M. 1999. Selective glutamate receptor antagonists can induce or prevent axonal sprouting in rat hippocampal slice cultures. *Proc Natl Acad Sci U S A*, 96, 11631-6.
- MILLER, A. R., HAWKINS, N. A., MCCOLLOM, C. E. & KEARNEY, J. A. 2014. Mapping genetic modifiers of survival in a mouse model of Dravet syndrome. *Genes Brain Behav*, 13, 163-72.
- MOHRMANN, R., KOHR, G., HATT, H., SPRENGEL, R. & GOTTMANN, K. 2002. Deletion of the C-terminal domain of the NR2B subunit alters channel properties and synaptic targeting of N-methyl-D-aspartate receptors in nascent neocortical synapses. *J Neurosci Res*, 68, 265-75.
- MONYER, H., BURNASHEV, N., LAURIE, D. J., SAKMANN, B. & SEEBURG, P. H. 1994. Developmental and regional expression in the rat brain and functional properties of four NMDA receptors. *Neuron*, 12, 529-40.
- MORI, T., KASEM, E. A., SUZUKI-KOUYAMA, E., CAO, X., LI, X., KURIHARA, T., UEMURA, T., YANAGAWA, T. & TABUCHI, K. 2019. Deficiency of calcium/calmodulin-dependent serine protein kinase disrupts the excitatory-inhibitory balance of synapses by down-regulating GluN2B. *Mol Psychiatry*, 24, 1079-1092.
- MORINI, R., FERRARA, S., PERRUCCI, F., ZAMBETTI, S., PELUCCHI, S., MARCELLO, E., GARDONI, F., ANTONUCCI, F., MATTEOLI, M. & MENNA, E. 2018. Lack of the Actin Capping Protein, Eps8, Affects NMDA-Type Glutamate Receptor Function and Composition. *Front Mol Neurosci*, 11, 313.
- MULLIER, B., WOLFF, C., SANDS, Z. A., GHISDAL, P., MUGLIA, P., KAMINSKI, R. M. & ANDRE, V. M. 2017. GRIN2B gain of function mutations are sensitive to radiprodil, a negative

- allosteric modulator of GluN2B-containing NMDA receptors. *Neuropharmacology*, 123, 322-331.
- MURPHY, J. A., STEIN, I. S., LAU, C. G., PEIXOTO, R. T., AMAN, T. K., KANEKO, N., AROMOLARAN, K., SAULNIER, J. L., POPESCU, G. K., SABATINI, B. L., HELL, J. W. & ZUKIN, R. S. 2014. Phosphorylation of Ser1166 on GluN2B by PKA is critical to synaptic NMDA receptor function and Ca²⁺ signaling in spines. *J Neurosci*, 34, 869-79.
- MYERS, C. T. & MEFFORD, H. C. 2015. Advancing epilepsy genetics in the genomic era. *Genome Med*, 7, 91.
- MYERS, R. A., CASALS, F., GAUTHIER, J., HAMDAN, F. F., KEEBLER, J., BOYKO, A. R., BUSTAMANTE, C. D., PITON, A. M., SPIEGELMAN, D., HENRION, E., ZILVERSMIT, M., HUSSIN, J., QUINLAN, J., YANG, Y., LAFRENIERE, R. G., GRIFFING, A. R., STONE, E. A., ROULEAU, G. A. & AWADALLA, P. 2011. A population genetic approach to mapping neurological disorder genes using deep resequencing. *PLoS Genet*, 7, e1001318.
- NAGY, A. 2000. Cre recombinase: the universal reagent for genome tailoring. *Genesis*, 26, 99-109.
- NAGY, J., KOLOK, S., BOROS, A. & DEZSO, P. 2005. Role of altered structure and function of NMDA receptors in development of alcohol dependence. *Curr Neuropharmacol*, 3, 281-97.
- NEVES, G., COOKE, S. F. & BLISS, T. V. P. 2008. Synaptic plasticity, memory and the hippocampus: a neural network approach to causality. *Nature Reviews Neuroscience*, 9, 65-75.
- NG, P. C. & HENIKOFF, S. 2001. Predicting deleterious amino acid substitutions. *Genome Res*, 11, 863-74.
- NICOLL, R. A. 2017. A Brief History of Long-Term Potentiation. *Neuron*, 93, 281-290.
- NILSSON, D., PETTERSSON, M., GUSTAVSSON, P., FORSTER, A., HOFMEISTER, W., WINCENT, J., ZACHARIADIS, V., ANDERLID, B. M., NORDGREN, A., MAKITIE, O., WIRTA, V., KALLER, M., VEZZI, F., LUPSKI, J. R., NORDENSKJOLD, M., LUNDBERG, E. S., CARVALHO, C. M. B. & LINDSTRAND, A. 2017. Whole-Genome Sequencing of Cytogenetically Balanced Chromosome Translocations Identifies Potentially Pathological Gene Disruptions and Highlights the Importance of Microhomology in the Mechanism of Formation. *Hum Mutat*, 38, 180-192.
- NOBELS, J. 2015. Pathway-driven discovery of epilepsy genes. *Nat Neurosci*, 18, 344-50.
- NOWAK, L., BREGESTOVSKI, P., ASCHER, P., HERBET, A. & PROCHIANTZ, A. 1984. Magnesium gates glutamate-activated channels in mouse central neurones. *Nature*, 307, 462-5.
- O'ROAK, B. J., VIVES, L., FU, W., EGERTSON, J. D., STANAWAY, I. B., PHELPS, I. G., CARVILL, G., KUMAR, A., LEE, C., ANKENMAN, K., MUNSON, J., HIATT, J. B., TURNER, E. H., LEVY, R., O'DAY, D. R., KRUMM, N., COE, B. P., MARTIN, B. K., BORENSTEIN, E., NICKERSON, D. A., MEFFORD, H. C., DOHERTY, D., AKEY, J. M., BERNIER, R., EICHLER, E. E. & SHENDURE, J. 2012. Multiplex Targeted Sequencing Identifies Recurrently Mutated Genes in Autism Spectrum Disorders. *Science*, 338, 1619-1622.
- OGDEN, K. K., CHEN, W., SWANGER, S. A., MCDANIEL, M. J., FAN, L. Z., HU, C., TANKOVIC, A., KUSUMOTO, H., KOSOBUECKI, G. J., SCHULIEN, A. J., SU, Z., PECHA, J., BHATTACHARYA, S., PETROVSKI, S., COHEN, A. E., AIZENMAN, E., TRAYNELIS, S. F. & YUAN, H. 2017. Molecular Mechanism of Disease-Associated Mutations in the Pre-M1 Helix of NMDA Receptors and Potential Rescue Pharmacology. *PLoS Genet*, 13, e1006536.
- PAN, Y., CHEN, J., GUO, H., OU, J., PENG, Y., LIU, Q., SHEN, Y., SHI, L., LIU, Y., XIONG, Z., ZHU, T., LUO, S., HU, Z., ZHAO, J. & XIA, K. 2015. Association of genetic variants of GRIN2B with autism. *Sci Rep*, 5, 8296.
- PAOLETTI, P., ASCHER, P. & NEYTON, J. 1997. High-Affinity Zinc Inhibition of NMDA NR1–NR2A Receptors. *The Journal of Neuroscience*, 17, 5711-5725.

- PAOLETTI, P., BELLONE, C. & ZHOU, Q. 2013. NMDA receptor subunit diversity: impact on receptor properties, synaptic plasticity and disease. *Nat Rev Neurosci*, 14, 383-400.
- PAOLETTI, P., VERGNANO, A. M., BARBOUR, B. & CASADO, M. 2009. Zinc at glutamatergic synapses. *Neuroscience*, 158, 126-36.
- PAPADIA, S. & HARDINGHAM, G. E. 2007. The dichotomy of NMDA receptor signaling. *Neuroscientist*, 13, 572-9.
- PAQUET, M. & SMITH, Y. 2000. Presynaptic NMDA receptor subunit immunoreactivity in GABAergic terminals in rat brain. *J Comp Neurol*, 423, 330-47.
- PENN, A. C., WILLIAMS, S. R. & GREGER, I. H. 2008. Gating motions underlie AMPA receptor secretion from the endoplasmic reticulum. *EMBO J*, 27, 3056-68.
- PENN, A. C., ZHANG, C. L., GEORGES, F., ROYER, L., BREILLAT, C., HOSY, E., PETERSEN, J. D., HUMEAU, Y. & CHOQUET, D. 2017. Hippocampal LTP and contextual learning require surface diffusion of AMPA receptors. *Nature*, 549, 384-388.
- PERIN-DUREAU, F., RACHLINE, J., NEYTON, J. & PAOLETTI, P. 2002. Mapping the binding site of the neuroprotectant ifenprodil on NMDA receptors. *J Neurosci*, 22, 5955-65.
- PHILPOT, B. D., SEKHAR, A. K., SHOUVAL, H. Z. & BEAR, M. F. 2001. Visual experience and deprivation bidirectionally modify the composition and function of NMDA receptors in visual cortex. *Neuron*, 29, 157-69.
- PIAN, J. P., CRIADO, J. R., MILNER, R. & EHLERS, C. L. 2010. N-methyl-D-aspartate receptor subunit expression in adult and adolescent brain following chronic ethanol exposure. *Neuroscience*, 170, 645-54.
- PIERSON, T. M., YUAN, H., MARSH, E. D., FUENTES-FAJARDO, K., ADAMS, D. R., MARKELLO, T., GOLAS, G., SIMEONOV, D. R., HOLLOMAN, C., TANKOVIC, A., KARAMCHANDANI, M. M., SCHREIBER, J. M., MULLIKIN, J. C., PH, D. F. T. N. C. S. P., TIFFT, C. J., TORO, C., BOERKOEL, C. F., TRAYNELIS, S. F. & GAHL, W. A. 2014. mutation and early-onset epileptic encephalopathy: personalized therapy with memantine. *Ann Clin Transl Neurol*, 1, 190-198.
- PLATZER, K., YUAN, H., SCHUTZ, H., WINSCHER, A., CHEN, W., HU, C., KUSUMOTO, H., HEYNE, H. O., HELBIG, K. L., TANG, S., WILLING, M. C., TINKLE, B. T., ADAMS, D. J., DEPIENNE, C., KEREN, B., MIGNOT, C., FRENGEN, E., STROMME, P., BISKUP, S., DOCKER, D., STROM, T. M., MEFFORD, H. C., MYERS, C. T., MUIR, A. M., LACROIX, A., SADLEIR, L., SCHEFFER, I. E., BRILSTRA, E., VAN HAELEST, M. M., VAN DER SMAGT, J. J., BOK, L. A., MOLLER, R. S., JENSEN, U. B., MILLICHAP, J. J., BERG, A. T., GOLDBERG, E. M., DE BIE, I., FOX, S., MAJOR, P., JONES, J. R., ZACKAI, E. H., ABOU JAMRA, R., ROLFS, A., LEVENTER, R. J., LAWSON, J. A., ROSCIOLI, T., JANSEN, F. E., RANZA, E., KORFF, C. M., LEHESJOKI, A. E., COURAGE, C., LINNANKIVI, T., SMITH, D. R., STANLEY, C., MINTZ, M., MCKNIGHT, D., DECKER, A., TAN, W. H., TARNOPOLSKY, M. A., BRADY, L. I., WOLFF, M., DONDIT, L., PEDRO, H. F., PARISOTTO, S. E., JONES, K. L., PATEL, A. D., FRANZ, D. N., VANZO, R., MARCO, E., RANELLS, J. D., DI DONATO, N., DOBYNS, W. B., LAUBE, B., TRAYNELIS, S. F. & LEMKE, J. R. 2017. GRIN2B encephalopathy: novel findings on phenotype, variant clustering, functional consequences and treatment aspects. *J Med Genet*, 54, 460-470.
- PUNNAKKAL, P. & DOMINIC, D. 2018. NMDA Receptor GluN2 Subtypes Control Epileptiform Events in the Hippocampus. *Neuromolecular Med*, 20, 90-96.
- PURPURA, D. P. 1974. Dendritic spine "dysgenesis" and mental retardation. *Science*, 186, 1126-8.
- QIU, S., ZHANG, X. M., CAO, J. Y., YANG, W., YAN, Y. G., SHAN, L., ZHENG, J. & LUO, J. H. 2009. An endoplasmic reticulum retention signal located in the extracellular amino-terminal domain of the NR2A subunit of N-Methyl-D-aspartate receptors. *J Biol Chem*, 284, 20285-98.
- RAOL, Y. H., LYNCH, D. R. & BROOKS-KAYAL, A. R. 2001. Role of excitatory amino acids in developmental epilepsies. *Ment Retard Dev Disabil Res Rev*, 7, 254-60.

- RAUNER, C. & KOHR, G. 2011. Triheteromeric NR1/NR2A/NR2B receptors constitute the major N-methyl-D-aspartate receptor population in adult hippocampal synapses. *J Biol Chem*, 286, 7558-66.
- REDDY, D. S. 2010. Neurosteroids: endogenous role in the human brain and therapeutic potentials. *Prog Brain Res*, 186, 113-37.
- REGAN, M. C., ZHU, Z., YUAN, H., MYERS, S. J., MENALDINO, D. S., TAHIROVIC, Y. A., LIOTTA, D. C., TRAYNELIS, S. F. & FURUKAWA, H. 2019. Structural elements of a pH-sensitive inhibitor binding site in NMDA receptors. *Nat Commun*, 10, 321.
- REIPRICH, P., KILB, W. & LUHMANN, H. J. 2005. Neonatal NMDA receptor blockade disturbs neuronal migration in rat somatosensory cortex in vivo. *Cereb Cortex*, 15, 349-58.
- REITTERER, K., JUUSOLA, J., CHO, M. T., VITAZKA, P., MILLAN, F., GIBELLINI, F., VERTINO-BELL, A., SMAOUI, N., NEIDICH, J., MONAGHAN, K. G., MCKNIGHT, D., BAI, R., SUCHY, S., FRIEDMAN, B., TAHILIANI, J., PINEDA-ALVAREZ, D., RICHARD, G., BRANDT, T., HAVERFIELD, E., CHUNG, W. K. & BALE, S. 2015. Clinical application of whole-exome sequencing across clinical indications. *Genetics in Medicine*, 18, 696-704.
- REUTLINGER, C., HELBIG, I., GAWELCZYK, B., SUBERO, J. I. M., TÖNNIES, H., MUHLE, H., FINSTERWALDER, K., VERMEER, S., PFUNDT, R., SPERNER, J., STEFANOVA, I., GILLESSEN-KAESBACH, G., VON SPICZAK, S., VAN BAALEN, A., BOOR, R., SIEBERT, R., STEPHANI, U. & CALIEBE, A. 2010. Deletions in 16p13 including GRIN2A in patients with intellectual disability, various dysmorphic features, and seizure disorders of the rolandic region. *Epilepsia*, 51, 1870-1873.
- ROZOV, A., SPRENGEL, R. & SEEBURG, P. H. 2012. GluA2-lacking AMPA receptors in hippocampal CA1 cell synapses: evidence from gene-targeted mice. *Front Mol Neurosci*, 5, 22.
- RUBENSTEIN, E., SCHIEVE, L., WIGGINS, L., RICE, C., VAN NAARDEN BRAUN, K., CHRISTENSEN, D., DURKIN, M., DANIELS, J. & LEE, L. C. 2018. Trends in documented co-occurring conditions in children with autism spectrum disorder, 2002-2010. *Res Dev Disabil*, 83, 168-178.
- RUBENSTEIN, J. L. & MERZENICH, M. M. 2003. Model of autism: increased ratio of excitation/inhibition in key neural systems. *Genes Brain Behav*, 2, 255-67.
- RUBENSTEIN, J. L. R. 2010. Three hypotheses for developmental defects that may underlie some forms of autism spectrum disorder. *Current Opinion in Neurology*, 23, 118-123.
- RUMBAUGH, G., PRYBYLOWSKI, K., WANG, J. F. & VICINI, S. 2000. Exon 5 and spermine regulate deactivation of NMDA receptor subtypes. *J Neurophysiol*, 83, 1300-6.
- RYAN, T. J., EMES, R. D., GRANT, S. G. & KOMIYAMA, N. H. 2008. Evolution of NMDA receptor cytoplasmic interaction domains: implications for organisation of synaptic signalling complexes. *BMC Neurosci*, 9, 6.
- RYAN, T. J., KOPANITSA, M. V., INDERSMITTEN, T., NITHIANANTHARAJAH, J., AFINOWI, N. O., PETTIT, C., STANFORD, L. E., SPRENGEL, R., SAKSIDA, L. M., BUSSEY, T. J., O'DELL, T. J., GRANT, S. G. & KOMIYAMA, N. H. 2013. Evolution of GluN2A/B cytoplasmic domains diversified vertebrate synaptic plasticity and behavior. *Nat Neurosci*, 16, 25-32.
- SAKIMURA, K., KUTSUWADA, T., ITO, I., MANABE, T., TAKAYAMA, C., KUSHIYA, E., YAGI, T., AIZAWA, S., INOUE, Y., SUGIYAMA, H. & ET AL. 1995. Reduced hippocampal LTP and spatial learning in mice lacking NMDA receptor epsilon 1 subunit. *Nature*, 373, 151-5.
- SALMI, M., BOLBOS, R., BAUER, S., MINLEBAEV, M., BURNASHEV, N. & SZEPETOWSKI, P. 2018. Transient microstructural brain anomalies and epileptiform discharges in mice defective for epilepsy and language-related NMDA receptor subunit gene Grin2a. *Epilepsia*, 59, 1919-1930.
- SALMI, M., DEL GALLO, F., MINLEBAEV, M., ZAKHAROV, A., PAULY, V., PERRON, P., PONS-BENNACEUR, A., CORBY-PELLEGRINO, S., ANIKSZTEJN, L., LENCK-SANTINI, P. P., EPSZTEIN, J., KHAZIPOV, R., BURNASHEV, N., BERTINI, G. & SZEPETOWSKI, P. 2019.

- Impaired vocal communication, sleep-related discharges, and transient alteration of slow-wave sleep in developing mice lacking the GluN2A subunit of N-methyl-D-aspartate receptors. *Epilepsia*, 60, 1424-1437.
- SANS, N., PRYBYLOWSKI, K., PETRALIA, R. S., CHANG, K., WANG, Y. X., RACCA, C., VICINI, S. & WENTHOLD, R. J. 2003. NMDA receptor trafficking through an interaction between PDZ proteins and the exocyst complex. *Nat Cell Biol*, 5, 520-30.
- SANZ-CLEMENTE, A., MATTA, J. A., ISAAC, J. T. & ROCHE, K. W. 2010. Casein kinase 2 regulates the NR2 subunit composition of synaptic NMDA receptors. *Neuron*, 67, 984-96.
- SANZ-CLEMENTE, A., NICOLL, R. A. & ROCHE, K. W. 2013. Diversity in NMDA receptor composition: many regulators, many consequences. *Neuroscientist*, 19, 62-75.
- SAUNDERS, C. T. & BAKER, D. 2002. Evaluation of structural and evolutionary contributions to deleterious mutation prediction. *J Mol Biol*, 322, 891-901.
- SCENIAK, M. P., FEDDER, K. N., WANG, Q., DROUBI, S., BABCOCK, K., PATWARDHAN, S., WRIGHT-ZORNES, J., PHAM, L. & SABO, S. L. 2019. A GluN2B mutation identified in Autism prevents NMDA receptor trafficking and interferes with dendrite growth. *J Cell Sci*.
- SCHNEIDER, R. & SANDER, C. 1996. The HSSP database of protein structure-sequence alignments. *Nucleic Acids Res*, 24, 201-5.
- SCHORGE, S. & COLQUHOUN, D. 2003. Studies of NMDA receptor function and stoichiometry with truncated and tandem subunits. *J Neurosci*, 23, 1151-8.
- SCHÜLER, T., MESIC, I., MADRY, C., BARTHOLOMÄUS, I. & LAUBE, B. 2008. Formation of NR1/NR2 and NR1/NR3 Heterodimers Constitutes the Initial Step in N-Methyl-D-aspartate Receptor Assembly. *Journal of Biological Chemistry*, 283, 37-46.
- SCHYMKOWITZ, J., BORG, J., STRICHER, F., NYS, R., ROUSSEAU, F. & SERRANO, L. 2005. The FoldX web server: an online force field. *Nucleic Acids Res*, 33, W382-8.
- SCULIER, C., TILMANT, A.-S., DE TIÈGE, X., GIURGEA, S., PAQUIER, P., RUDOLF, G., LESCA, G. & VAN BOGAERT, P. 2017. Acquired epileptic opercular syndrome related to a heterozygous deleterious substitution in GRIN2A. *Epileptic Disorders*, 19, 345-350.
- SEEBURG, P. H., BURNASHEV, N., KOHR, G., KUNER, T., SPRENGEL, R. & MONYER, H. 1995. The NMDA receptor channel: molecular design of a coincidence detector. *Recent Prog Horm Res*, 50, 19-34.
- SERRAZ, B., GRAND, T. & PAOLETTI, P. 2016. Altered zinc sensitivity of NMDA receptors harboring clinically-relevant mutations. *Neuropharmacology*, 109, 196-204.
- SHE, K., FERREIRA, J. S., CARVALHO, A. L. & CRAIG, A. M. 2012. Glutamate binding to the GluN2B subunit controls surface trafficking of N-methyl-D-aspartate (NMDA) receptors. *J Biol Chem*, 287, 27432-45.
- SHENG, M., CUMMINGS, J., ROLDAN, L. A., JAN, Y. N. & JAN, L. Y. 1994. Changing subunit composition of heteromeric NMDA receptors during development of rat cortex. *Nature*, 368, 144-7.
- SHENG, M. & PAK, D. T. S. 2000. Ligand-Gated Ion Channel Interactions with Cytoskeletal and Signaling Proteins. *Annual Review of Physiology*, 62, 755-778.
- SHINOHARA, Y., HIRASE, H., WATANABE, M., ITAKURA, M., TAKAHASHI, M. & SHIGEMOTO, R. 2008. Left-right asymmetry of the hippocampal synapses with differential subunit allocation of glutamate receptors. *Proc Natl Acad Sci U S A*, 105, 19498-503.
- SHIPTON, O. A. & PAULSEN, O. 2014. GluN2A and GluN2B subunit-containing NMDA receptors in hippocampal plasticity. *Philos Trans R Soc Lond B Biol Sci*, 369, 20130163.
- SIBAROV, D. A., BRUNEAU, N., ANTONOV, S. M., SZEPETOWSKI, P., BURNASHEV, N. & GINIATULLIN, R. 2017. Functional Properties of Human NMDA Receptors Associated with Epilepsy-Related Mutations of GluN2A Subunit. *Front Cell Neurosci*, 11, 155.

- SIL'KIS, I. G. 2007. What are the mechanisms underlying the involvement of different subtypes of NMDA receptors in inducing long-term potentiation and depression in the hippocampus? *Neurosci Behav Physiol*, 37, 477-80.
- SINGLE, F. N., ROZOV, A., BURNASHEV, N., ZIMMERMANN, F., HANLEY, D. F., FORREST, D., CURRAN, T., JENSEN, V., HVALBY, O., SPRENGEL, R. & SEEBURG, P. H. 2000. Dysfunctions in mice by NMDA receptor point mutations NR1(N598Q) and NR1(N598R). *J Neurosci*, 20, 2558-66.
- SOTO, D., OLIVELLA, M., GRAU, C., ARMSTRONG, J., ALCON, C., GASULL, X., SANTOS-GOMEZ, A., LOCUBICHE, S., GOMEZ DE SALAZAR, M., GARCIA-DIAZ, R., GRATACOS-BATLLE, E., RAMOS-VICENTE, D., CHU-VAN, E., COLSCH, B., FERNANDEZ-DUENAS, V., CIRUELA, F., BAYES, A., SINDREU, C., LOPEZ-SALA, A., GARCIA-CAZORLA, A. & ALTAFAJ, X. 2019. l-Serine dietary supplementation is associated with clinical improvement of loss-of-function GRIN2B-related pediatric encephalopathy. *Sci Signal*, 12.
- SPRENGEL, R., ELTOKHI, A. & SINGLE, F. N. 2017. Gene Targeted Mice with Conditional Knock-In (-Out) of NMDAR Mutations. *Methods Mol Biol*, 1677, 201-230.
- SPRENGEL, R., SUCHANEK, B., AMICO, C., BRUSA, R., BURNASHEV, N., ROZOV, A., HVALBY, O., JENSEN, V., PAULSEN, O., ANDERSEN, P., KIM, J. J., THOMPSON, R. F., SUN, W., WEBSTER, L. C., GRANT, S. G., EILERS, J., KONNERTH, A., LI, J., MCNAMARA, J. O. & SEEBURG, P. H. 1998. Importance of the intracellular domain of NR2 subunits for NMDA receptor function in vivo. *Cell*, 92, 279-89.
- STANDLEY, S., ROCHE, K. W., MCCALLUM, J., SANS, N. & WENTHOLD, R. J. 2000. PDZ Domain Suppression of an ER Retention Signal in NMDA Receptor NR1 Splice Variants. *Neuron*, 28, 887-898.
- STEIGERWALD, F., SCHULZ, T. W., SCHENKER, L. T., KENNEDY, M. B., SEEBURG, P. H. & KOHR, G. 2000. C-Terminal truncation of NR2A subunits impairs synaptic but not extrasynaptic localization of NMDA receptors. *J Neurosci*, 20, 4573-81.
- STOCCA, G. & VICINI, S. 1998. Increased contribution of NR2A subunit to synaptic NMDA receptors in developing rat cortical neurons. *J Physiol*, 507 (Pt 1), 13-24.
- STOREY, G. P., OPITZ-ARAYA, X. & BARRIA, A. 2011. Molecular determinants controlling NMDA receptor synaptic incorporation. *J Neurosci*, 31, 6311-6.
- STREHLOW, V., HEYNE, H. O., VLASKAMP, D. R. M., MARWICK, K. F. M., RUDOLF, G., DE BELLESCIZE, J., BISKUP, S., BRILSTRA, E. H., BROUWER, O. F., CALLENBACH, P. M. C., HENTSCHEL, J., HIRSCH, E., KIND, P. C., MIGNOT, C., PLATZER, K., RUMP, P., SKEHEL, P. A., WYLLIE, D. J. A., HARDINGHAM, G. E., VAN RAVENSWAAL-ARTS, C. M. A., LESCA, G., LEMKE, J. R. & GROUP, G. A. S. 2019. GRIN2A-related disorders: genotype and functional consequence predict phenotype. *Brain*, 142, 80-92.
- STROEBEL, D., CASADO, M. & PAOLETTI, P. 2018. Triheteromeric NMDA receptors: from structure to synaptic physiology. *Curr Opin Physiol*, 2, 1-12.
- SU, T., LU, Y., GENG, Y., LU, W. & CHEN, Y. 2018. How could N-Methyl-D-Aspartate Receptor Antagonists Lead to Excitation Instead of Inhibition? *Brain Science Advances*, 4, 73-98.
- SUBRAMANIAN, J. & NEDIVI, E. 2016. Filling the (SR)GAP in Excitatory/Inhibitory Balance. *Neuron*, 91, 205-7.
- SULLIVAN, J. A., ZHANG, X. L., SULLIVAN, A. P., VOSE, L. R., MOGHADAM, A. A., FRIED, V. A. & STANTON, P. K. 2018. Zinc enhances hippocampal long-term potentiation at CA1 synapses through NR2B containing NMDA receptors. *PLoS One*, 13, e0205907.
- SUN, Y., CHENG, X., ZHANG, L., HU, J., CHEN, Y., ZHAN, L. & GAO, Z. 2017. The Functional and Molecular Properties, Physiological Functions, and Pathophysiological Roles of GluN2A in the Central Nervous System. *Mol Neurobiol*, 54, 1008-1021.
- SUN, Y. Y., CAI, W., YU, J., LIU, S. S., ZHUO, M., LI, B. M. & ZHANG, X. H. 2016. Surface expression of hippocampal NMDA GluN2B receptors regulated by fear conditioning determines its contribution to memory consolidation in adult rats. *Sci Rep*, 6, 30743.

- SUTTON, M. A., ITO, H. T., CRESSY, P., KEMPF, C., WOO, J. C. & SCHUMAN, E. M. 2006. Miniature neurotransmission stabilizes synaptic function via tonic suppression of local dendritic protein synthesis. *Cell*, 125, 785-99.
- SUZUKI, Y., GOETZE, T. A., STROEBEL, D., BALASURIYA, D., YOSHIMURA, S. H., HENDERSON, R. M., PAOLETTI, P., TAKEYASU, K. & EDWARDSON, J. M. 2013. Visualization of structural changes accompanying activation of N-methyl-D-aspartate (NMDA) receptors using fast-scan atomic force microscopy imaging. *J Biol Chem*, 288, 778-84.
- SVEINBJORNSDOTTIR, S., SANDER, J. W., UPTON, D., THOMPSON, P. J., PATSALOS, P. N., HIRT, D., EMRE, M., LOWE, D. & DUNCAN, J. S. 1993. The excitatory amino acid antagonist D-CPP-ene (SDZ EAA-494) in patients with epilepsy. *Epilepsy Res*, 16, 165-74.
- SWANGER, S. A., CHEN, W., WELLS, G., BURGER, P. B., TANKOVIC, A., BHATTACHARYA, S., STRONG, K. L., HU, C., KUSUMOTO, H., ZHANG, J., ADAMS, D. R., MILLICHAP, J. J., PETROVSKI, S., TRAYNELIS, S. F. & YUAN, H. 2016. Mechanistic Insight into NMDA Receptor Dysregulation by Rare Variants in the GluN2A and GluN2B Agonist Binding Domains. *Am J Hum Genet*, 99, 1261-1280.
- SZABADITS, E., CSEREP, C., SZONYI, A., FUKAZAWA, Y., SHIGEMOTO, R., WATANABE, M., ITOHARA, S., FREUND, T. F. & NYIRI, G. 2011. NMDA receptors in hippocampal GABAergic synapses and their role in nitric oxide signaling. *J Neurosci*, 31, 5893-904.
- TABUCHI, K., BLUNDELL, J., ETHERTON, M. R., HAMMER, R. E., LIU, X., POWELL, C. M. & SUDHOF, T. C. 2007. A neuroligin-3 mutation implicated in autism increases inhibitory synaptic transmission in mice. *Science*, 318, 71-6.
- TAKARAE, Y. & SWEENEY, J. 2017. Neural Hyperexcitability in Autism Spectrum Disorders. *Brain Sci*, 7.
- TAKASAKI, Y., KOIDE, T., WANG, C., KIMURA, H., XING, J., KUSHIMA, I., ISHIZUKA, K., MORI, D., SEKIGUCHI, M., IKEDA, M., AIZAWA, M., TSURUMARU, N., IWAYAMA, Y., YOSHIMI, A., ARIOKA, Y., YOSHIDA, M., NOMA, H., OYA-ITO, T., NAKAMURA, Y., KUNIMOTO, S., ALEKSIC, B., UNO, Y., OKADA, T., UJIKE, H., EGAWA, J., KUWABARA, H., SOMEYA, T., YOSHIKAWA, T., IWATA, N. & OZAKI, N. 2016. Mutation screening of GRIN2B in schizophrenia and autism spectrum disorder in a Japanese population. *Sci Rep*, 6, 33311.
- TALKOWSKI, M. E., ROSENFELD, J. A., BLUMENTHAL, I., PILLALAMARRI, V., CHIANG, C., HEILBUT, A., ERNST, C., HANSCOM, C., ROSSIN, E., LINDGREN, A. M., PEREIRA, S., RUDERFER, D., KIRBY, A., RIPKE, S., HARRIS, D. J., LEE, J. H., HA, K., KIM, H. G., SOLOMON, B. D., GROPMAN, A. L., LUCENTE, D., SIMS, K., OHSUMI, T. K., BOROWSKY, M. L., LORANGER, S., QUADE, B., LAGE, K., MILES, J., WU, B. L., SHEN, Y., NEALE, B., SHAFFER, L. G., DALY, M. J., MORTON, C. C. & GUSELLA, J. F. 2012. Sequencing chromosomal abnormalities reveals neurodevelopmental loci that confer risk across diagnostic boundaries. *Cell*, 149, 525-37.
- TANG, T. T., BADGER, J. D., 2ND, ROCHE, P. A. & ROCHE, K. W. 2010. Novel approach to probe subunit-specific contributions to N-methyl-D-aspartate (NMDA) receptor trafficking reveals a dominant role for NR2B in receptor recycling. *J Biol Chem*, 285, 20975-81.
- TANG, Y. P., SHIMIZU, E., DUBE, G. R., RAMPON, C., KERCHNER, G. A., ZHUO, M., LIU, G. & TSIEN, J. Z. 1999. Genetic enhancement of learning and memory in mice. *Nature*, 401, 63-9.
- TARABEUX, J., KEBIR, O., GAUTHIER, J., HAMDAN, F. F., XIONG, L., PITON, A., SPIEGELMAN, D., HENRION, É., MILLET, B., FATHALLI, F., JOOBER, R., RAPOPORT, J. L., DELISI, L. E., FOMBONNE, É., MOTTRON, L., FORGET-DUBOIS, N., BOIVIN, M., MICHAUD, J. L., DRAPEAU, P., LAFRENIÈRE, R. G., ROULEAU, G. A. & KREBS, M. O. 2011. Rare mutations in N-methyl-D-aspartate glutamate receptors in autism spectrum disorders and schizophrenia. *Translational Psychiatry*, 1, e55-e55.

- THOMAS, P. & SMART, T. G. 2005. HEK293 cell line: a vehicle for the expression of recombinant proteins. *J Pharmacol Toxicol Methods*, 51, 187-200.
- TOLLE, T. R., BERTHELE, A., LAURIE, D. J., SEEBURG, P. H. & ZIEGLGANSBERGER, W. 1995. Cellular and subcellular distribution of NMDAR1 splice variant mRNA in the rat lumbar spinal cord. *Eur J Neurosci*, 7, 1235-44.
- TOVAR, K. R., MCGINLEY, M. J. & WESTBROOK, G. L. 2013. Triheteromeric NMDA receptors at hippocampal synapses. *J Neurosci*, 33, 9150-60.
- TOVAR, K. R. & WESTBROOK, G. L. 2012. Amino-terminal ligands prolong NMDA Receptor-mediated EPSCs. *J Neurosci*, 32, 8065-73.
- TRAYNELIS, S. F., HARTLEY, M. & HEINEMANN, S. F. 1995. Control of proton sensitivity of the NMDA receptor by RNA splicing and polyamines. *Science*, 268, 873-6.
- TRUJILLANO, D., BERTOLI-AVELLA, A. M., KUMAR KANDASWAMY, K., WEISS, M. E., KOSTER, J., MARAIS, A., PAKNIA, O., SCHRODER, R., GARCIA-AZNAR, J. M., WERBER, M., BRANDAU, O., CALVO DEL CASTILLO, M., BALDI, C., WESSEL, K., KISHORE, S., NAHAVANDI, N., EYAD, W., AL RIFAI, M. T., AL-RUMAYYAN, A., AL-TWAIJRI, W., ALOTHAIM, A., ALHASHEM, A., AL-SANNAA, N., AL-BALWI, M., ALFADHEL, M., ROLFS, A. & ABOU JAMRA, R. 2017. Clinical exome sequencing: results from 2819 samples reflecting 1000 families. *Eur J Hum Genet*, 25, 176-182.
- TSIEN, J. Z., HUERTA, P. T. & TONEGAWA, S. 1996. The essential role of hippocampal CA1 NMDA receptor-dependent synaptic plasticity in spatial memory. *Cell*, 87, 1327-38.
- TUCHMAN, R. & CUCCARO, M. 2011. Epilepsy and Autism: Neurodevelopmental Perspective. *Current Neurology and Neuroscience Reports*, 11, 428-434.
- TWOMEY, E. C. & SOBOLEVSKY, A. I. 2017. Structural Mechanisms of Gating in Ionotropic Glutamate Receptors. *Biochemistry*, 57, 267-276.
- VAN ZUNDERT, B., YOSHII, A. & CONSTANTINE-PATON, M. 2004. Receptor compartmentalization and trafficking at glutamate synapses: a developmental proposal. *Trends Neurosci*, 27, 428-37.
- VANCE, K. M., HANSEN, K. B. & TRAYNELIS, S. F. 2012. GluN1 splice variant control of GluN1/GluN2D NMDA receptors. *J Physiol*, 590, 3857-75.
- VENKATESWARAN, S., MYERS, K. A., SMITH, A. C., BEAULIEU, C. L., SCHWARTZENTRUBER, J. A., MAJEWSKI, J., BULMAN, D., BOYCOTT, K. M. & DYMENT, D. A. 2014. Whole-exome sequencing in an individual with severe global developmental delay and intractable epilepsy identifies a novel, de novo GRIN2A mutation. *Epilepsia*, 55, e75-e79.
- VENSELAAR, H., TE BEEK, T. A., KUIPERS, R. K., HEKKELMAN, M. L. & VRIEND, G. 2010. Protein structure analysis of mutations causing inheritable diseases. An e-Science approach with life scientist friendly interfaces. *BMC Bioinformatics*, 11, 548.
- VERGNANO, A. M., REBOLA, N., SAVTCHENKO, L. P., PINHEIRO, P. S., CASADO, M., KIEFFER, B. L., RUSAKOV, D. A., MULLE, C. & PAOLETTI, P. 2014. Zinc dynamics and action at excitatory synapses. *Neuron*, 82, 1101-14.
- VERMA, V., PAUL, A., AMRAPALI VISHWANATH, A., VAIDYA, B. & CLEMENT, J. P. 2019. Understanding intellectual disability and autism spectrum disorders from common mouse models: synapses to behaviour. *Open Biol*, 9, 180265.
- VICINI, S., WANG, J. F., LI, J. H., ZHU, W. J., WANG, Y. H., LUO, J. H., WOLFE, B. B. & GRAYSON, D. R. 1998. Functional and pharmacological differences between recombinant N-methyl-D-aspartate receptors. *J Neurophysiol*, 79, 555-66.
- VILLARROEL, A., BURNASHEV, N. & SAKMANN, B. 1995. Dimensions of the narrow portion of a recombinant NMDA receptor channel. *Biophys J*, 68, 866-75.
- VILLEMURE, E., VOLGRAF, M., JIANG, Y., WU, G., LY, C. Q., YUEN, P. W., LU, A., LUO, X., LIU, M., ZHANG, S., LUPARDUS, P. J., WALLWEBER, H. J., LIEDERER, B. M., DESHMUKH, G., PLISE, E., TAY, S., WANG, T. M., HANSON, J. E., HACKOS, D. H., SCEARCE-LEVIE, K., SCHWARZ, J. B. & SELLERS, B. D. 2017. GluN2A-Selective Pyridopyrimidinone Series of

- NMDAR Positive Allosteric Modulators with an Improved in Vivo Profile. *ACS Med Chem Lett*, 8, 84-89.
- VISSERS, L., VAN NIMWEGEN, K. J. M., SCHIEVING, J. H., KAMSTEEG, E. J., KLEEFSTRA, T., YNTEMA, H. G., PFUNDT, R., VAN DER WILT, G. J., KRABBENBORG, L., BRUNNER, H. G., VAN DER BURG, S., GRUTTERS, J., VELTMAN, J. A. & WILLEMSSEN, M. 2017. A clinical utility study of exome sequencing versus conventional genetic testing in pediatric neurology. *Genet Med*, 19, 1055-1063.
- VOLGRAF, M., SELLERS, B. D., JIANG, Y., WU, G., LY, C. Q., VILLEMURE, E., PASTOR, R. M., YUEN, P. W., LU, A., LUO, X., LIU, M., ZHANG, S., SUN, L., FU, Y., LUPARDUS, P. J., WALLWEBER, H. J., LIEDERER, B. M., DESHMUKH, G., PLISE, E., TAY, S., REYNEN, P., HERRINGTON, J., GUSTAFSON, A., LIU, Y., DIRKSEN, A., DIETZ, M. G., LIU, Y., WANG, T. M., HANSON, J. E., HACKOS, D., SCEARCE-LEVIE, K. & SCHWARZ, J. B. 2016. Discovery of GluN2A-Selective NMDA Receptor Positive Allosteric Modulators (PAMs): Tuning Deactivation Kinetics via Structure-Based Design. *J Med Chem*, 59, 2760-79.
- VON ENGELHARDT, J., BOCKLISCH, C., TONGES, L., HERB, A., MISHINA, M. & MONYER, H. 2015. GluN2D-containing NMDA receptors mediate synaptic currents in hippocampal interneurons and pyramidal cells in juvenile mice. *Front Cell Neurosci*, 9, 95.
- VON ENGELHARDT, J., DOGANCI, B., JENSEN, V., HVALBY, O., GONGRICH, C., TAYLOR, A., BARKUS, C., SANDERSON, D. J., RAWLINS, J. N., SEEBURG, P. H., BANNERMAN, D. M. & MONYER, H. 2008. Contribution of hippocampal and extra-hippocampal NR2B-containing NMDA receptors to performance on spatial learning tasks. *Neuron*, 60, 846-60.
- VON SPICZAK, S., FINSTERWALDER, K., MUHLE, H., FRANKE, A., SCHILHABEL, M., STEPHANI, U. & HELBIG, I. 2011. Comprehensive analysis of candidate genes for photosensitivity using a complementary bioinformatic and experimental approach. *Epilepsia*, 52, e143-e147.
- VON STULPNAGEL, C., ENSSLEN, M., MOLLER, R. S., PAL, D. K., MASNADA, S., VEGGIOTTI, P., PIAZZA, E., DREESMANN, M., HARTLIEB, T., HERBERHOLD, T., HUGHES, E., KOCH, M., KUTZER, C., HOERTNAGEL, K., NITANDA, J., POHL, M., ROSTASY, K., HAACK, T. B., STOHR, K., KLUGER, G. & BORGGRAEFE, I. 2017. Epilepsy in patients with GRIN2A alterations: Genetics, neurodevelopment, epileptic phenotype and response to anticonvulsive drugs. *Eur J Paediatr Neurol*, 21, 530-541.
- VRIEND, G. 1990. WHAT IF: a molecular modeling and drug design program. *J Mol Graph*, 8, 52-6, 29.
- VYKLYCKY, V., KORINEK, M., SMEJKALOVA, T., BALIK, A., KRAUSOVA, B., KANIAKOVA, M., LICHNEROVA, K., CERNY, J., KRUSEK, J., DITTERT, I., HORAK, M. & VYKLYCKY, L. 2014. Structure, function, and pharmacology of NMDA receptor channels. *Physiol Res*, 63 Suppl 1, S191-203.
- VYKLYCKY, V., KRAUSOVA, B., CERNY, J., LADISLAV, M., SMEJKALOVA, T., KYSILOV, B., KORINEK, M., DANACIKOVA, S., HORAK, M., CHODOUNSKA, H., KUDOVA, E. & VYKLYCKY, L. 2018. Surface Expression, Function, and Pharmacology of Disease-Associated Mutations in the Membrane Domain of the Human GluN2B Subunit. *Front Mol Neurosci*, 11, 110.
- WANG, C. C., HELD, R. G., CHANG, S. C., YANG, L., DELPIRE, E., GHOSH, A. & HALL, B. J. 2011. A critical role for GluN2B-containing NMDA receptors in cortical development and function. *Neuron*, 72, 789-805.
- WANG, D., CUI, Z., ZENG, Q., KUANG, H., WANG, L. P., TSIEN, J. Z. & CAO, X. 2009. Genetic enhancement of memory and long-term potentiation but not CA1 long-term depression in NR2B transgenic rats. *PLoS One*, 4, e7486.
- WANG, J. X. & FURUKAWA, H. 2019. Dissecting diverse functions of NMDA receptors by structural biology. *Curr Opin Struct Biol*, 54, 34-42.

- WANG, T., GUO, H., XIONG, B., STESSMAN, H. A., WU, H., COE, B. P., TURNER, T. N., LIU, Y., ZHAO, W., HOEKZEMA, K., VIVES, L., XIA, L., TANG, M., OU, J., CHEN, B., SHEN, Y., XUN, G., LONG, M., LIN, J., KRONENBERG, Z. N., PENG, Y., BAI, T., LI, H., KE, X., HU, Z., ZHAO, J., ZOU, X., XIA, K. & EICHLER, E. E. 2016. De novo genic mutations among a Chinese autism spectrum disorder cohort. *Nat Commun*, 7, 13316.
- WANG, X. H., ZHU, W. J., CORSI, L., IKONOMOVIC, S., PALJUG, W. R., VICINI, S. & GRAYSON, D. R. 1998. Chronic dizocilpine (MK-801) reversibly delays GABA(A) receptor maturation in cerebellar granule neurons in vitro. *J Neurochem*, 71, 693-704.
- WATANABE, M., INOUE, Y., SAKIMURA, K. & MISHINA, M. 1992. Developmental changes in distribution of NMDA receptor channel subunit mRNAs. *Neuroreport*, 3, 1138-40.
- WELLS, G., YUAN, H., MCDANIEL, M. J., KUSUMOTO, H., SNYDER, J. P., LIOTTA, D. C. & TRAYNELIS, S. F. 2018. The GluN2B-Glu413Gly NMDA receptor variant arising from a de novo GRIN2B mutation promotes ligand-unbinding and domain opening. *Proteins*, 86, 1265-1276.
- WENTHOLD, R. J., PRYBYLOWSKI, K., STANDLEY, S., SANS, N. & PETRALIA, R. S. 2003a. Trafficking of NMDA receptors. *Annu Rev Pharmacol Toxicol*, 43, 335-58.
- WENTHOLD, R. J., SANS, N., STANDLEY, S., PRYBYLOWSKI, K. & PETRALIA, R. S. 2003b. Early events in the trafficking of N-methyl-D-aspartate (NMDA) receptors. *Biochem Soc Trans*, 31, 885-8.
- WRIGHT, J. L., GREGORY, T. F., BIGGE, C. F., BOXER, P. A., SERPA, K., MELTZER, L. T., WISE, L. D., CAI, S. X., HAWKINSON, J. E., KONKOY, C. S., WHITTEMORE, E. R., WOODWARD, R. M. & ZHOU, Z. L. 1999. Subtype-selective N-methyl-D-aspartate receptor antagonists: synthesis and biological evaluation of 1-(arylalkynyl)-4-benzylpiperidines. *J Med Chem*, 42, 2469-77.
- WU, D., BACAJ, T., MORISHITA, W., GOSWAMI, D., ARENDT, K. L., XU, W., CHEN, L., MALENKA, R. C. & SÜDHOF, T. C. 2017. Postsynaptic synaptotagmins mediate AMPA receptor exocytosis during LTP. *Nature*, 544, 316-321.
- WYLLIE, D. J., LIVESEY, M. R. & HARDINGHAM, G. E. 2013. Influence of GluN2 subunit identity on NMDA receptor function. *Neuropharmacology*, 74, 4-17.
- XIANGWEI, W., JIANG, Y. & YUAN, H. 2018. De Novo Mutations and Rare Variants Occurring in NMDA Receptors. *Curr Opin Physiol*, 2, 27-35.
- XU, X. X., LIU, X. R., FAN, C. Y., LAI, J. X., SHI, Y. W., YANG, W., SU, T., XU, J. Y., LUO, J. H. & LIAO, W. P. 2018. Functional Investigation of a GRIN2A Variant Associated with Rolandic Epilepsy. *Neurosci Bull*, 34, 237-246.
- XU, X. X. & LUO, J. H. 2018. Mutations of N-Methyl-D-Aspartate Receptor Subunits in Epilepsy. *Neurosci Bull*, 34, 549-565.
- YANG, W., ZHENG, C., SONG, Q., YANG, X., QIU, S., LIU, C., CHEN, Z., DUAN, S. & LUO, J. 2007. A three amino acid tail following the TM4 region of the N-methyl-D-aspartate receptor (NR) 2 subunits is sufficient to overcome endoplasmic reticulum retention of NR1-1a subunit. *J Biol Chem*, 282, 9269-78.
- YAO, L., GRAND, T., HANSON, J. E., PAOLETTI, P. & ZHOU, Q. 2018. Higher ambient synaptic glutamate at inhibitory versus excitatory neurons differentially impacts NMDA receptor activity. *Nat Commun*, 9, 4000.
- YI, F., ZACHARIASSEN, L. G., DORSETT, K. N. & HANSEN, K. B. 2018. Properties of Triheteromeric N-Methyl-d-Aspartate Receptors Containing Two Distinct GluN1 Isoforms. *Mol Pharmacol*, 93, 453-467.
- YU, A. & LAU, A. Y. 2018. Glutamate and Glycine Binding to the NMDA Receptor. *Structure*, 26, 1035-1043 e2.
- YU, F. H., MANTEGAZZA, M., WESTENBROEK, R. E., ROBBINS, C. A., KALUME, F., BURTON, K. A., SPAIN, W. J., MCKNIGHT, G. S., SCHEUER, T. & CATTERALL, W. A. 2006. Reduced

- sodium current in GABAergic interneurons in a mouse model of severe myoclonic epilepsy in infancy. *Nat Neurosci*, 9, 1142-9.
- YU, Y., LIN, Y., TAKASAKI, Y., WANG, C., KIMURA, H., XING, J., ISHIZUKA, K., TOYAMA, M., KUSHIMA, I., MORI, D., ARIOKA, Y., UNO, Y., SHIINO, T., NAKAMURA, Y., OKADA, T., MORIKAWA, M., IKEDA, M., IWATA, N., OKAHISA, Y., TAKAKI, M., SAKAMOTO, S., SOMEYA, T., EGAWA, J., USAMI, M., KODAIRA, M., YOSHIMI, A., OYA-ITO, T., ALEKSIC, B., OHNO, K. & OZAKI, N. 2018. Rare loss of function mutations in N-methyl-d-aspartate glutamate receptors and their contributions to schizophrenia susceptibility. *Translational Psychiatry*, 8.
- YUAN, H., HANSEN, K. B., ZHANG, J., PIERSON, T. M., MARKELLO, T. C., FAJARDO, K. V., HOLLOMAN, C. M., GOLAS, G., ADAMS, D. R., BOERKOEL, C. F., GAHL, W. A. & TRAYNELIS, S. F. 2014. Functional analysis of a de novo GRIN2A missense mutation associated with early-onset epileptic encephalopathy. *Nat Commun*, 5, 3251.
- YUAN, H., LOW, C. M., MOODY, O. A., JENKINS, A. & TRAYNELIS, S. F. 2015. Ionotropic GABA and Glutamate Receptor Mutations and Human Neurologic Diseases. *Mol Pharmacol*, 88, 203-17.
- ZAREI, M. M. & DANI, J. A. 1994. Ionic permeability characteristics of the N-methyl-D-aspartate receptor channel. *J Gen Physiol*, 103, 231-48.
- ZHANG, Y., KONG, W., GAO, Y., LIU, X., GAO, K., XIE, H., WU, Y., ZHANG, Y., WANG, J., GAO, F., WU, X. & JIANG, Y. 2015. Gene Mutation Analysis in 253 Chinese Children with Unexplained Epilepsy and Intellectual/Developmental Disabilities. *PLoS One*, 10, e0141782.
- ZHENG, W., WEN, H., IACOBUCCI, G. J. & POPESCU, G. K. 2017. Probing the Structural Dynamics of the NMDA Receptor Activation by Coarse-Grained Modeling. *Biophys J*, 112, 2589-2601.
- ZHOU, C., SUN, H., KLEIN, P. M. & JENSEN, F. E. 2015. Neonatal seizures alter NMDA glutamate receptor GluN2A and 3A subunit expression and function in hippocampal CA1 neurons. *Front Cell Neurosci*, 9, 362.
- ZHOU, Z. L., CAI, S. X., WHITTEMORE, E. R., KONKOY, C. S., ESPITIA, S. A., TRAN, M., ROCK, D. M., COUGHENOUR, L. L., HAWKINSON, J. E., BOXER, P. A., BIGGE, C. F., WISE, L. D., WEBER, E., WOODWARD, R. M. & KEANA, J. F. 1999. 4-Hydroxy-1-[2-(4-hydroxyphenoxy)ethyl]-4-(4-methylbenzyl)piperidine: a novel, potent, and selective NR1/2B NMDA receptor antagonist. *J Med Chem*, 42, 2993-3000.
- ZHU, S. & GOUAUX, E. 2017. Structure and symmetry inform gating principles of ionotropic glutamate receptors. *Neuropharmacology*, 112, 11-15.

Appendix

Appendix A: Raw and ranked scores of static and dynamic features

	LBD mutation	Raw Scores											Ranked scores												
		Constrf norm.	HSP sequence entropy	c-beta accessibility	c-beta density	average POPMUSIC solvent accessibility	Normalized B-factor	FOLDX Saturation	MAESTRO Saturation	SIFT	PROVEAN	Polyphe n2	average POPMUSIC residue's ΔΔG	Constrf norm.	HSP sequence entropy	c-beta accessibility	c-beta density	average POPMUSIC solvent accessibility	Normalized B-factor	FOLDX Saturation	MAESTRO Saturation	SIFT	PROVEAN	Polyphe n2	average POPMUSIC residue's ΔΔG
GRIN2A	C436R	-0.68	-0.84	0	27	2.91	-0.39	3.03	0.79	0	-11.77	1	2.32	3	5.5	2.5	4	11	11	4	3	9	1	4.5	3
	V452M	0.76	2.31	8.39	14	34.09	-0.51	0.57	0.20	0.13	-1.53	0.58	0.83	23	26	21	23	20	9	20	21	24	25	25	15
	G483R	-0.69	-0.76	3.84	17	47.25	-0.2	0.9	0.27	0.01	-7.63	1	2.12	1	8	14	20	21	16	13	15	19.5	4	4.5	6
	R504W	0.43	-0.15	8.56	15	50.07	-0.06	0.45	0.17	0	-6.6	0.96	0.27	21.5	18.5	22.5	21.5	22.5	18.5	23.5	23.5	9	7	18	24.5
	R504P	0.43	-0.15	8.56	15	50.07	-0.06	0.45	0.17	0	-5.33	0.84	0.95	21.5	18.5	22.5	21.5	22.5	18.5	23.5	23.5	9	9	20	10
	V506A	1.16	1.42	4.54	22	17.8	0.08	0.39	0.64	0.49	-0.36	0.88	2.16	24	25	18	9.5	17	20	26	6	26	26	19	5
	R518H	-0.54	-0.84	1.05	27	1.19	-1.02	0.78	0.63	0	-4.82	1	0.88	13	5.5	6	4	6	5	15	8	9	10	4.5	11.5
	T531M	-0.6	-0.84	0	25	0.57	-1.2	3.22	0.75	0	-5.79	1	0.31	6	5.5	2.5	6	4	3	3	4	9	8	4.5	23
	K669N	-0.38	-0.25	4.19	20	15.95	-0.34	0.79	0.25	0	-4.74	1	0.98	18	16	15.5	14.5	16	13	14	18	9	12	4.5	9
	I694T	-0.59	-0.5	2.97	22	0.46	-1.01	1.5	0.25	0.01	-4.79	1	2.56	7	15	12	9.5	3	6	7	17	19.5	11	4.5	1
	P699S	2.73	0.99	18.52	10	59.78	-0.87	0.48	0.11	0.04	-4.04	0.98	0.48	26	22	25.5	26	25	8	21	25	23	16	16	21
	M705V	-0.30	-0.51	2.45	21	1.92	-0.37	1.33	0.20	0	-3.81	1	1.3	20	14	10	11.5	8	12	9	20	9	19	14	7
	E714K	2.66	0.85	18.52	11	58.91	0.21	0.46	0.11	0.02	-2.5	0.17	0.36	25	21	25.5	24.5	24	21	22	26	22	23	26	22
	A716T	-0.50	-0.62	0	27	0	-0.46	6.21	0.63	0	-3.86	1	0.85	15	11	2.5	4	1.5	10	1	7	9	18	10.5	13
	A727I	-0.58	-0.59	0	24	0	-0.92	3.91	0.88	0.01	-3.57	0.98	0.88	11	12.5	2.5	7	1.5	7	2	2	19.5	20	17	11.5
GRIN2B	D731N	-0.55	-0.93	3.5	28	5.28	-1.10	0.63	0.96	0	-4.46	0.66	0.27	12	1	13	1.5	13	4	19	1	9	15	24	24.5
	V734L	-0.59	-0.84	1.75	20	0.93	-1.36	1.1	0.35	0.01	-2.63	0.71	0.59	8	5.5	9	14.5	5	1	11	12	19.5	22	23	18
	K772E	-0.50	-0.76	6.64	18	31.89	0.27	0.75	0.24	0	-3.48	0.81	0.57	16	9	20	19	18	23	16	19	9	21	21	19.5
	A778P	-0.33	-0.59	1.22	21	3.93	-0.10	1.48	0.31	0	-4.5	1	2.49	19	12.5	7	11.5	12	17	8	13	9	13	10.5	2
	M788I	-0.41	1.04	6.29	19	5.85	0.43	0.68	0.25	0.22	-1.57	1	0.84	17	24	19	17.5	14	24	18	16	25	24	13	14
	E413G	-0.68	-0.23	4.19	23	14.76	-0.23	0.75	0.67	0	-6.87	1	0.57	2	17	15.5	8	15	15	17	5	9	6	10.5	19.5
	C456Y	-0.63	-0.76	1.4	20	2.88	0.24	1.62	0.53	0	-10.72	1	1.1	4.5	10	8	14.5	10	22	6	9	9	3	4.5	8
	C461F	-0.63	-0.86	0.35	28	1.52	-1.22	1.64	0.39	0	-10.79	1	0.76	4.5	2.5	5	1.5	7	2	5	11	9	2	4.5	16
	R540H	-0.59	-0.86	12.41	11	63.26	0.92	0.44	0.2	0	-4.49	0.72	0.13	9	2.5	24	24.5	26	26	25	22	9	14	22	26
	R682C	-0.58	0.39	4.37	19	33.83	0.66	0.92	0.46	0	-7.51	1	0.69	10	20	17	17.5	19	25	12	10	9	5	10.5	17
	M789K	-0.53	1.03	2.8	20	2.08	-0.27	1.10	0.31	0	-3.94	1	2.17	14	23	11	14.5	9	14	10	14	9	17	15	4

Appendix B: Order of mutations from most to least damaging

	Principle Component values				Difference from 3 SDs from the mean			Distance from 3 SDs of the mean*	Ordered distance from 3 SDs of the mean	Order of mutations: Most to least damaging	
LBD mutation	Static	Dynamic	Static	Dynamic	dsPC1	dsPC2	ddPC1	ddPC2			
Explains % of variability	sPC1	sPC2	dPC1	dPC2							
	64.7	12.6	54.40	29.60							
GRIN2A	C436R	-0.60	-1.45	-1.09	-1.35	-2.4	-1.55	-1.91	-1.65	3.81	C436R
	V452M	0.18	1.76	1.81	0.41	-3.18	-4.76	-4.81	-3.41	8.22	C461F
	G483R	1.15	-1.58	-0.17	-1.47	-4.15	-1.42	-2.83	-1.53	5.45	C456Y
	R504W	1.05	0.81	-0.9	1.43	-4.05	-3.81	-2.10	-4.43	7.41	R518H
	R504P	1.05	0.81	-0.33	0.2	-4.05	-3.81	-2.67	-3.2	6.94	T531M
	V506A	0.04	1.17	2.11	-0.93	-3.04	-4.17	-5.11	-2.07	7.55	I694T
	R518H	-0.93	-0.27	-0.77	-0.53	-2.07	-2.73	-2.23	-2.47	4.78	A778P
	T531M	-1.28	-0.78	-1.2	0.54	-1.72	-2.22	-1.80	-3.54	4.86	A716T
	K669N	0.03	0.57	-0.59	-0.75	-3.03	-3.57	-2.41	-2.25	5.73	G483R
	I694T	-0.88	0.16	0.38	-1.91	-2.12	-3.16	-3.38	-1.09	5.21	E413G
	P699S	0.65	1.71	0.76	0.48	-3.65	-4.71	-3.76	-3.48	7.86	K669N
	M705V	-0.71	0.84	0.17	-0.38	-2.29	-3.84	-3.17	-2.62	6.07	A727T
	E714K	1.2	1.19	1.37	1.19	-4.2	-4.19	-4.37	-4.19	8.48	R682C
	A716T	-1.60	0.19	-0.16	-0.02	-1.4	-3.19	-2.84	-2.98	5.39	M789K
	A727T	-1.59	-0.02	1.01	-0.20	-1.41	-2.98	-4.01	-2.8	5.90	M705V
	D731N	-0.37	-0.92	-0.24	1.79	-2.63	-2.08	-2.76	-4.79	6.47	D731N
GRIN2B	V734L	-0.67	-0.42	1.14	0.75	-2.33	-2.58	-4.14	-3.75	6.58	V734L
	K772E	1.09	-0.41	0.16	1.18	-4.09	-2.59	-3.16	-4.18	7.13	R504P
	A778P	-0.45	0.26	-0.16	-1.07	-2.55	-3.26	-2.84	-1.93	5.38	K772E
	M788I	0.47	0.71	1.5	-0.39	-3.47	-3.71	-4.5	-2.61	7.27	M788I
	E413G	0.28	-0.89	-1.05	0.54	-3.28	-2.11	-1.95	-3.54	5.62	R504W
	C456Y	0.20	-1.23	-1.1	-0.88	-3.20	-1.77	-1.90	-2.12	4.64	V506A
	C461F	-0.99	-1	-1.37	-0.13	-2.01	-2.00	-1.63	-2.87	4.35	R540H
	R540H	2.48	-1.63	-0.40	1.82	-5.48	-1.37	-2.6	-4.82	7.86	P699S
GRIN2C	R682C	0.77	-0.38	-1.04	0.30	-3.77	-2.62	-1.96	-3.30	5.98	V452M
	M789K	-0.57	0.8	0.16	-0.62	-2.43	-3.8	-3.16	-2.38	6	E714K

* $\sqrt{\left(\frac{dsPC1^2 + dsPC2^2}{+ddPC1^2 + ddPC2^2}\right)}$ SD: Standard deviation

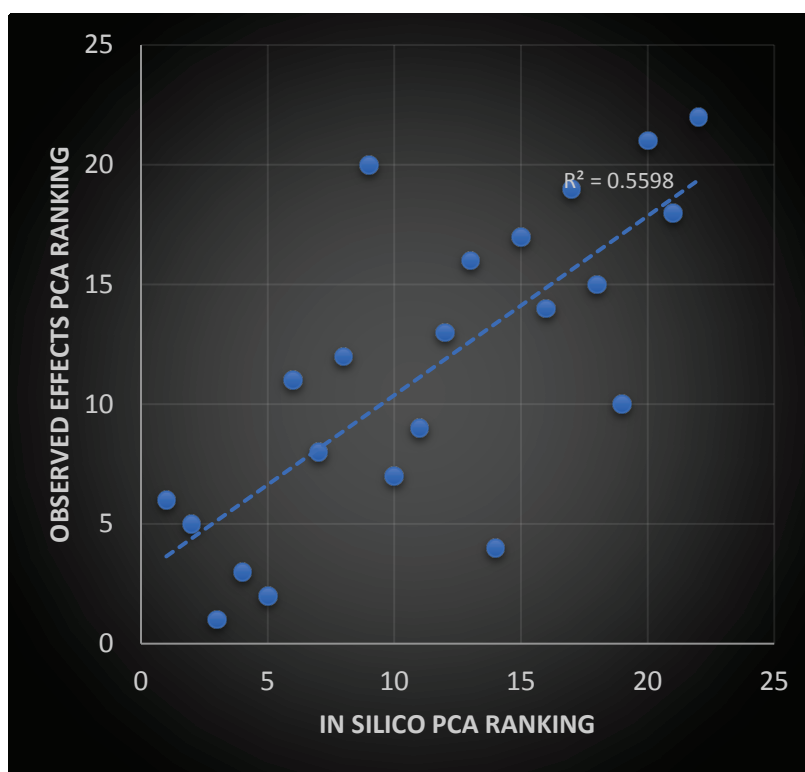
Appendix C: Extraction Method for Principal Component Analysis.

Rotated Component Matrix		
Static features	PC 1	PC 2
Consurf norm. score		0.896
HSSP sequence entropy		0.820
c-beta accessibility	0.858	0.443
c-beta density	0.812	0.397
average PoPMuSiC solvent accessibility	0.924	
Normalized B-factor	0.749	
FOLDX Saturation mutagenesis MAD	0.765	0.372
MAESTRO Saturation mutagenesis MAD	0.635	0.520

Rotated Component Matrix		
Dynamic features	PC 1	PC 2
SIFT	0.866	
PROVEAN	0.896	
Polyphen2	0.610	0.697
average PoPMuSiC residue's $\Delta\Delta G$		0.933

PCs were rotated using the Varimax with Kaiser Normalization method in SPSS. This method adjusts the data to identify the correlations of the generated PCs to the original variables.

Appendix D: Correlation between rankings of predicted deleterious effects and observed effects in heterologous cells of *GRIN2A* and *GRIN2B* mutations.



A PCA was performed for data obtained from Swanger et al. (2016). This data included glutamate and glycine EC_{50} s, τ_w and peak amplitudes for responses from NMDARs with *GRIN2A* and *GRIN2B* mutations measured in heterologous cells. R504P, A778P and M788I from *GRIN2A* and M789K from *GRIN2B* were not included in the analysis since they were not included by Swanger et al. (2016). First, mutations were ranked for each feature (glutamate and glycine EC_{50} s, τ_w and peak amplitude) based on the fold-change in mutant values with respect to the WT values. A larger difference between the mutant and WT values was equivalent to a more damaging mutation as it caused a greater perturbation in NMDAR function. The PCA produced a single component that represented 70% of the variability within the data. The rank of these mutations was then correlated to the rank produced by the PCA of the in silico data from the various bioinformatics programmes ($n = 22$, $r = 0.748$, $p < 0.0001$).

Appendix E: Unadjusted p values for mutant data

Unadjusted p values	+ 20 mV NMDAR*		- 40 mV		AMPA*		RI# (-40 mV / +20 mV)
	Peak Amplitude (nS)	Decay (ms)	Peak Amplitude (nS)	Decay (ms)	Peak Amplitude (pA)	Decay (ms)	
GluN2							
GluN2A KO	<0.00001	<0.00001					
K669N	0.1308	0.03	0.5059		0.4906	0.3989	0.2348
L812M	0.0001	0.0002	0.2671		0.0723	0.0259	0.0053
T531M	0.0003	<0.00001	0.0028		0.2064	0.1675	0.0425
C436R	0.005	<0.00001	0.0546		0.5384	0.3152	0.1313
R518H	0.0003	<0.00001	0.0213		0.8816	0.4655	0.3613
I694T	0.0021	0.844	0.0249		0.4099	0.2404	0.6725
GluN2B KO	<0.00001	<0.00001					
C461F	0.1259	0.0001	0.2788		0.0518	0.6177	0.0756
C456Y	0.0402	<0.00001	0.0654		0.5003	0.0559	0.2961
C436R	0.0195	<0.00001	0.1357		0.0515	0.8022	0.5425
R540H	0.0386	0.0005	0.9623		0.3363	0.4349	0.1716
R696H	0.0037	0.0037	0.1284		0.6963	0.7267	0.9866

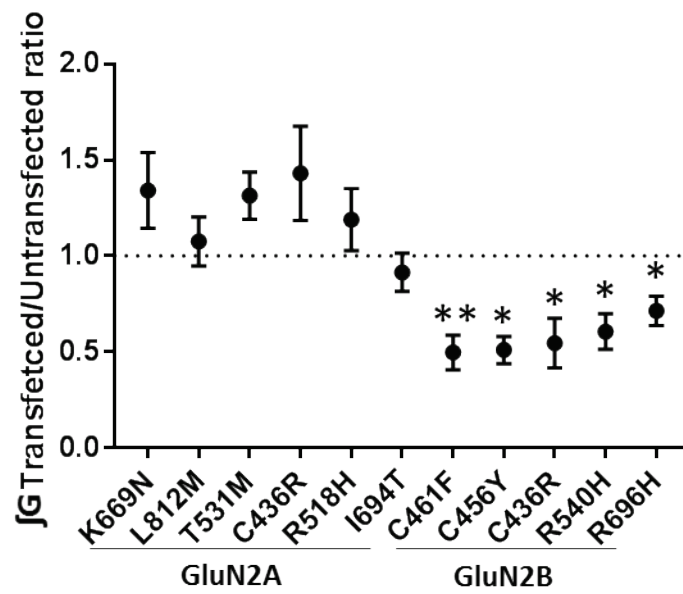
*MLM and #paired t-test unadjusted p values. Significant values are highlighted in red.

Appendix F: Adjusted p values for mutant data

adjusted p values	+ 20 mV NMDAR		- 40 mV NMDAR		AMPA		RI (-40 mV / +20 mV)
GluN2	Peak Amplitude (nS)	Decay (ms)	Peak Amplitude (nS)	Decay (ms)	Peak Amplitude (pA)	Decay (ms)	
GluN2A KO	<0.00001	<0.00001					
K669N	0.6540	0.18	1	1	1	1	0.93913
L812M	0.0006	0.001	0.2671	0.0777	0.1446	0.0777	0.021224
T531M	0.0015	<0.00001	0.0112	0.335	0.335	0.335	0.127399
C436R	0.025	<0.00001	0.2184	0.6304	0.6304	0.6304	0.393983
R518H	0.0015	<0.00001	0.0852	1	1	1	1
I694T	0.0126	1	0.1245	0.9616	1	0.9616	1
GluN2B KO	<0.00001	<0.00001					
C461F	0.3778	0.0006	0.5576	0.6177	0.259	0.6177	0.302311
C456Y	0.2010	<0.00001	0.2236	0.2236	0.592146	0.2236	0.592146
C436R	0.0974	<0.00001	0.4071	1	0.206	1	1
R540H	0.1931	0.003	1	1	1	1	0.686338
R696H	0.0222	0.0222	0.5136	1	1	1	1

p values from Appendix E adjusted for multiple comparisons with MATLAB 9.2 multcomp, Holm-Bonferroni. p values of all six variables (+20 mV peak and decay, -40 mV peak, AMPAR peak and decay, and RI) were adjusted for each mutant separately (a MC test was performed for each mutant: each row of the table). Significant values are highlighted in red. P values that lost significance are highlighted orange.

Appendix G: Integral of conductance for mutant NMDAR subunits



Paired t-tests used to compare transfected vs untransfected values with MATLAB 9.2 multicomp, Holm-Bonferroni correction for multiple comparisons

Appendix H: NMDAR Current-Voltage curves for untransfected cells and cells transfected with mutant GluN2 subunits.

For the 0 mV data, mixed NMDAR and AMPAR current was used due to the conversion of conductance to current which required a division by zero for pure NMDAR current.

